THE EFFECT OF THE COUNTERFACE ON THE WEAR RESISTANCE OF CERTAIN ALLOYS AT ROOM TEMPERATURE AND 750°C

Philip David Wood

Ph.D.

March 1997

THE EFFECT OF THE COUNTERFACE ON THE WEAR RESISTANCE OF CERTAIN ALLOYS AT ROOM TEMPERATURE AND 750°C

Philip David Wood

A thesis submitted in part fulfilment of the requirements
for the degree of Doctor of Philosophy

In collaboration with EPSRC and British Gas

Surface Engineering Research Group
School of Engineering
University of Northumbria

March 1997

'If you steal from one author, it's plagiarism;
if you steal from many, it's research.'

Wilson Mizner

CONTENTS

		Page
CHAPTER 1	**INTRODUCTION**	1
CHAPTER 2	**LITERATURE REVIEW**	8
2.1	**Introduction to Wear**	8
2.2	**Classification and Mechanisms of Wear**	8
2.2.1	Adhesive Wear	9
2.2.2	Abrasive Wear	11
2.2.3	Fatigue Wear	14
2.2.4	Combined Wear Types	15
2.3	**Theories of Wear**	16
2.3.1	Room Temperature	16
2.3.2	Elevated Temperature	20
2.4	**Factors Affecting Wear Behaviour**	30
2.4.1	Hardness	30
2.4.2	Mutual Solubility	32
2.4.3	Crystal Structure and Microstructure	34
2.4.4	Processing Route of Material	35
2.4.5	Formation of Protective Oxide Films	38
2.5	**Ceramic/Metal Sliding**	48
CHAPTER 3	**INTRODUCTION TO EXPERIMENTAL WORK**	54
CHAPTER 4	**EXPERIMENTAL**	58
4.1	**Materials**	58
4.2	**Design and Experimental Conditions for Wear Rig**	59

4.3 Experimental Methods 62

4.3.1 Specimen Preparation 62

4.3.2 Experimental Procedure 62

4.3.3 Analysis 63

CHAPTER 5 RESULTS 65

5.1 XRD Analysis of the As-Received Materials 65

5.2 Air Oxidation 66

5.3 Wear Studies Using Different Counterfaces at Room Temperature and 750°C for 4 Hours 67

5.3.1 Weight Changes 67

5.3.2 Friction Coefficient 72

5.3.3 XRD Analysis 78

5.3.4 SEM Morphological Analysis 82

5.3.5 Hardness Testing 88

5.3.6 EDX Analysis 89

5.3.7 Cross-Sectional EDX of the Block Alloys and EDX Analysis of Wear Debris 92

5.4 Wear Testing of Nimonic 90 and Ma956 Against Incoloy 800 and Stellite 6 at 750°C for 2 Minutes to 1 Hour 107

5.4.1 Weight Changes 107

5.4.2 XRD Analysis 107

5.4.3 SEM Morphological Analysis 110

5.4.4 Hardness Testing 115

5.4.5 Cross-Sectional EDX of Block Alloys/EDX Analysis of Counterface and EDX Analysis of Wear Debris 116

5.5 Effect of Temperature on the Wear Resistance of Ma956 Wearing Against Stellite 6 132

5.5.1 Weight Changes 132

5.5.2 Friction Coefficient 132

5.5.3 XRD Analysis 133

5.5.4 Hardness Testing 134

5.5.5 SEM/Cross-Sectional EDX of Ma956 and EDX Analysis of Wear Debris 135

5.6 Effect of Preoxidation on the Wear Resistance of ODS Alloys Wearing Against Incoloy 800 at 750°C 139

5.6.1 Weight Changes 139

5.6.2 Friction Coefficient 140

5.6.3 XRD Analysis 140

5.6.4 SEM Morphological Analysis 141

5.6.5 Cross-Sectional EDX of Preoxidised Alloys and EDX analysis of Wear Debris 143

CHAPTER 6 DISCUSSION 144

6.1 Wear Studies Using Different Counterfaces at Room Temperature and 750°C for 4 Hours 144

6.1.1 ODS Alloys vs Different Counterfaces 144

6.1.2 Nimonics vs Different Counterfaces 149

6.1.3 TiAl vs Different Counterfaces 153

6.2 Wear Testing of Nimonic 90 and Ma956 Against Incoloy 800 and Stellite 6 at 750°C for 2 Minutes to 1 Hour 158

6.2.1 Nimonic 90 vs Incoloy 800 at 750°C 158

6.2.2 Nimonic 90 vs Stellite 6 at 750°C 163

6.2.3 Ma956 vs Incoloy 800 at 750°C 168

6.2.4 Ma956 vs Stellite 6 at 750°C 172

6.3 Effect of Temperature on the Wear Resistance of Ma956 Wearing Against Stellite 6 180

6.4 Effect of Preoxidation on the Wear Resistance of the ODS Alloys 181

CHAPTER 7 CONCLUSIONS AND SUGGESTIONS FOR FUTURE WORK 183

7.1 Wear Studies Using Different Counterfaces at Room Temperature and 750°C for 4 Hours 183

7.1.1 Ma956, PM2000 and PM2000SD 183

7.1.2 Nimonic 80A (cast + HIPped) and Nimonic 90 184

7.1.3 TiAl 185

7.1.4 Comparisons 186

7.2 Wear Testing of Nimonic 90 and Ma956 Against Incoloy 800 and Stellite 6 for 2 Minutes to 4 Hours at 750°C 187

7.2.1 Nimonic 90 vs Incoloy 800 187

7.2.2 Nimonic 90 vs Stellite 6 187

7.2.3 Ma956 vs Incoloy 800 188

7.2.4 Ma956 vs Stellite 6 188

7.2.5 Comparisons 189

7.3 Effect of Temperature on the Wear Resistance of Ma956 Wearing Against Stellite 6 190

7.4 Effect of Preoxidation on the Wear Resistance of the ODS Alloys 190

7.5 Future Work 192

REFERENCES 194

LIST OF TABLES

		Page
Table 1.1	Summary of environmental factors found in different engines	1
Table 1.2	Composition of existing valve materials and hard-facing alloys	3
Table 1.3	Properties of some existing valve materials	4
Table 2.1	Wear coefficient values for various materials sliding against tool steel in unlubricated pin-on-disc tests in air	11
Table 2.2	Summary of selected investigations and conclusions conducted by Stott et al.	26
Table 2.3	Composition of the alloys used in investigations by Stott et al.	27
Table 2.4	Composition of alloys used by Hickl for west testing	31
Table 2.5	Comparison of wear coefficients and compatibility ratings of material pairs	32
Table 2.6	Composition and hardness values of the counterface material used by Subramanian	33
Table 2.7	Composition of LV21-43 alloy	37
Table 2.8	Selected investigations into the effect of microstructure on wear resistance	36
Table 2.9	Chemical composition of 321 stainless steel and Jethete 152	39
Table 2.10	Transition times for severe-to-mild wear rates for like-on-like sliding of a 9% chromium steel	42
Table 2.11	Average friction coefficient values for the wearing of an Al_2O_3 pin against various discs	49
Table 2.12	Variation in the volume loss of Si_3N_4 and high chromium cast iron with hardness of the cast iron	50
Table 2.13	Metallic alloys and ceramic materials used in ceramic/metal wear testing	53

Table 4.1	Composition of block materials	58
Table 4.2	Composition of wheel materials	59
Table 4.3	Experimental conditions chosen for wear testing	59
Table 4.4	Description and properties of materials used in the investigation	60
Table 5.1	XRD analysis of the surface of the as-received materials	65
Table 5.2	Weight change of alloys after air oxidation at 750°C for 4 hours	66
Table 5.3	XRD analysis of the surface of the block alloys after wearing against Incoloy 800 at room temperature and 750°C	79
Table 5.4	XRD analysis of the surface of the block alloys after wearing against Stellite 6 at room temperature and 750°C	80
Table 5.5	XRD analysis of the surface of the block alloys after wearing against Si_3N_4 at room temperature and 750°C	81
Table 5.6	Hardness values of block alloys prior to and after wearing against various counterfaces at room temperature and 750°C	89
Table 5.7	Composition of the surface of the block alloys after wearing against various counterfaces at room temperature	90
Table 5.8	Composition of the surface of the block alloys after wearing against various counterfaces at 750°C	91
Table 5.9	Cross-sectional EDX of the block alloys and analysis of the collected wear debris after testing against Incoloy 800 at room temperature	95
Table 5.10	Cross-sectional EDX of the block alloys and analysis of the collected wear debris after testing against Incoloy 800 at 750°C	96
Table 5.11	Cross-sectional EDX of the block alloys and analysis of the collected wear debris after testing against Stellite 6 at room temperature	97
Table 5.12	Cross-sectional EDX of the block alloys and analysis of the collected wear debris after testing against Stellite 6 at 750°C	98

Table 5.13	Cross-sectional EDX of the block alloys and analysis of the collected wear debris after testing against Si_3N_4 at room temperature	99
Table 5.14	Cross-sectional EDX of the block alloys and analysis of the collected wear debris after testing against Si_3N_4 at 750°C	100
Table 5.15	XRD analysis of the surface of Nimonic 90 and Ma956 after wearing against Incoloy 800 and Stellite 6 at 750°C for 2 minutes to 1 hour	109
Table 5.16	Hardness of Ma956 and Nimonic 90 after wearing against Incoloy 800 and Stellite 6 at 750°C for 2 minutes to 1 hour	115
Table 5.17	Summary of the analysis of the wearing system: Nimonic 90 vs Incoloy 800 for 2 minutes to 1 hour at 750°C	118
Table 5.18	Summary of the analysis of the wearing system: Nimonic 90 vs Stellite 6 for 2 minutes to 1 hour at 750°C	119
Table 5.19	Summary of the analysis of the wearing system: Ma956 vs Incoloy 800 for 2 minutes to 1 hour at 750°C	120
Table 5.20	Summary of the analysis of the wearing system: Ma956 vs Stellite 6 for 2 minutes to 1 hour at 750°C	121
Table 5.21	XRD analysis of the surface of Ma956 after wearing against Stellite 6 at different temperatures	134
Table 5.22	Hardness of Ma956 after wearing against Stellite 6 at room temperature, 350°C, 550°C and 750°C	135
Table 5.23	Summary of analysis of selected features after the wearing of Ma956 against Stellite 6 between room temperature and 750°C	137
Table 5.24	XRD analysis of the surface of the preoxidised ODS alloys after wearing against Incoloy 800 at 750°C	141
Table 5.25	Summary of analysis of preoxidised ODS alloys after wearing against Incoloy 800 at 750°C	143

Table 6.1	Comparison of the mechanical properties of Nimonic 90 and Nimonic 80A	152
Table 6.2	Atomic radius and covalent radius of certain elements	156
Table 7.1	Comparison of wear performances of the alloys against different counterfaces	191

LIST OF FIGURES

		Page
Fig.1.1	Nomenclature of the valve and seat insert	2
Fig.2.1	Schematic of the three abrasive modes	12
Fig.2.2	Abrasive wear due to an idealised conical particle and a surface	13
Fig.2.3	Plot of stress against the number of cycles to failure, N	15
Fig.2.4	Longitudinal section of a wear specimen	18
Fig.2.5	Idealised cell microstructure after wear	19
Fig.2.6	Stages of metallic adhesion between asperities leading to material transfer and high wear rates	20
Fig.2.7	Stages of metallic oxide adhesion leading to a small amount of material transfer and low wear rates	21
Fig.2.8	Wear rate vs W/p_m for pin-on-disc sliding of medium carbon steel at room temperature and a sliding speed of 650cms^{-1}	23
Fig.2.9	Coefficient of friction vs time plots for like-on-like sliding of C263 in air at 20°C to 600°C	27
Fig.2.10	Wear rate of 1040 steel pins wearing against 4140 steel discs	30
Fig.2.11	Volume loss of different alloys wearing against a carburised SAE 4620 steel	31
Fig.2.12	Variation of the normalised wear rates of the Al-Si alloy slid against various counterface materials	34
Fig.2.13	Schematic of Todsen's test rig	37
Fig.2.14	Results of Todsen's rig testing on cast and PM LV21-43	38
Fig.2.15	Coefficient of friction vs time plots during like-on-like sliding at 300°C for as-received and preoxidised 321 stainless steel	40
Fig.2.16	Coefficient of friction vs time plot during like-on-like sliding at 300°C for as-received and preoxidised Jethete M152	40

Fig.2.17	Effects of preoxidation on the wearing of S45C at 20°C	41
Fig.2.18	Friction coefficient of Fe-4.9%Cr during like-on-like sliding in various oxygen partial pressures at 20°C	44
Fig.2.19	Wear of Fe-4.9%Cr during like-on-like sliding in various oxygen partial pressures at 20°C	44
Fig.2.20	Coefficient of friction as a function of time for like-on-like sliding of Ni-20%Cr	45
Fig.2.21	Wear curve for like-on-like sliding of Nimonic 80A at 20°C	46
Fig.2.22	Influence of load on sliding wear	47
Fig.2.23	The change of the wear coefficient with speed for 60/40 brass on steel	48
Fig.2.24	Variation of the friction coefficient with relative humidity for various metal/ceramic couples	51
Fig.4.1	Schematic of wear rig	61
Fig.5.1	Weight change of the ODS alloys after wearing against various counterfaces at room temperature and 750°C	68
Fig.5.2	Weight change of the Nimonics after wearing against various counterfaces at room temperature and 750°C	70
Fig.5.3	Weight changes of Stellite 6 and TiAl after wearing against various counterfaces at room temperature and 750°C	71
Fig.5.4	Friction coefficient vs time plot for Ma956 wearing against various counterfaces at room temperature and 750°C	73
Fig.5.5	Friction coefficient vs time plot for PM2000 wearing against various counterfaces at room temperature and 750°C	73
Fig.5.6	Friction coefficient vs time plot for PM2000SD wearing against various counterfaces at room temperature and 750°C	74
Fig.5.7	Friction coefficient vs time plot for Nimonic 80A (HIPped) wearing against various counterfaces at room temperature and 750°C	75

Fig.5.8	Friction coefficient vs time plot for Nimonic 80A (cast) wearing against various counterfaces at room temperature and 750°C	76
Fig.5.9	Friction coefficient vs time plot for Nimonic 90 wearing against various counterfaces at room temperature and 750°C	76
Fig.5.10	Friction coefficient vs time plot for TiAl wearing against various counterfaces at room temperature and 750°C	77
Fig.5.11	SEM micrographs of Ma956 worn against various counterfaces at room temperature and 750°C	84
Fig.5.12	SEM micrographs of Nimonic 80A (cast) worn against various counterfaces at room temperature and 750°C	85
Fig.5.13	SEM micrographs of Nimonic 90 worn against various counterfaces at room temperature and 750°C	86
Fig.5.14	SEM micrographs of TiAl worn against various counterfaces at room temperature and 750°C	87
Fig.5.15	Cross-sectional EDX of Ma956 worn against Incoloy 800 at room temperature and 750°C	101
Fig.5.16	Cross-sectional EDX of Nimonic 90 worn against Incoloy 800 at room temperature and 750°C	102
Fig.5.17	Cross-sectional EDX of TiAl worn against Incoloy 800 at room temperature and 750°C	103
Fig.5.18	Cross-sectional EDX of Ma956 worn against Stellite 6 at room temperature and 750°C	104
Fig.5.19	Cross-sectional EDX of TiAl worn against Si_3N_4 at room temperature and 750°C	105
Fig.5.20	Selected SEM micrographs of wear debris from the alloys wearing against various counterfaces	106

Fig.5.21	Weight changes of Nimonic 90 and Ma956 after wearing against Incoloy 800 at 750°C for 2 minutes to 4 hours	109
Fig.5.22	Weight changes of Nimonic 90 and Ma956 after wearing against Stellite 6 at 750°C for 2 minutes to 4 hours	109
Fig.5.23	SEM micrographs of Nimonic 90 worn against Incoloy 800 at 750°C for 2 minutes to 1 hour	111
Fig.5.24	SEM micrographs of Nimonic 90 worn against Stellite 6 at 750°C for 2 minutes to 1 hour	112
Fig.5.25	SEM micrographs of Ma956 worn against Incoloy 800 at 750°C for 2 minutes to 1 hour	113
Fig.5.26	SEM micrographs of Ma956 worn against Incoloy 800 at 750°C for 2 minutes to 1 hour	114
Fig.5.27	Cross-sectional EDX of Nimonic 90 worn against Incoloy 800 at 750°C for 2 minutes to 1 hour	122
Fig.5.28	Cross-sectional EDX of Nimonic 90 worn against Stellite 6 at 750°C for 2 minutes to 1 hour	123
Fig.5.29	SEM micrographs and EDX analysis of Incoloy 800 after wearing against Nimonic 90 at 750°C for 2 minutes to 1 hour	124
Fig.5.30	SEM micrographs and EDX analysis of Stellite 6 after wearing against Nimonic 90 at 750°C for 2 minutes to 1 hour	125
Fig.5.31	SEM micrographs and EDX analysis of wear debris from Nimonic 90 worn against Incoloy 800 and Stellite 6 at 750°C for 2 minutes to 1 hour	126
Fig.5.32	Cross-sectional EDX of Ma956 worn against Incoloy 800 at 750°C for 2 minutes to 1 hour	127
Fig.5.33	Cross-sectional EDX of Ma956 worn against Stellite 6 at 750°C for 2 minutes to 1 hour	128

Fig.5.34	SEM micrographs and EDX analysis of Incoloy 800 after wearing against Ma956 at 750°C for 2 minutes to 1 hour	129
Fig.5.35	SEM micrographs and EDX analysis of Stellite 6 after wearing against Ma956 at 750°C for 2 minutes to 1 hour	130
Fig.5.36	SEM micrographs and EDX analysis of wear debris from Ma956 worn against Incoloy 800 and Stellite 6 at 750°C for 2 minutes to 1 hour	131
Fig.5.37	Weight change of Ma956 after wearing against Stellite 6 at room temperature, 350°C, 550°C and 750°C	132
Fig.5.38	Friction coefficient vs time plot for Ma956 wearing against Stellite 6 at room temperature, 350°C, 550°C and 750°C	133
Fig.5.39	SEM micrographs and cross-sectional EDX of Ma956 worn against Stellite 6 at 350°C and 550°C	138
Fig.5.40	Weight change of preoxidised ODS alloys after wearing against Incoloy 800 at 750°C	139
Fig.5.41	Friction coefficient vs time plot for preoxidised ODS alloys wearing against Incoloy 800 at 750°C	140
Fig.5.42	SEM micrographs of preoxidised Ma956 worn against Incoloy 800 at 750°C	142
Fig.6.1	Schematic of Nimonic 90 wearing against Incoloy 800 at 750°C for 2 minutes, 10 minutes and 20 minutes	159
Fig.6.2	Schematic of Nimonic 90 wearing against Incoloy 800 at 750°C for 1 hour and 4 hours	160
Fig.6.3	Schematic of Nimonic 90 wearing against Stellite 6 at 750°C for 2 minutes, 10 minutes and 20 minutes	165
Fig.6.4	Schematic of Nimonic 90 wearing against Stellite 6 at 750°C for 1 hour and 4 hours	166

Fig.6.5	Schematic of Ma956 wearing against Incoloy 800 at 750°C for 2 minutes, 10 minutes and 20 minutes	169
Fig.6.6	Schematic of Ma956 wearing against Incoloy 800 at 750°C for 1 hour and 4 hours	170
Fig.6.7	Variation of the tensile strength and yield strength with temperature for Nimonic 90 and Ma956	173
Fig.6.8	Schematic of Ma956 wearing against Stellite 6 at 750°C for 2 minutes, 10 minutes and 20 minutes	175
Fig.6.9	Schematic of Ma956 wearing against Stellite 6 at 750°C for 1 hour and 4 hours	176

ACKNOWLEDGEMENTS

I wish to express my thanks and appreciation to Professor P.K.Datta of the Surface Engineering Research Group, University of Northumbria for his supervision and encouragement provided throughout the course of my study. Thanks also go to Dr J.S.Burnell-Gray of the Surface Engineering Research Group, University of Northumbria for the discussion and help given during the preparation of the thesis.

I am also appreciative for the assistance given to me by the technical staff, especially Mr R. Best within the Surface Engineering Research Group.

In addition, the author is also grateful to the Engineering and Physical Sciences Research Council and British Gas for funding the research project, particularly the help given by Mr. N.Wood at British Gas.

Finally, I would like to thank my parents for their continuous support throughout my undergraduate and postgraduate days.

I hereby declare that:

during the periods I have been registered for the degree of PhD, for which the thesis is submitted, I have not been a registered candidate for any other award of a university.

and

that I have attended: selected lectures from the Integrated Graduate Diploma Scheme in Corrosion and Materials engineering; internal seminars within the Surface Engineering Research Group of University of Northumbria; annual symposia of the Institute of Corrosion; presented papers at selected conferences in the UK and abroad within the field of high temperature wear; and followed the course of guided reading laid down by my supervisors.

ABSTRACT

THE EFFECT OF THE COUNTERFACE ON THE WEAR RESISTANCE OF CERTAIN ALLOYS AT ROOM TEMPERATURE AND 750°C

by

Philip D. Wood

The overall aim of this research was to investigate the room temperature and high temperature wear of a group of alloys, Ma956, PM2000, PM2000SD, TiAl, Nimonic 90 and Nimonic 80A (cast and HIPped), selected to portray candidate engine valve materials, when in contact with different counterfaces (Incoloy 800, Stellite 6 and Si_3N_4). The counterfaces were chosen to represent seat insert materials. Wear testing was conducted on a specially constructed reciprocating wear rig designed to simulate valve seat/seat insert wear. The test conditions included: 7N load, rotation speed of 12.5m/min, 3 reciprocation cycles per minute and temperatures of 21°C and 750°C. Testing was carried out in a laboratory air environment for 4 hours.

The counterface was seen to have a major effect on the wear resistance of the alloys. The process of wear at room temperature was associated with the transfer of counterface material to the alloy surface. The degree of such transfer was dependant on the hardness of the counterface. No glaze formation occurred at room temperature.

At 750°C, the type of counterface influenced the formation of oxidised wear-resistant plateaux ('glazes'). Glaze formation resulted in low friction and low weight losses. Preoxidation improved the wear resistance of the ODS alloys worn against Incoloy 800 at 750°C by forming a wear-protective oxide film on the surface of the alloy, though it did not encourage the formation of glazes. Temperature, however, did have a major influence on glaze formation on Ma956 when worn against Stellite 6. The mechanism of glaze formation involved transfer of material, oxidation, mixing, fracture, agglomeration and compaction.

CHAPTER 1

INTRODUCTION

1. INTRODUCTION

Significant efforts are now being made to develop a new type of engine. These engines operate at higher efficiency rates compared to conventional engines making energy savings of around 36%. The engines also experience different internal environmental conditions to traditional diesel and gasoline engines as shown in ***Table 1.1***.

Table 1.1 Summary of environmental factors found in different engines [1-5]

Valve	Condition	Engine Type		
		Gasoline	Diesel	New engine
Inlet	Max. temp. Pressure Deposits	350-500°C 60-80 MPa Fuel-derived deposits (not corrosive)	350°C-500°C >100 MPa Fuel-derived deposits (corrosive)	400°C-550°C <60 MPa No deposits
Exhaust	Max. temp Pressure Deposits	600-750°C 60-80 MPa Lead deposits on valve seat (lubrication)	450-600°C > 100 MPa Fuel-derived deposits (very corrosive)	650-850°C <60 MPa No deposits

One of the problems in producing such high efficiency engines is the occurrence of high temperature corrosion and wear of the engine valves. A particular problem exists where the engine valve contacts the engine block at valve seat face/ seat insert interface (see **Fig.1.1**).

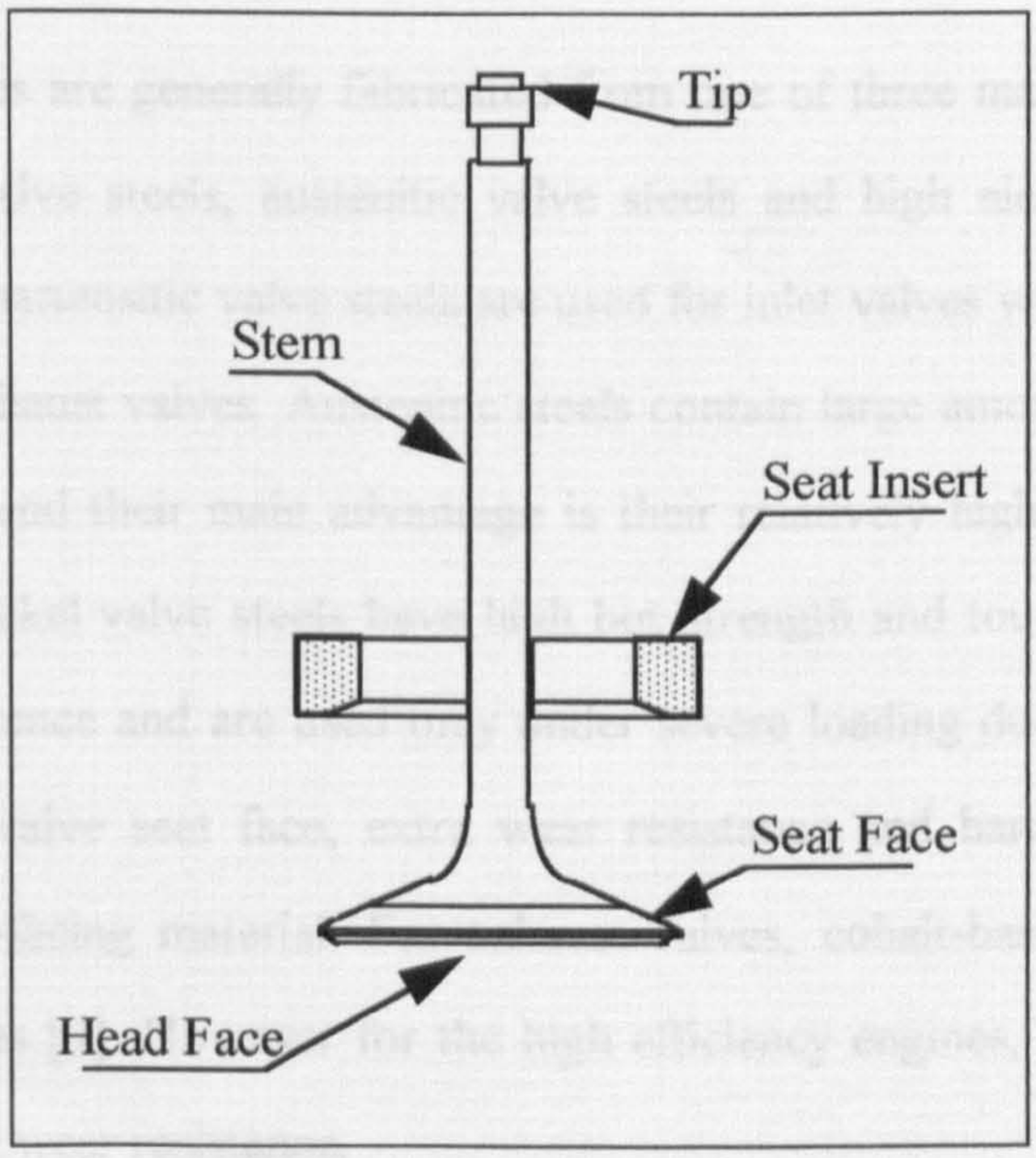

Fig.1.1 Nomenclature of the valve and seat insert

At the valve seat face/seat insert interface, temperatures can reach up to 750°C for the high efficiency engines, though lower temperatures are experienced for diesel and gasoline engines. Contact pressures are also high and values as high as 100 MPa have been recorded for diesel engines. This causes high temperature adhesive and abrasive wear of the valve face and seat insert. Wear of the valve seat face can lead to the formation of small pits which, after a while, may join together to form channels [6-7]. These channels reduce the gas sealing ability of the valve and allow hot gases to escape from the combustion chamber. This causes rapid temperature rises of the valve seat face (200-300°C) leading to severe high temperature wear and corrosion.

In gasoline engines running on leaded fuels, lead compounds deposit on the valve seat face which act as a lubricant resulting in reduced wear. In the high efficiency engines, lead additives are not present and protective deposits do not form on the valve seat face, thereby leading to higher wear rates.

Existing valves are generally fabricated from one of three materials [8]. These are ferritic martensitic valve steels, austenitic valve steels and high nickel valve steels (see ***Table 1.2***). Ferritic martensitic valve steels are used for inlet valves which operate at lower temperatures than exhaust valves. Austenitic steels contain large amounts of chromium for oxidation resistance and their main advantage is their relatively high strength at elevated temperature. High nickel valve steels have high hot strength and toughness in addition to good oxidation resistance and are used only under severe loading due their high cost (see ***Table 1.3***). At the valve seat face, extra wear resistance and hardness is provided by coating with a hard-facing material. For exhaust valves, cobalt-base materials are used known as the Stellites [9]. However for the high efficiency engines, existing materials do not provide sufficient wear resistance.

Table 1.2 Composition of existing valve materials and hard-facing alloys [8]

Valve material	Composition (%wt)							
	C	Si	Mn	Cr	Ni	Co	Fe	Others
X45CrSi93 ferritic-martensitic	0.45	3.0	<0.8	9.0	<0.5	-	bal.	-
21-4N austenitic	0.56	<0.2	9.0	21.0	3.9	-	bal.	N 0.4
Nimonic 80A high nickel	0.10	0.25	1.0	20.5	bal.	1.0	2.0	Ti 2.4 Al 1.3
Stellite 6	1.1	1.0	-	28.0	3.0	bal.	3.0	W 4.5

Table 1.3 Properties of some existing valve materials [8]

Valve Material	0.2%proof stress (Nmm^{-2}) at 700°C	Rupture strength 1000h (Nmm^{-2}) at 650°C
X45 CrSi 93 ferritic-martensitic	80	40
21-4N austenitic	250	200
Nimonic 80A high-nickel	750	500

High temperature wear is a complex phenomenon and is accompanied by oxidation. The complexity arises because of the conjoint action of wear and oxidation. High temperature wear involves several processes - material loss due to wear between two bodies, physical transfer of materials between the bodies, oxidation of the participating materials, diffusional transport of cations and oxygen, formation and breakdown of scales and generation of wear particles and their participation in the subsequent process. All these processes are influenced by temperature, load and speed which produce deformation and fracture.

This project is concerned with the study of room temperature and high temperature wear behaviour of a number of potential exhaust valve materials - titanium aluminides, oxide dispersion strengthened (ODS) alloys, and Nimonics, wearing against a number of different seat insert materials (Incoloy 800, Stellite 6 and Si_3N_4). The materials were selected on the basis of their mechanical properties and oxidation resistance.

Engine testing is very expensive and therefore it's often necessary to find other methods to simulate the conditions experienced by an engine valve. Studies [10-11] have

shown that a major failure of engine valves in related high efficiency engines is valve seat face/seat insert wear and therefore it is necessary to concentrate on wear of the materials. Hence, a reciprocating rotating wear rig was used for the testing. In this rig the sample (valve material) was reciprocated against a rotating wheel (seat insert) which was all confined in a furnace. The main wear process using this rig has shown to be adhesive wear.

During adhesive wear, a commonly observed phenomenon is a change from severe to mild wear with sliding time. This, particularly at elevated temperature, has been attributed to the formation of oxides. Stott et al. [12] have suggested these oxides are formed from wear debris which have been comminuted, agglomerated and finally compacted onto the wear surface. Under certain conditions a thin, physically homogenous surface layer forms on top consisting of fine crystalline oxide particles typically 10-50 nm in diameter. This layer is often referred to as a 'glaze'.

The speed of glaze formation increases with temperature and therefore oxidation has a very important role in wear particularly at elevated temperature. Studies [13-15] have been conducted to encourage the formation of glazes through preoxidation. A preoxidised layer should either provide a substrate for the glaze to form on or supply wear debris from which glazes may also form. Stott and Mitchell [13] observed that glaze formation occurred almost immediately when samples were preoxidised. However, investigators including Sullivan and Granville [14] stated that preoxidation alone had no effect on the reduction of the wear rate i.e. the formation of glazes.

A number of models and equations [16-23] have been put forward to estimate wear rates in a system. In all of the equations, either the parameters are very difficult to measure experimentally and/or the equation can only be used under very specific conditions i.e. similar loading, temperature, counterface etc. The most frequently stated wear equation is that suggested by Archard [24]:

$$V = \frac{k.L.S}{3H} \qquad \{1.1\}$$

V = Wear volume

k = Wear Coefficient

L = Load

S = Sliding Distance

H = Hardness of the wearing surface

Even this simplified equation does not correlate to a number of experimental findings. For example according to the equation wear volume should be inversely proportional to the hardness. However, studies [25] have not found a correlation between hardness and wear rates of different groups of alloys. In addition the hardness used for this equation is room temperature hardness whereas the wearing surface will be at elevated temperature. Therefore the hot hardness of the material would be more applicable. Wear can never be correlated to one particular factor but must be seen as a complex mechanism involving a number of different interactions which are affected by numerous external factors i.e. temperature, load, sliding speed, sample geometry etc. and internal factors such as material properties. Therefore, there are in fact so many variables that it is difficult to see wear equations being able to predict wear rates in different systems. In this investigation work has concentrated on working out the mechanisms of wear against different counterfaces and not on wear modelling in which a numerical equation is formed.

The overall aims of the investigation were to investigate the room temperature and high temperature wear properties of a group of ODS alloys, two Nimonics, and a titanium aluminide wearing against three different counterfaces in terms of weight change, scale morphology, phase type and distribution of elements and to establish the mechanism responsible for the degradation of these materials. In detail the purpose was to:

- Investigate the effect on the formation of wear protective oxides of:
  - increasing the temperature
  - preoxidising the samples

- using different counterfaces

- Derive mechanisms for the high temperature wear of Ma956 and Nimonic 90 when worn against various counterfaces.
- Assess the effect of different processing methods on wear resistance.
- Evaluate the effect of hardness on the wear resistance.

The thesis is presented in seven chapters. Chapter 2 critically reviews existing wear theories and observations particularly concentrating on high temperature wear. The rationale for this research programme and the details of the experimental aspects are presented in Chapter 3 and Chapter 4 respectively. The experimental results obtained are outlined in Chapter 5 and discussed in Chapter 6, while Chapter 7 comprises the main conclusions derived from the present research and lists possible future work.

CHAPTER 2

LITERATURE REVIEW

2. LITERATURE REVIEW

This Chapter provides a critical review of available literature pertaining to wear and the various factors that influence it. The aim is to provide a context for the present project and a framework to facilitate interpretation of the results in the study. There are four main sections in this chapter: the first section gives a brief review of classifications of wear; the second section deals with the theories of wear; whilst the third and fourth sections contain information on the factors affecting wear behaviour and features of ceramic/metal sliding.

2.1 Introduction to Wear

Wear can be defined as the removal of material from two interacting surfaces. This is a complex process consisting of many different mechanisms. The main variables which affect the degree and type of wear can be divided into two groups:-

(1) external factors - e.g. speed, load speed, temperature and environment.

(2) internal factors - material properties such as hot hardness, crystal structure and microstructure.

2.2 Classification and Mechanisms of Wear

Archard and Hurst [26] originally classified the sliding wear of metals and alloys into two main categories - mild and severe wear. Severe wear is characterised by large metallic debris particles (10μm to 1mm) and usually occurs in the early stages of wear. Mild wear is characterised by small debris particles size (0.01-1.0μm); smooth wear surfaces and high contact resistance occurring in the later stages of wear. Mild wear is associated with the development of oxides on the wearing metallic surfaces and is also known as "oxidational wear ".

Subsequently other classifications emerged [27] involving four main groups:

- adhesive wear;

- abrasive wear;
- fatigue wear; and
- combined types
    - (a) fretting
    - (b) corrosive wear.

2.2.1 Adhesive Wear

When two surfaces are in contact, they touch only at a small number of asperities. Consequently, the apparent area of contact appears much larger than the true contact area. The asperities support the full load of the two surfaces and are therefore under great stress. This causes the asperities to plastically deform increasing the true contact area. This continues until mechanical equilibrium is reached and the force of the applied load W is balanced by the strength of the supporting area. The mechanical equilibrium can be expressed by:

$$a = \frac{W}{\sigma_y} \qquad \{2.1\}$$

where W = applied load

a = true area of contact

σ_y = compressive yield stress of the softer surface.

For a number of materials the yield stress is directly proportional to the hardness:

$$\sigma_y = \frac{H}{3} \qquad \{2.2\}$$

By combining equations {2.1} and {2.2} the true area of contact can be expressed by :

$$a = \frac{3W}{H} \qquad \{2.3\}$$

A simple model of adhesive wear was first suggested by Archard [24]. In the model it is assumed that the wear particles are geometrically similar and that the wear volume (V) is both proportional to the real areas of contact (a) and to the sliding distance (L).

Therefore :

$$V \propto a \times L \qquad \{2.4\}$$

Combining equations {2.3} and {2.4} leads to the expression

$$V = K\frac{WL}{H} \qquad \{2.5\}$$

This is known as the Archard wear equation. K is dimensionless and is defined as the probability of each asperity interaction resulting in the production of a wear particle. From the equation it can be seen that wear volume should increase linearly with an increase in load or an increase in sliding distance. The equation also shows that wear volume is inversely proportional to the hardness.

The Archard equation is an over simplification but the complexity of wear processes have prevented the development of a more sophisticated equation. For example, investigations [25] have not shown a correlation between room temperature hardness and wear volume. This is hardly suprising as the asperities will be at an elevated temperature and will not have the same hardness as at room temperature. However, the equation does allow the severity of wear to be compared using the wear coefficient, K. Some values for K are listed in ***Table 2.1*** for dry sliding in pin-on-ring tests for a range of materials at room temperature against tool steel.

Ploughing occurs when a wear particle cannot be clearly seen at the interface between the material and the counterface. Only a shallow groove is formed plastically on the material. Ploughing occurs when the adhesion at the interface is weak and the penetration of an abrasive asperity is relatively small.

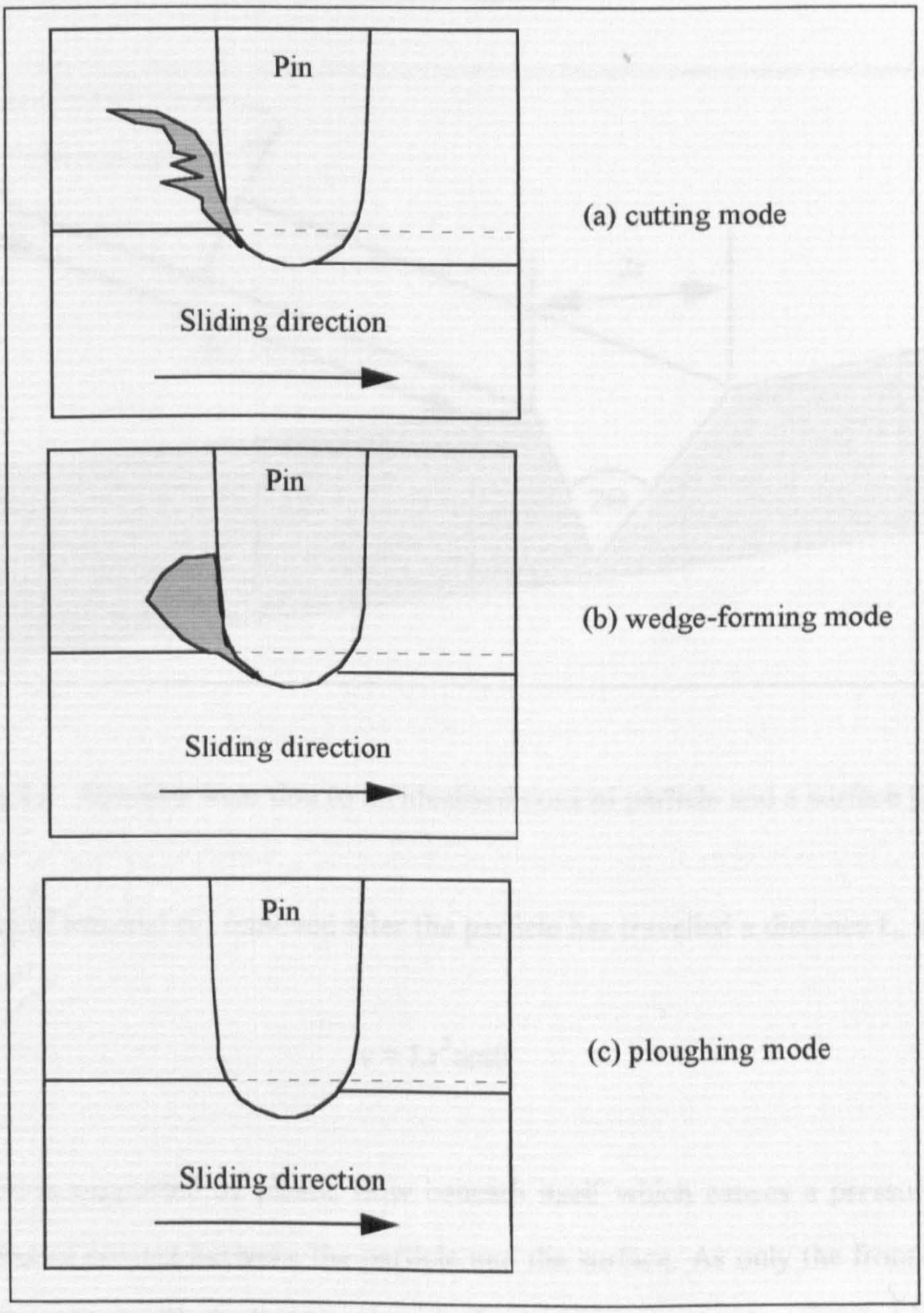

Fig.2.1 Schematic of three abrasive modes: (a) cutting mode, (b) wedge forming and (c) ploughing mode [29]

Abrasive wear normally involves both plastic flow and brittle fracture, though in some cases plastic flow can occur alone. Simple models have been developed to describe abrasive wear [30].

In the plastic flow model the idealised abrasive particle is a cone of semiangle θ, traversing a surface of a ductile material (see **Fig.2.2**).

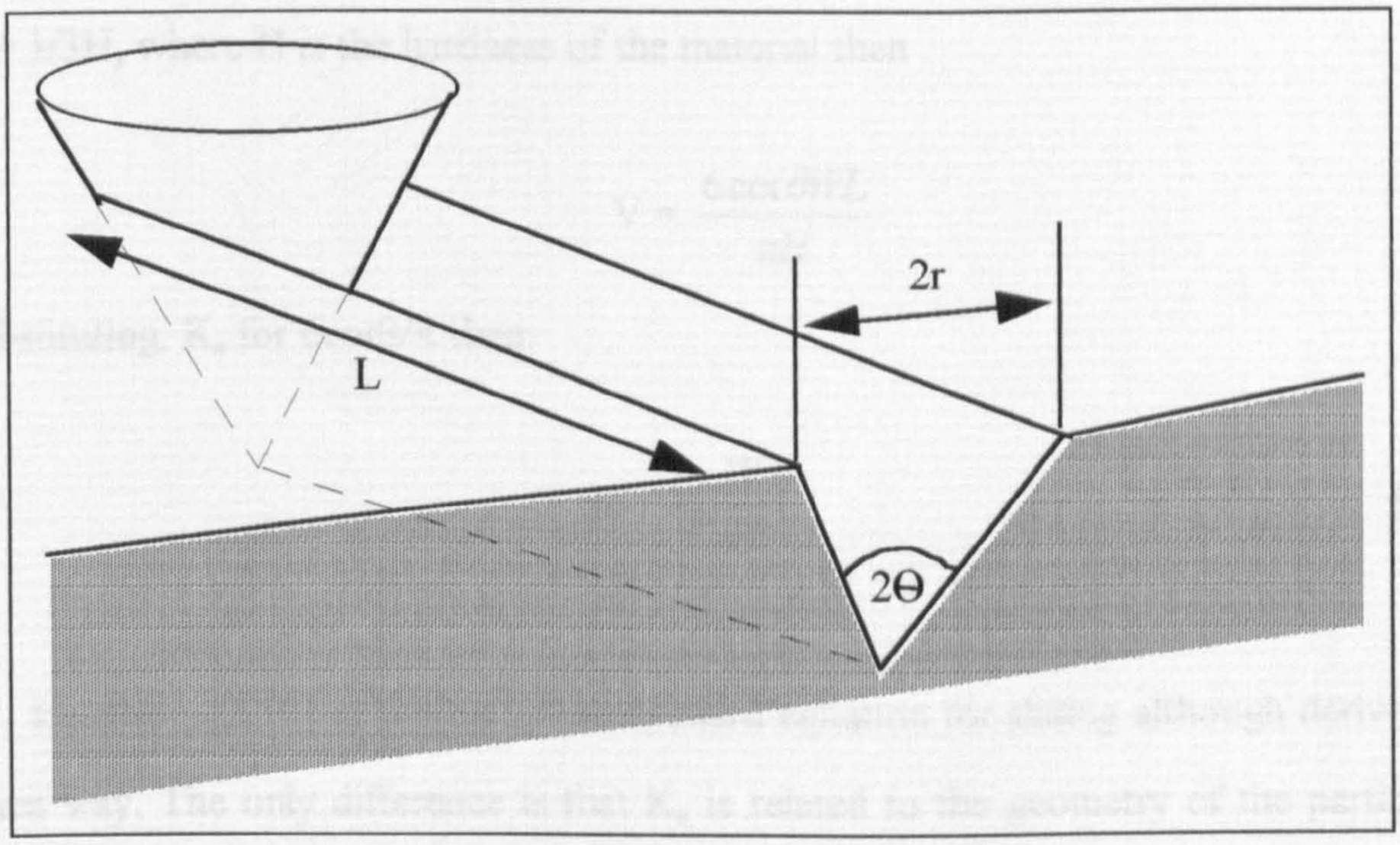

Fig.2.2 Abrasive wear due to an idealised conical particle and a surface [30]

The volume of material (v) removed after the particle has travelled a distance L, is

$$v = Lr^2\cot\theta \qquad \{2.6\}$$

The particle is supported by plastic flow beneath itself which causes a pressure P to act over the area of contact between the particle and the surface. As only the front half of the particle is in contact with the front surface the load (W) carried by the particle is:

$$W = P\frac{\pi r^2}{2} \qquad \{2.7\}$$

Combining equations {2.6} and {2.7} for n number particles, then

$$V = \frac{2\cot\theta WL}{\pi P} \qquad \{2.8\}$$

As P = 1/3H, where H is the hardness of the material then

$$V = \frac{6\cot\theta WL}{\pi H} \qquad \{2.9\}$$

By substituting, K_a for $6\cot\theta/\pi$ then:

$$V = K_a\frac{W}{H}L \qquad \{2.10\}$$

Equation {2.10} is similar to the Archard equation for sliding although derived in a different way. The only difference is that K_a is related to the geometry of the particles as described by the angle θ. The problem with the model is that brittle fracture is ignored which is commonly observed in combination with plastic flow during abrasive wear. Typical values of K for two body abrasion of metals lie between $\sim 5x10^{-3}$ and $\sim 50x10^{-3}$.

2.2.3 Fatigue Wear

Wear by fatigue occurs when the surface of a material is repeatedly stressed, due to cyclic loading. The stresses induced in the substrate, as a result, lead to the nucleation and subsequent propagation of subsurface cracks to the surface leading to large scale surface damage and pitting. Fatigue failure can therefore occur at loads much lower than those expected to produce failure in a single load application. **Fig.2.3** shows a plot of stress

against the number of cycles to failure N indicating that the lower the applied cyclical stress the longer the life of the material before failure occurs.

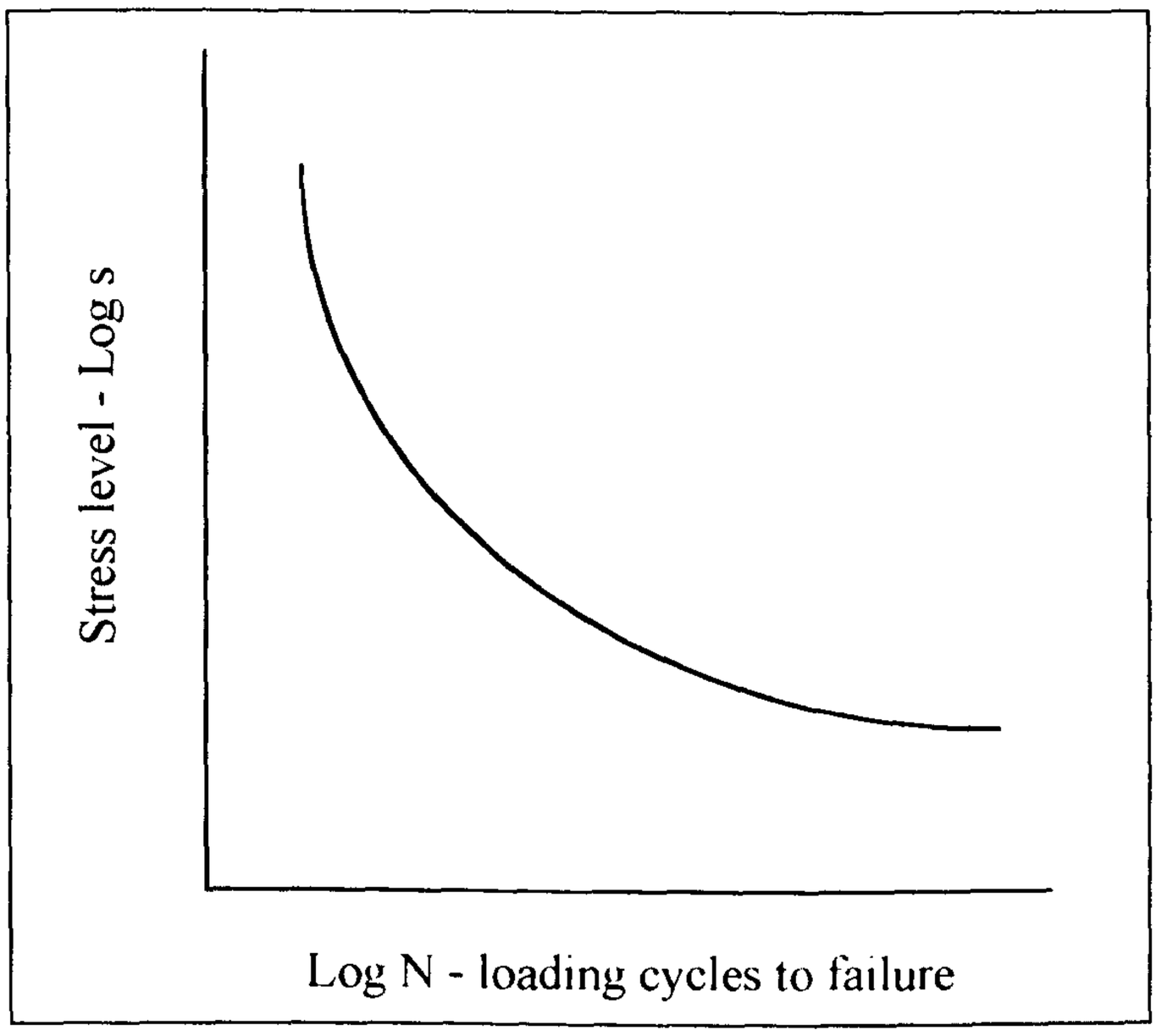

Fig.2.3 Plot of stress against the number of cycles to failure, N

Fatigue wear is a particular problem during rolling contact when material is compressed at the front of the contact zone and is then released as the element rolls forward. The maximum stress of a rolling contact occurs just below the surface initiating fatigue failure. This leads to cracks below the surface which propagate to eventually form large debris particles.

2.2.4 Combined Wear Types

It is often observed that wear involves more than one process. These processes combine to produce further unique wear processes such as fretting and corrosive wear.

(a) Fretting Fretting wear occurs when contacting surfaces slide in an oscillation motion of relatively small amplitude, often micrometres. Under these conditions of reciprocating

sliding, the oxide wear particles become trapped between the sliding surfaces, thereby inducing severe stresses within the substrates. In addition, the oxide particles can act as a third body cutting agent producing abrasion of the surfaces. The wear debris produced comprises of finely oxidised particles which often flow out of the contact area.

(b) Corrosive Wear In a gaseous or liquid environment the products of corrosion form a film on the interacting surfaces of the sliding members, which appreciably reduce the corrosion rate. This film may be partially or wholly removed due to the action of sliding resulting in the exposure of the bare metal and allowing further corrosion. This mechanism of repeated removal and formation of the film is known as corrosive wear.

2.3 Theories of Wear

2.3.1 Room Temperature

The *delamination theory of wear* was proposed by Suh [22]. The theory is based on dislocation theory and the plastic deformation and fracture of metals near the surface. According to the theory during sliding, material within a small surface layer at the wearing surface does not attain a high dislocation density because of the action of the image forces (acting parallel to the surface) which tend to eliminate dislocation. The image force itself arises because of the presence of a stress-free surface. This creates a near-surface zone of low dislocation density capable of undergoing relatively large amounts of plastic deformation without appreciable work-hardening. With continued sliding the dislocations pile up at and beneath a critical distance from the surface. This leads to the formation of voids. With further sliding, the voids coalesce either by the growth or by the shearing of connecting matrix material. This results in the generation of a crack parallel to the wearing interface at or near a certain critical depth. When this crack reaches a certain critical length, the material between the crack plane and the surface shears creating plate-like wear particles.

Suh derived an expression for the total wear volume (V) of a hard surface sliding against a soft surface. The following assumptions were made:

(a) metals wear layer by layer, each layer comprising N wear sheets (particles);

(b) the number of wear sheets per layer (N) is proportional to the number of asperities in contact, at any one time, between the contacting surfaces; and

(c) the rate of void and crack nucleation can be expressed in terms of a critical distance parameter, S_o, where S_o is defined as the interfacial sliding distance required for the complete removal of one layer of N wear sheets.

Using these assumptions, the total volume of wear of a soft surface sliding on a hard counterface is given by:

$$V = N_1\left(\frac{S}{So_1}\right)A_1h_1 + N_2\left(\frac{S}{So_2}\right)A_2h_2 \qquad \{2.11\}$$

A = average area of the delaminated sheet

h = thickness of the sheet

S = total distance slid

N = number of wear sheets in material removed

So = critical sliding distance required to remove a complete layer of material

Subscripts = denotes soft and hard materials 1 or 2

The delamination theory provides an insight into factors controlling wear behaviour and establishes a link between wear observations and microstructure. However, it contains constants such as S_o which are difficult to establish empirically and hence render the wear equation of little practical use, other than as a guide to the material wear behaviour.

In later work by Rigney and Glaeser [31], it was suggested that the plate-like wear debris sometimes observed were due to a change in the microstructure of the material in the highly deformed surface region (see **Fig.2.4**).

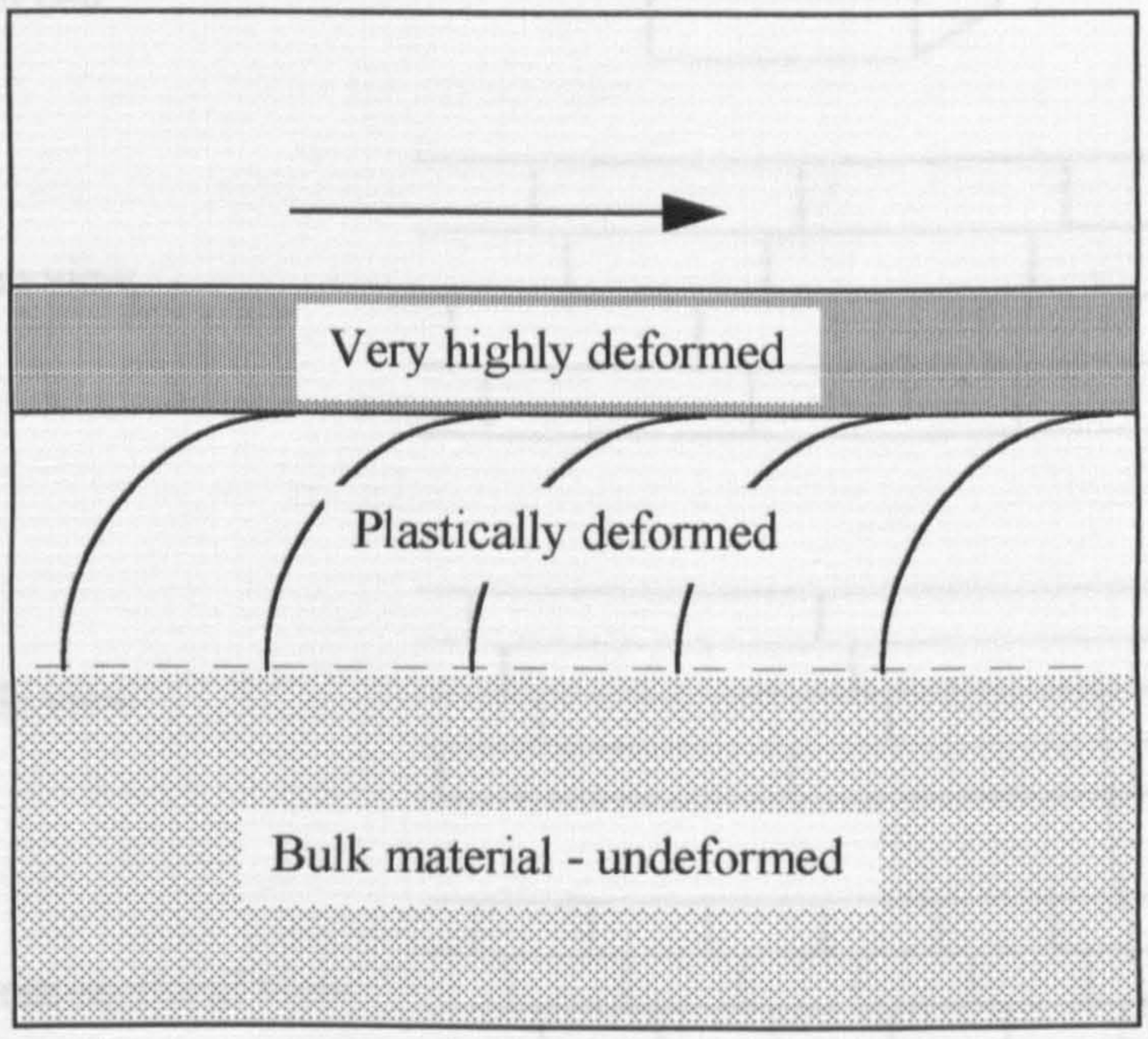

Fig.2.4 Longitudinal section of a wear specimen: the curved lines indicate strain and the arrow indicates the sliding direction [31]

According to the theory, during sliding, repeated ploughing of the asperity contacts over a counterface surface can produce high dislocation densities, changing the microstructure to a cell-type structure (see **Fig.2.5**). The cell sizes depend on material characteristics such as the applied stress, stacking fault energy and temperature. This cell structure is capable of accommodating large strains in the sliding direction. Subsurface cracks can therefore form at the cell boundaries eventually leading to production of the flake-like wear debris.

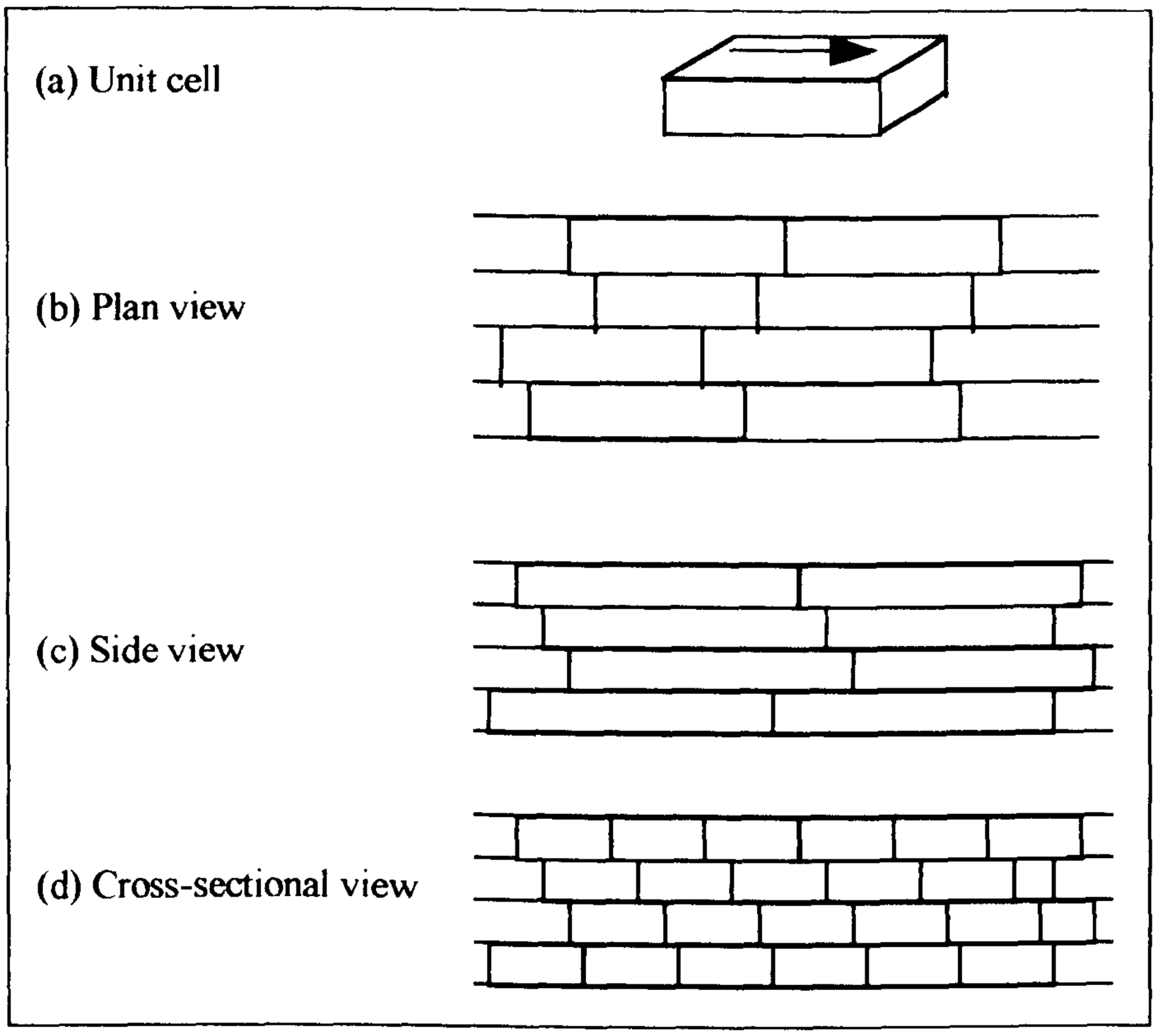

Fig.2.5 Idealised cell microstructure after wear. The arrow indicates the direction of sliding [31]

Under steady state conditions the average cell structure at a given distance from the surface remains constant, and the average thickness *t* of the cell region is a constant which depends on material properties and experimental conditions.

However, Rigney and Glaeser analysed the cell structure only through TEM and it is unclear if the cell structure is formed only from the substrate or from material transfer from the counterface.

2.3.2 Elevated Temperature

It has been observed that for many alloys, at a critical load or critical speed, the friction and wear rates decrease especially at elevated temperature. These observations are thought to be related to the presence of oxide films that form on the surface [32-33].

During sliding, interactions between asperities result in the development of junctions . If the asperities are metallic, these junctions can grow significantly, resulting in relatively high coefficients of friction while subsequent wear can be substantial (see **Fig.2.6**). However, with oxide asperities, the junctions grow relatively little before failure occurs resulting in lower coefficients of friction and wear rates (see **Fig.2.7**). The termination of junction growth occurs when the contact area has increased to such an extent that the reduced pressure over the points of contact results in the oxide reverting to its brittle nature. Thus, under high contact pressures, small cracks, which cause a reduction in the effective shear strength of the oxide, are partially healed. However, as junction growth proceeds, and the contact pressure is reduced, such cracks enlarge and act more effectively as stress-raisers, leading to a reduction in the shear strength of the oxide and ultimately brittle failure of the junctions.

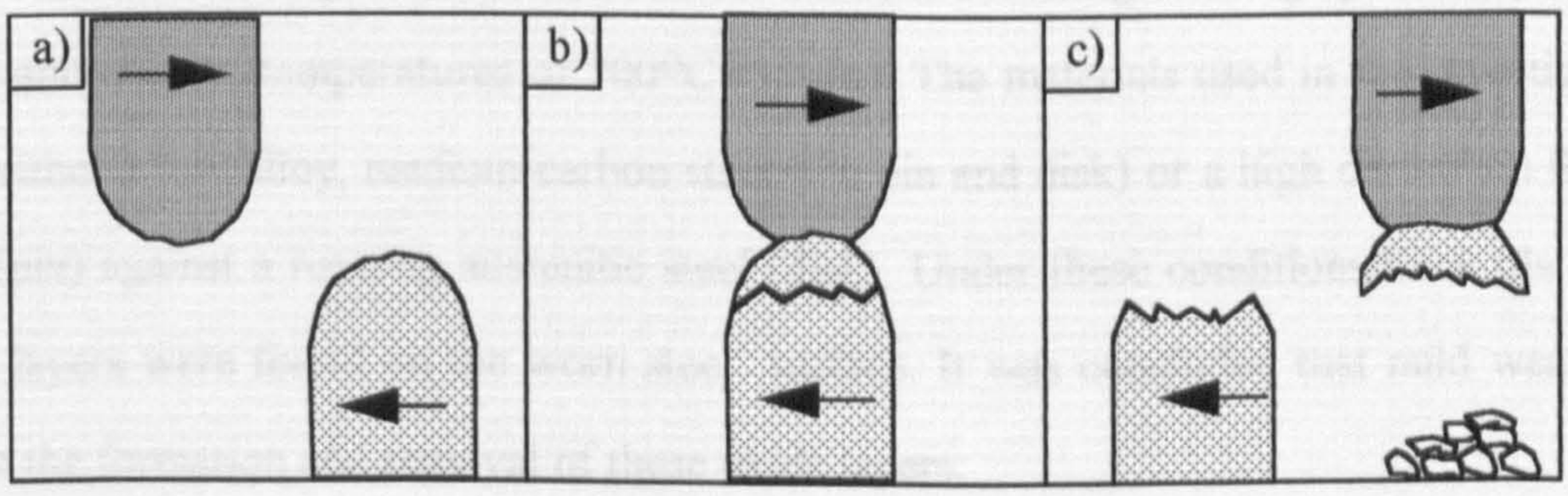

Fig.2.6 Stages of metallic adhesion between asperities leading to material transfer and high wear rates

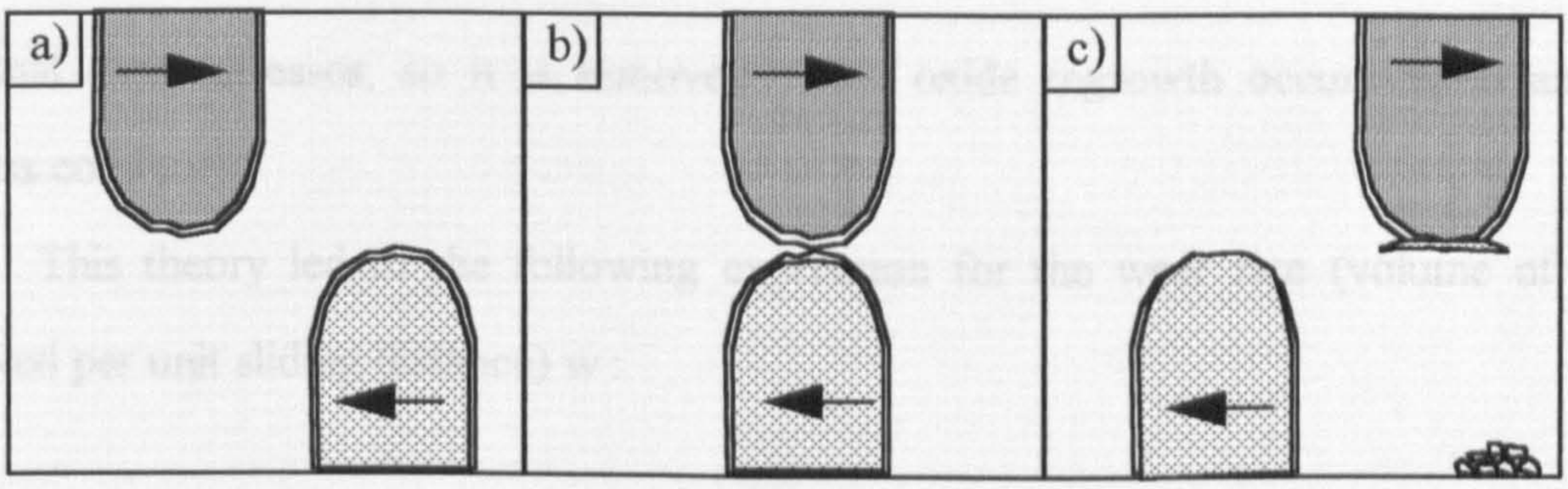

Fig.2.7 Stages of metallic oxide adhesion leading to small material transfer and low wear rates

The behaviour of oxide films during mild wear has been studied by a number of authors [12,18-19]. It has been observed that the wear rate is related to the growth of the oxide film which is strongly influenced by temperature. However, it is not known whether the controlling temperature is the brief "flash temperature" which exists during the short period of asperity contact or the bulk temperatures which occurs for much longer periods between contacts. The estimates of the flash temperatures have ranged between 250-600°C to greater than 900°C [34].

Quinns investigations of mild wear were carried at high sliding speeds (up to 3.3 ms^{-1}) and contact temperatures of 700°C [35-36]. The materials used in the investigation were either a low-alloy, medium-carbon steel (the pin and disk) or a high chromium ferritic steel (pin) against a rotating austenitic steel (disk). Under these conditions thick plate-like oxide layers were found on the worn steel surface. It was concluded that mild wear was due to the formation and removal of these oxide layers.

During the initial period of wear, the oxide films found on the unworn surface are destroyed and severe wear commences. This wear rate then declines drastically as a thick oxide layer is established and a state of mild wear is reached. The thick oxide forms at the contacting asperity peaks where the frictional contact temperatures are very high. When each oxide layer reaches a critical thickness it becomes too weak to withstand the load and

frictional shear stresses, so it is removed. Slow oxide regrowth occurs again and the process continues.

This theory led to the following expression for the wear rate (volume of oxide removed per unit sliding distance) w :

$$w = \left[\frac{d.A_p.e^{\left(\frac{Q_p}{R}(T_o+273)\right)}}{\xi_c^2.\rho_0^2.f^2.V} \right].A_r \qquad \{2.12\}$$

d = distance of sliding

A_p= Arrhenius constant

Q_p = activation energy

R = gas constant

ρ_o = density of oxide

f = fraction of oxide which is oxygen

V = linear sliding speed

T_o = temperature at which oxidation occurs

ξ_c = critical oxide film thickness

A_r = real area of contact.

Comparison of Oxidational Wear Equation with Experimental Data

A comparison was made between the oxidational wear equation and experimental data using the following calculations:-

(1) It was assumed that w= KA [24] and A=W/p_m [37] and therefore the gradient of a plot of w vs. W/p_m gave the experimental K-factor,

where w = wear rate

A = real area of contact

K = wear constant

W = load

p_m = hardness

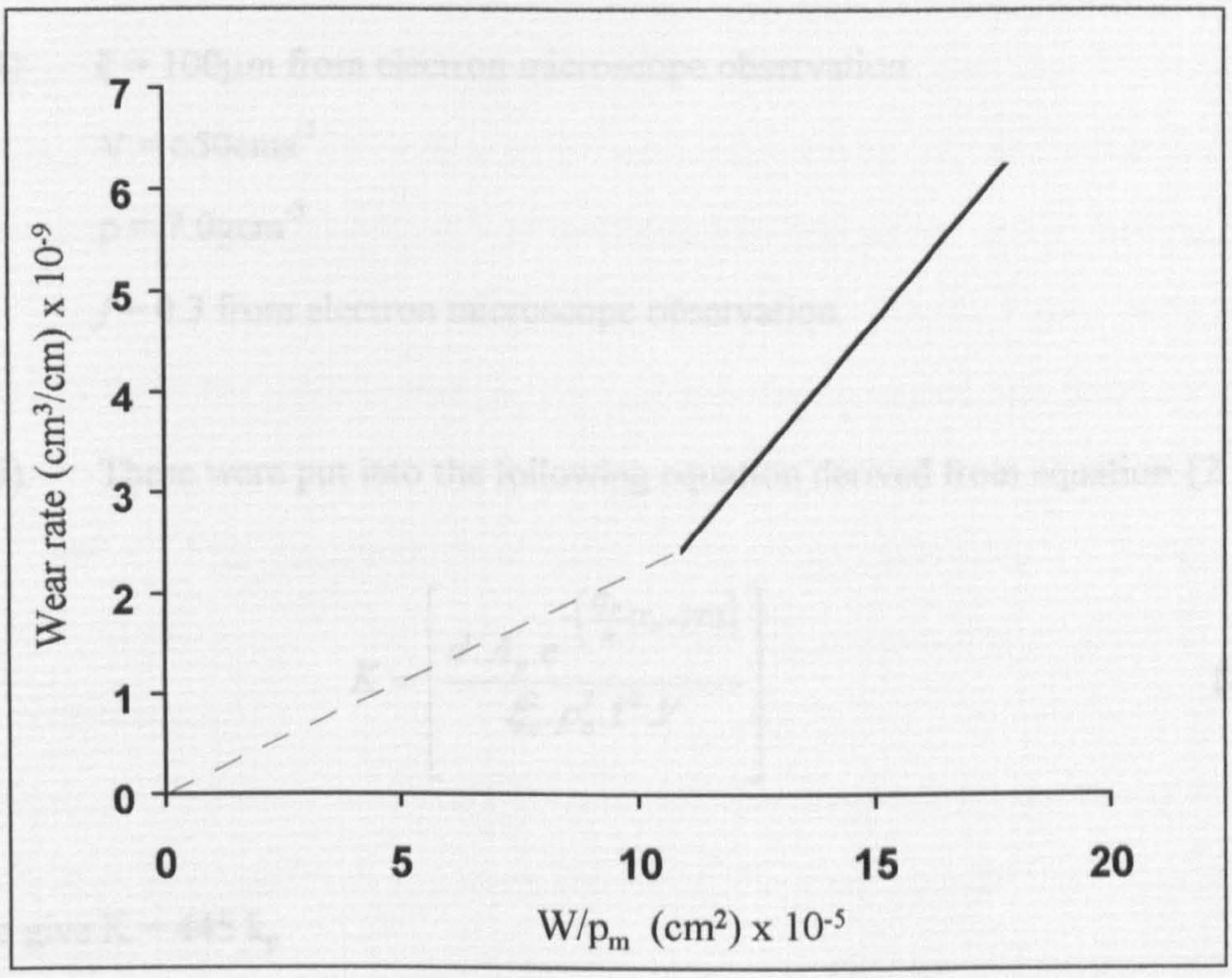

Fig.2.8 Wear rate vs. W/p_m for pin-on-disc sliding of medium carbon steel at room temperature and a sliding speed of $650 cms^{-1}$ [36]

K = gradient of line = 6×10^{-3} (above W/p_m value of 10^{-4})

The change in slope was thought to be associated with a change in oxide composition i.e. formation of Fe_3O_4 and α-Fe_2O_3 .

(2) From the graph, at $W = 2 \times 10^{-9} cm^3/cm$, $W/p_m(A) = 12 \times 10^{-5}\ cm^2$ and therefore $A = 12 \times 10^{-5}\ cm^2$

(3) As real area of contact (A) =12 x 10^{-5} cm^2 then diameter (d) of real area of contact was $1.2x10^{-2}$ cm

(4) ξ = 100μm from electron microscope observation

$V = 650cms^{-1}$

$\rho = 7.0gcm^{-3}$

$f = 0.3$ from electron microscope observation.

(5) These were put into the following equation derived from equation {2.12}:

$$K = \left[\frac{d.A_p.e^{\left(\frac{Q_P}{R}(T_o+273)\right)}}{\xi_c^2.\rho_0^2.f^2.V} \right] \qquad \{2.13\}$$

to give K = 445 k_p

(6) From a plot of log (k_p) vs ($1/T_o$) using data provided by Kubaschewski and Hopkins [38] the value of k_p implied an oxidation temperature (T_o), of about 830°C.

(7) T_a (the average surface temperature) was about 150°C for the experiment making θ_m (the excess temperature at a hot spot over the general surface temperature) to be ~ 680°C.

The value of θ_m was compared to values determined by extrapolation of Fureys measurements [39] and X-ray diffraction analysis [40] which was calculated as 350°C. The results showed a difference of about 500°C. Quinn concluded that the reason for the

difference was that the static oxidation activation energy and Arrhenius constant were different to wearing oxidation. Quinn stated that if these were calculated then the oxidational wear mechanism could be applicable. However, this is difficult to do and other parameters such as ξ_c, d, and T_o - are very difficult to determine. One interesting point concerning the equation is that values of the activation energy (Q_p) and Arrehnius constant (A_p) were calculated. Originally, it was assumed that the values of Q_p and A_p could be calculated from static oxidation results but this work showed the values for tribological wear are half those for static oxidation. For example the Q_p values calculated by Quinn for the mild wear process were $26\pm4 kJmol^{-1}$ for $100°C<T<300°C$ and about $76kJmol^{-1}$ for $300°C<T<450°C$. This compares to a static oxidation Q_p calculated at $193kJmol^{-1}$ [38] Therefore, it is easier to oxidise a wearing surface than a static one exposed to the same ambient temperature.

Stott et al. [41-44] have studied quite different wear conditions from Quinn. They have studied wear at much lower speeds ($\leq 0.02 ms^{-1}$) and have studied the effect of oxygen partial pressure and ambient temperature on wear. Selected investigations are shown in ***Table 2.2*** and the composition of the materials used are displayed in ***Table 2.3***.

Table 2.2 Summary of selected investigations and conclusions conducted by Stott et al.

Material	Test	Conclusions	Ref
Like-on-like sliding of Nimonic 75, Nimonic C263, Nimonic 108 and Incoloy 901	Reciprocator Load = 15N Speed = 0.021ms^{-1} Temp. = 150-800°C	Clearly defined temperature/time when a reduction in the friction and wear rate occurs (see **Fig.2.9**) This is due to the formation on a thin, physically homogeneous surface layer known as a 'glaze.'	[41]
Like-on-like sliding of Fe-12%Cr (Jethete M152 & Rex 152)	Reciprocator Load = 15N Speed = 0.02ms^{-1} Temp. = 100-400°C	Generation of wear-formed oxide due to removal of transient oxide (300-400°C) and oxidation of metallic wear debris at (100-400°C)	[42]
Like-on-like sliding of Fe-5%Cr	Reciprocator Load = 0.7N Speed = 0.002ms^{-1} Temp. = RT O_2 Pressure = 10^{-6}Pa - 1atm	Development of wear protective oxide islands increase rapidly as the oxygen partial pressure increases.	[43]
Like-on-like sliding of Ni-1%Cr to Ni-40%Cr	Reciprocator Load = 15N Speed = 0.002ms^{-1} Temp. = 20-800°C	Similar friction and wear rates decreases were observed. The transition time changed with differing chromium content. The change was associated with the formation of 'glazes'.	[44]

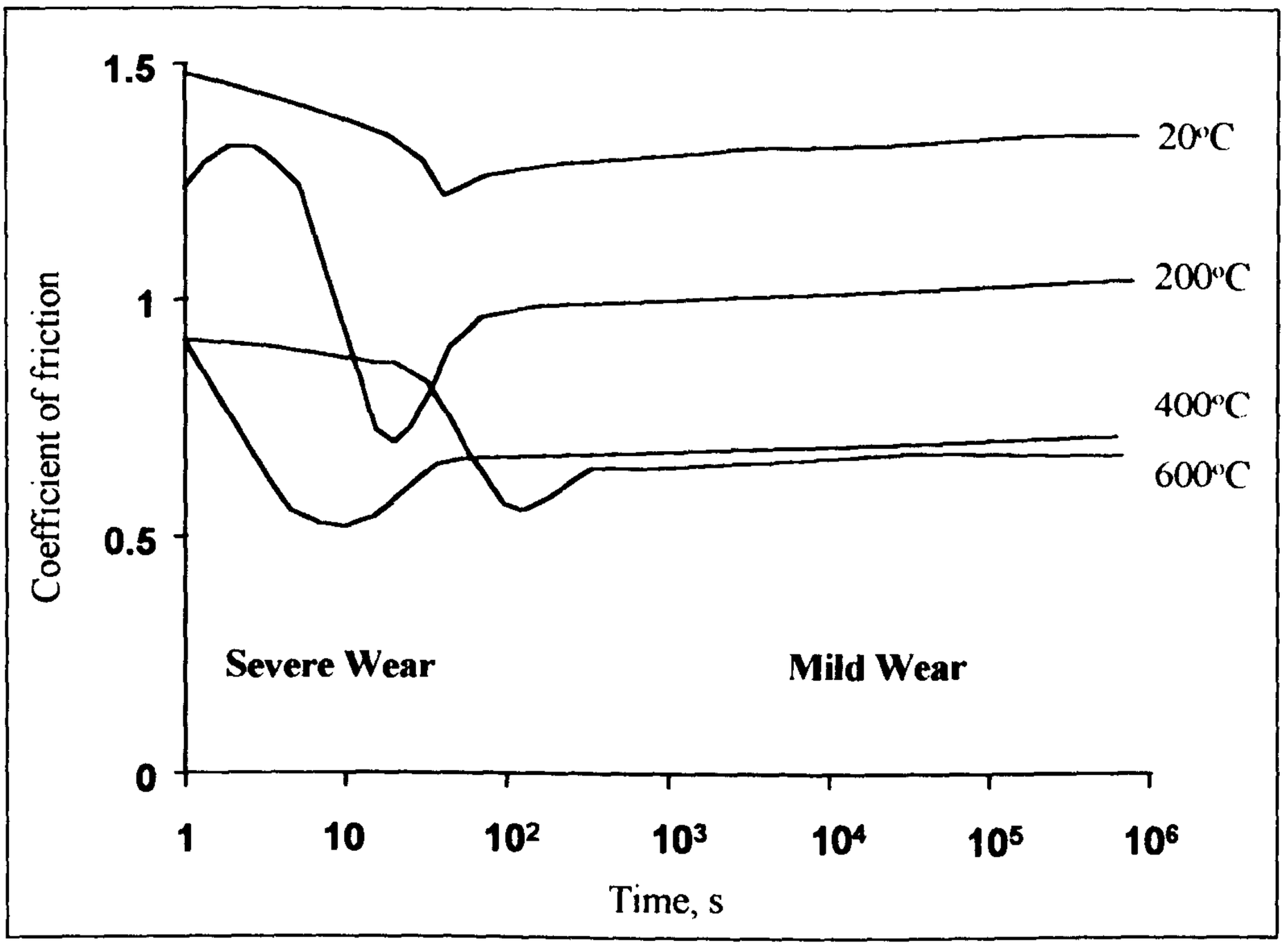

Fig.2.9 Coefficient of friction versus time plots for like-on-like sliding of C263 in air at 20° to 600°C [41]

Table 2.3 Composition of the alloys used in investigations by Lin et al. [41]

Alloy	Composition (wt.%)										
	C	Si	Cu	Fe	Mn	Cr	Ti	Al	Co	Mo	Ni
N75	0.08-0.15	≤1.0	≤0.5	≤5.0	≤1.0	18.0-21.0	0.2-0.6	-	-	-	bal.
C263	0.03	0.25	≤0.2	≤0.7	0.40	20.0	2.15	0.45	20.0	5.9	bal.
N108	≤0.2	≤1.0	≤0.5	≤2.0	≤1.0	13.5-15.7	0.9-1.5	4.5-4.9	18.0-22.0	4.5-5.5	bal.
Incoloy 901	≤0.1	≤0.6	≤0.5	bal.	≤2.0	11.0-14.0	2.3-3.0	≤0.3	-	5.0-7.0	40.0-45.0

Through these extensive investigations, Stott et al. formulated a theory to explain the observations. It was suggested that, at the start of wear, the films found on an unworn surface are progressively destroyed and a period of severe wear ensues. During this time metallic and oxide wear debris accumulates to form thick oxide layers. On top of this compacted wear debris, a thin physically homogeneous surface layer (made up of particles 10-50nm) may form known as a 'glaze'. The glaze may also be supported by an oxide film, formed prior to sliding. Once the glaze forms the wear rate and friction coefficient fall sharply and a period of mild wear follows. The glaze and the underlying oxide contained all the alloying elements, approximately in the same proportions as in the alloy, with the concentrations of the metal elements remaining fairly constant across the glaze.

The general conclusion was that the development of a 'glaze' probably involves three simultaneous stages: formation, agglomeration and compaction of wear debris. Three main processes have been suggested to be responsible for the generation of glazes [45-46]:

1. Metal debris mechanism Metallic wear debris formed in the early stages of sliding is gradually fractured and refractured exposing clean metal surfaces for further oxidation. This eventually produces a number of oxide and oxide-covered particles. Following the formation of oxide debris, a relatively weak bond develops between the debris particles causing them to adhere. Glaze formation occurs at the surface of the compacted debris where pressures are higher leading to closer packing of the particles. The pressure also leads to fragmentation of the particles until they reach such a size (10-50nm) where only plastic deformation can occur.

2. Oxidation-scrape-reoxidation mechanism Oxide may be produced by oxidation of metallic asperities in contact or by more general oxidation in the apparent area of contact. In both cases the oxide may be removed by a subsequent traverse exposing clean metal to the environment which is quickly re-oxidised. The formation of the glaze from the oxide debris follows in the same way as the metal debris mechanism.

3. Total oxide mechanism The oxide developed during sliding may only be partially removed or not at all during sliding. This would leave the remaining film to thicken slowly on subsequent traversals. If the oxide developed on the substrate is coherent and adherent and can withstand the severity of the sliding action, then a plastically deformed wear protective surface or glaze may develop.

The glaze under sliding conditions can undergo plastic flow which increases as the temperature increases. The ability of the glaze to undergo plastic flow is due to two factors. The first factor is connected with the very small size of the oxide particles that make up the glaze. The smaller the size of the particle the higher the maximum tensile strength to fracture. Therefore contacting pressures may be high enough to cause plastic deformation of the oxide particles but not to fracture them. Secondly, it has been found that brittle materials can undergo extensive plastic deformation when subjected to hydrostatic pressures. This may occur during sliding leading to plastic flow of the compacted oxides.

Glazes reduce friction and wear rates for two reasons:-

(1) When sliding occurs opposing asperities contact leading to the formation of junctions. If the asperities are metal, considerable junction growth can occur before fracture occurs leading to high friction coefficients. However, with oxide asperities, the junction growth is small before failure occurs and therefore lower friction coefficients are observed.

(2) Low wear rates are observed because any wear debris produced consists of small oxide particles which are easily compacted back onto the wear surface.

However, testing has been limited to like-on-like sliding and therefore the effects of a different material transferred from the counterface onto the wear scar have not been investigated. This may hinder glaze formation or produce glaze compositions which are very different from the substrate.

2.4 Factors Affecting Wear Behaviour

2.4.1 Hardness

According to the Archard equation [24] an increase in hardness should decrease the wear rate of a material. Generally, as the load increases, the wear rate increases rapidly as the nominal contact pressure approaches H/3, where H is the indentation hardness. Such a transition from mild to severe wear is associated with a plastic yielding of the material immediately below the asperities. Since all sliding results in a high local temperature rise in the region of contact, the hot hardness characteristics of materials are particularly significant. However, in literature a number of investigations [47-50] have compared room temperature hardness with wear resistance - this information may be misleading. Investigations [47-48] have found a correlation when using alloys within a group (see **Fig.2.10**) but in general a correlation cannot be found between the hardness and wear resistance of different groups of alloys [25]. **Fig.2.11** presents results of wear tests carried out on different groups of alloys and ***Table 2.4*** shows the composition of the alloys used.

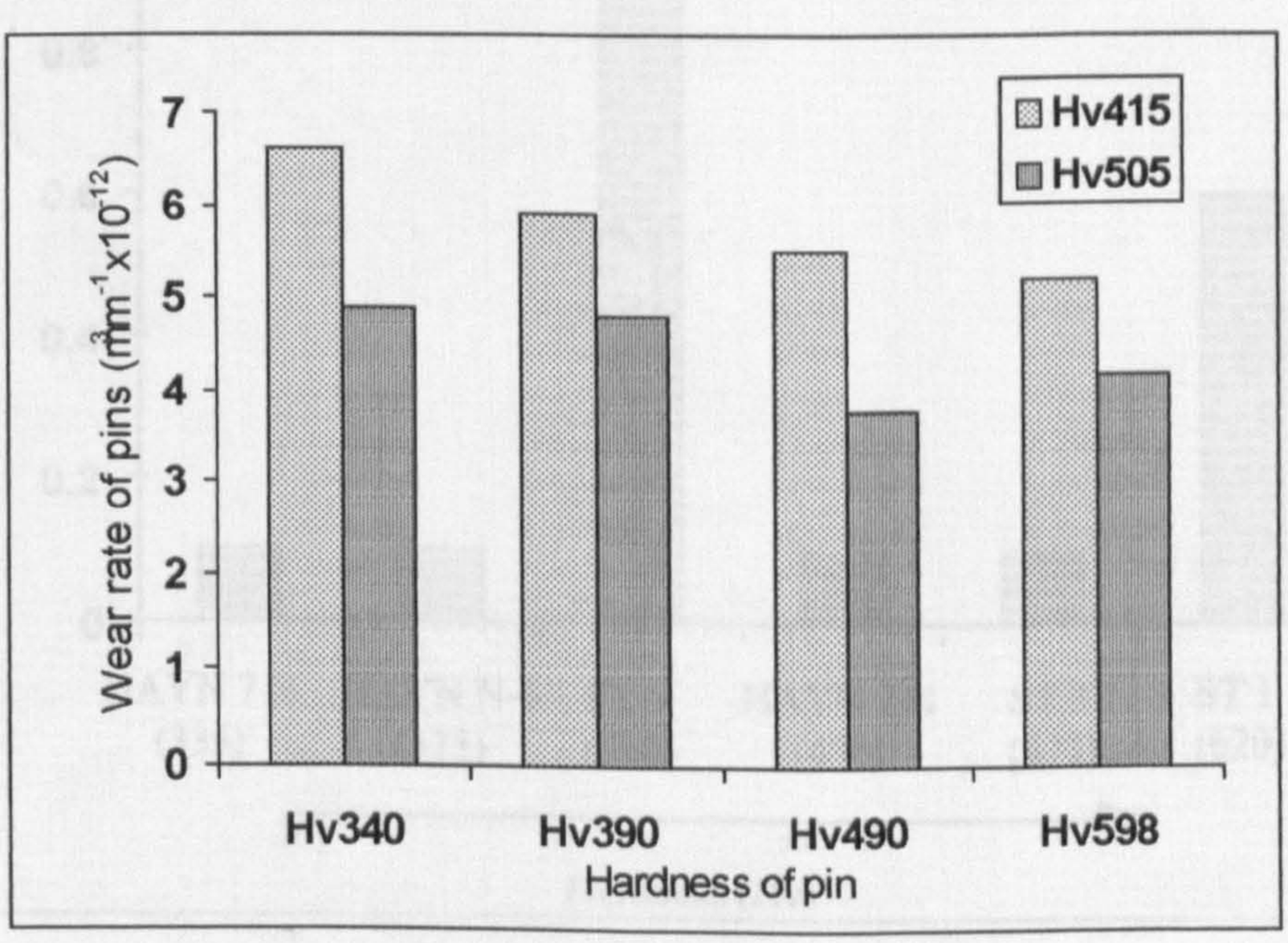

Fig.2.10 Wear rate of 1040 steel pins wearing against 4140 steel discs (load = 133N, sliding speed=1ms^{-1}) [48]

Table 2.4 Composition of alloys used for wear testing [25]

Alloy	Composition %wt								
	Cr	W	Mo	C	Si	B	Ni	Fe	Co
HAYN 716	26	3.5	3.0	1.1	1.5	0.4	23	29	12
HAYN N-6	29	2.0	4.0	1.1	1.5	0.6	bal.	-	-
ST6	28	4.0	-	1.1	1.0	-	-	-	bal.
HAYN 711	27	3.0	7.0	2.7	1.0	-	bal.	23	12
ST3	31	12.5	-	2.3	1.0	1.0	-	-	bal
ST1	30	12.0	-	2.5	1.0	-	-	-	bal

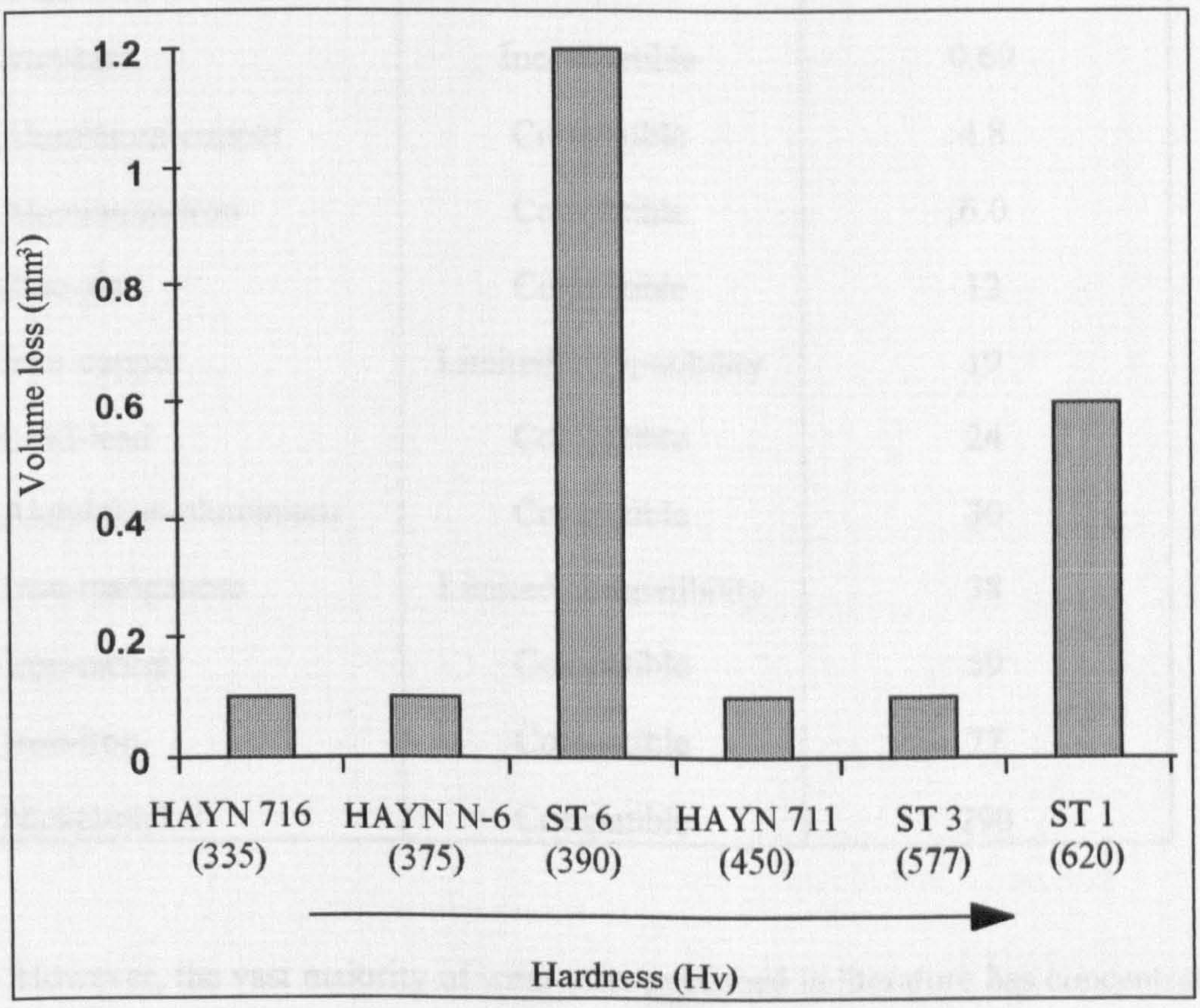

Fig.2.11 Volume loss of different alloys wearing against a carburised SAE 4620 steel, Load=410N, sliding speed = $0.15ms^{-1}$ [25]

2.4.2 Mutual Solubility

Studies [51-53] have shown that the mutual solubility, or compatibility, of materials in contact can be correlated with the wear rate. Wear is generally less where mutual solubility is low and is greatest where it is high (see ***Table 2.5***). Therefore, greatest wear occurs between identical metals in contact, where the mutual solubility is 100 per cent.

Table 2.5 Comparison of wear coefficients and compatibility ratings of metal pairs [30]

Metal Pair	Compatibility (solubility)	Wear coefficient, K $x10^{-4}$
Copper-lead	Incompatible	0.1
Iron-lead	Incompatible	0.69
Aluminium-copper	Compatible	4.8
Aluminium-iron	Compatible	6.0
Zinc-zinc	Compatible	12
Iron-copper	Limited compatibility	19
Lead-lead	Compatible	24
Aluminium-aluminium	Compatible	30
Iron-manganese	Limited compatibility	38
Iron-nickel	Compatible	59
Iron-iron	Compatible	77
Nickel-nickel	Compatible	290

However, the vast majority of wear tests published in literature has concentrated on wear testing with one counterface at room temperature and little attention has been focused on the effect of different counterfaces (different solubilities).

Subramanian [51] investigated the effects of different counterfaces on the wear of a Al-12.3Si alloy pin at room temperature (see ***Table 2.6***). Testing was conducted at room temperature using a pin-on-ring wear testing machine at loads from 4.5 to 225N and speed from 0.1 to 10 ms^{-1}. Copper was chosen as a counterface, as aluminium has a greater solubility in copper than in iron. Therefore, it was expected that a greater tendency of adhesion in aluminium/copper pairs would result in more friction and wear than in aluminium/steel pairs. In addition, copper aluminium alloys were also used as counterfaces as it was thought that copper, partially or fully saturated with aluminium, would adhere less to the aluminium alloy pin compared to a pure copper counterface.

Table 2.6 Composition and hardness of the materials used by Subramanian [51]

Counterface Material	Composition (wt%)	Hardness Hv 5kg
Copper	-	52
Cu-4.6Al	4.6 Al	76
Cu-7.5Al	7.5Al	114
Mild Steel	0.15C 0.1Si	114

The results are shown in **Fig.2.12** as a function of normalised wear rate vs. normalised pressure/normalised velocity. The following equations were used to calculate the normalised values:

Normalised pressure = F/(AH) where F = load

A = nominal area of contact

H = room temperature hardness of pin

Normalised velocity = Vr/a where V = velocity

r = radius of the pin

a = thermal diffusivity

Normalised wear rate =W/A where W= wear rate.

The results indicated that the highest wear rates of the Al-Si alloy pin were achieved with a copper disc, followed by Cu-4.5Al, mild steel with Cu-7.5Al offering the lowest wear rate. Subramaniam concluded that a counterface material which has a low solubility in Al-Si (e.g. Cu-7.5Al) results in low wear rates.

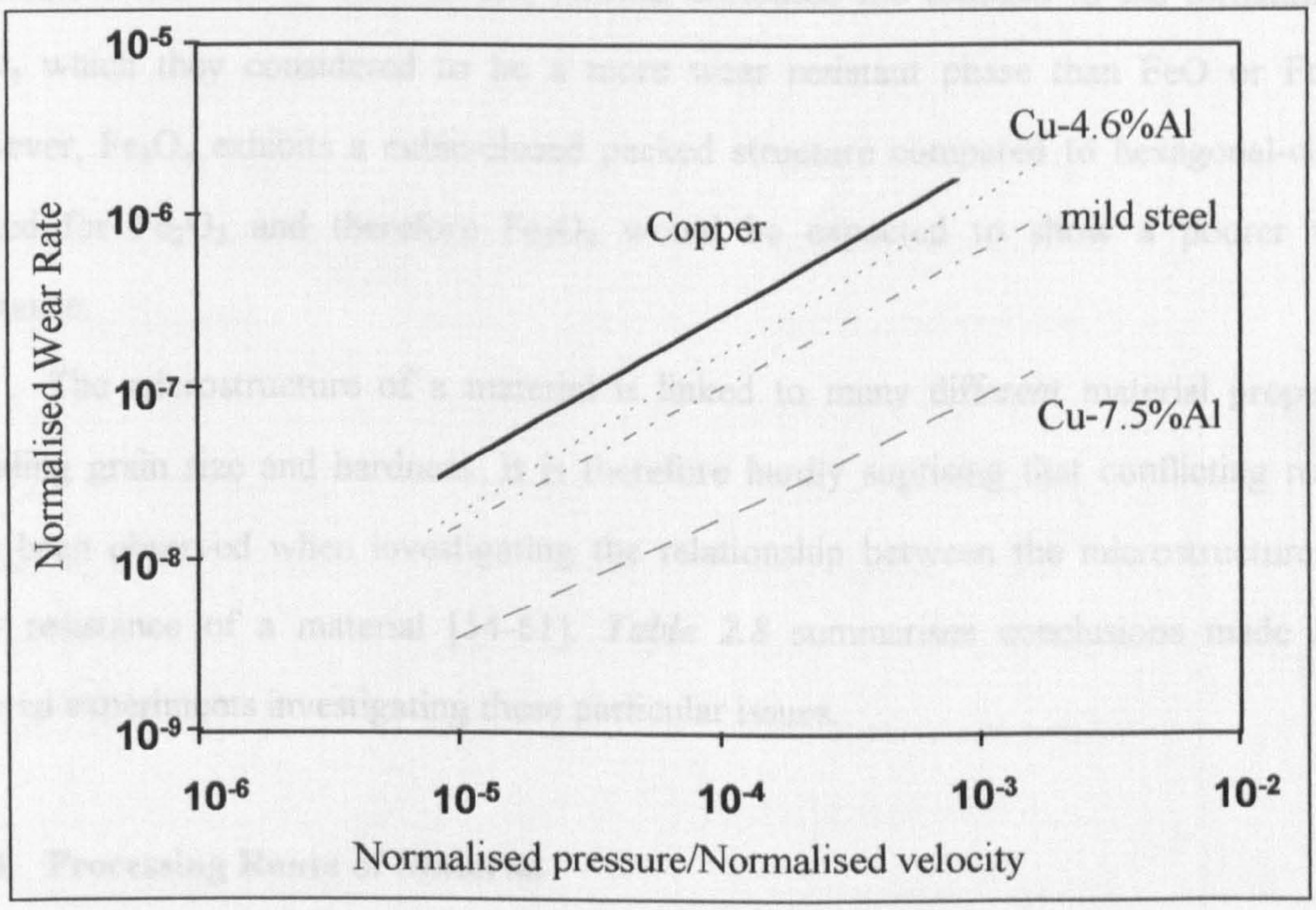

Fig.2.12 Variation of the normalised wear rates of the Al-Si alloy slid against various counterface materials [51]

2.4.3 Crystal Structure and Microstructure

The majority of metals have one of three crystal structures: body-centred cubic (bcc), face-centred cubic (fcc) or hexagonal-close packed (hcp). The hexagonal close-packed structure has the most limited deformation characteristics as it can only deform by slip along the basal plane. Since wear is associated with plastic deformation, metals which

have a hexagonal close packed structure such as cobalt generally give good wear resistance. However, above a contact temperature of 417°C the wear rate of cobalt increases one hundred-fold. This is associated with a change in crystal structure to face-centred cubic.

Sullivan and Athwal [20] observed transitions in wear rates at critical loads, during pin-on-disc wear testing of like-on-like 52100 steel (1.0%C 1.3%Cr - Fe) between room temperature and 500°C. Sullivan and Athwal attributed the changes to the formation of Fe_3O_4 which they considered to be a more wear resistant phase than FeO or Fe_2O_3. However, Fe_3O_4 exhibits a cubic-closed packed structure compared to hexagonal-closed packed for Fe_2O_3 and therefore Fe_3O_4 would be expected to show a poorer wear resistance.

The microstructure of a material is linked to many different material properties including grain size and hardness. It is therefore hardly suprising that conflicting results have been observed when investigating the relationship between the microstructure and wear resistance of a material [54-61]. ***Table 2.8*** summarises conclusions made from selected experiments investigating these particular issues.

2.4.4 Processing Route of Material

Investigations have shown that the processing route of a material can effect it's wear behaviour. Todsen [62] has compared the wear resistance of a valve steel, LV 21-43 (see ***Table 2.7***) produced in two different ways:-

Route 1: ingot casting with subsequent rolling into bars; and

Route 2: melt is atomised and the resulting powder is pressed isostatically (hot or cold) to ingots. These are deformed to valve material bars using the hot extrusion method.

From this stage the valve materials were fabricated into valves in a similar manner.

Table 2.8 Selected investigations into the effect of microstructure on wear resistance

Material	Test	Conclusions	Ref.
Range of Co-, Fe- and Ni-base alloys cast in either sand or graphite moulds (block) SAE 4620 steel (ring)	Block-on-wheel Load = 410N Speed = 0.14ms^{-1} Temp. = RT	Little effect of the microstructure on wear rates.	[47]
Like-on-like sliding of Co-Cr-Mo alloy solution treated and aged in different ways	Pin-on-disc Load = 0-63.8N Speed = 0.57ms^{-1} Temp. = RT	The presence of varying contents of carbides in the microstructure had little effect on the wear resistance.	[54]
Steel 1080 tempered and isothermalised for various times (pin) WC-8%Co (ring)	Pin-on-ring Load = 20-140N Speed = 0.6-2.0ms^{-1} Temp. = RT	Under conditions of severe wear, wear increased in the following order: spherodized carbide, martensite, bainite and lamenar pearlite.	[55]
Stellite 6 produced by chill casting and laser surface cladding (pin) WC-Co 90/10 (disc)	Pin-on-disc Load = 50N Speed = 2ms^{-1} Temp. = RT	No dependence of the wear rate on microstructure was observed.	[56]
Ductile cast iron (pin) austempered for various times Flat hardened tool steel (disc)	Pin-on-disc Load = 10.5-19.6N Speed = 1.15ms^{-1} Temp. = RT	The alloys containing the higher proportion of martensite showed the greater wear resistance.	[59]

Table 2.7 Composition of LV21-43 alloy [62]

Composition %wt							
C	Si	Mn	Cr	Ni	W	Ti	Fe
0.50	≤0.45	8.0-10.0	20.0-22.0	3.5-5.0	0.8-1.5	1.8-2.5	bal.

Testing was conducted in a rig in which the valve was subjected to thermal shock cycles whilst wearing against a seat insert (see **Fig.2.13**). The thermal shock cycles were achieved through the valve being heated in a combustion chamber (1100°C) and then cooled when it made contact with the valve seat insert.

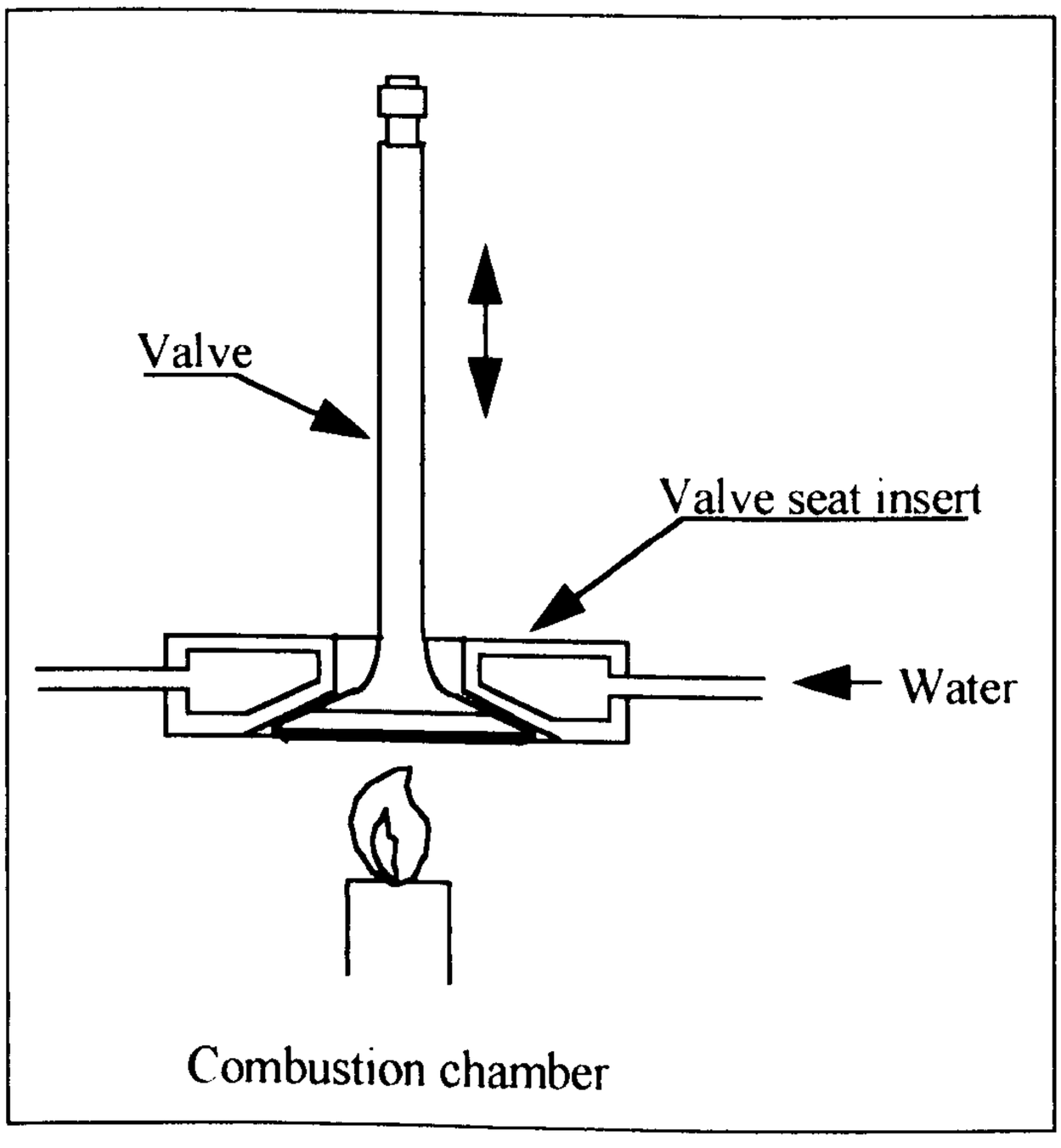

Fig.2.13 Schematic of Todsen's test rig [62]

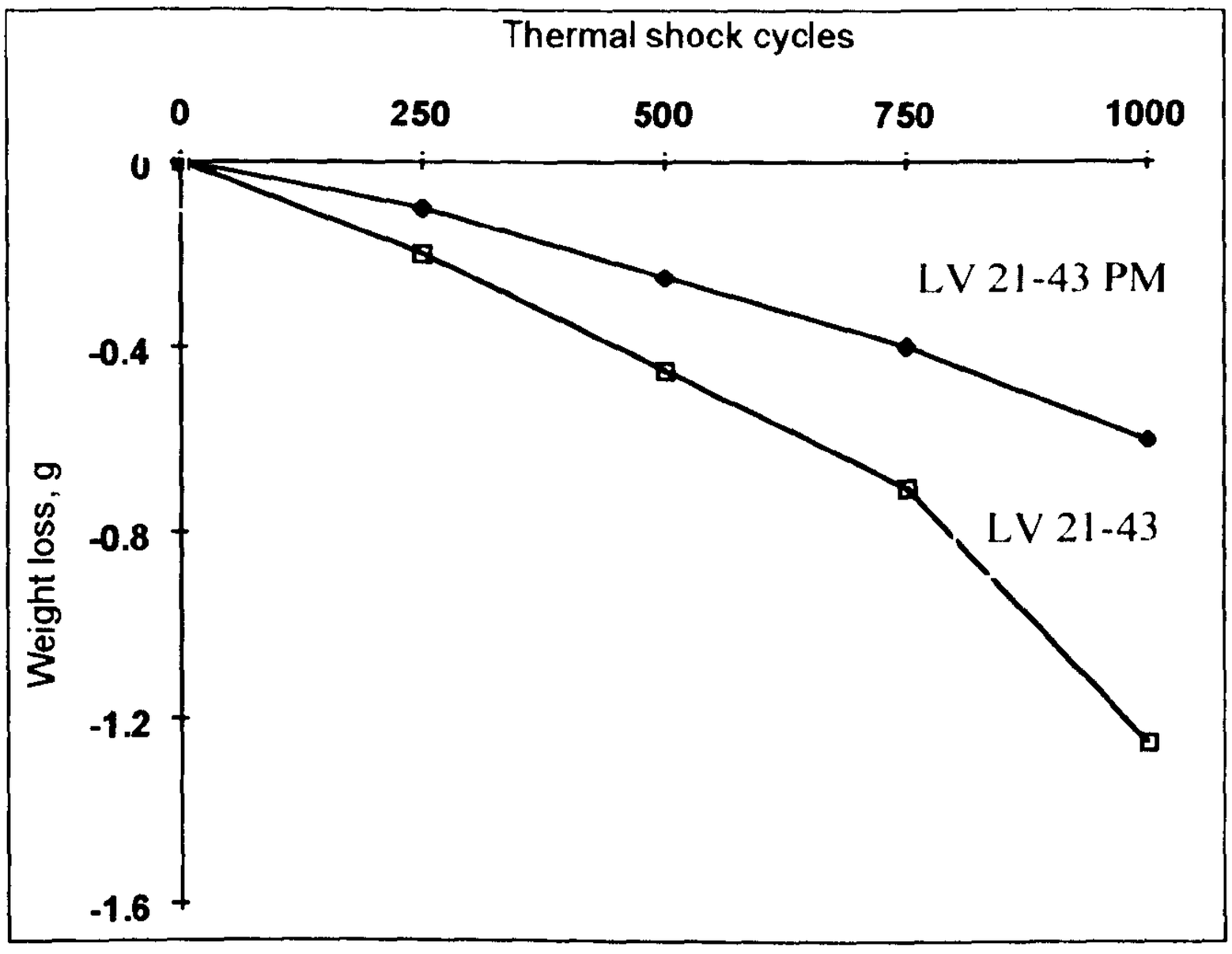

Fig.2.14 Results of Todsen's rig testing on cast and PM LV21-43 [62]

The results (see **Fig.2.14**) revealed a lower weight loss of the valve manufactured by the powder metallurgy route compared to the cast route. Todsen attributed this to the finer distribution of alloying elements in the matrix of the PM material compared to the cast material. The greater uniform distribution of the elements allowed a more homogeneous precipitation behaviour which in turn improved strength and resistance to hot corrosion.

2.4.5 Formation of Protective Oxide Films

The formation of protective oxide films is very important in the process of wear as it is often accompanied by a large drop in friction and wear rates. The formation of the oxide is itself affected by a number of different factors, viz.:

(a) Preoxidation

Attempts [13-15] have been made to pre-form oxides through preoxidation on alloys prior to sliding and thus possibly aid the development of the protective oxides. In general, mixed conclusions have been made. Stott and Mitchell [13] investigated the effect of preoxidation on the like-on-like wear of two materials, 321 stainless steel and Jethete 152 (see ***Table 2.9***). Preoxidation of 321 stainless steel was carried out in carbon dioxide containing 1% carbon monoxide and 400 to 600 ppm water vapour at 3.1 MPa pressure for 3000 hrs at 700°C. Jethete M152 specimens were preoxidised by exposure to laboratory air for 4h at 800°C. A pin-on-disc machine was used, at a load of 15 N for Jethete M152 and 16N for 321 stainless steel, to obtain the wear data.

Table 2.9 Chemical composition of 321 stainless steel and Jethete 152 [13]

Material	Chemical composition %wt						
	Cr	Ni	Mn	Si	Mo	Fe	Other
321 stainless steel	18	8.1	1.1	0.4	0.1	bal.	Ti 0.6
Jethete M152	12	2	0.6	0.3	1.6	bal.	V 0.3

The results revealed that a surface glaze was formed almost immediately on sliding preoxidised 321 stainless steel at 300°C and metal-to metal contact never occurred (see **Fig.2.15**). This resulted in less wear and a lower coefficient of friction in the first few seconds of sliding compared to the results obtained with the corresponding as-received specimens. Similar observations were reported for Jethete M152 at 300°C (see **Fig.2.16**).

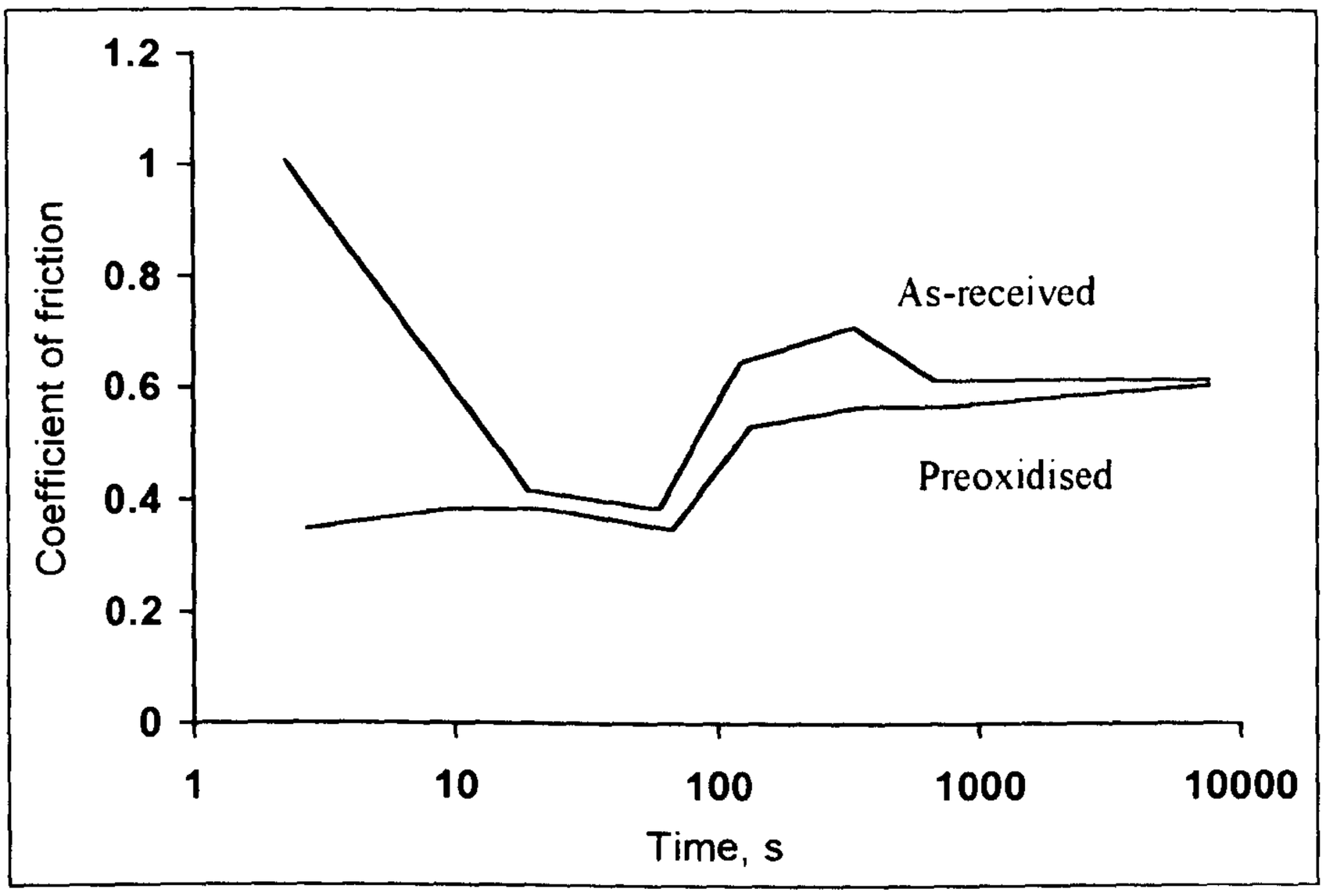

Fig.2.15 Coefficient of friction vs time plot during like-on-like sliding at 300°C for as-received and preoxidised 321 stainless steel [13]

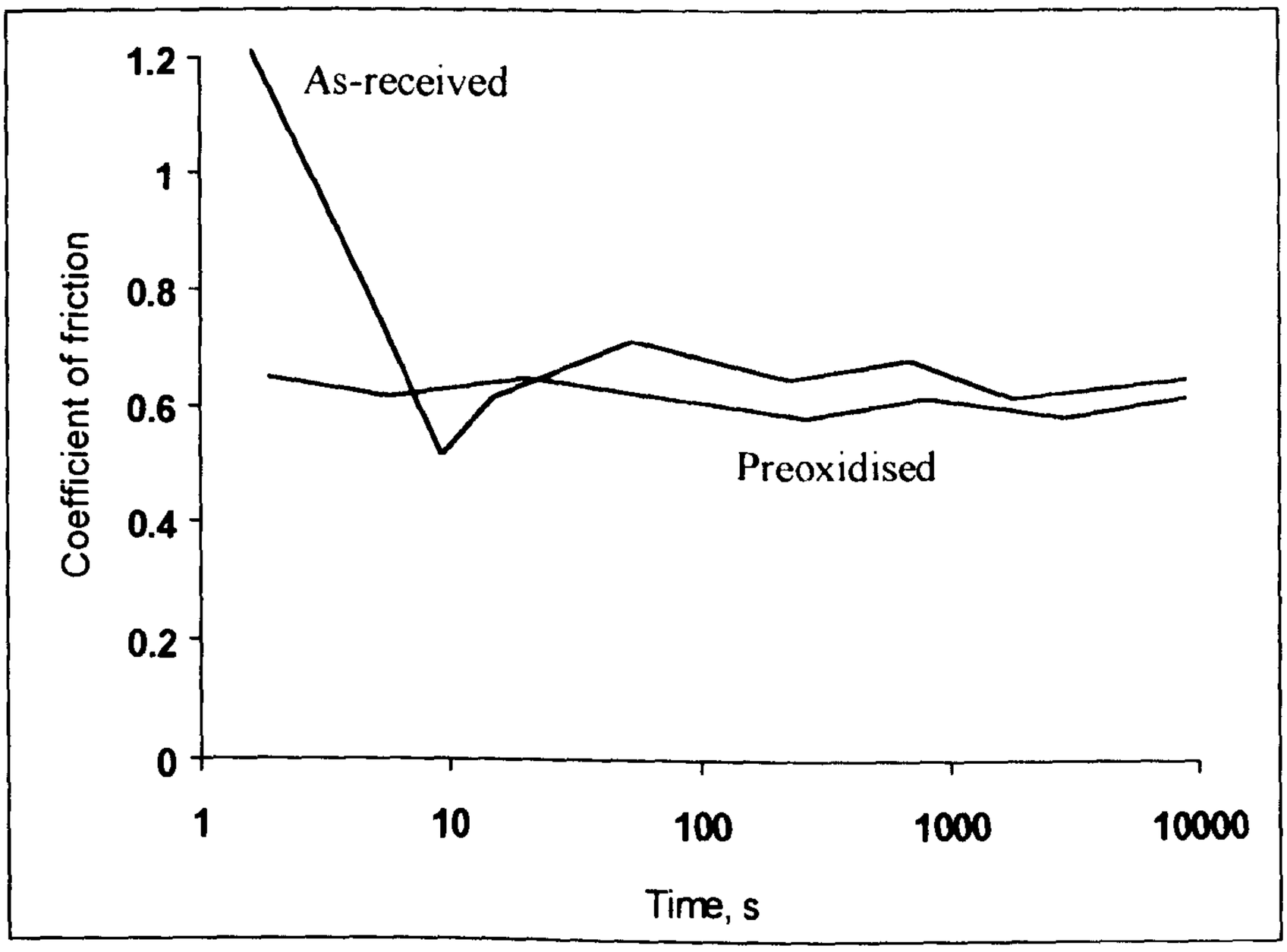

Fig.2.16 Coefficient of friction vs time plot during like-on-like sliding at 300°C for as-received and preoxidised Jethete M152 [13]

Iwabuchi et al. [14] observed similar positive effects of preoxidation. Testing was conducted using both a 0.4%C steel (S45C) and a 18%Cr-8%Ni austenitic stainless steel (SUS304) under a normal load of 39N and a mean velocity of 83.5mm/s using a flat-on-flat configuration. S45C was chosen as it was a oxidisable metal compared to SUS304 which was a oxidation resistant metal. Preoxidation of S45C was carried out at 300°C for 5 minutes, 1 hour and 3 hours in air. The results of wear testing of preoxidised S45C at 20°C indicated that preoxidation reduced the severe wear volume produced. The extent of the reduction increased with oxidation time, as shown in **Fig.2.17**. However, beyond one hour preoxidation, the reduction was constant. SUS304 stainless steel was preoxidised at 300°C for up to 10 hours. However, wear testing at 300°C revealed little beneficial effect of preoxidation. The investigators concluded that, as SUS304 was an oxidation resistant alloy, sufficient oxide to form wear resistant oxide plateaux had not formed.

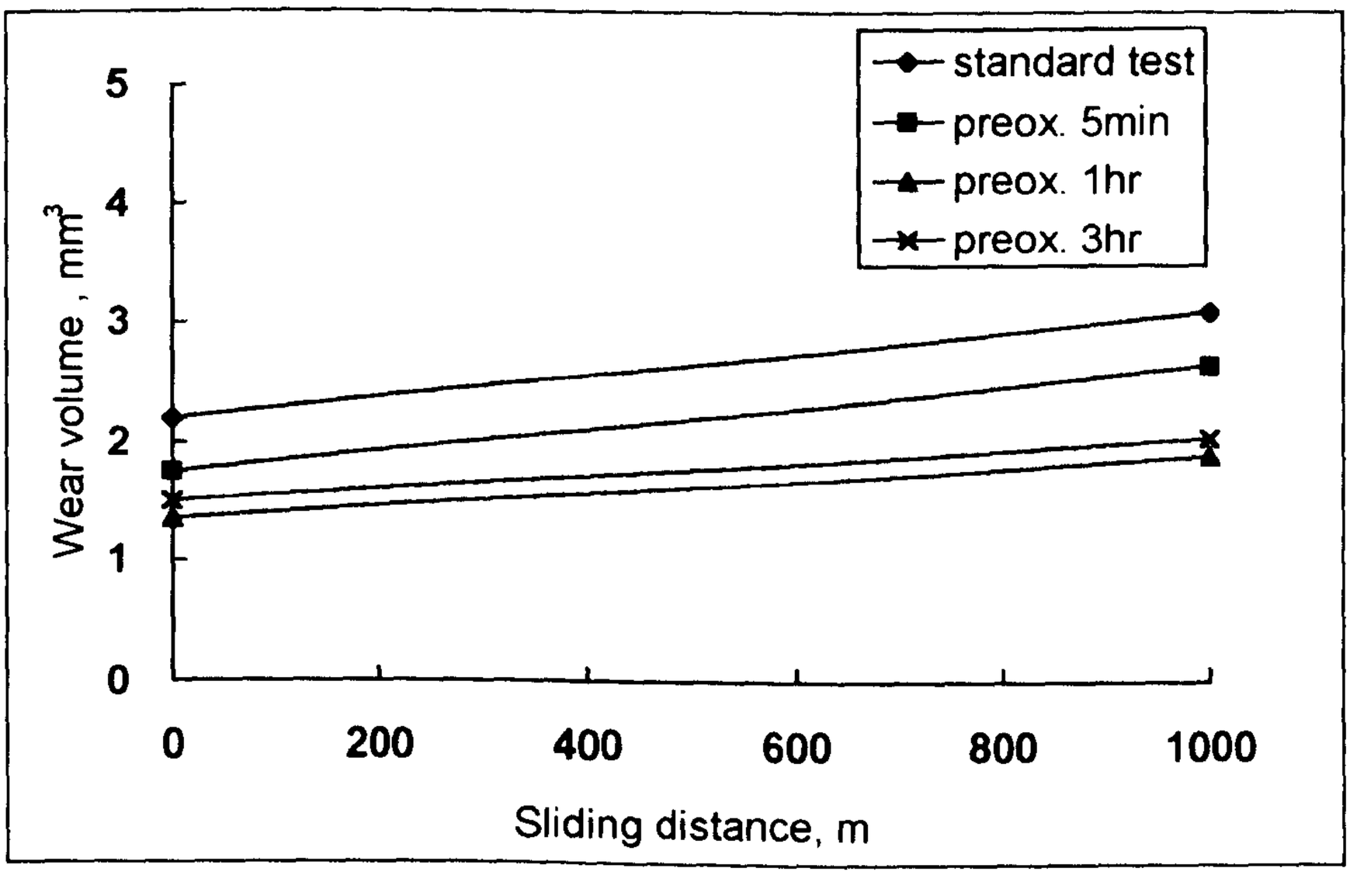

Fig.2.17 Effects of preoxidation on the wearing of S45C at 20°C [14]

One important observation that Iwabuchi et al. failed to record was the thickness of oxide films produced during preoxidation. Results indicated that beyond 1 hour's preoxidation time for S45C there was no increased reduction in wear volume and this may

have been linked to a limiting oxide film thickness. In addition it would have been useful to compare the thickness of the oxide films after preoxidation between the supposed oxidisable sample (S45C) and the oxidation resistant sample (SUS304).

Sullivan and Granville [15] however, stated that preoxidation alone had no effect on the reduction of wear rate. They conducted experiments on the initial stages of like-on-like reciprocating sliding wear of a 9% chromium steel in an environment of carbon dioxide at different temperatures, loads, dwell periods and initial sliding distances. The results are shown in ***Table 2.10***. The values in brackets are the transition distances from severe to mild wear without any dwell periods or initial sliding distances.

Table 2.10 Transition times marking severe-to-mild wear rates under different dwell periods and initial sliding distances for like-on-like sliding of a 9% chromium steel [15]

Load, N	Temperature, ^{0}C	Initial sliding distance, m	Dwell period, h	Transition distance, m
22	290	0	750	5400 (6100)
22	290	180	96	585 (6100)
41	300	180	96	960 (9000)
22	450	36	4	225 (216)

The samples preoxidised in the carbon dioxide environment for 750 hours at 290^{0}C showed no statistically significant reduction in the transition distance (5400m cf. 6100m without preoxidation). Sullivan and Granville stated that the reason for this was that a tribologically disturbed sub-surface was necessary for the formation of an oxide layer capable of giving protective regenerative properties. The absence of the hard sub-surface layer needed to support the oxide was responsible for this result.

Sullivan and Granville did observe a significant effect on wear of oxidation interspersed between sliding periods where transition sliding distances were reduced by an

order of magnitude. When the 9% chromium steel was slid for 180m at 290°C and left for 96 hours, subsequent sliding reduced the transition distance to 585m compared to 6100m without the prior sliding and dwell time. The only explanation was that the static oxidation somehow consolidated the glaze formation.

The reason for the difference in conclusions of Sullivan and Granville to other authors [13-14] could be connected with the thickness of the preoxidised film formed on the 9% Cr steel. The steel was preoxidised for 750 hours at 290°C which is a long duration and therefore a thick oxide film would be expected. However, the preoxidation was carried out in carbon dioxide and, as the oxide film thickness was not measured, this may have produced only a thin oxide film. Subsequent wear testing would have shown only a minor reduction in the severe wear period which indeed were reflected in the observed results.

(b) Partial Pressure of Oxygen

The importance of oxygen pressure on the formation of glazes has been shown by Stott and Wood [63]. Friction and wear experiments were carried out in an ultra-high vacuum apparatus at a gas pressure of 10^{-8}Pa. It was found that iron and Fe-Cr alloys containing up to 30%Cr gave coefficient of friction values between 1.5 and 3 during like-on-like sliding at 20°C. On heating the specimens, the coefficients of friction increased rapidly between 450°C and 600°C and eventually seizure occurred . When oxygen was leaked into the system and the partial pressure raised to 10^{-5} Pa, seizure still occurred for Fe-4.9%Cr when the temperature was increased to 500°C. Seizure was however prevented when the oxygen partial pressure was increased to 10^{-4} Pa even when the temperature was increased to 800°C. Further work showed that as the oxygen partial pressure was increased, glaze coverage of both wearing surfaces increased.

Stott and Wood also investigated the formation of glazes during like-on-like sliding in a pin-on-disc wear rig for a Fe-4.9% Cr alloy in oxygen partial pressures of between 10^{-6} Pa and atmospheric pressure (see **Fig.2.18-2.19**).

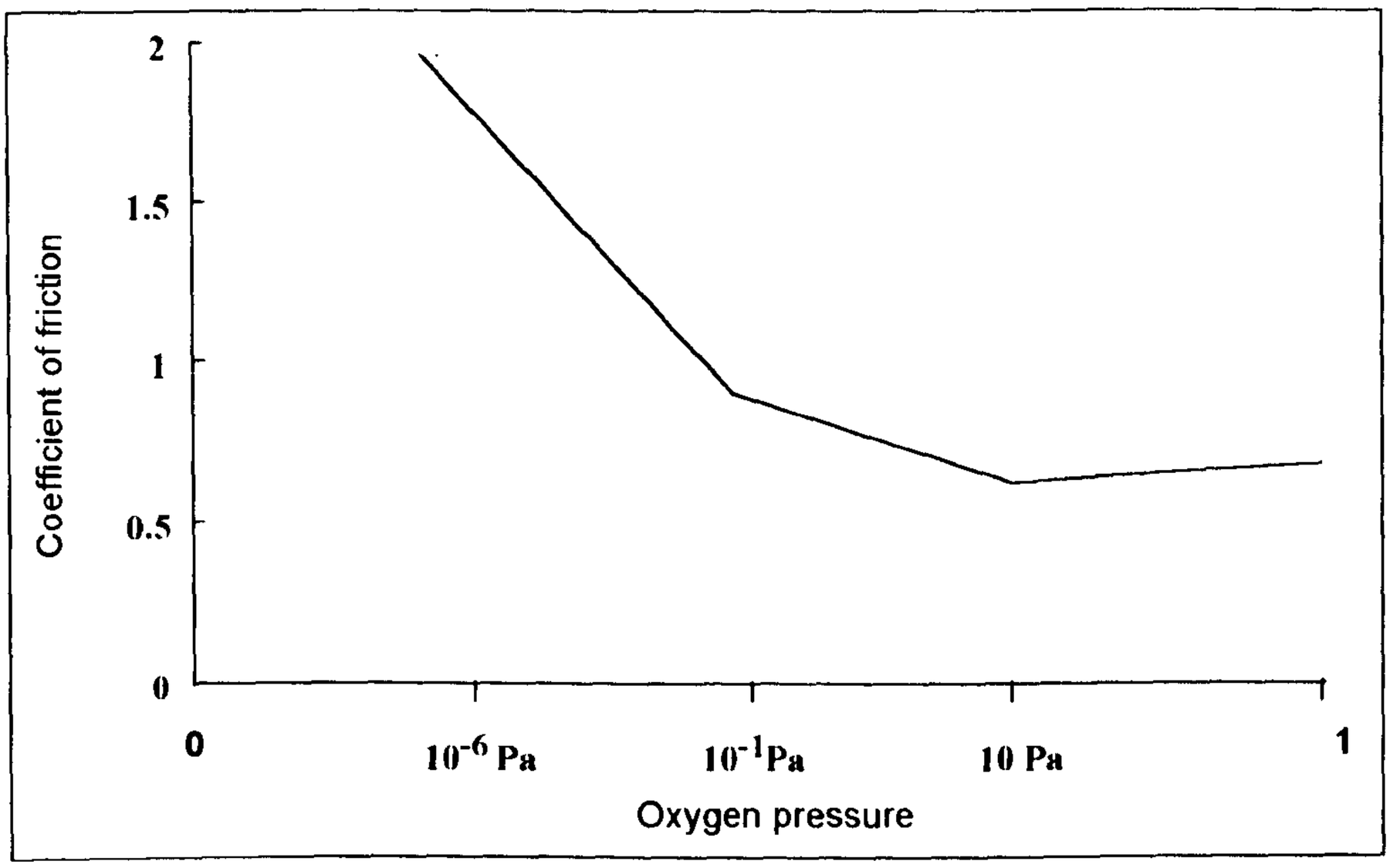

Fig.2.18 Friction coefficient of Fe-4.9%Cr during like-on-like sliding in various oxygen partial pressures at 20°C [63]

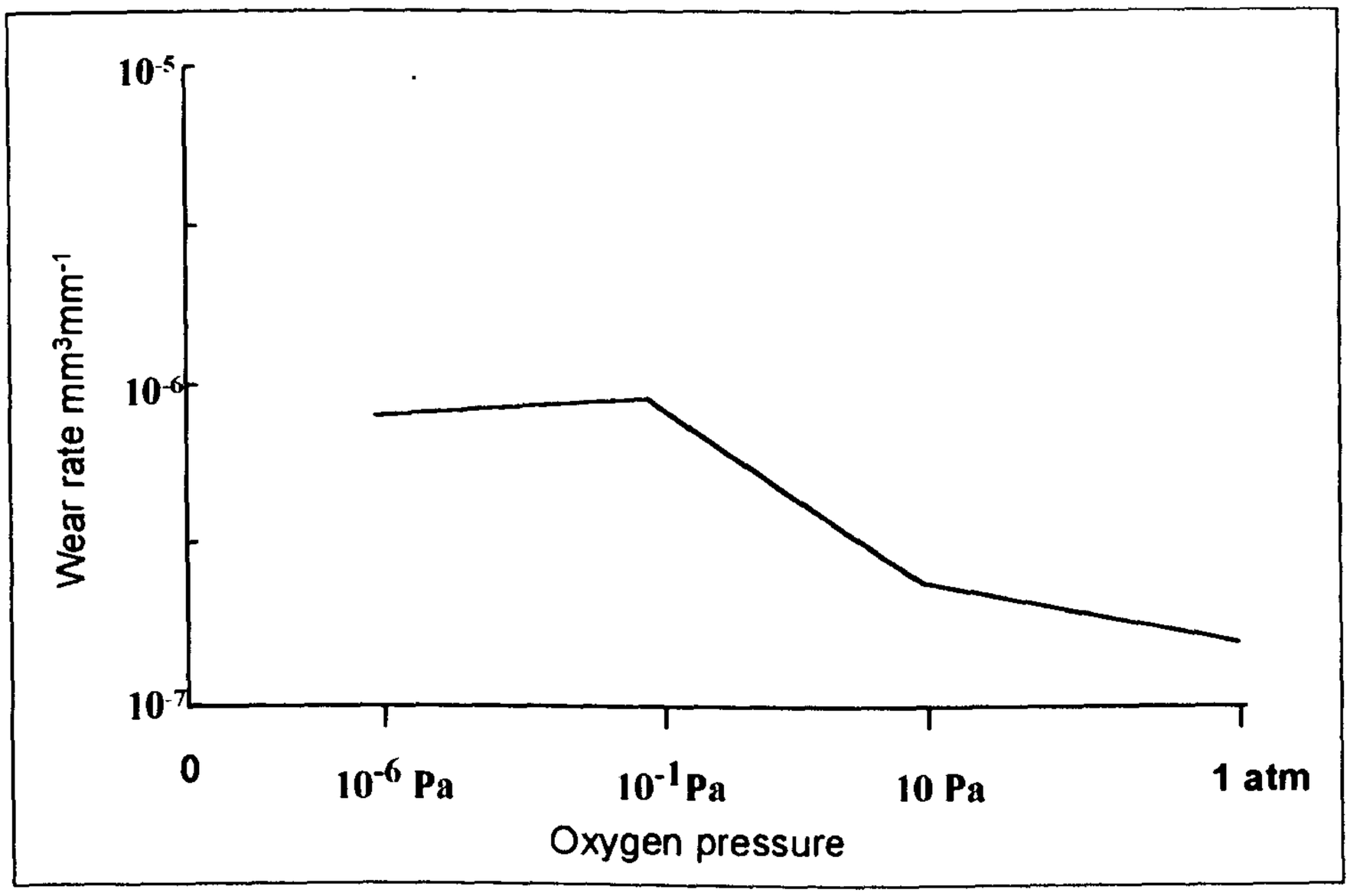

Fig.2.19 Wear of Fe-4.9%Cr during like-on-like sliding in various oxygen partial pressures at 20°C [63]

Stott and Wood observed that the glazes developed gradually but increased rapidly as the oxygen partial pressure increased, and persisted even in an evacuated environment. A corresponding reduction in the coefficient and wear rate was noticed as the oxygen partial pressure increased.

(c) Temperature

It has been observed [12] that for a number of alloys, a rise in temperature shortens the period of time of sliding to form a wear protective oxide. **Fig.2.20** shows this as a function of the reduction in the coefficient of friction for a Ni-20%Cr alloy during like-on-like sliding.

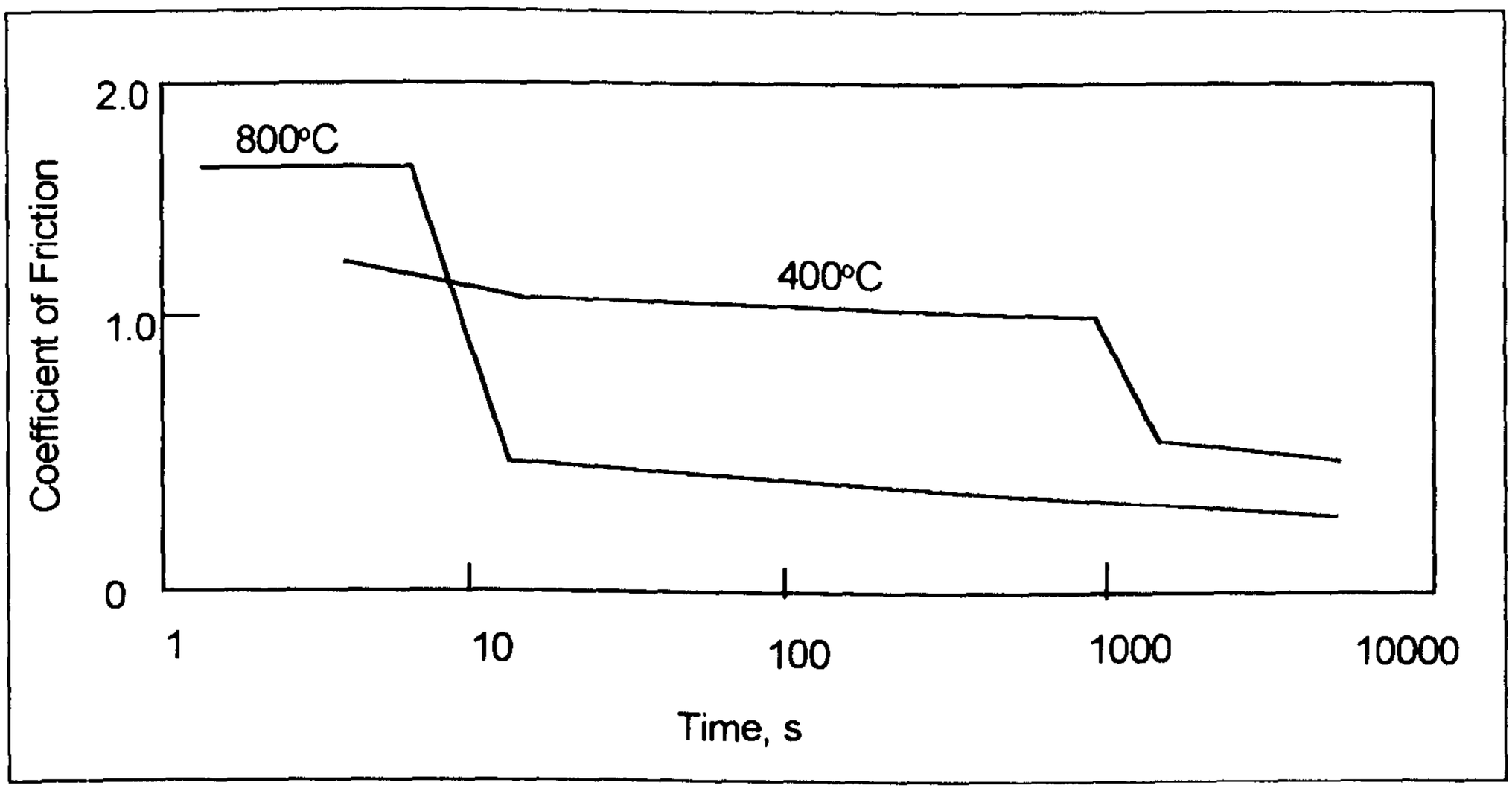

Fig.2.20 Coefficient of friction as a function of time for like-on-like sliding of Ni-20%Cr [12]

However, contrasting conclusions have been made to the role of protective oxide films at room temperature. Lin et al. [41] investigated the friction and wear properties

during like-on-like sliding of Nimonic 75, C263, Nimonic 108 and Incoloy 901 at room temperature (see ***Table 2.3***).

The investigators found that the friction and wear properties of the alloys during sliding were correlated with work hardening, and possibly some degree of age-hardening of the load-bearing areas, owing to the severe mechanical and thermal stresses developed. No evidence was found that suggested oxide film or wear debris had any major effect on the friction and wear behaviour of the alloys. However, testing under similar sliding conditions by Jiang et al. [64] for Nimonic 80A at 20°C revealed compacted, oxidised and agglomerated wear debris had a major effect on the friction and wear properties of the alloy. Results indicated that once wear debris had compacted onto the surface the total amount of wear increased with further sliding (see **Fig.2.21**). The reason for the difference is unclear as the experimental conditions were similar and the geometry of the two wear rigs (therefore wear debris retention) were also similar.

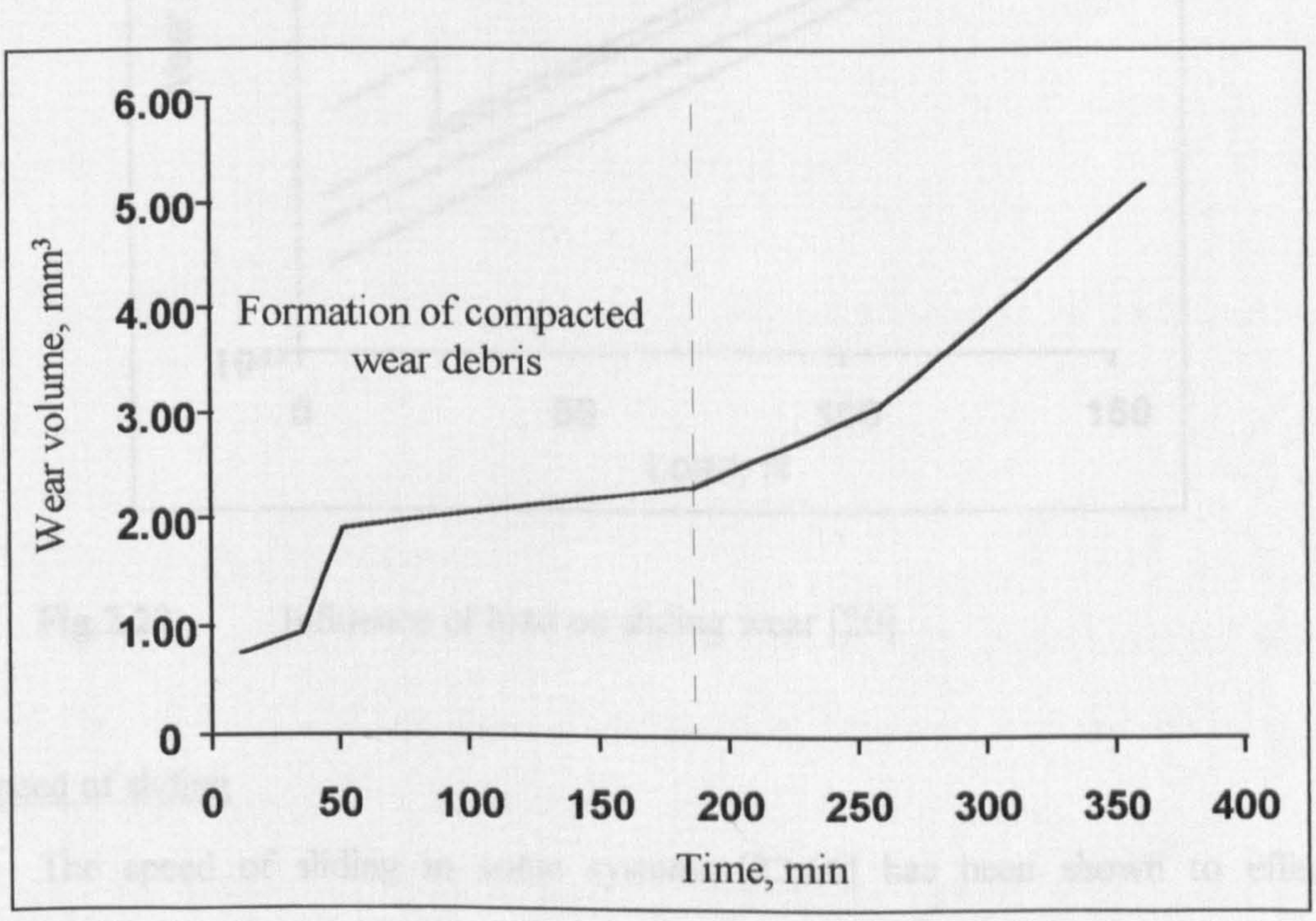

Fig.2.21 Wear curve for like-on-like sliding of Nimonic 80A at 20°C [64]

(d) Load

The Archard equation [24] indicates that the wear rate should increase linearly with the applied load. However, in some systems a change in load can change the wear mechanism leading to mild→severe wear transitions or vice versa. These effects are less common at elevated temperature [20,34,65]. At higher temperatures protective oxide plateaux form which protect the surface through a range of different loads. **Fig.2.22** show the results of like-on-like pin-on-disc testing of 52100 steel at a sliding speed of $2ms^{-1}$ [20].

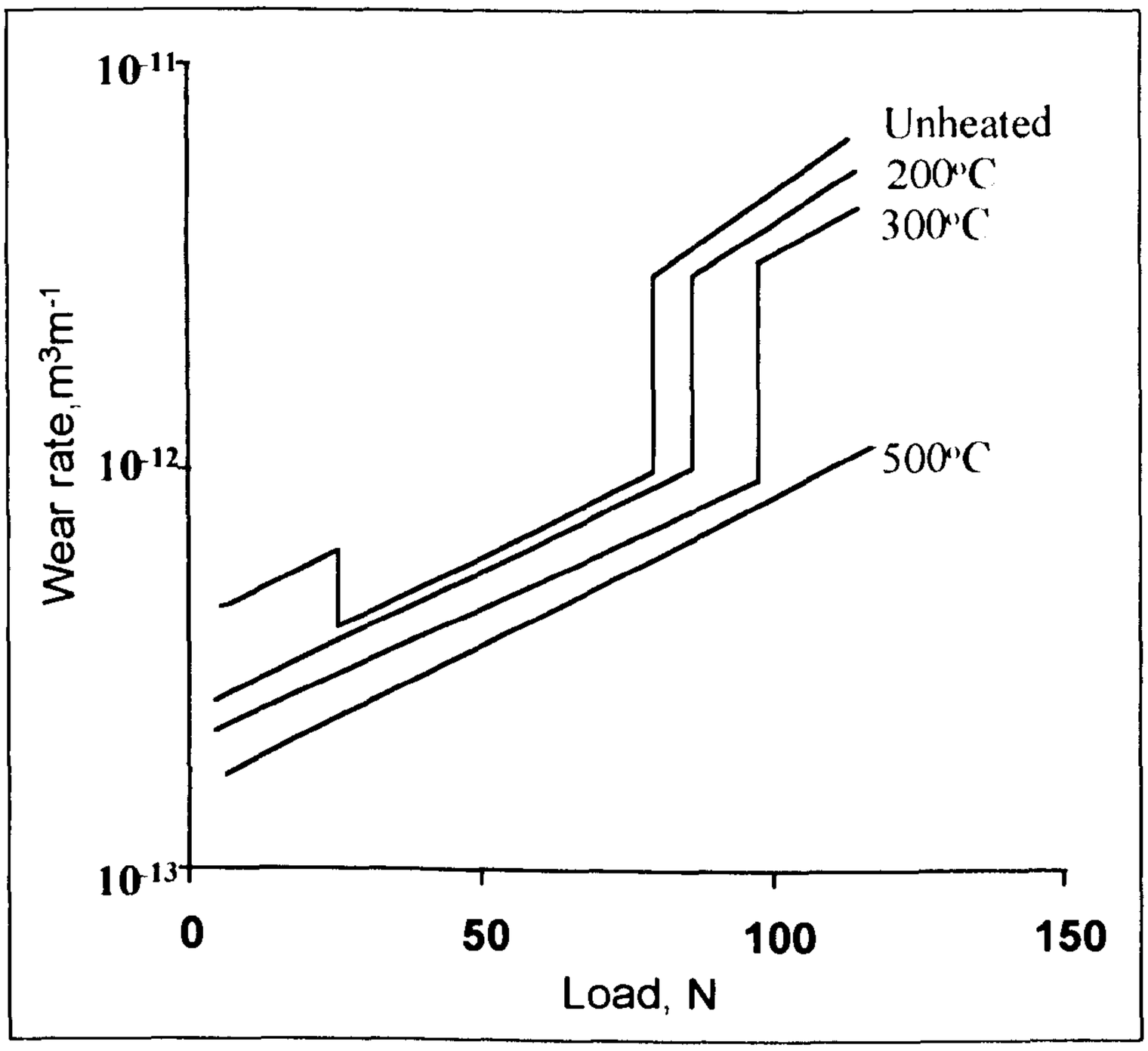

Fig.2.22 Influence of load on sliding wear [20]

(e) Speed of sliding

The speed of sliding in some systems [32,66] has been shown to effect the formation of protective oxide films. Lancaster [66] investigated the wear properties of 60/40 brass sliding against a hard steel surface under a load of 30N and at an ambient

temperature of 300°C. Lancaster observed a region of severe wear at intermediate speeds (0.02-0.3ms^{-1}) separating regions of mild wear at high and low speeds (see **Fig.2.23**). Testing with an oxygen-enriched atmosphere reduced the range of severe wear (0.07-0.2ms^{-1}) indicating the importance of the formation of protective oxide films.

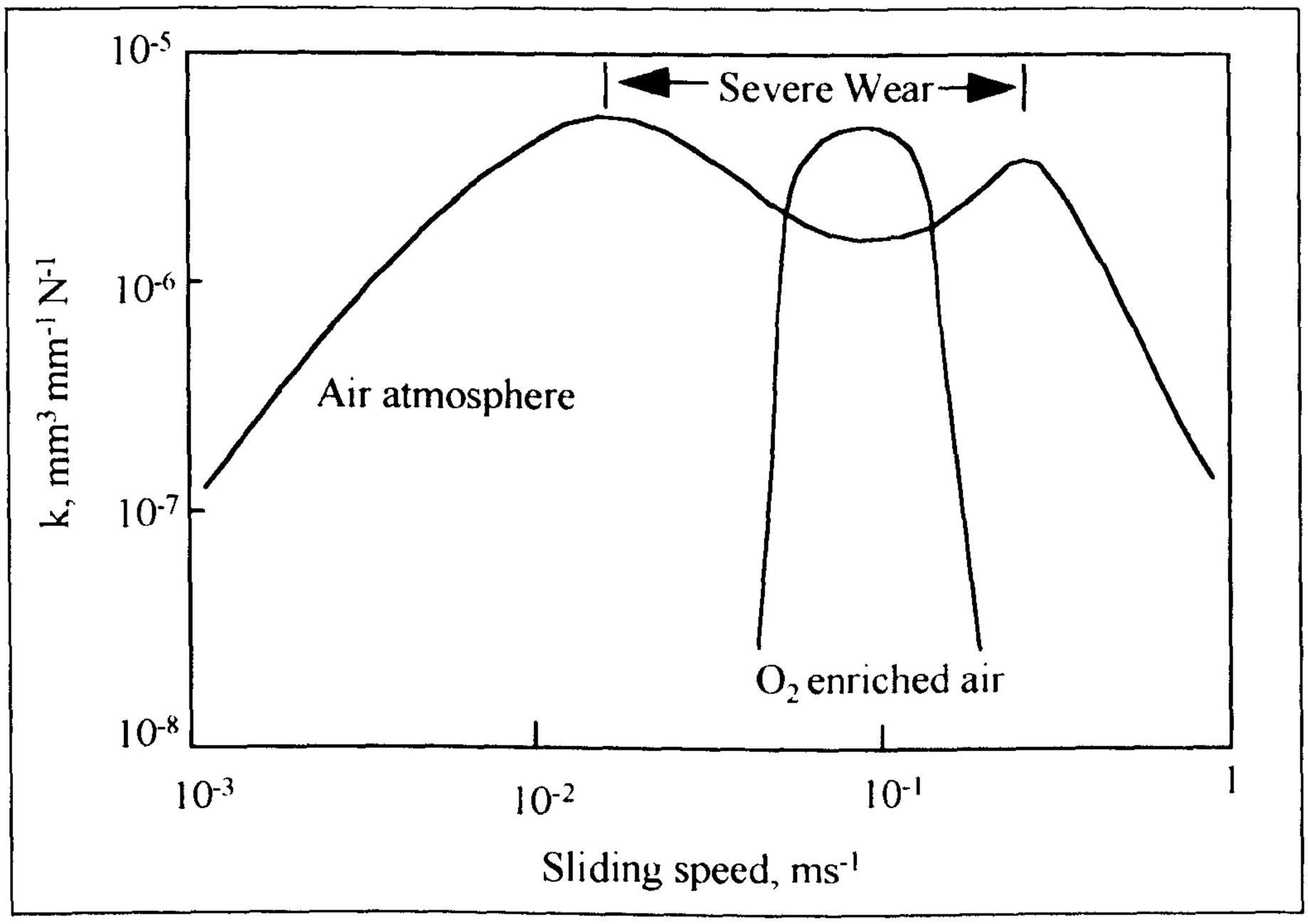

Fig.2.23 The change of the wear coefficient with speed for 60/40 brass on steel [66]

2.5 Ceramic/Metal Sliding

The review presented so far has concentrated on the unlubricated wear of metal-on-metal sliding. Metal-on-ceramic contact can act very differently and the following pages summarise certain essential points concerning the wear of this system.

The main influence during the wear of metal against ceramic is the transfer of metal to the ceramic surface. This is affected by the mechanical properties and oxidation activity of the metal. A number of investigations [67-70] have found that a metal with a high

oxygen affinity is transferred to the ceramic surface more readily than a metal with a low oxygen affinity. This results in like-on-like sliding causing high friction coefficients.

Takadoum and Roques-Carmes [67] investigated the friction and wear properties of polycrystalline Al_2O_3 sliding on different metals, namely titanium, aluminium, nickel and copper. Dry pin-on-disc tests were conducted in air at room temperature under an applied load of 5N and at a sliding speed of 0.29m/min. Electron microprobe analysis revealed the presence of large amounts of aluminium and titanium transferred to the Al_2O_3; little transfer from nickel to the Al_2O_3 surface was observed, while for copper no transfer was detected. ***Table 2.11*** displays the friction coefficients recorded with the aluminium disc showing the highest value of 0.8 compared to only 0.3 for the copper disc. Takadoum and Roques-Carmes concluded that the affinity of the metal for oxygen is the key factor which determines the strength of adhesion and affects friction and wear. It was stated that the oxygen affinity increased in the following order: copper, nickel, titanium and aluminium. The greater the oxygen affinity of the metal, the higher the material transfer and friction coefficient. However, in the study no values were given for the oxygen affinities and therefore a comparison could not be made with the observations.

Table 2.11 Average friction coefficient values for the wearing of an Al_2O_3 pin against various discs [67]

Disc	Average friction coefficient	
	Initial	After 5m sliding
Copper	0.1	0.3
Nickel	0.4	0.5
Titanium	0.4	0.6
Aluminium	0.5	0.8

The mechanical properties of the metal, i.e. hardness, have also been suggested to influence the wear of ceramic/metal pairs [71-72]. Zhou et al. [71] studied the unlubricated sliding behaviour of hot-pressed ceramic Si_3N_4 against high-chromium cast iron (2.9%C 0.2%Si 0.3%Mn 18.6%Cr 1.0%Mo - Fe). The cast iron was heat treated to obtain various different microstructures and consequently hardnesses. Testing was conducted using a block-on-ring rig at room temperature, with a load of 30N and at a speed of 200rpm. The results are shown in ***Table 2.12***.

Table 2.12 Variation in the volume loss of Si_3N_4 and high chromium cast iron with hardness of the cast iron [71]

Hardness of heat treated cast iron (Hv)	Volume loss of Si_3N_4 (mm^3)	Volume loss of high chromium cast iron (mm^3)
1020	0.331	0.24
959	0.268	0.17
847	0.442	0.40
744	0.578	0.59
767	0.383	0.20
564	0.640	0.21
377	0.376	0.54

Zhou et al. concluded that the wear of the Si_3N_4 decreased with increasing hardness of the high chromium steel. It was also reported that the wear of the high chromium cast iron depended upon two factors: matrix hardness and plastic deformation of the matrix. However, the results indicate for both statements that discrepancies exist. For example, the highest hardness of the cast iron was Hv1020 and therefore the lowest volume loss of Si_3N_4 and cast iron should have been observed. The actual volume loss of Si_3N_4 and the cast iron

was 0.331mm^3 and 0.24mm^3 respectively, higher than corresponding values of lower hardness cast irons.

The wear and friction properties of the ceramic/metal wearing has also been stated to be influenced by environmental factors - load, temperatures, sliding speed and humidity [73-77].

Takadoum [69] conducted pin-on-disc wear tests in air with different relative humidity levels (RHL). The pins were Al_2O_3 and the discs were samples of copper, nickel, titanium and aluminium. It was found that aluminium and titanium adhere strongly to the ceramic counterface, leading to large metal transfer whatever the RHL was (20%, 50%, 90%). However, copper and nickel were sensitive to the RHL during wear testing. Increasing RHL led to a decrease in the metal/ceramic bond strength, and consequently, in the friction coefficient (see **Fig.2.24**). Adhesive wear took place at low RHL while the metals wore by ploughing at the high RHL.

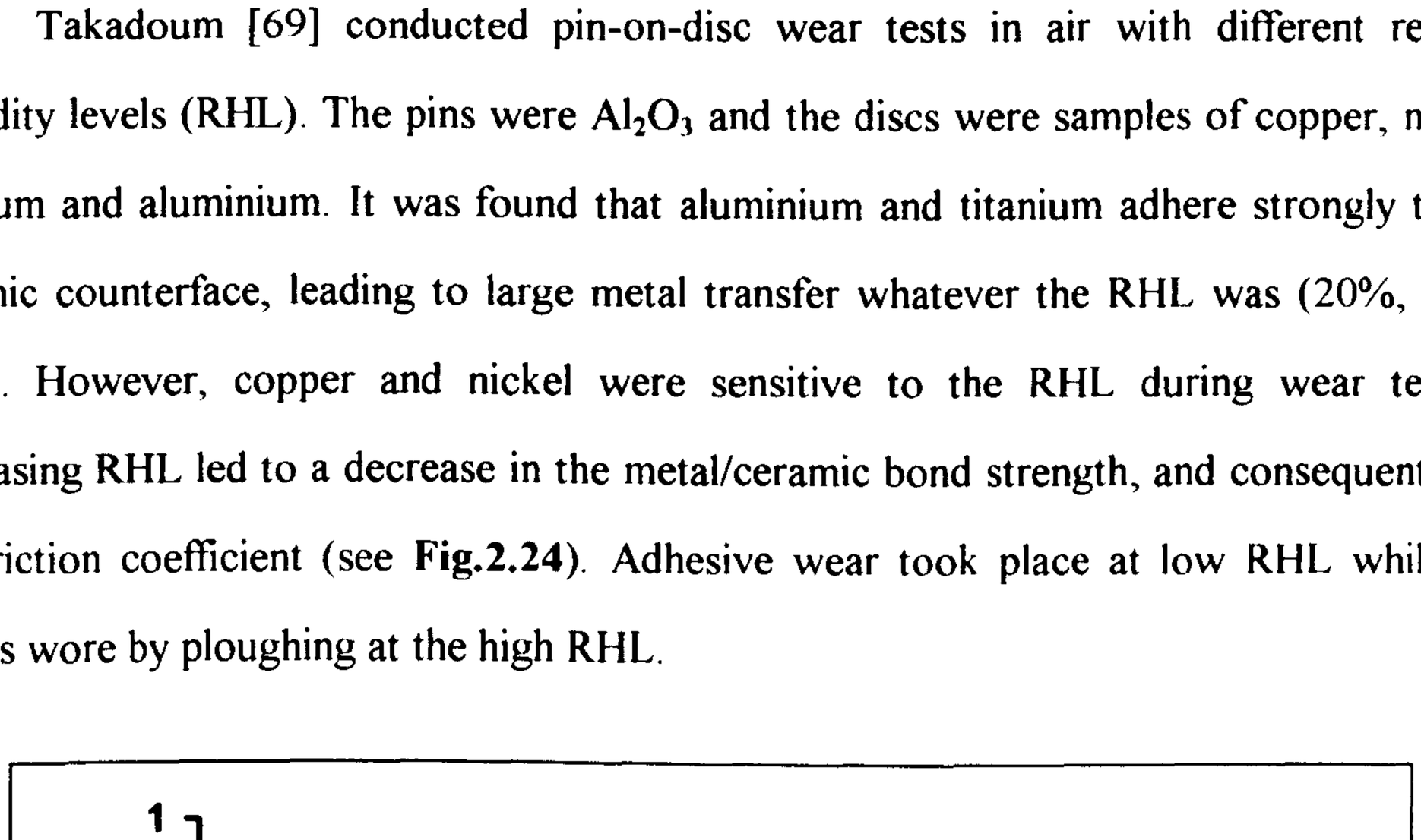

Fig.2.24 Variation of the friction coefficient with relative humidity for various metal/ceramic couples [69]

Ravikiran and Pramila Bai [73] investigated the influence of speed on the sliding of Si_3N_4 (pin) against a steel disc and found four different regions corresponding to certain tribochemical reactions occurring on the surface. The speeds chosen were between 0.1 ms^{-1} to 12 ms^{-1} at a load of 15.5 MPa and the results were as follows:-

Region 1 (0.1-1.25 ms^{-1})	Friction high (0.7-0.8), high wear rate of pin (1.3-2.0 x $10^{-13}m^3m^{-1}$) and negligible wear rate of disc. Si_3N_4 reacted with water vapour to form hydrated silica ($SiO_2.nH_2O$).
Region 2 (1.25-3.5 ms^{-1})	Friction low (0.3-0.4), wear rate of pin is negligible and high wear rate of disc (5.5 x $10^{-13}m^3m^{-1}$). Controlled by softening of $SiO_2.nH_2O$.
Region 3 (3.5-6.5 ms^{-1})	Friction high (0.55-0.6), wear rate of pin is low (0.4 x $10^{-13}m^3m^{-1}$) and high wear rate of disk (6.2 x $10^{-13}m^3m^{-1}$). Characterised by the microfracture of Si_3N_4 and limited formation of Y_2SiO_5.
Region 4 (6.5-12.0 ms-1)	Friction low (0.35-0.4), wear rate of pin is high (0.4-0.5 x $10^{-13}m^3m^{-1}$) and very low wear rate of disc (0.2 x $10^{-13}m^3m^{-1}$). Associated with increased formation of $YSiO_5$ and SiO_2.

One criticism of the work of Ravikiran and Pramila Bai is that the various friction and wear rate changes have been related mainly to changes in tribochemical reactions and other factors have been ignored. It is possible that in *regions 2, 3* and *4*, metal transferred

from the disc onto the Si_3N_4 pin caused a reduction of the wear rates of the pin. Similarly in *region 1*, the high wear rate was probably caused by the absence of metal transfer.

Murray and Calabrese [78] reported wear testing using a metal pin and a ceramic disc at a load of 142.2N over a temperature range of 25 to 800°C. The ceramic materials and alloys chosen are shown in ***Table 2.13***.

Table 2.13 Metallic alloys and ceramic materials used in ceramic/metal wear testing [78]

Ceramic material - disc	Metallic alloy (%wt) - pin
Hot-pressed Si_3N_4	Fe-15Mo 15Co
Hot-pressed beta-sialon	Co-0.08C 20Cr 11Ni 16W 1.6Fe
Pressureless sintered α-SiC	Co-0.25C 27Cr 2.5Ni 5.5Mo 2Fe
Hot-pressed 70%Al_2O_3 + 30% TiC	Co-0.08C 2Si 28Mo 8Cr
Hot-pressed 50%Al_2O_3 + 50% SiC whiskers	Ni-0.08C 15Cr 7Fe 2.5Ti 0.5Al 1Nb 1Co

Murray and Calabrese observed that material transfer from the metals to the ceramics played a major role in most of the results. In the low-to-intermediate temperature range (up to 300°C), the transferred films coated the ceramic surface and sliding was essentially metal vs. the transferred metal film. At higher temperatures, for some of the alloys, the transferred films oxidised leading to low friction and, in some cases, very low wear rates, i.e. approaching $2.1x10^{-7}mm^3N^{-1}m^{-1}$.

CHAPTER 3

INTRODUCTION TO THE PRESENT EXPERIMENTAL WORK

3. INTRODUCTION TO THE PRESENT EXPERIMENTAL WORK

Wear has been shown to be a complicated process affected by numerous parameters including material properties and external factors such as load, speed and geometry. [32,34,65-66]. Extensive studies have been conducted into the process of wear, particularly at room temperature, and usually involving only one pair of materials. The most common parameters investigated are the effect of load and sliding speed on wear rates. However, few investigations have considered the process of wear when a number of different types of counterfaces are used. Even with these investigations, testing has mostly been limited to room temperature [79-84]. Therefore a more detailed understanding of the effect of differing counterfaces on the overall process of wear is needed, particularly at high temperature.

This research programme has concentrated on the effect of the counterface in the formation of wear resistant oxide plateaux, often referred to as 'glazes'. These have been shown by a number of authors [85-90] to have a very important role in the wear resistance of an alloy especially at elevated temperature. The 'glazes' are very fine crystalline oxide particles which can undergo plastic deformation during the process of high temperature wear leading to very low wear rates and greatly reduced friction coefficients. The glazes can form on top of either wear debris which has undergone fragmentation, agglomeration and compaction, or on relatively thick oxide present on the alloy prior to sliding.

Attempts [13-15] have been made to preform these glazes through the process of preoxidation. Theoretically, this can encourage formation of glazes by either providing material using the removed oxide film debris, or by providing a stable oxide film on which the glaze can form. However, no agreed conclusion has been made describing the effect of preoxidation on glaze formation. Consequently, it was this proposition that was investigated in the research programme.

Glaze formation has been shown to be affected by temperature. Higher temperatures increase the speed of oxidation. Hence, oxide films or oxidised wear debris,

from which glazes can develop, are formed more quickly. In the present research programme, glazes formed at various temperatures were analysed for compositional differences, morphological differences and variations in wear resistance.

Several investigations have centred on comparing wear resistance to hardness. This stems from the widely stated Archard equation [24] in which wear volume produced is inversely proportional to the hardness of the material. In the present investigation the hardnesses of the wear sample and counterface were compared and the relationship with the wear resistance examined.

Research has also suggested the processing route of an alloy can have an effect on its wear resistance. The wear resistance of similar composition cast and HIPped materials have been compared and investigations [67] have concluded that HIPped materials have an improved wear resistance. This stemmed from the more uniform distribution of the elements in the HIPped samples allowing a more homogeneous precipitation behaviour which, in turn, improved strength and resistance to hot corrosion. In the present research programme the wear resistance of cast and HIPped Nimonic 80A was compared.

Wear testing was conducted in a reciprocating block-on-wheel rig mainly at room temperature or 750°C, at a rotation speed of 250rpm and a load of 7N. In addition, the block was reciprocated at 3 cycles per minute against the rotating wheel. These conditions were chosen to simulate the conditions as closely as possible to that experienced by an exhaust valve in the newly designed engine. Testing was carried out for a duration of 4 hours. In addition, a more detailed investigation was pursued for four different block/wheel combinations in which testing was conducted between 2 minutes to 1 hour at 750°C.

A range of different alloys had been chosen to assess suitability as valve materials in the new engine. In addition, studies have shown the importance of finding the appropriate material pairing, and therefore three seat insert materials have also been investigated. The candidate valve materials chosen were Ma956, PM2000, PM2000SD, Nimonic 80A (Cast), Nimonic 80A (HIPped), Nimonic 90 and titanium aluminide. Particular interest was centred

on MA956, PM2000 and PM2000SD. These are iron-based oxide dispersion strengthened alloys which have been manufactured through a mechanical alloying process. In this process fine yttrium oxide particles are dispersed uniformly in the alloy matrix. These particles interfere with the dislocation movement imparting high temperature strength in addition to creep and deformation resistance. In addition, ODS alloys have excellent corrosion resistance up to 1300°C due to a slowly growing protective α-alumina film [91-102]. These properties indicate suitability for a valve material at the high temperatures experienced in the new engines.

Titanium alloys have been used in engine valve systems in race cars for many years because of their high temperature strength and corrosion resistance [103-106]. The materials also have the added advantage of having a very low density ($3.8gcm^{-3}$) which makes the valve train lighter and therefore more efficient. However, the use of titanium aluminides for this purpose has not been fully investigated.

Nimonic 80A is used as an existing exhaust valve material in high loading conditions [8]. In the present study Nimonic 80A, produced by two different processing methods, was investigated. Studies have shown an improvement in wear resistance when HIPped materials have been compared to cast materials.

Nimonic 90 is similar to Nimonic 80A as both are nickel-base superalloys. However, in Nimonic 90, 16wt% cobalt has been substituted for nickel which increases the solubility of the γ′ phase and therefore increases the maximum operating temperature of the alloy [107].

Three materials were also chosen to act as the seat insert material. These were Incoloy 800, Stellite 6 and Si_3N_4. The ceramic, Si_3N_4, is particularly promising as previous studies using natural gas engines [108-109] have observed low wear rates when testing with silicon nitride seat inserts and metal valves.

The rationale of the investigation can be summarised as follows:

1. to compare the effect of the counterface on the wear resistance of three groups of alloys (ODS, Nimonics, intermetallics) at room temperature and 750°C with a view to understanding the role of the counterface in glaze formation;
2. to investigate the role of preoxidation (in air) of the ODS alloys in the subsequent formation and development of glazes;
3. to carry out studies into the effect of temperature on glaze formation on Ma956 from room temperature up to 750°C;
4. to ascertain if a relationship exists between the processing route and wear resistance of Nimonic 80A; and
5. to investigate the effect of hardness of the block and wheel on wear resistance.

The overall information derived from the present programme was designed to yield mechanistic information on the wearing of materials against different counterfaces. In particular, a clearer picture should be gained to the effect of various factors on glaze formation.

CHAPTER 4

EXPERIMENTAL

4. EXPERIMENTAL

This Chapter is structured in three main sections. The first section details the materials used for the investigation. The second section describes the design, construction and experimental conditions of the experimental wear rig used for the testing. The third section presents the experimental methods and the methods of analysis.

4.1 Materials

The experimental alloys employed in this research programme were chosen from a range of different alloys. The compositions of the block materials are shown in ***Table 4.1*** and the composition of the wheel materials are presented in ***Table 4.2***. A brief description and some properties of the materials are displayed in ***Table 4.4***.

Table 4.1 Composition of block materials

Alloy	Composition (wt%)									
	C	Si	Mn	Co	Al	Fe	Ni	Cr	Ti	Other
PM2000	<0.04	-	-	-	5.5	bal.	-	20	0.5	Y 0.5
MA956	0.05	-	-	-	4.5	bal.	-	20	0.5	Y 0.5
PM2000SD	<0.04	-	-	-	5.5	bal.	-	20	0.5	Y 0.5
TiAl	-	-	1.3	-	bal.	-	-	-	35.2	Nb 0.7
Nimonic 80A (cast)	0.08	0.1	-	-	1.4	0.7	bal.	19.4	2.5	
Nimonic 80A (HIPped)	0.11	0.3	-	-	1.2	0.8	bal.	18.5	2.1	
Nimonic 90	0.08	0.3	-	15.9	1.4	0.6	bal.	19.2	2.4	

Table 4.2 Composition of wheel materials

Alloy	Composition (wt%)									
	C	Si	Mn	Co	Al	Fe	Ni	Cr	Ti	Other
Incoloy 800	0.1	0.4	0.7	0.3	0.5	bal.	30.8	20.0	0.6	Cu 0.4
Silicon nitride	-	bal.	-	-	-	-	-	-	-	N 39.9
Stellite 6	1.1	1.0	-	bal.	-	3.0	3.0	28.0	-	W 4.5

4.2 Design and Experimental Conditions for Wear Rig

A schematic of the wear rig used in the investigation is shown in **Fig.4.1**. This particular design was used because it was the best compromise between ease of construction, close simulation of valve and seat insert conditions and quick sample preparation. Originally the wear testing was to be conducted in an exhaust gas atmosphere but problems with leakage in the split furnace prevented testing other than in laboratory air. The experimental conditions are shown in ***Table 4.3***.

Table 4.3 Experimental conditions chosen for wear testing

Condition	Value
Load	7N
Temperature	RT, 350°C, 550°C, 750°C
Speed of rotation	250rpm
Speed of reciprocation	3 cycles per min
Duration	2 mins-4 hrs

Table 4.4 Description and properties of the materials used in the investigation

Alloy	Description	Hv500g	Av. grain size (μm)
Ma956	ODS alloy strengthened through a yttria dispersion in Fe-Cr-Al matrix	303	3000
PM2000	ODS alloy strengthened through a yttria dispersion in Fe-Cr-Al matrix	311	500
PM2000SD	ODS alloy strengthened through a yttria dispersion in Fe-Cr-Al matrix. Rolled at higher temperature than PM2000 imparting greater ductility	363	80
Nimonic 80A (cast)	Precipitation hardened alloy through a $Ni_3(Al, Ti)$ phase	223	90
Nimonic 80A (HIPped)	Precipitation hardened alloy through a $Ni_3(Al, Ti)$ phase. Hot pressed at 1200°C at 30kN	308	30
Nimonic 90	Similar to Nimonic 80A apart from 16wt% cobalt has been substituted for nickel which increases the solubility of the γ′ phase improving the maximum operating temperature of the alloy	242	80
Stellite 6	Solid solution strengthened matrix in which carbides (Cr_7C_3) are distributed	464	50
Incoloy 800	Solid solution strengthened iron-based superalloy containing an austenitic matrix	183	90
TiAl	γ-TiAl ordered intermetallic containing laminar/duplex structure	345	<5
Si_3N_4	Reaction bonded silicon nitride	1301	8

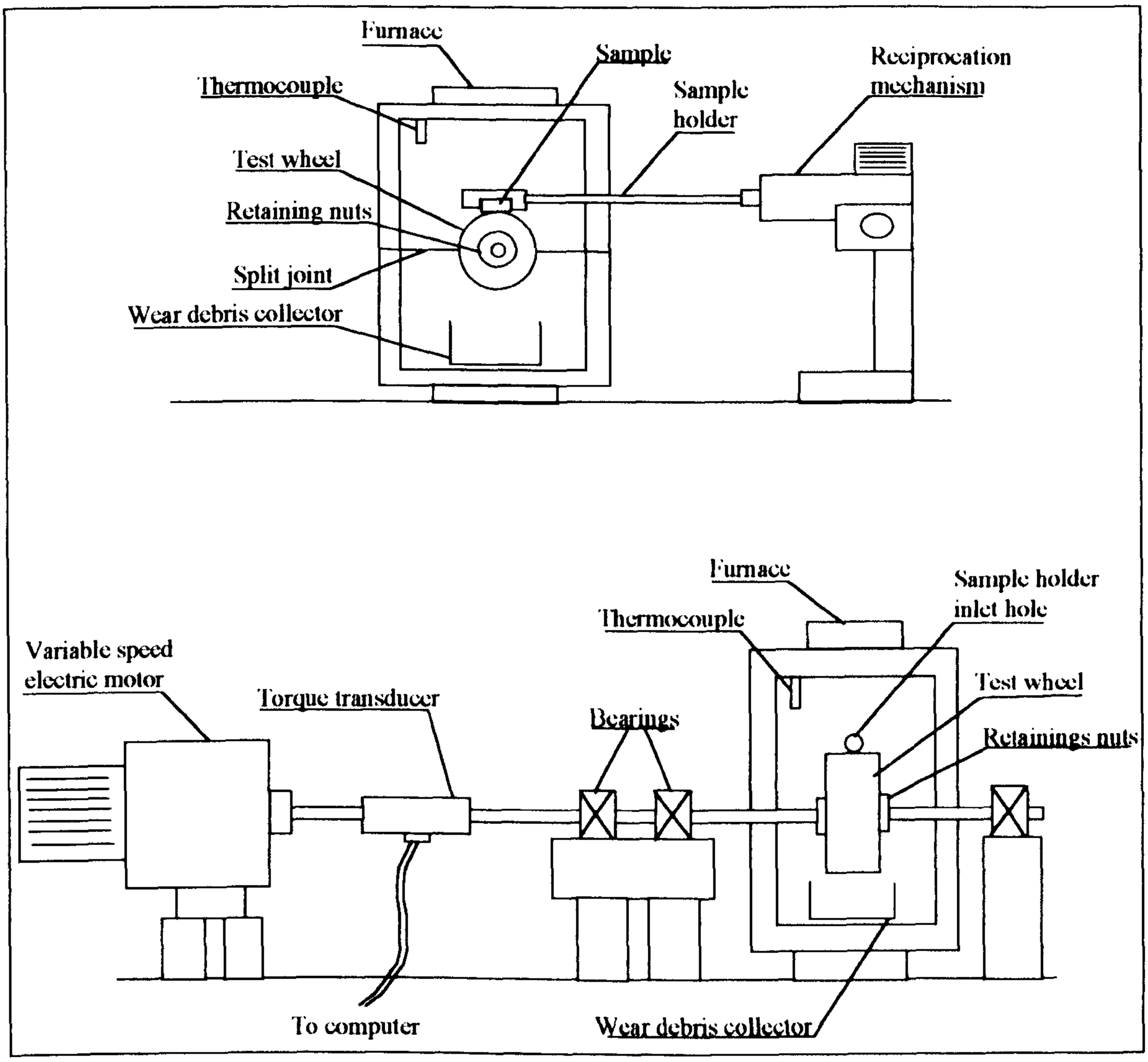

Fig.4.1 Schematic of wear rig

Previous investigations [110] adopting similar geometry rigs to simulate valve seat wear used a load of 22N which corresponded to a peak Hertzian stress of 80MPa. This stress is similar to the closing pressure of a typical diesel valve. However in this investigation a load of 7N was used as it was assumed it closely resembled the load in the new engine [111]. This load was achieved without external weighting but just through the weight of the sample holder. The highest temperature used during the testing was 750°C as this is a typical temperature experienced by the valve seat face of the exhaust valve in the new engine. In addition the sample block was reciprocated at a speed of 3

cycles per min, with a constant velocity and a stroke 12mm, at a tangent to the wheel surface. This was achieved using a motorised cam which pushed the sample holder back and forth. This was designed to simulate the valve stress cycle.

4.3 Experimental Methods

4.3.1 Specimen Preparation

The block materials were cut into 5 x 5 x 40mm samples and polished to a surface finish of 1μm. This was achieved by polishing the samples on SiC papers from 400 (through 600 and 800 grit) to 1200 grit and further polishing with diamond paste (9 to 1μm).The polished block materials were ultrasonically cleaned for 15 minutes in distilled water and then 15 minutes in acetone to remove grease and other residues. The block materials were dried in air. These test samples were weighed before and after exposure on a *Mettler HL52* microbalance to a resolution of +/- 0.00005g. The dimensions were measured using vernier callipers to the resolution of 0.05mm.

The counterface materials were cut into 50mm diameter x 50mm length wheels, polished to a surface finish of 1200 grit and cleaned using a similar method to that described previously.

4.3.2 Experimental Procedure

Wear Testing The wheel (Incoloy 800, Stellite 6 or Si_3N_4) was placed onto the shaft and secured tightly with locking nuts (see **Fig.4.1**). The shaft was fastened onto the rig and the rig switched on without the block material present. This was to allow the torque transducer values to stabilise and/or allow the furnace to reach the appropriate temperature (350, 550 or 750°C). After the test temperature was reached (or the torque transducer readings stabilised for room temperature testing) the block material was placed onto the wheel, using a sample holder which was pushed through a hole in the furnace, and the time recorded as t=0. Torque transducer readings were then recorded at 5 minutes intervals for a

4 hour test. After the appropriate test run time (2 minutes to 4 hours) the block material was removed from the furnace, allowed to cool and weighed. The torque transducer value was recorded and the rig switched off. Collected wear debris was removed from the crucible in the furnace and stored in a dessicator for further analyses.

Oxidation testing Oxidation tests were carried out in laboratory air. The furnace was switched on and heated to 750°C. When the test temperature was reached the block materials were inserted into the hot zone of the furnace. After 4 hours the samples were removed, left to cool and weighed.

Preoxidation Only ODS block materials were used for preoxidation tests. Samples of MA956, PM2000 and PM2000SD were preoxidised in laboratory air at 1000°C for 1 hour. In addition, MA956 was also preoxidised in laboratory air at 1000°C for 10 hours and 100 hours.

4.3.3 Analysis

The as-received materials and the worn block materials were examined by various methods: XRD, EDX and SEM to ascertain the composition and morphology of the wear scars. The SEM used was an *Hitachi SN2400* and the diffractometer was a *Siemens Diffraktometer 5000*. The worn block materials were examined using SEM to study their structure in plan and through the cross-section of the wear scars formed. This also included cross-sectional EDX analysis of the wear scar. Micro-hardness testing was performed on selected worn block materials using a *Buehler Micromet II Indentor*. The wear scars on the selected samples comprised of flat plateaux from which reproducible hardness values could be attained and an average hardness calculated from.

Friction coefficient results were calculated from torque transducer values using the following equations:

$$F = T/r \qquad \{4.1\}$$

where T = torque reading [Nm]

r = radius of wheel [m]

F = friction force [N]

and $$\mu = F/W \quad \{4.2\}$$

where μ = friction coefficient

W = load [N]

X-ray diffraction was used as the main means to identify the phases present in the wear scars on the block alloys. The XRD analysis was conducted using Cu K_{α} radiation at a scan rate of 0.2mm/s with a Ni filter. Wear debris analysis was performed using EDX spot analysis of numerous debris particles to find the main types of particles present.

Selected wear scars on the worn counterface wheels were analysed using EDX and SEM.

Weight changes of the worn block materials were converted into weight change/ per unit area by dividing by the wear scar area. Normally, in wear situations, weight loss is described in terms of volume loss. However, in this investigation the wear scar was long and wide (12mm x 5mm) and therefore accurate volume loss was difficult to record even with a tallysurf.

Stellite 6 was used as a block material in addition to being employed as a counterface material. The reason for this was to compare the wear resistance of the block alloys to a widely used wear-resistant alloy, i.e. Stellite 6. The Stellite 6 block alloy was not analysed in anyway apart from weight change measurements.

By comparing all the results obtained using different and complimentary analytical facilities, it was then possible to obtain comprehensive, accurate and detailed information on the morphology, phases present and the compositional profiles of the wear scars developed on the worn samples.

CHAPTER 5

RESULTS

5. RESULTS

This chapter is divided into six main sections. The first section displays phases identified on the as-received samples. The second section presents the results of oxidation studies of the alloys. The third and fourth section describe results of wear tests conducted for 4 hours and between 2 minutes to 1 hour. The results obtained from wear testing of Ma956 at room temperature up to 750°C are given in the fifth section and the sixth section deals with information derived from preoxidation studies.

5.1 XRD Analysis of the As-Received Materials

XRD analysis of the as-received materials is shown in ***Table 5.1***

Table 5.1 XRD analysis of the as-received materials

Alloy	Phase
Ma956	Fe-Cr solid solution
PM2000	Fe-Cr solid solution
PM2000SD	Fe-Cr solid solution
Nimonic 80A (cast)	$Ni_{2.9}Cr_{0.7}Fe_{0.36}$
Nimonic 80A (HIPped)	$Ni_{2.9}Cr_{0.7}Fe_{0.36}$
Nimonic 90	$Ni_{2.9}Cr_{0.7}Fe_{0.36}$
TiAl	Al_3Ti, AlTi
Incoloy 800	$Ni_{2.9}Cr_{0.7}Fe_{0.36}$
Stellite 6	CoCr
Si_3N_4	Si_3N_4

A similar phase of a Fe-Cr solid solution was detected on the as-received ODS alloys. A $Ni_{2.9}Cr_{0.7}Fe_{0.36}$ phase was identified on Nimonic 90, Incoloy 800 and Nimonic 80A

(cast and HIPped). Two phases of Al_3Ti and AlTi were observed on the surface of the as-received TiAl. CoCr was identified on Stellite 6 and a Si_3N_4 phase was detected on Si_3N_4.

5.2 Air Oxidation

The measured values of the weight changes of the alloys after air oxidation at 750°C for 4 hours are shown in ***Table 5.2.***

Table 5.2 Weight change of alloys after air oxidation at 750°C for 4 hours

Alloy	Weight change ($mgcm^{-2}$)
MA956	+0.01
PM2000	+0.02
PM2000SD	-0.02
Nimonic 80A (cast)	+0.03
Nimonic 80A (HIPped)	-0.01
Nimonic 90	+0.02
TiAl	+0.01
Stellite 6	+0.02

The data show a similar very low weight change for all of the alloys varying between $+0.03mgcm^{-2}$ for Nimonic 80A (Cast) to $-0.02mgcm^{-2}$ for PM2000SD. These values are well within the error of the balance ($\pm 0.05mgcm^{-2}$) indicating little or no weight change. Therefore any weight changes of the block alloys during wearing at 750°C was at the wear scar and not through oxidation of the remaining alloy.

5.3 Wear Studies using Different Counterfaces at Room Temperature and 750°C for 4 Hours

5.3.1 Weight Changes

The wear data in terms of weight changes of the ODS block samples worn against different counterfaces at room temperature and 750°C are presented in **Fig.5.1**. Ma956 showed weight losses for all of the wear tests. Particularly large weight losses were observed when worn against Incoloy 800 (-1020.7mgcm^{-2}) at 750°C and Si_3N_4 at room temperature (-95.3mgcm^{-2}). A very low weight loss of -1.4mgcm^{-2} was noted when Ma956 was worn against Si_3N_4 at 750°C.

PM2000 showed similar trends to Ma956 with a large weight loss when worn against Incoloy 800 at 750°C (-594.7mgcm^{-2}). However, only a small weight loss of -2.4mgcm^{-2} was observed when PM2000 was worn against Si_3N_4 at room temperature. Against the Stellite 6 counterface the values of weight losses were between -1.4mgcm^{-2} at 750°C and -22.8mgcm^{-2} at room temperature.

PM2000SD again showed similar trends to those obtained for Ma956 and PM2000 but the weight loss values were generally lower. The largest weight loss was displayed when PM2000SD was worn against Incoloy 800 at 750°C (-280.3mgcm^{-2}) which was much lower than showed by Ma956 and PM2000 (-1020.7 and -594.7mgcm^{-2} respectively) in a similar test. The lowest weight loss was achieved when PM2000SD was worn against Incoloy 800 at room temperature (-0.7mgcm^{-2}).

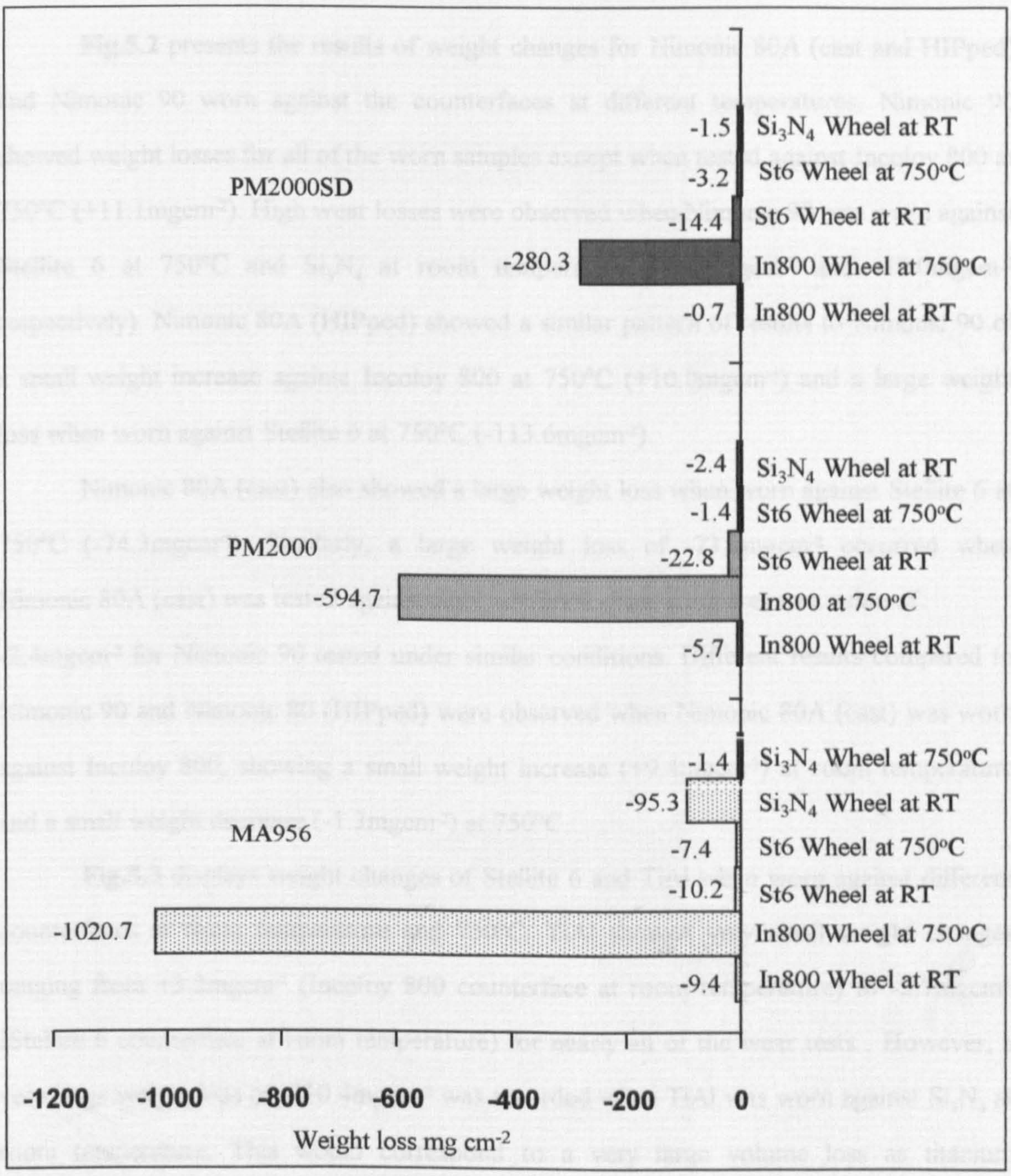

Fig.5.1 Weight change of the ODS alloys after wearing against various counterfaces at room temperature and 750°C

Fig.5.2 presents the results of weight changes for Nimonic 80A (cast and HIPped) and Nimonic 90 worn against the counterfaces at different temperatures. Nimonic 90 showed weight losses for all of the worn samples except when tested against Incoloy 800 at 750°C (+11.1mgcm^{-2}). High wear losses were observed when Nimonic 90 was worn against Stellite 6 at 750°C and Si_3N_4 at room temperature (-68.0mgcm^{-2} and -40.0mgcm^{-2} respectively). Nimonic 80A (HIPped) showed a similar pattern of results to Nimonic 90 of a small weight increase against Incoloy 800 at 750°C (+10.0mgcm^{-2}) and a large weight loss when worn against Stellite 6 at 750°C (-113.6mgcm^{-2}).

Nimonic 80A (cast) also showed a large weight loss when worn against Stellite 6 at 750°C (-74.3mgcm^{-2}). Similarly, a large weight loss of -73.3mgcm^{-2} occurred when Nimonic 80A (cast) was tested against Si_3N_4 at 750°C. This compares to a value of -2.4mgcm^{-2} for Nimonic 90 tested under similar conditions. Different results compared to Nimonic 90 and Nimonic 80 (HIPped) were observed when Nimonic 80A (cast) was worn against Incoloy 800, showing a small weight increase (+9.4mgcm^{-2}) at room temperature and a small weight decrease (-1.3mgcm^{-2}) at 750°C.

Fig.5.3 displays weight changes of Stellite 6 and TiAl when worn against different counterfaces at room temperature and 750°C. TiAl showed very small weight changes ranging from +3.2mgcm^{-2} (Incoloy 800 counterface at room temperature) to -2.7mgcm^{-2} (Stellite 6 counterface at room temperature) for nearly all of the wear tests . However, a very large weight loss of -210.4mgcm^{-2} was recorded when TiAl was worn against Si_3N_4 at room temperature. This would correspond to a very large volume loss as titanium aluminide has a low density.

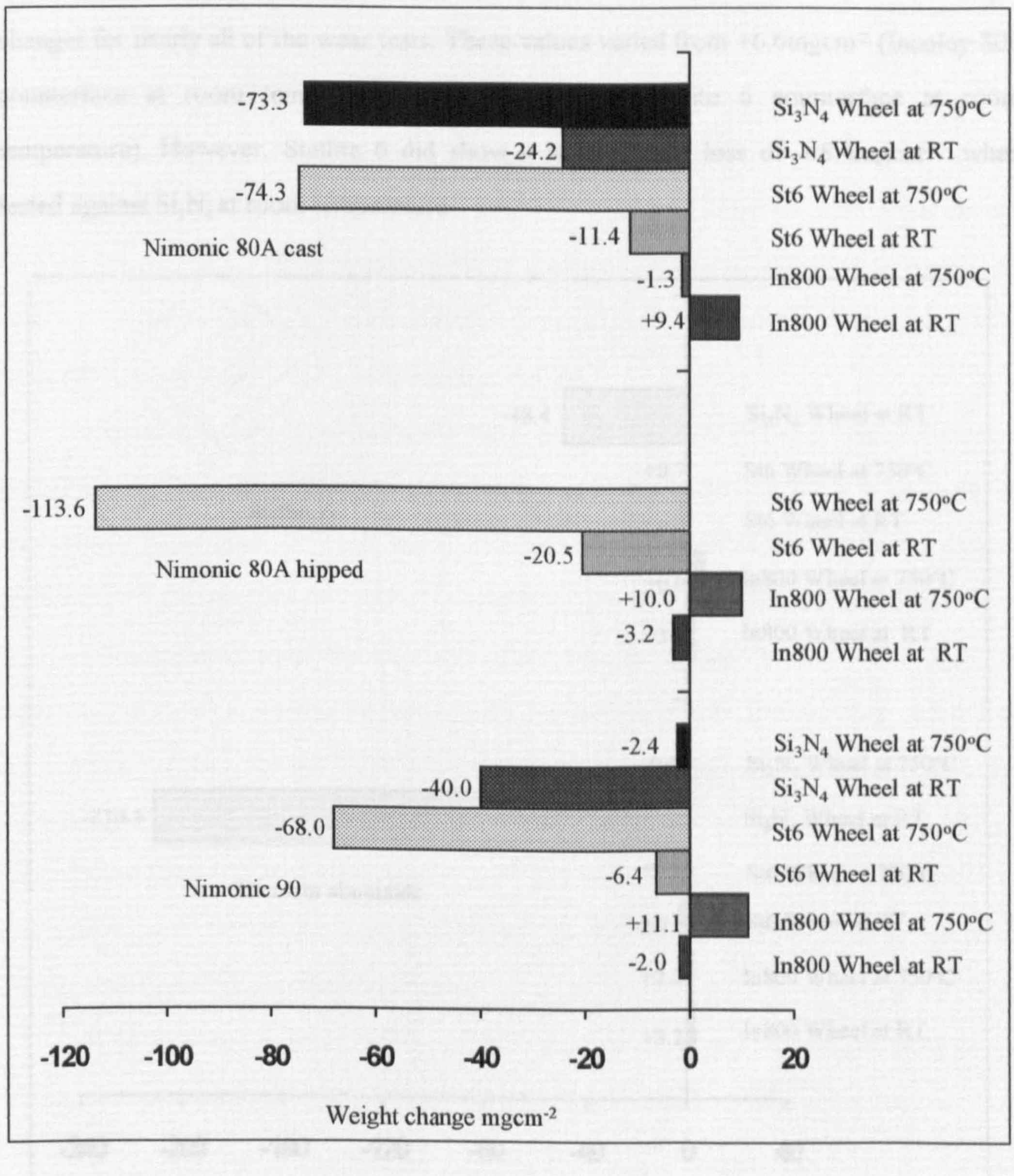

Fig.5.2 Weight changes of the Nimonics after wearing against various counterfaces at room temperature and 750°C

Stellite 6 showed excellent wear resistance as reflected by very small weight changes for nearly all of the wear tests. These values varied from +6.6mgcm^{-2} (Incoloy 800 counterface at room temperature) to -2.0mgcm^{-2} (Stellite 6 counterface at room temperature). However, Stellite 6 did show a large weight loss of -48.4mgcm^{-2} when tested against Si_3N_4 at room temperature

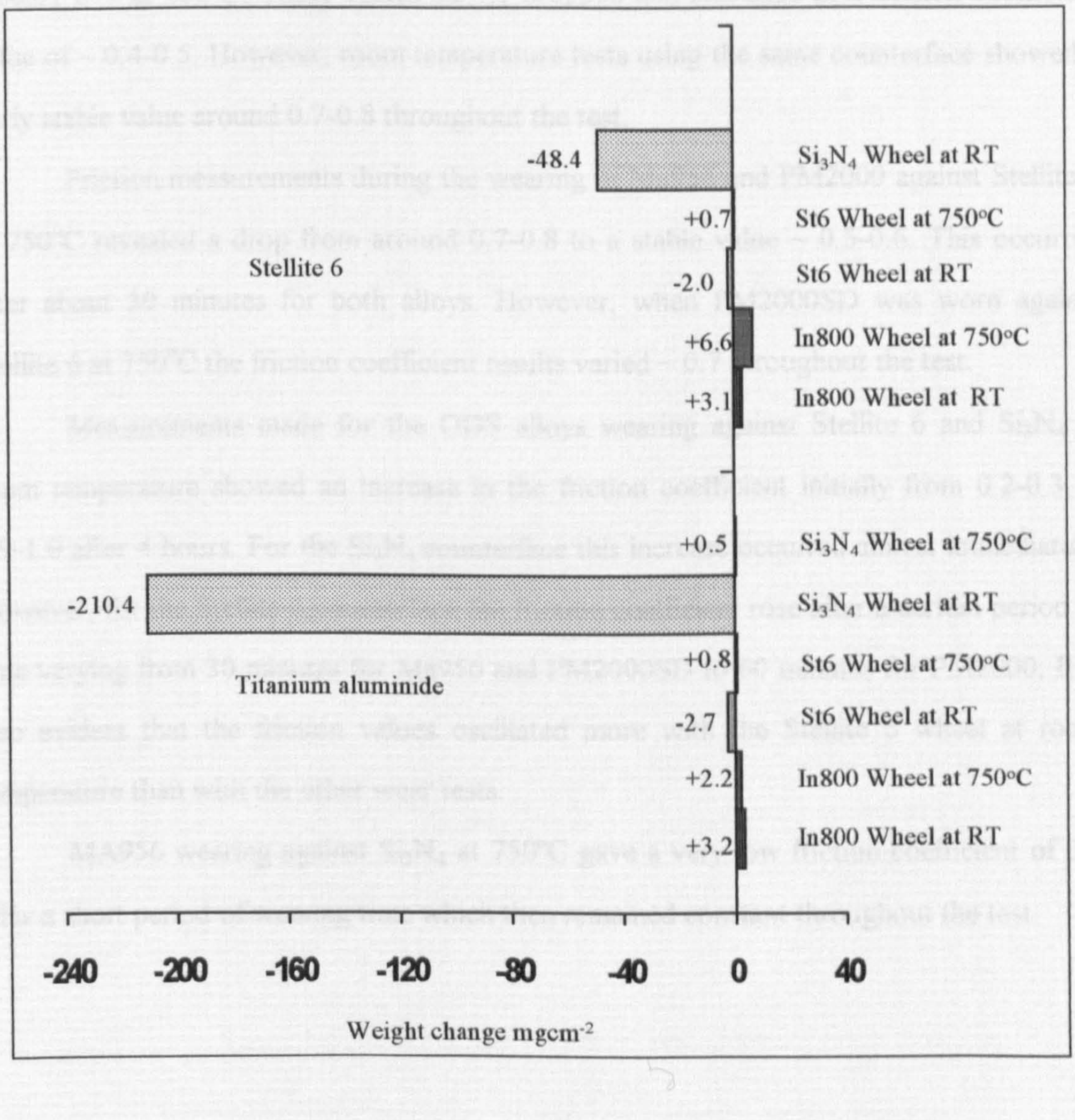

Fig.5.3 Weight changes of Stellite 6 and titanium aluminide after wearing against various counterfaces at room temperature and 750°C

5.3.2 Friction Coefficient

The friction coefficient values of Ma956, PM2000 and PM2000SD wearing against various counterfaces at room temperature and 750°C are shown in **Fig.5.4-5.6**. A similar pattern of results were observed with all the tests for the ODS alloys. In all cases high initial friction coefficients were recorded (~1.1) when the ODS alloys were worn against Incoloy 800 at 750°C. These values slowly dropped and stabilised at a friction coefficient value of ~ 0.4-0.5. However, room temperature tests using the same counterface showed a fairly stable value around 0.7-0.8 throughout the test.

Friction measurements during the wearing of Ma956 and PM2000 against Stellite 6 at 750°C revealed a drop from around 0.7-0.8 to a stable value ~ 0.5-0.6. This occurred after about 30 minutes for both alloys. However, when PM2000SD was worn against Stellite 6 at 750°C the friction coefficient results varied ~ 0.7 throughout the test.

Measurements made for the ODS alloys wearing against Stellite 6 and Si_3N_4 at room temperature showed an increase in the friction coefficient initially from 0.2-0.3 to 0.9-1.0 after 4 hours. For the Si_3N_4 counterface this increase occurred almost immediately. However, for the Stellite 6 counterface the friction coefficient rose after a certain period of time varying from 30 minutes for Ma956 and PM2000SD to 60 minutes for PM2000. It is also evident that the friction values oscillated more with the Stellite 6 wheel at room temperature than with the other wear tests.

MA956 wearing against Si_3N_4 at 750°C gave a very low friction coefficient of 0.2 after a short period of wearing time which then remained constant throughout the test.

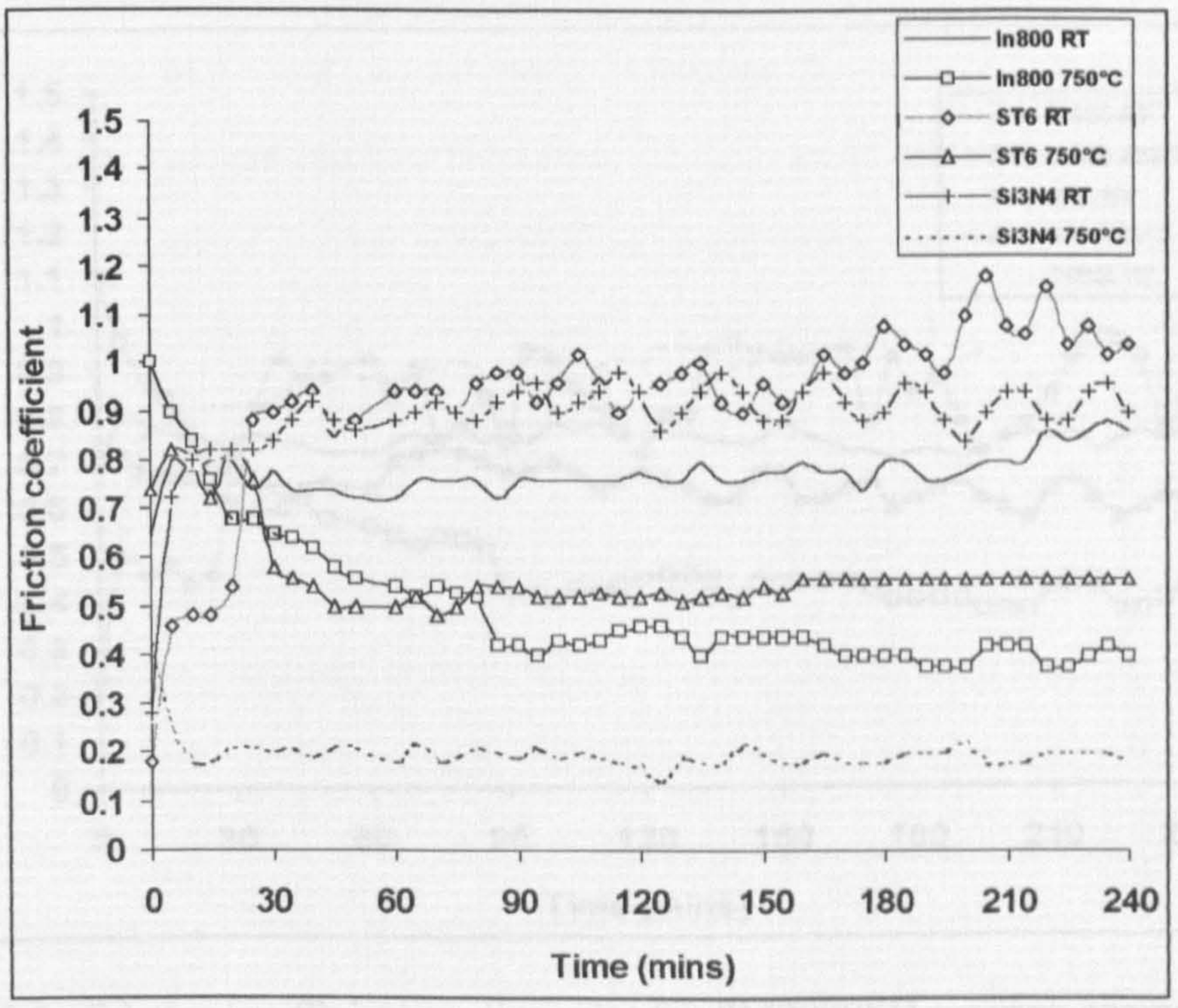

Fig.5.4 Friction coefficient vs. time plot for Ma956 wearing against various counterfaces at room temperature and 750°C

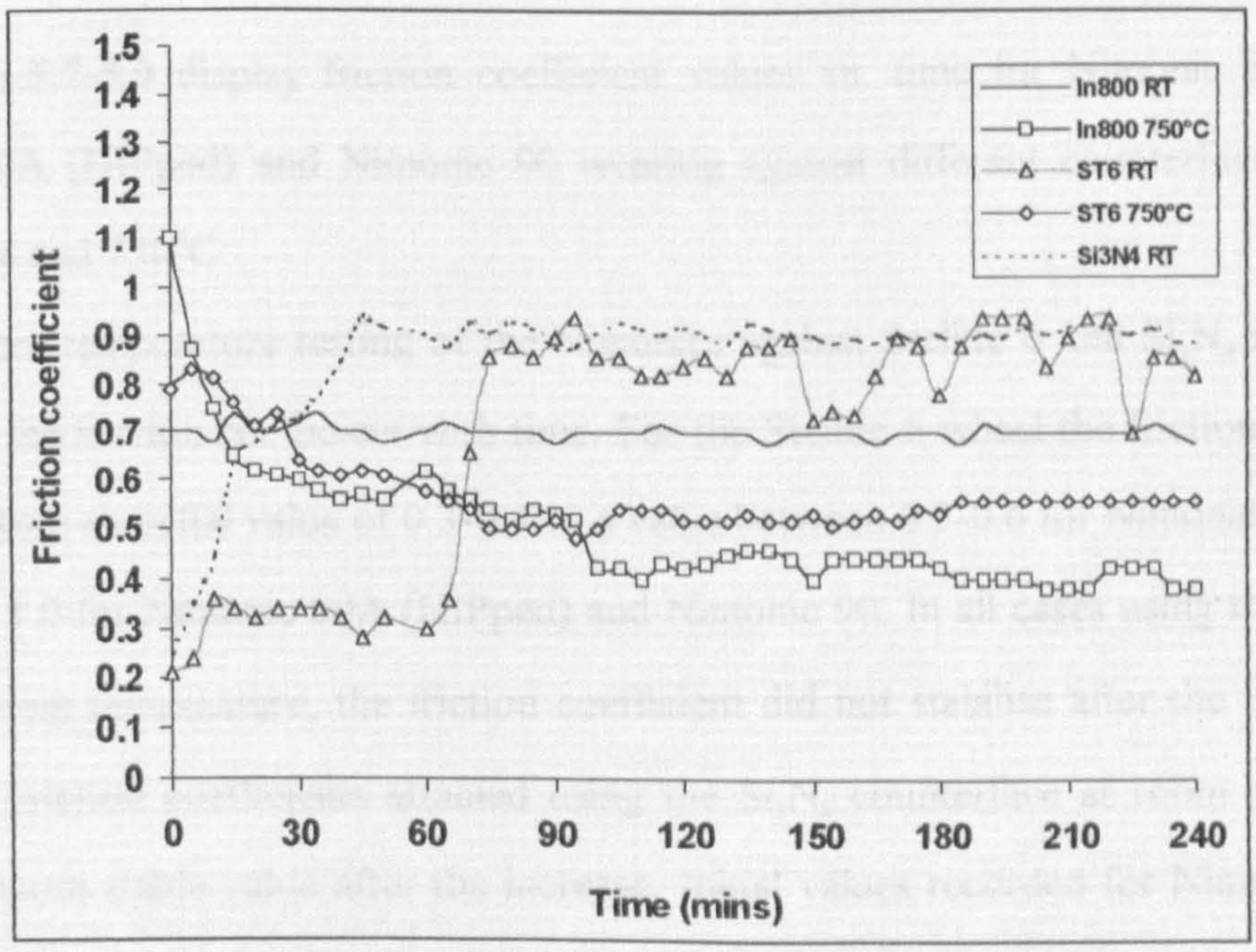

Fig.5.5 Friction coefficient vs. time plot for PM2000 wearing against different counterfaces at room temperature and 750°C

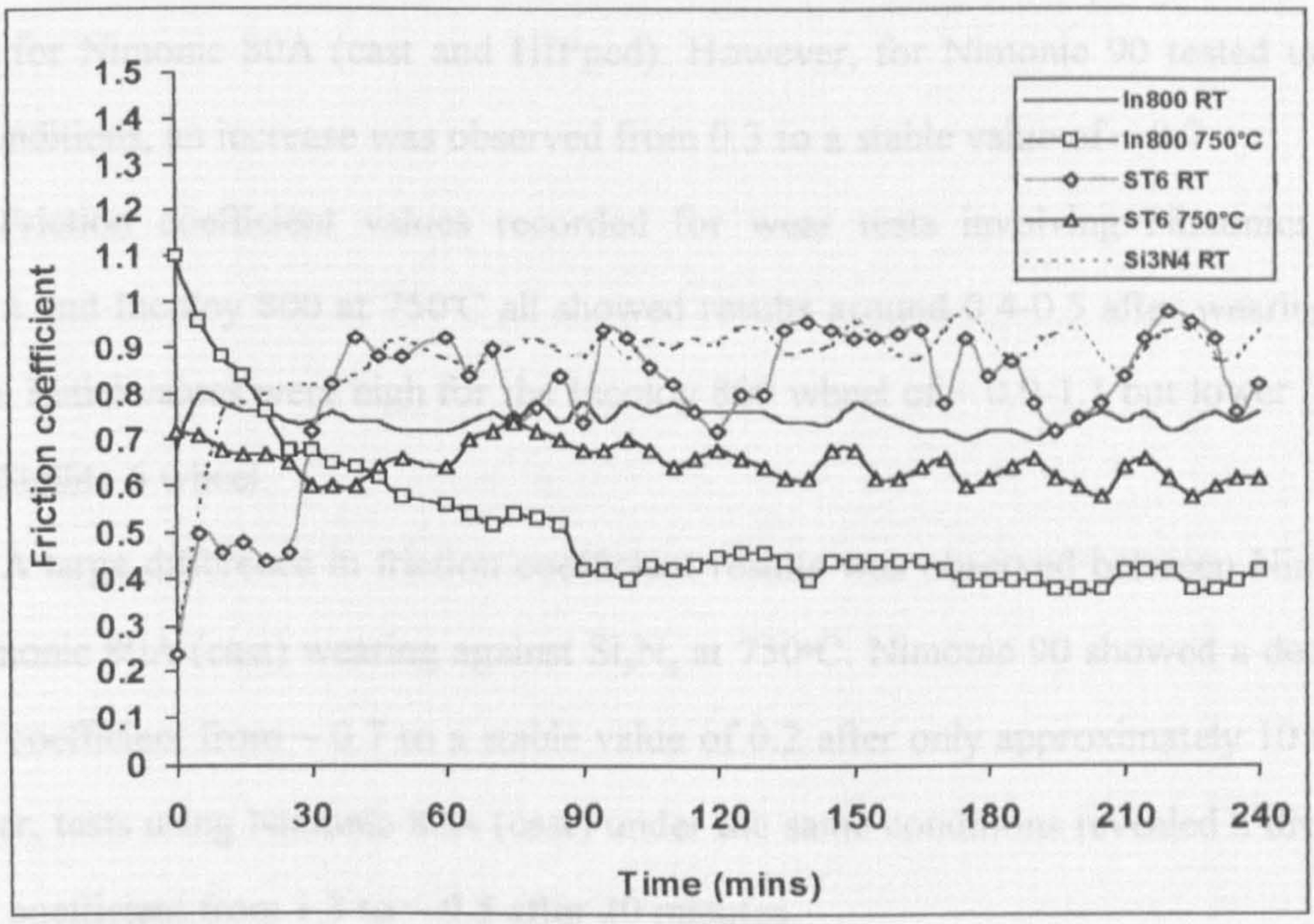

Fig.5.6 Friction coefficient vs. time plot for PM2000SD wearing against different counterfaces at room temperature and 750°C

Figs.5.7-5.9 display friction coefficient values vs. time for Nimonic 80A (cast), Nimonic 80A (HIPped) and Nimonic 90 wearing against different counterfaces at room temperature and 750°C.

Room temperature testing of the Nimonics against Stellite 6 and Si_3N_4 revealed an increase in the friction coefficient with time. For the Stellite 6 wheel the friction coefficient increased from an initial value of 0.3-0.4 to a value between 0.5-0.6 for Nimonic 80A (cast) and to 0.7-1.0 for Nimonic 80A (HIPped) and Nimonic 90. In all cases using the Stellite 6 wheel at room temperature, the friction coefficient did not stabilise after the increase but oscillated. Friction coefficients attained using the Si_3N_4 counterface at room temperature showed a more stable value after the increase. Initial values recorded for Nimonic 90 and Nimonic 80A were between 0.3-0.5 increasing to a value of 0.9-1.0.

Measurements made during wear testing using the Incoloy 800 wheel at room temperature against the Nimonics, showed a steady friction coefficient of ~ 0.9 throughout

the test for Nimonic 80A (cast and HIPped). However, for Nimonic 90 tested under the same conditions, an increase was observed from 0.3 to a stable value of ~ 0.7.

Friction coefficient values recorded for wear tests involving Nimonics against Stellite 6 and Incoloy 800 at 750°C all showed results around 0.4-0.5 after wearing for 30 minutes. Initial values were high for the Incoloy 800 wheel of ~ 0.9-1.1 but lower (0.5-0.7) for the Stellite 6 wheel.

A large difference in friction coefficient results was observed between Nimonic 90 and Nimonic 80A (cast) wearing against Si_3N_4 at 750°C. Nimonic 90 showed a decrease in friction coefficient from ~ 0.7 to a stable value of 0.2 after only approximately 10 minutes. However, tests using Nimonic 80A (cast) under the same conditions revealed a drop in the friction coefficient from 1.3 to ~ 0.5 after 30 minutes.

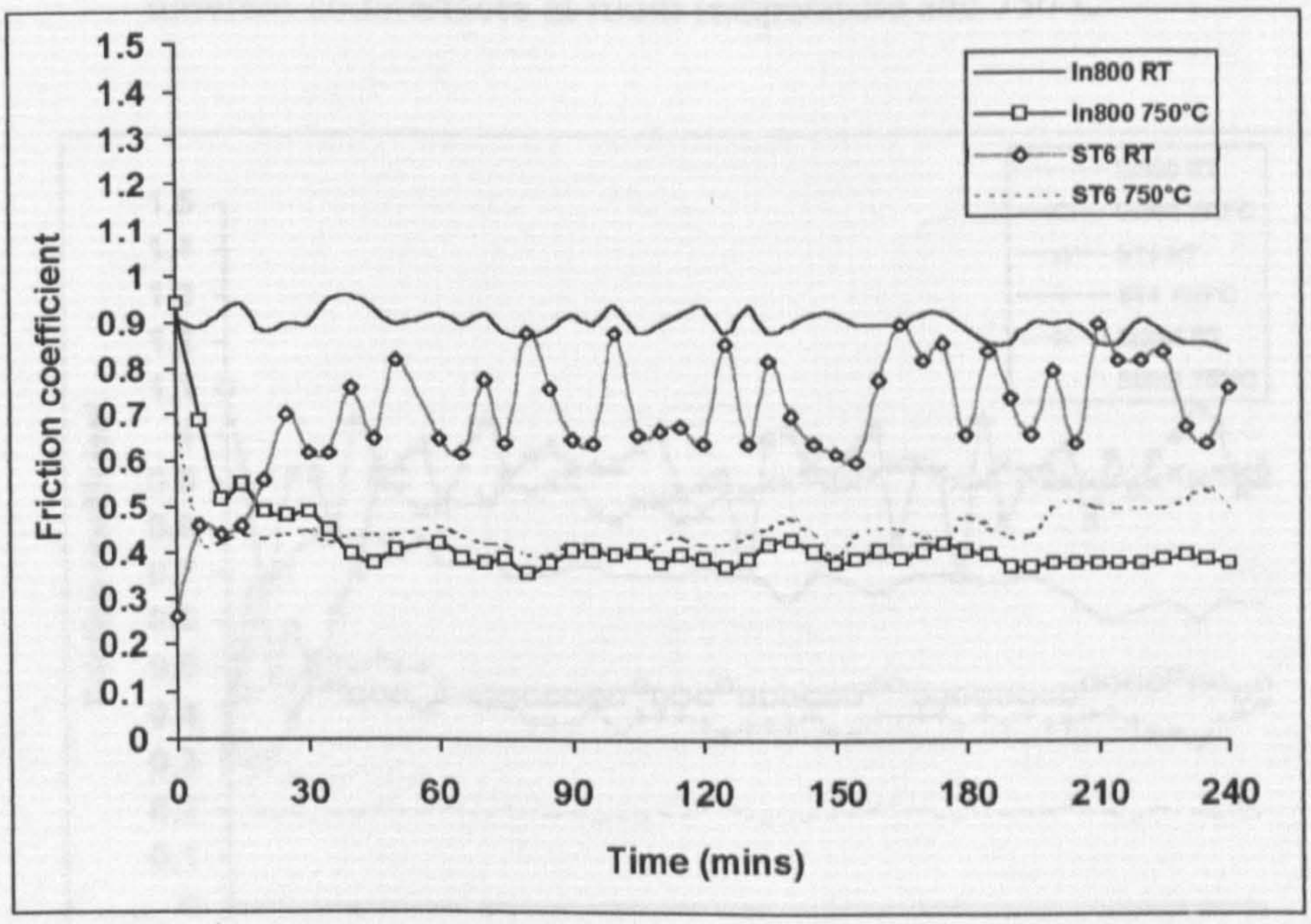

Fig.5.7 Friction coefficient vs. time for Nimonic 80A (HIPped) wearing against different counterfaces at room temperature and 750°C

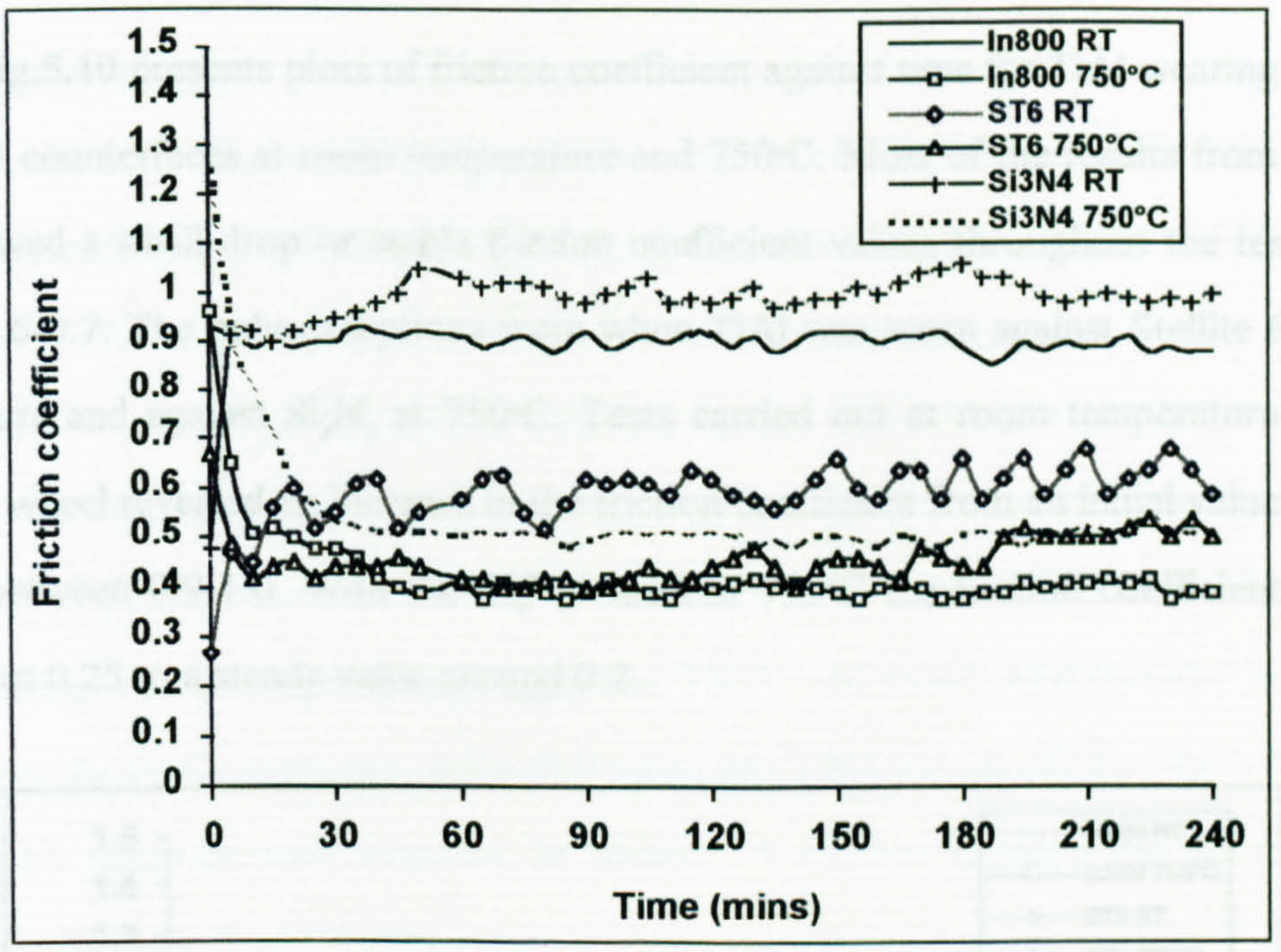

Fig.5.8 Friction coefficient vs. time plot for Nimonic 80A (cast) wearing against different counterfaces at room temperature and 750°C

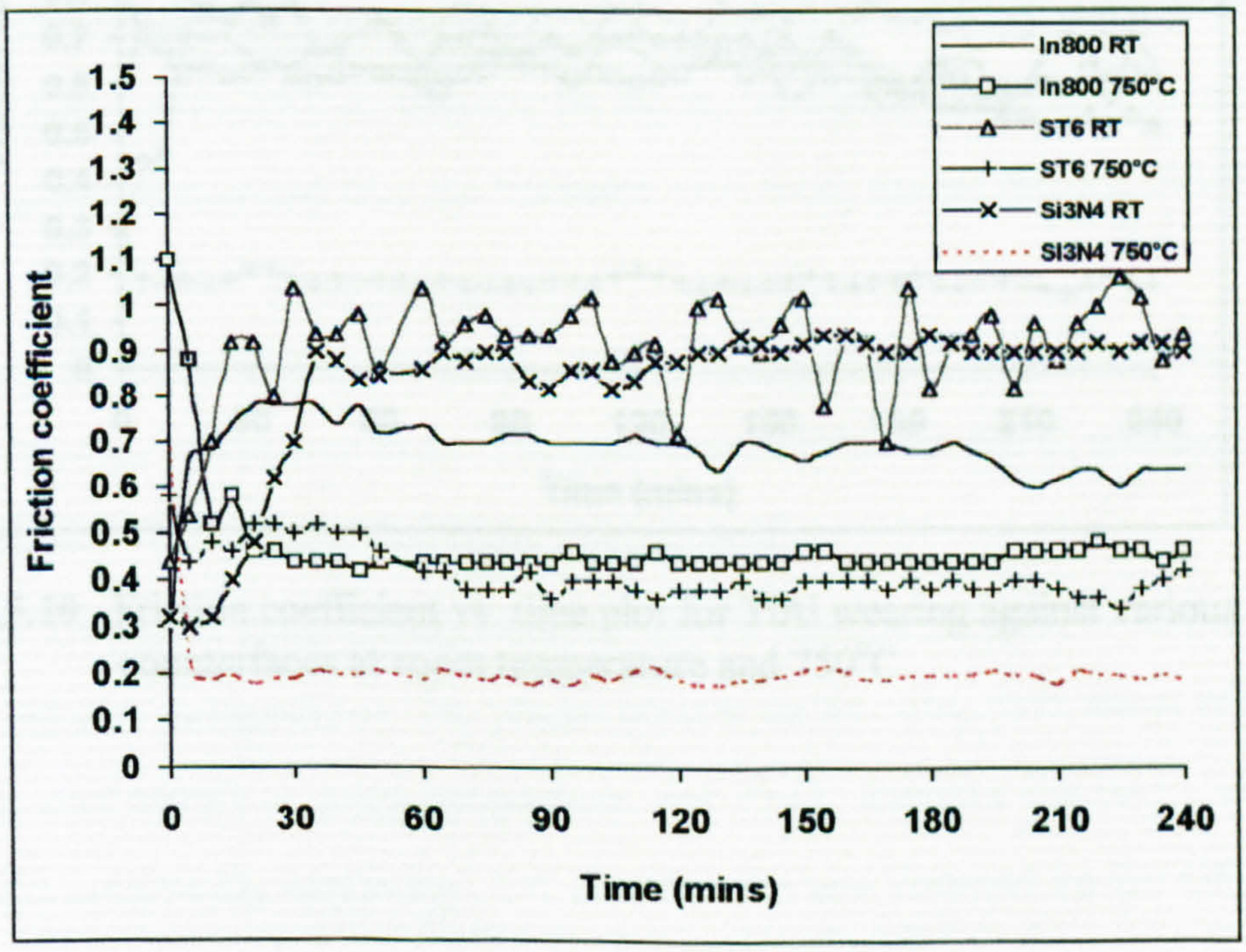

Fig.5.9 Friction coefficient vs. time plot for Nimonic 90 wearing against various counterfaces at room temperature and 750°C

Fig.5.10 presents plots of friction coefficient against time for TiAl wearing against a variety of counterfaces at room temperature and 750°C. Most of the results from the wear tests showed a small drop or stable friction coefficient values throughout the test varying around 0.6-0.7. The only exceptions were when TiAl was worn against Stellite 6 at room temperature and against Si_3N_4 at 750°C. Tests carried out at room temperature with the Stellite 6 wheel revealed an increase in the friction coefficient from an initial value of 0.3 to a value between 0.9-1.0. With the Si_3N_4 wheel at 750°C the friction coefficient dropped from about 0.25 to a steady value around 0.2.

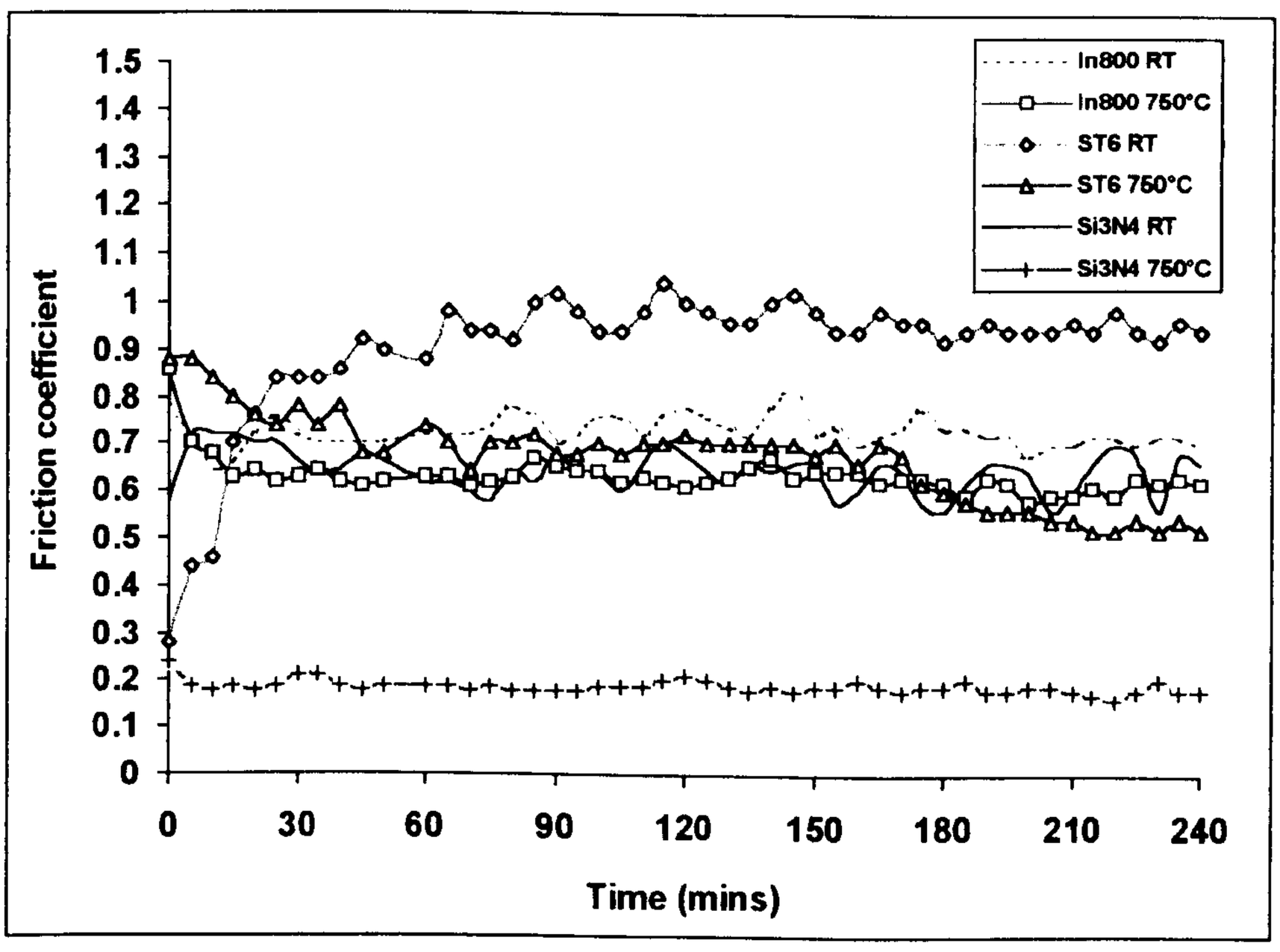

Fig.5.10 Friction coefficient vs. time plot for TiAl wearing against various counterfaces at room temperature and 750°C

Fig.5.10 presents plots of friction coefficient against time for TiAl wearing against a variety of counterfaces at room temperature and 750°C. Most of the results from the wear tests showed a small drop or stable friction coefficient values throughout the test varying around 0.6-0.7. The only exceptions were when TiAl was worn against Stellite 6 at room temperature and against Si_3N_4 at 750°C. Tests carried out at room temperature with the Stellite 6 wheel revealed an increase in the friction coefficient from an initial value of 0.3 to a value between 0.9-1.0. With the Si_3N_4 wheel at 750°C the friction coefficient dropped from about 0.25 to a steady value around 0.2.

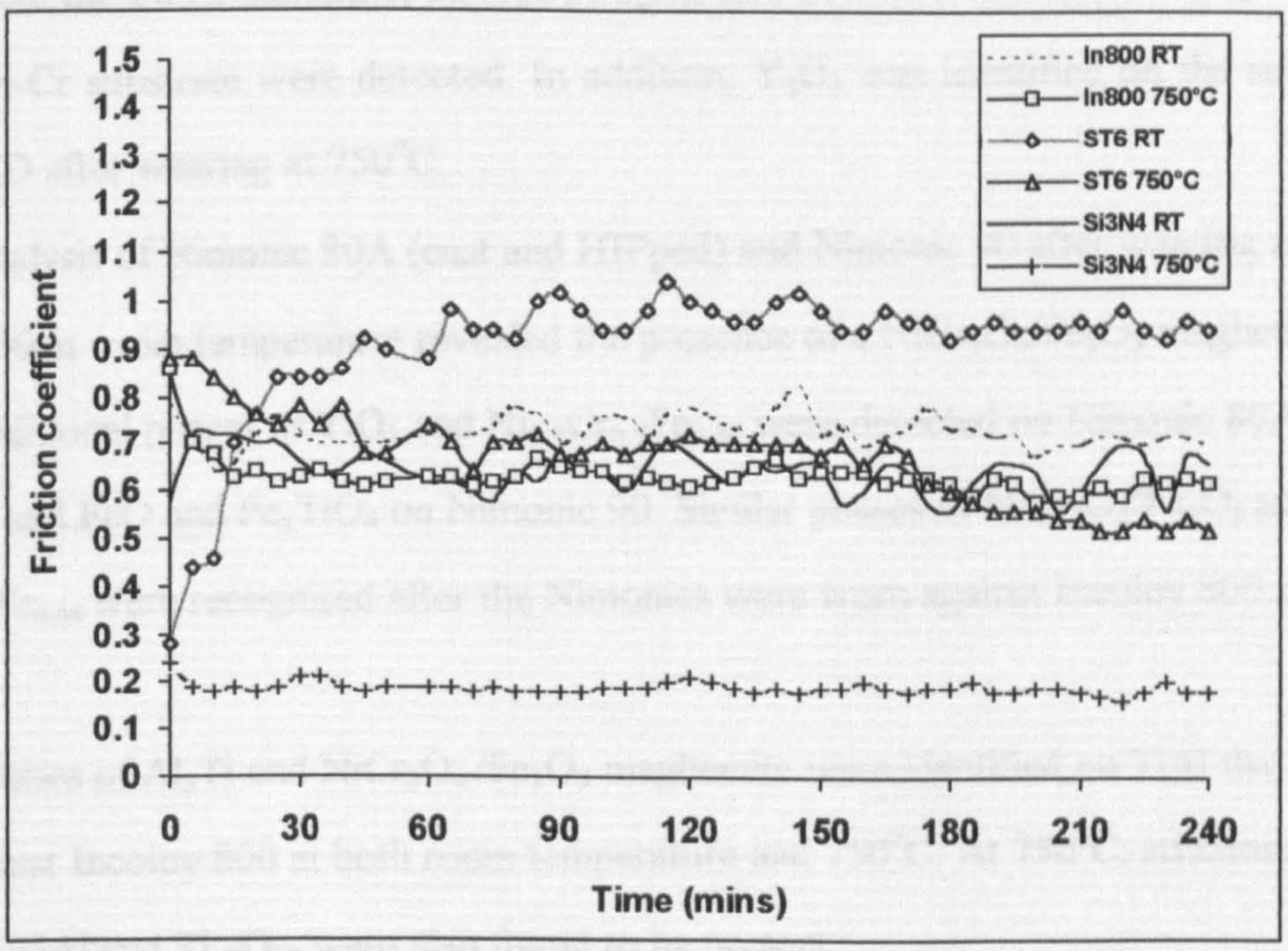

Fig.5.10 Friction coefficient vs. time plot for TiAl wearing against various counterfaces at room temperature and 750°C

5.3.3 XRD Analysis

One difficulty that arose during XRD analysis was that some of the phases had nearly identical diffraction patterns to one another and it was not possible to distinguish between them. Therefore in these cases both phases were given.

Table 5.3 presents the phases detected by the XRD analyses performed on the surfaces of the block alloys after wearing against Incoloy 800 at room temperature and 750°C. Similar phases were detected on Ma956, PM2000 and PM2000SD when worn against Incoloy 800 at room temperature and 750°C. At room temperature the phases present were the Fe-Cr substrate, $NiCr_2O_4/Fe_2O_3$, and FeO and at 750°C, Cr_2O_3 eskolaite and the Fe-Cr substrate were detected. In addition, Y_2O_3 was identified on the surface of PM2000SD after wearing at 750°C.

Analysis of Nimonic 80A (cast and HIPped) and Nimonic 90 after wearing against Incoloy 800 at room temperature revealed the presence of a $NiCr_2O_4/Fe_2O_3$ maghemite phase. Additional phases of TiO_2 and $Ni_{2.9}Cr_{0.7}Fe_{0.36}$ were detected on Nimonic 80A (HIPped) and FeO and Fe_2TiO_4 on Nimonic 90. Similar phases of $NiCr_2O_4/Fe_2O_3$ and $Ni_{2.9}Cr_{0.7}Fe_{0.36}$ were recognised after the Nimonics were worn against Incoloy 800 at 750°C.

Phases of Al_3Ti and $NiCr_2O_4/Fe_2O_3$ maghemite were identified on TiAl that had worn against Incoloy 800 at both room temperature and 750°C. At 750°C, additional phases of TiAl and $Ti_{10}O_{19}$ were also found to be present.

Table 5.4 shows XRD phases detected on the block alloys after wearing against Stellite 6 at different temperatures. The phases present on the worn ODS alloys of Ma956, PM2000 and PM2000SD at room temperature and 750°C included the Fe-Cr substrate, Y_2O_3, and $CoCr_2O_4/Fe_2O_3$ maghemite. $Cr_{1.3}Fe_{0.7}O_3$ was also detected on the ODS alloys after wearing at 750°C.

Table 5.3 XRD analysis of the surface of the block alloys after wearing against Incoloy 800 at room temperature and 750°C

Alloy	Phase detected by XRD	
	RT wear test	750°C wear test
MA956	$NiCr_2O_4/Fe_2O_3$ maghemite, FeO, Fe-Cr substrate	Cr_2O_3 eskolaite, Fe-Cr substrate
PM2000	$NiCr_2O_4/Fe_2O_3$ maghemite, FeO, Fe-Cr substrate	Cr_2O_3 eskolaite, Fe-Cr substrate
PM2000SD	$NiCr_2O_4/Fe_2O_3$ maghemite, FeO, Fe-Cr substrate	Cr_2O_3 eskolaite, Fe-Cr substrate, Y_2O_3
Nimonic 90	$NiCr_2O_4/Fe_2O_3$ maghemite, FeO Fe_2TiO_4 ulvospinel	$Ni_{2.9}Cr_{0.7}Fe_{0.36}$, $NiCr_2O_4/Fe_2O_3$ maghemite
Nimonic 80A (cast)	$Ni_{2.9}Cr_{0.7}Fe_{0.36}$, TiO_2 rutile, $NiCr_2O_4/Fe_2O_3$ maghemite	$Ni_{2.9}Cr_{0.7}Fe_{0.36}$, $NiCr_2O_4/Fe_2O_3$ maghemite
Nimonic 80A (HIPped)	$NiCr_2O_4/Fe_2O_3$ maghemite	$Ni_{2.9}Cr_{0.7}Fe_{0.36}$, $NiCr_2O_4/Fe_2O_3$ maghemite
TiAl	Al_3Ti, $NiCr_2O_4/Fe_2O_3$ maghemite	Al_3Ti, $NiCr_2O_4/Fe_2O_3$ maghemite, AlTi, $Ti_{10}O_{19}$

Table 5.4 XRD analysis of the surface of the block alloys after wearing against Stellite 6 at room temperature and 750°C

Alloy	Phase detected by XRD	
	RT wear test	750°C wear test
MA956	Fe-Cr substrate, Y_2O_3 yttria, Fe_2O_3 maghemite /$CoCr_2O_4$	Fe-Cr substrate, $Cr_{1.3}Fe_{0.7}O_3$, Y_2O_3 yttria, Fe_2O_3 maghemite /$CoCr_2O_4$
PM2000	Fe-Cr substrate, Y_2O_3 yttria, Fe_2O_3 maghemite /$CoCr_2O_4$	Fe-Cr substrate, $Cr_{1.3}Fe_{0.7}O_3$, Y_2O_3 yttria, Fe_2O_3 maghemite /$CoCr_2O_4$
PM2000SD	Fe-Cr substrate, Y_2O_3 yttria, Fe_2O_3 maghemite /$CoCr_2O_4$	Fe-Cr substrate, $Cr_{1.3}Fe_{0.7}O_3$, Y_2O_3 yttria, Fe_2O_3 maghemite /$CoCr_2O_4$
Nimonic 90	$Ni_{2.9}Cr_{0.7}Fe_{0.36}$	$Ni_{2.9}Cr_{0.7}Fe_{0.36}$, $NiCr_2O_4$/$CoCr_2O_4$
Nimonic 80A (cast)	$Ni_{2.9}Cr_{0.7}Fe_{0.36}$	$Ni_{2.9}Cr_{0.7}Fe_{0.36}$, $NiCr_2O_4$/$CoCr_2O_4$
Nimonic 80A (HIPped)	$Ni_{2.9}Cr_{0.7}Fe_{0.36}$	$Ni_{2.9}Cr_{0.7}Fe_{0.36}$, $NiCr_2O_4$/$CoCr_2O_4$
TiAl	Al_3Ti, AlTi, $CoCr_2O_4$,	Al_3Ti, AlTi, $CoCr_2O_4$

Analysis of the Nimonics after wearing against Stellite 6 at room temperature revealed only the substrate phase of $Ni_{2.9}Cr_{0.7}Fe_{0.36}$. In addition to this phase, $NiCr_2O_4/CoCr_2O_4$ was found to be present after the 750°C test.

Al_3Ti, AlTi and $CoCr_2O_4$ were detected on TiAl worn against Stellite 6 both at room temperature and 750°C.

Table 5.5 presents phases detected by XRD on block alloys worn against Si_3N_4 at room temperature and 750°C. For nearly all of the worn samples the only phase identified was the substrate. However, for Nimonic 80A (cast) and Nimonic 90 after wearing against the Si_3N_4 counterface at room temperature, a $NiCr_2O_4$ phase was identified on both materials. This phase was also present on Nimonic 80A (cast) after wearing against Si_3N_4 at 750°C.

Table 5.5 XRD analysis of the surface of the block alloys after wearing against Si_3N_4 at room temperature and 750°C

Alloy	Phase detected by XRD	
	RT wear test	750°C wear test
MA956	Fe-Cr substrate	Fe-Cr substrate
PM2000	Fe-Cr substrate	-
PM2000SD	Fe-Cr substrate	-
Nimonic 90	$Ni_{2.9}Cr_{0.7}Fe_{0.36}$, $CoCr_2O_4/NiCr_2O_4$	$Ni_{2.9}Cr_{0.7}Fe_{0.36}$
Nimonic 80A (cast)	$Ni_{2.9}Cr_{0.7}Fe_{0.36}$, $NiCr_2O_4$	$Ni_{2.9}Cr_{0.7}Fe_{0.36}$, $NiCr_2O_4$
TiAl	AlTi, $AlTi_3$	AlTi, $AlTi_3$

5.3.4 SEM Morphological Analysis

SEM micrographs of the worn block alloys are illustrated in **Figs.5.11-5.14**. The morphologies of worn Ma956, PM2000 and PM2000SD were very similar and therefore only micrographs of worn Ma956 are shown in **Fig.5.11**. The micrograph of Ma956 worn against Incoloy 800 at room temperature - displayed in **Fig.5.11a** - revealed the wear scar to be comprised of smooth plateaux made up of flat layers with little or no wear debris present. Testing under the same conditions at 750°C, shown in **Fig.5.11b**., produced a very smooth wear scar without any plateaux but with cracking and spalling in places. Wear testing using a Stellite 6 counterface against Ma956 formed a powder-like morphology at room temperature (see **Fig.5.11c**.) but a surface covered with glazes at 750°C (see **Fig.5.11d**.). Testing using a Si_3N_4 counterface against Ma956 produced a wear scar containing small plateaux at room temperature (**Fig.5.11e**.) but a worn surface covered with a glazes layer of material at 750°C (**Fig.5.11f**).

SEM analysis of worn Nimonic 80A, cast and HIPped, revealed similar surface morphologies and results for Nimonic 80A (cast) are only presented. **Fig.5.12a**. shows a micrograph of Nimonic 80A (cast) after wearing against Incoloy 800 at room temperature revealing a wear scar comprised of plateaux with very little, if any, wear debris present at room temperature. However, testing under the same conditions at 750°C produced a glazed surface (**Fig.5.12b**.) with wear debris present in the hollows.

Micrographs of Nimonic 80A (cast) after being worn against Stellite 6, illustrated in **Fig.5.12c**., show a powder-like appearance of the wear scar at room temperature testing but a heavily scarred surface at 750°C (**Fig.5.12d**). Observations, after wearing against a Si_3N_4 counterface (**Fig.5.12e**) showed the surface of Nimonic 80A (cast) to be comprised of a thin powder-like layer at room temperature testing. Testing under similar conditions at 750°C (**Fig.5.12f**.) produced a wear scar on Nimonic 80A (cast) that was heavily grooved with plateaux not being present.

The micrographs of Nimonic 80A (cast) worn against different counterfaces were also very similar to the micrographs of Nimonic 90 worn under similar conditions, presented in **Fig.5.13**. The morphologies, however, differed only when tested at 750°C against the Si_3N_4 . Under these conditions a heavily scarred region was produced on Nimonic 80A (cast) but a region of small glazes on top of a scarred surface was observed on the Nimonic 90 sample as shown in **Fig.5.13f**.

The SEM micrographs of TiAl tested against various counterfaces are presented in **Fig.5.14**. The surface of the TiAl worn against Incoloy 800 at room temperature (**Fig.5.14a**) was characterised by flat plateaux comprised of layers of material, with little or no wear debris being observed in the hollows. However, when the same combination of materials was worn at 750°C, glaze formation was observed (see **Fig.5.14b**).

The micrographs of TiAl after wearing against Stellite 6, shown in **Fig.5.14c**, revealed a powder-like wear scar surface after testing at room temperature. However, the TiAl tested at 750°C under the same conditions produced a wear surface covered in very thin glazes with wear debris observed in the hollows (**Fig.5.14d**). Small plateaux comprised of coarse wear particles were formed on TiAl after wearing against a Si_3N_4 counterface at room temperature (**Fig.5.14e**). However, micrographs (**Fig.5.14f**.) of the same combination wearing at 750°C, revealed the wear scar to be comprised of a smooth glazed layer which was scuffed and worn in places through to the substrate.

Fig.5.11 SEM micrographs of Ma956 worn for 4 hours against:

a - Incoloy 800 counterface at room temperature
b - Incoloy 800 counterface at 750°C
c - Stellite 6 counterface at room temperature
d - Stellite 6 counterface at 750°C
e - Si_3N_4 counterface at room temperature
f - Si_3N_4 counterface at 750°C

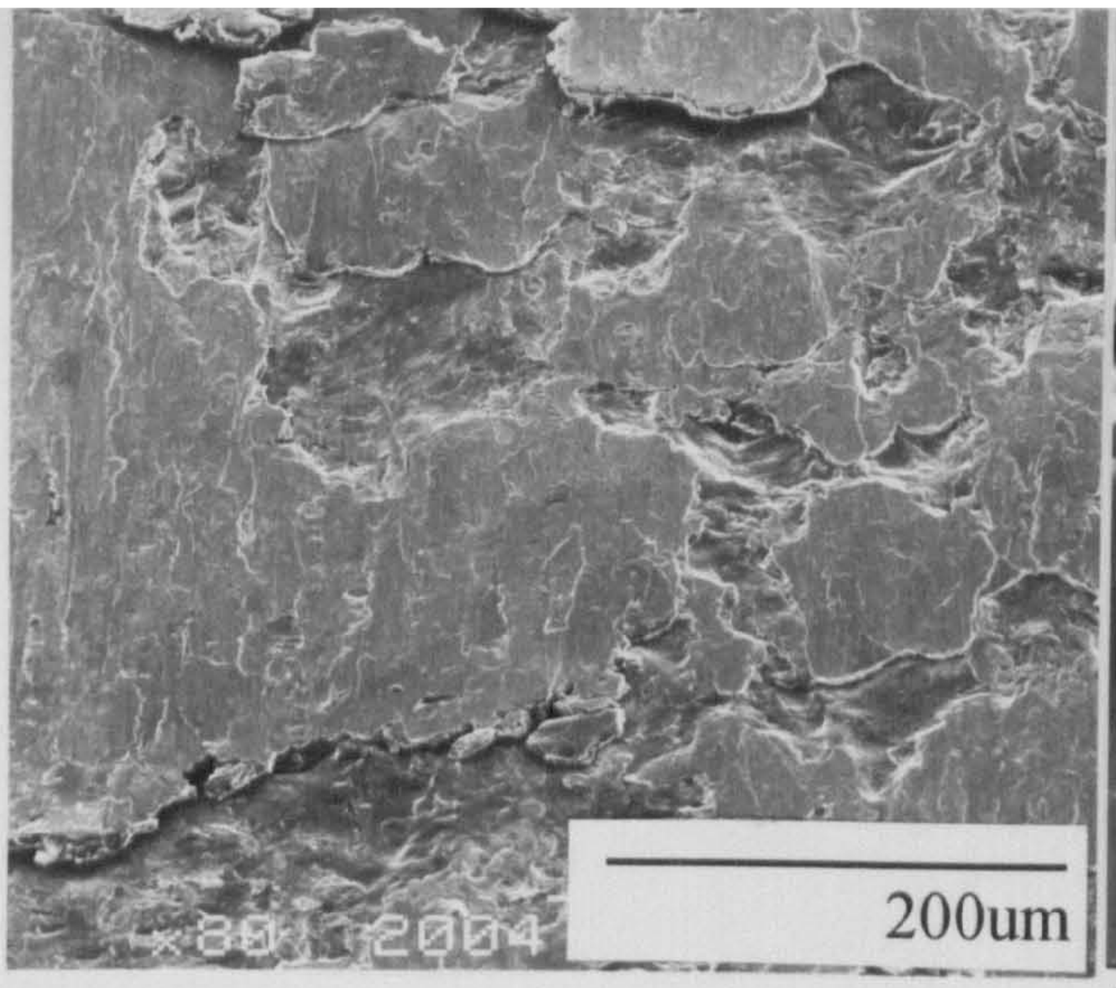

a

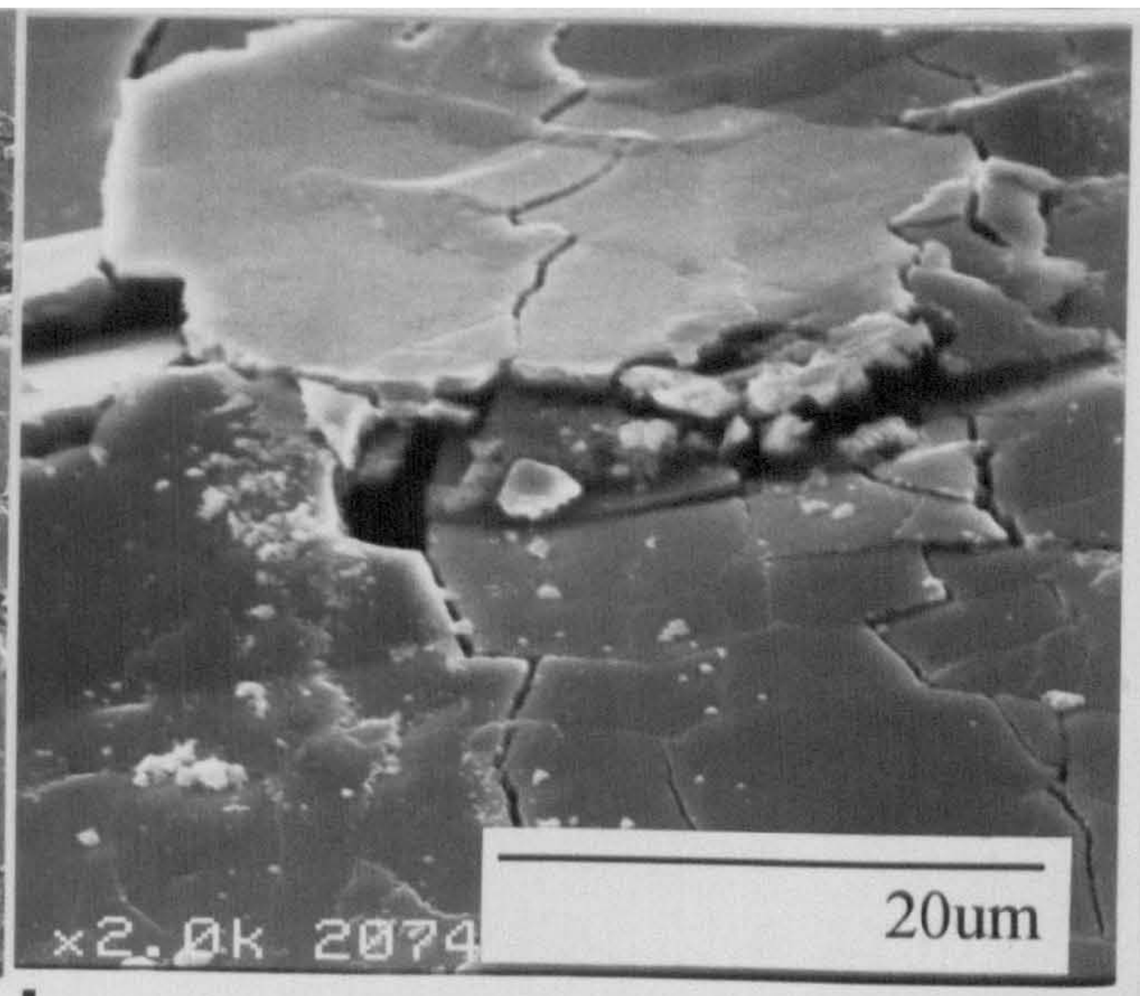

b

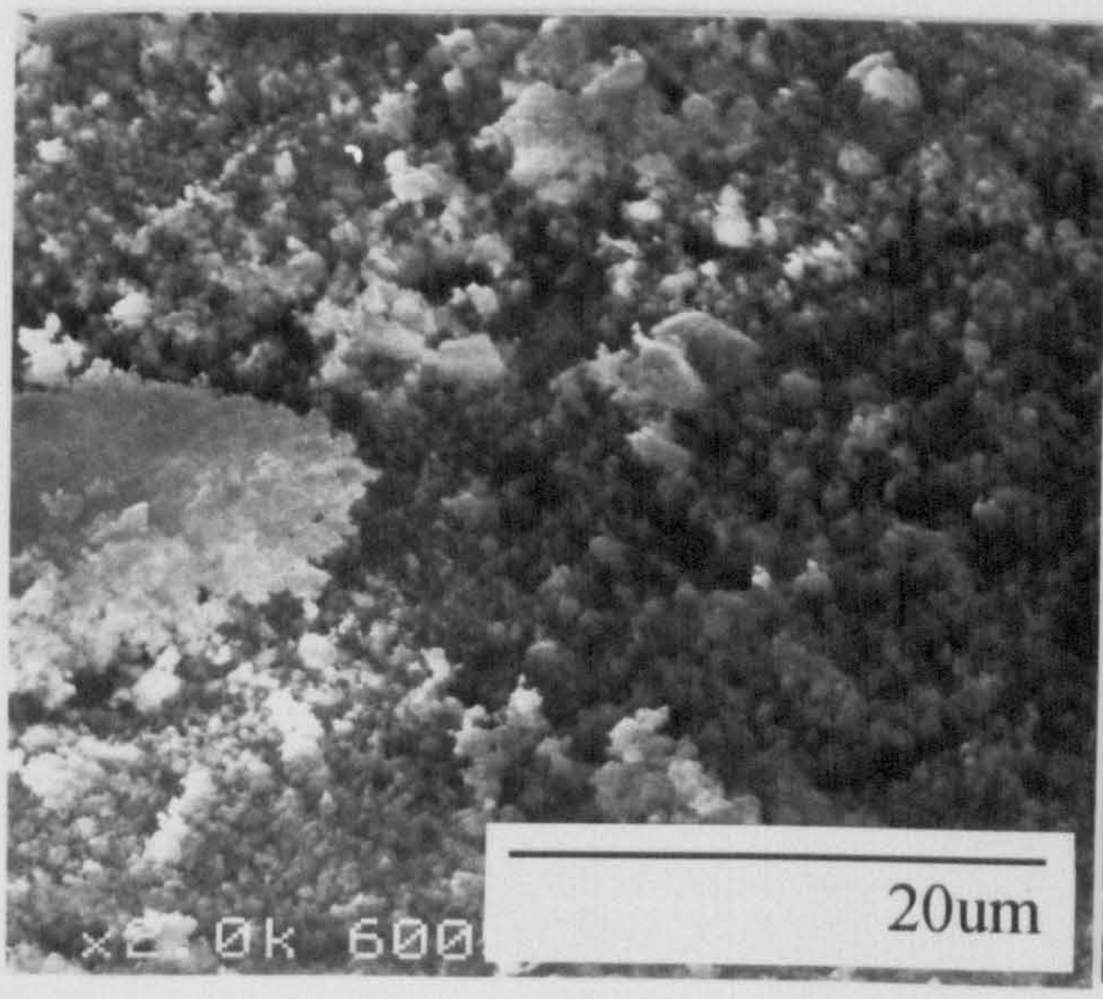

c

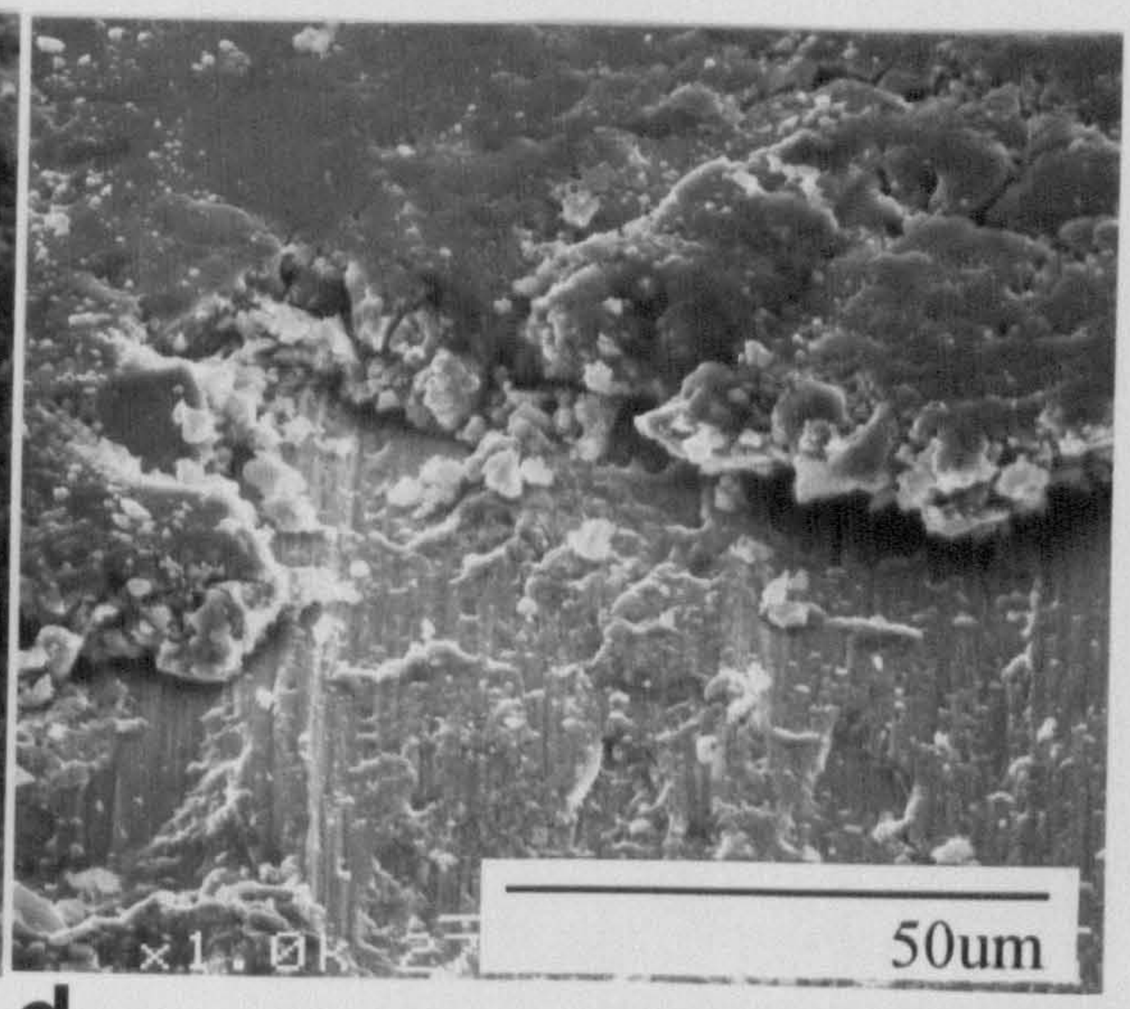

d

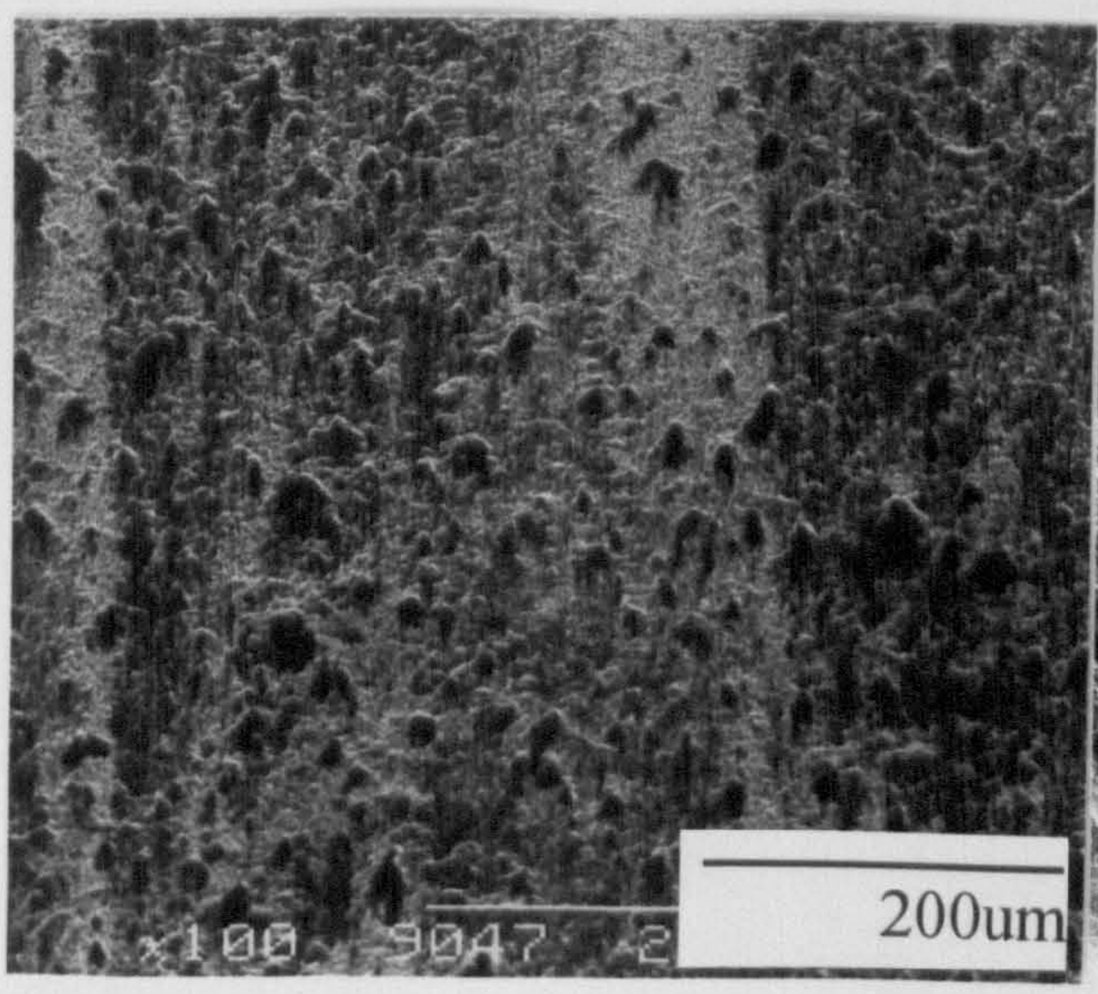

e

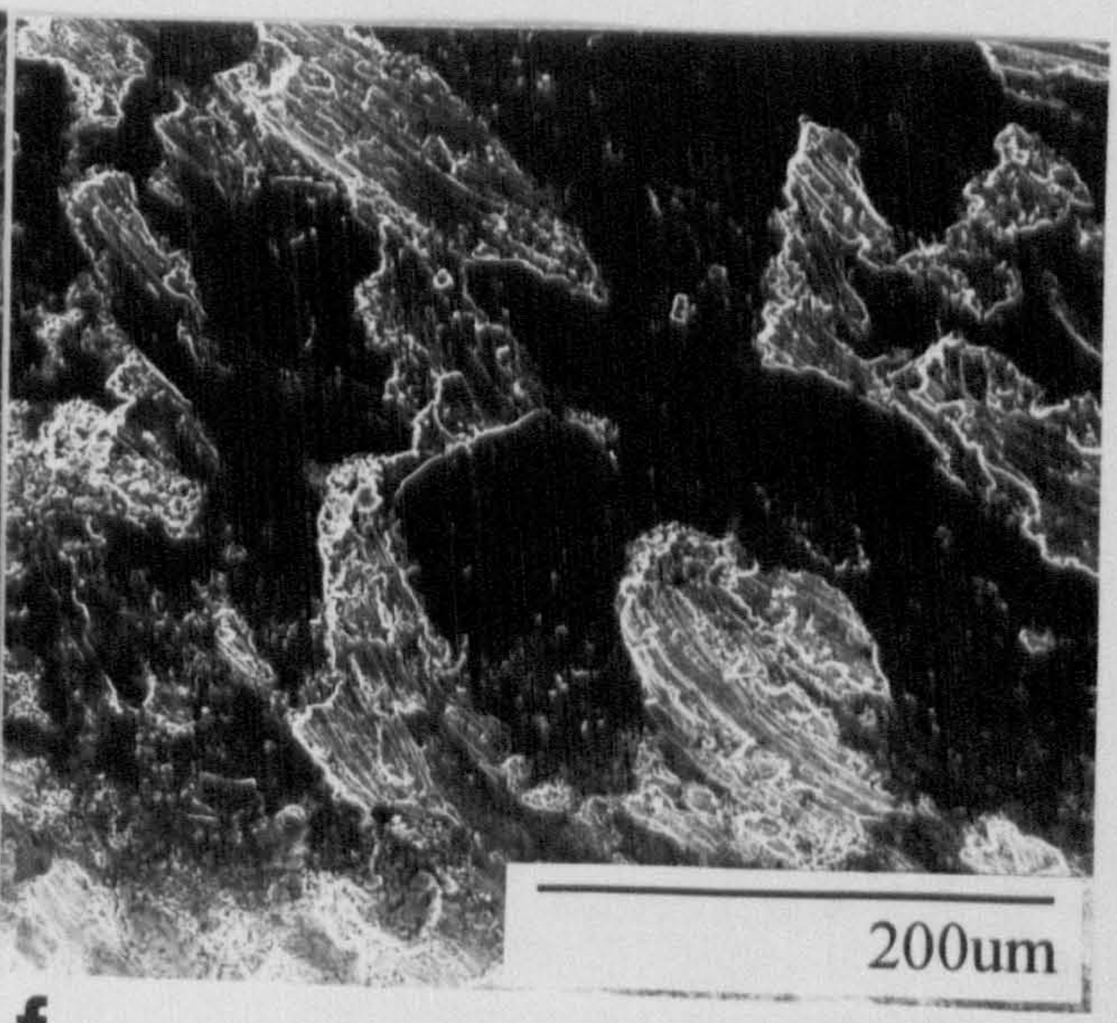

f

Fig.5.12 SEM micrographs of Nimonic 80A (cast) worn for 4 hours **against**:

a - Incoloy 800 counterface at room temperature
b - Incoloy 800 counterface at 750°C
c - Stellite 6 counterface at room temperature
d - Stellite 6 counterface at 750°C
e - Si_3N_4 counterface at room temperature
f - Si_3N_4 counterface at 750°C

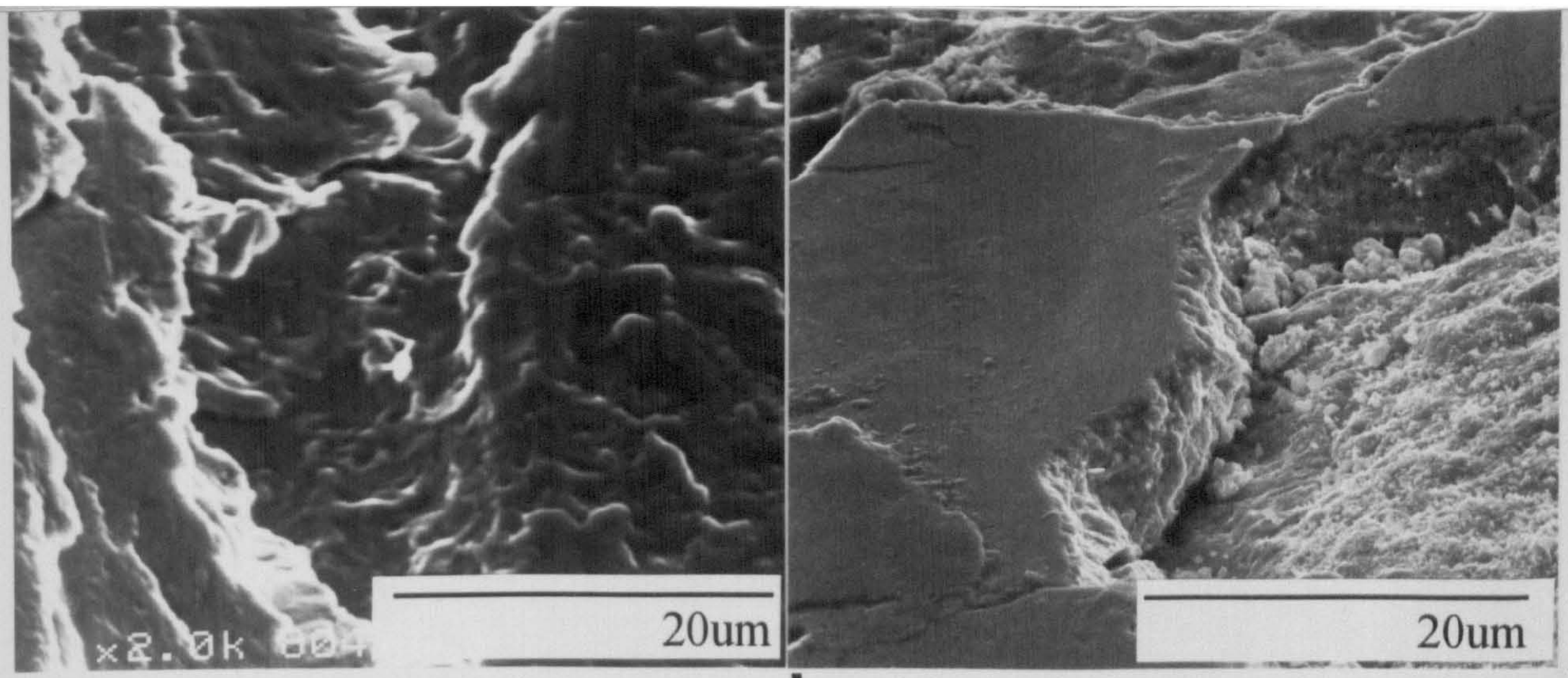

a b

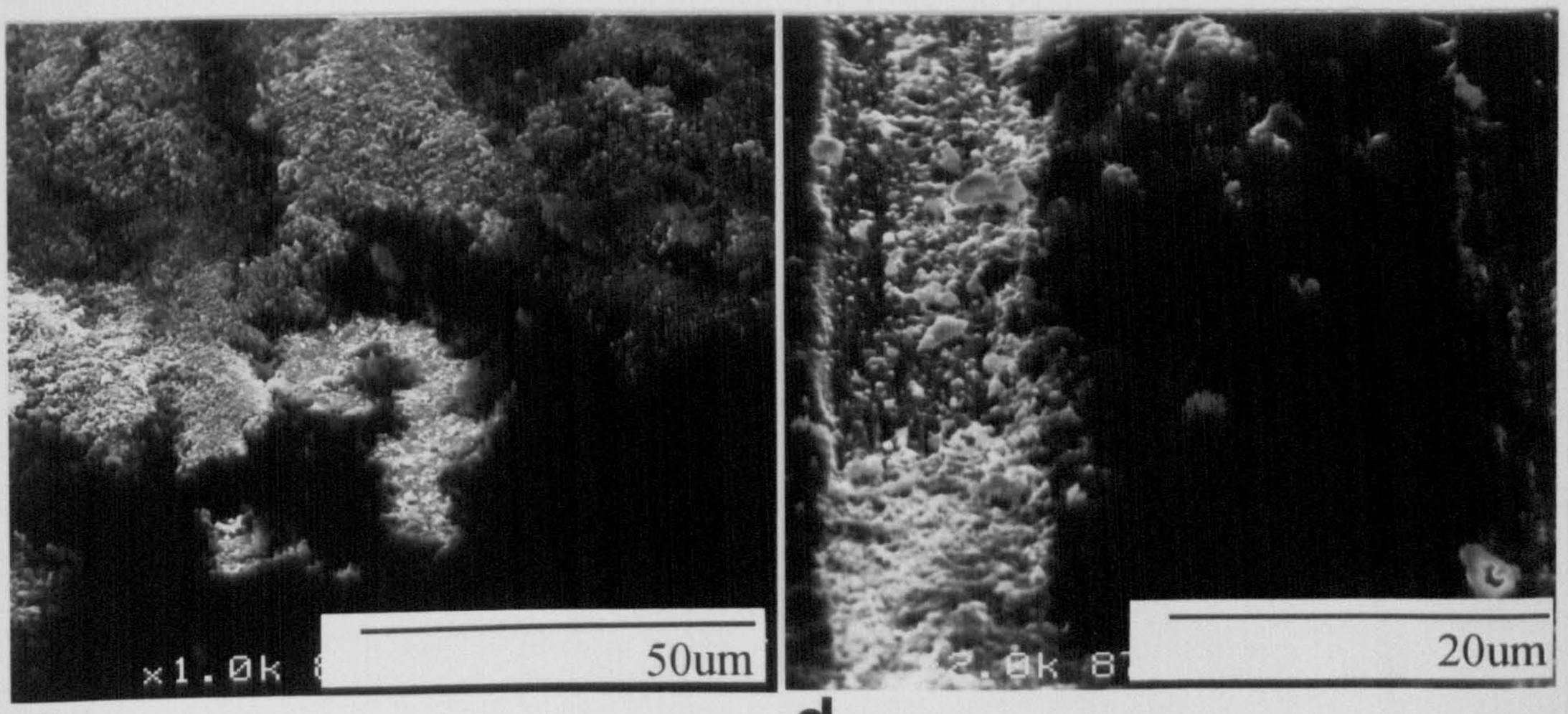

c d

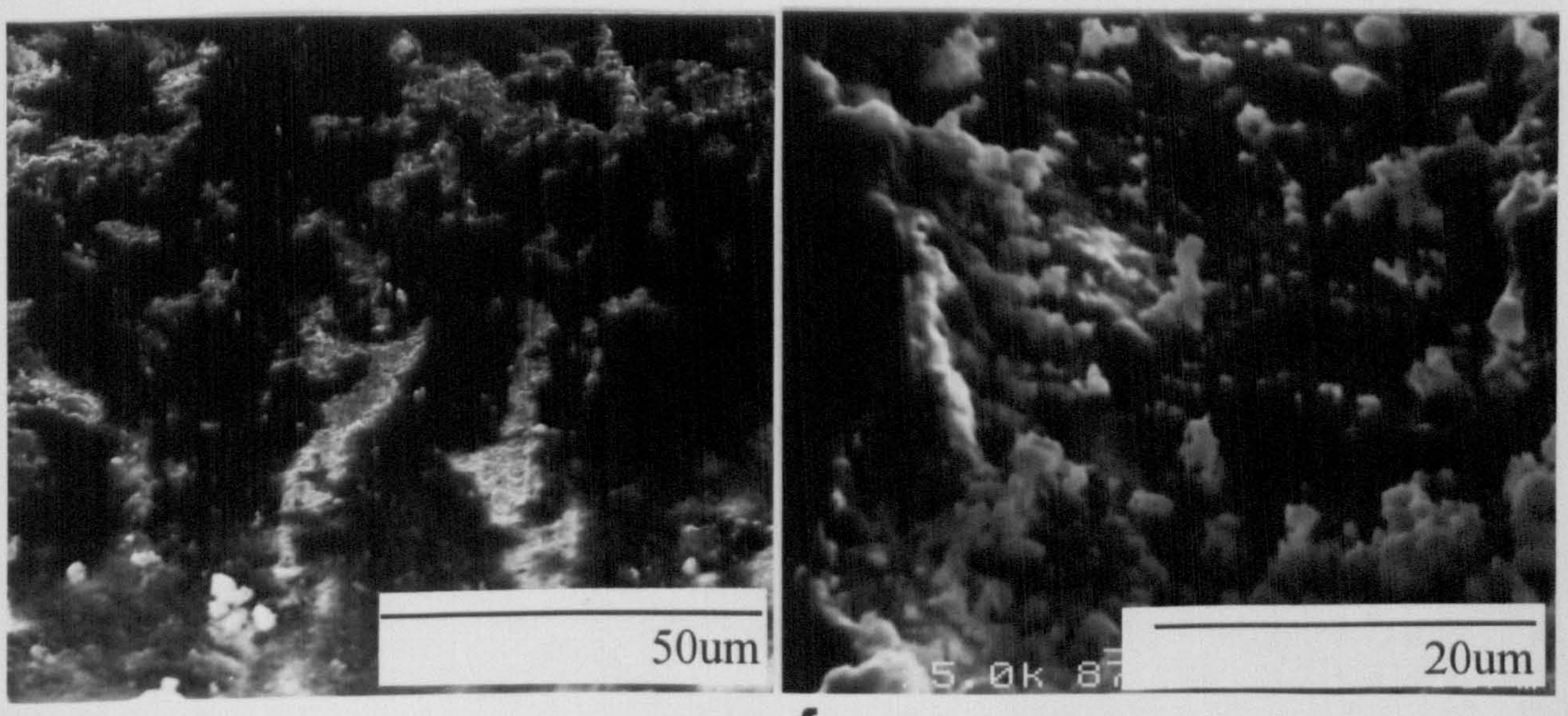

e f

Fig.5.13 SEM micrographs of Nimonic 90 worn for 4 hours against:

a - Incoloy 800 counterface at room temperature
b - Incoloy 800 counterface at 750°C
c - Stellite 6 counterface at room temperature
d - Stellite 6 counterface at 750°C
e - Si_3N_4 counterface at room temperature
f - Si_3N_4 counterface at 750°C

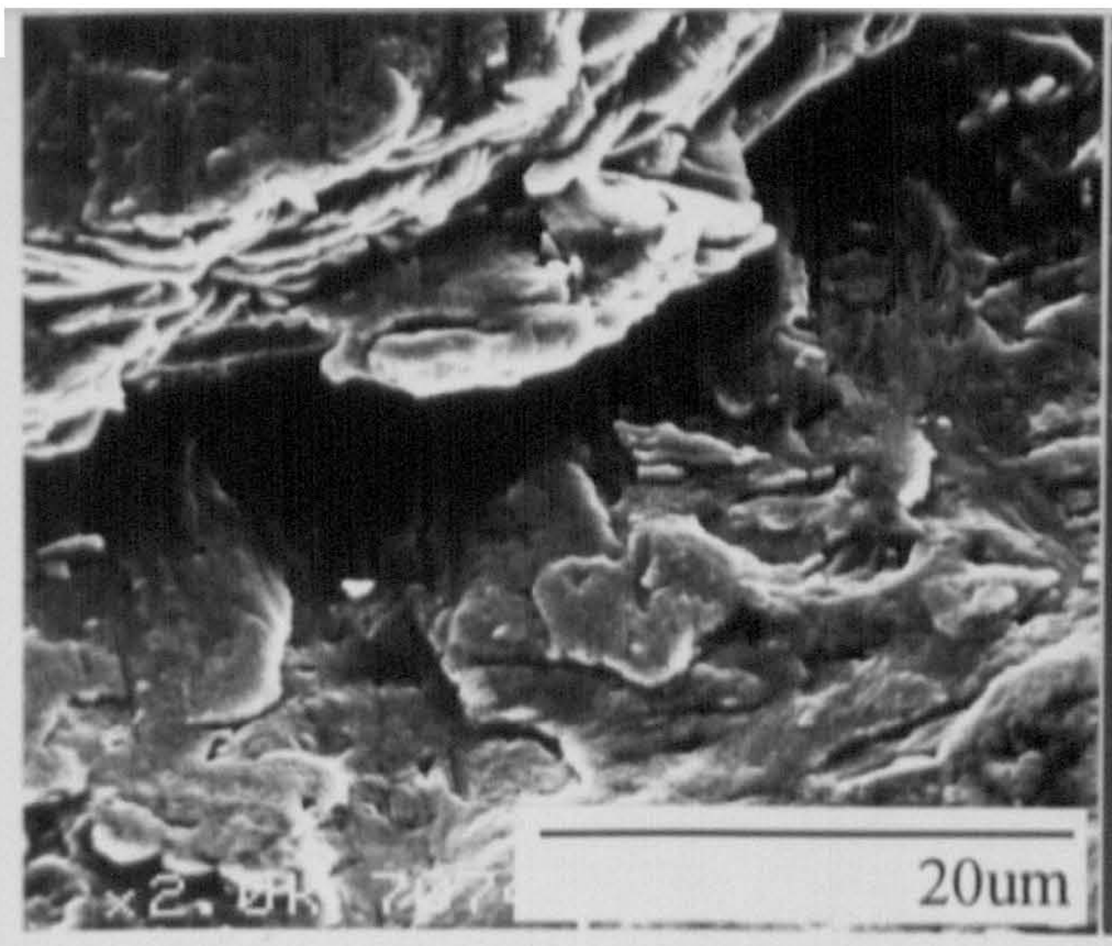

a

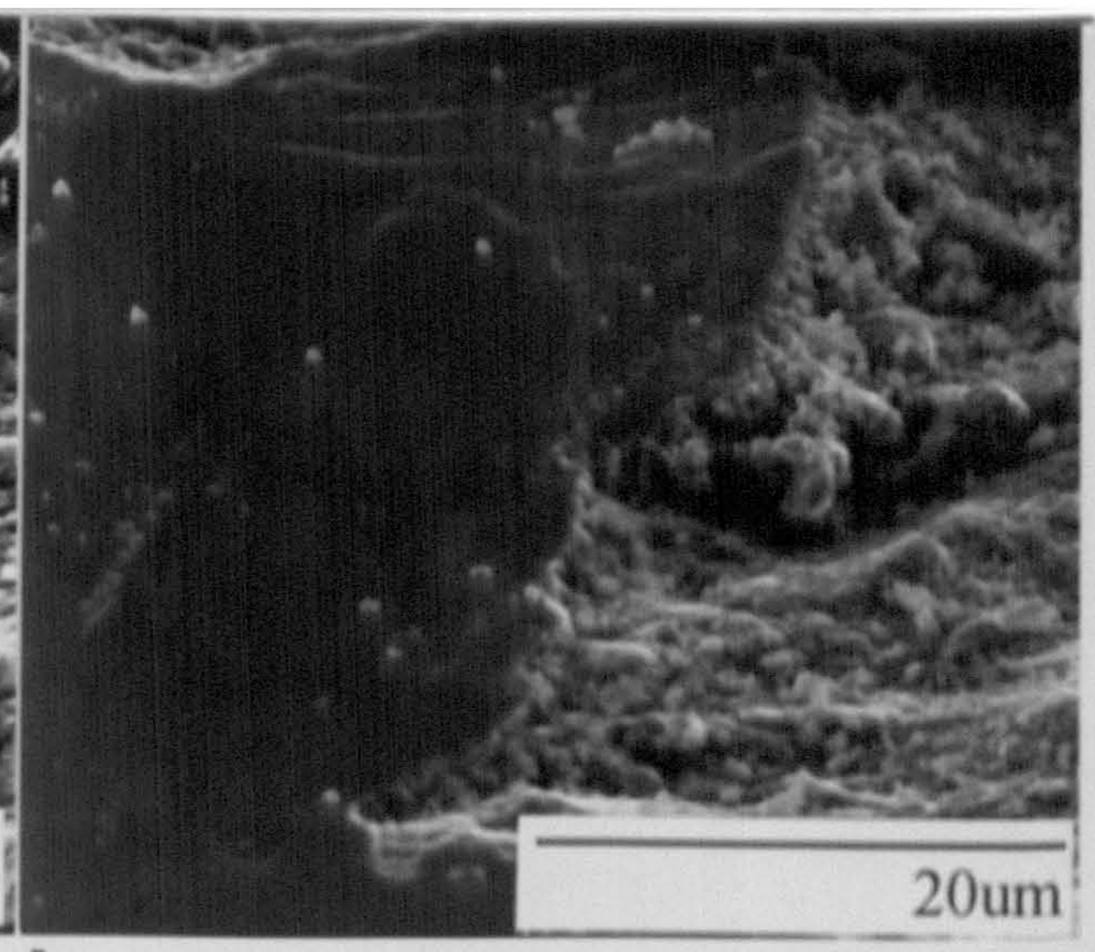

b

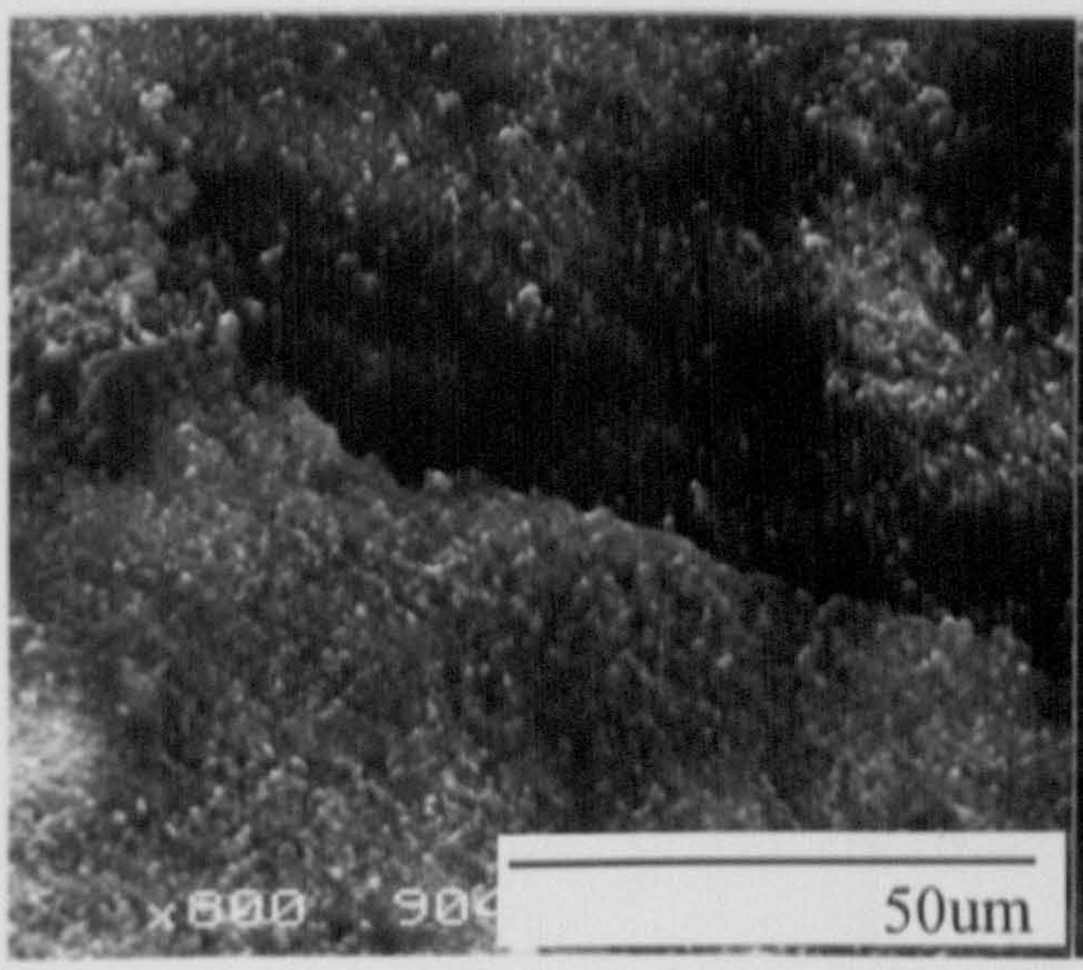

c

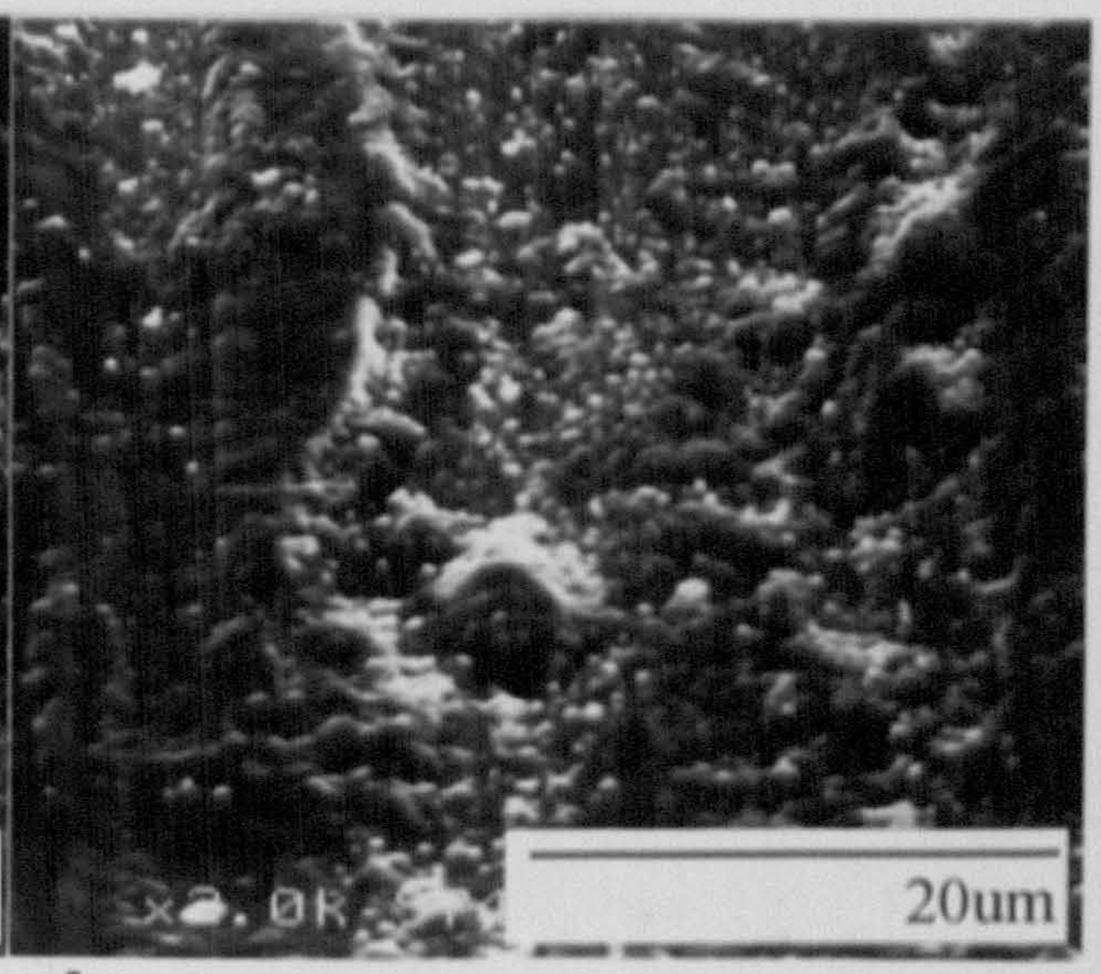

d

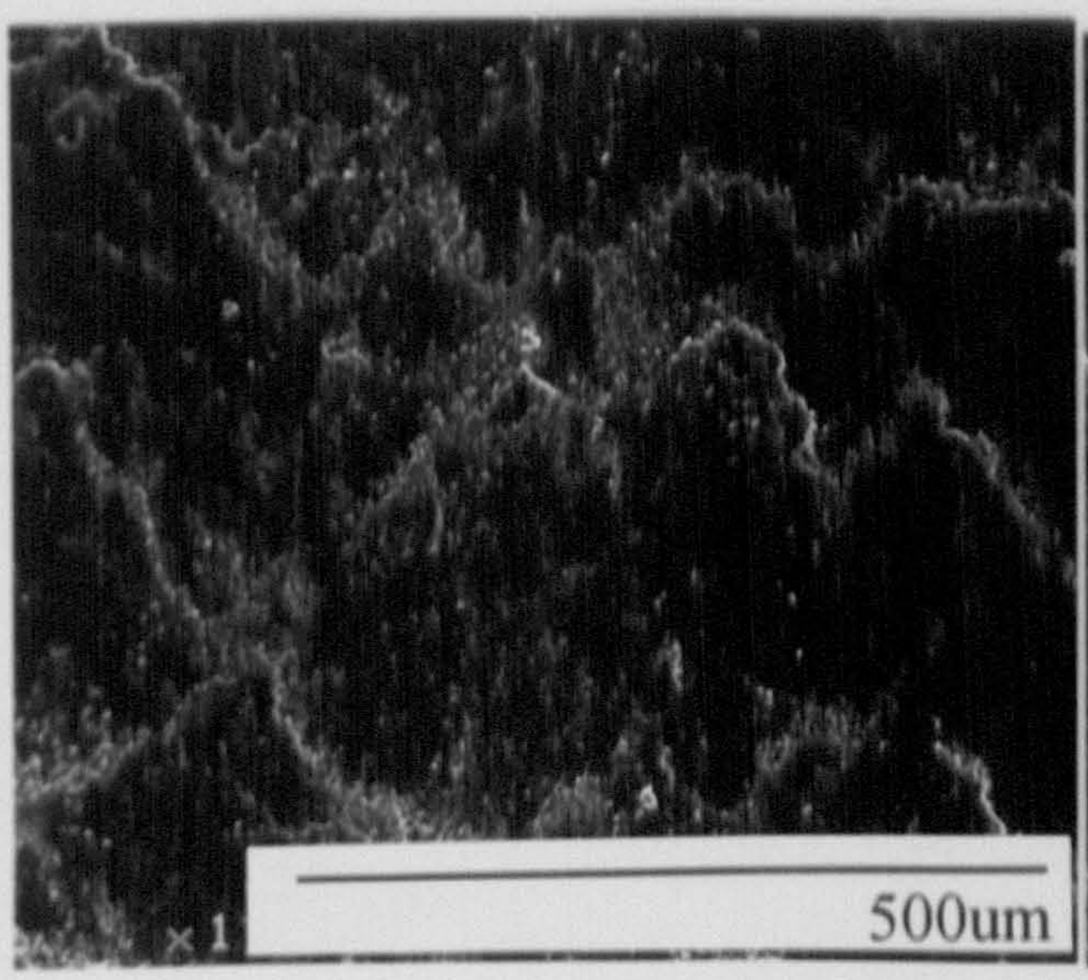

e

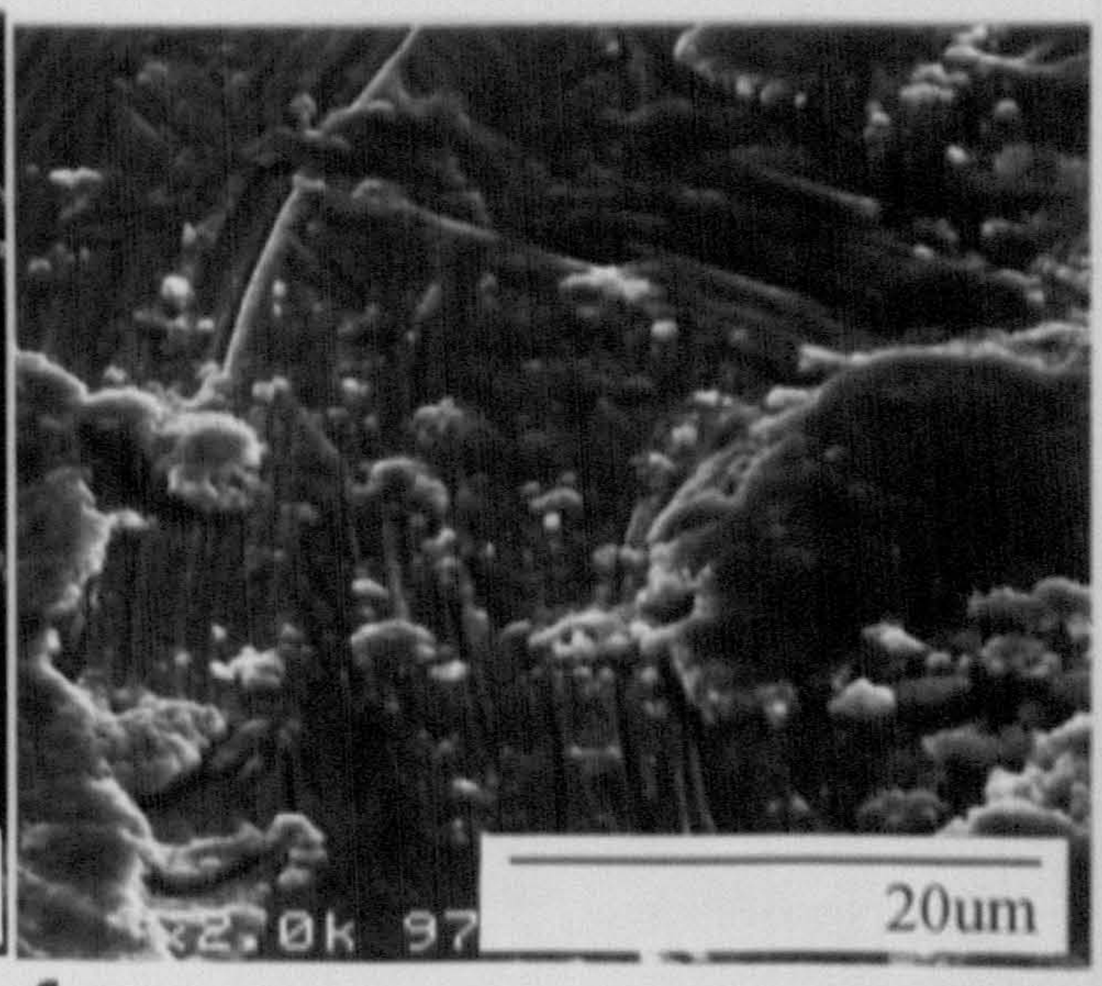

f

Fig.5.14 SEM micrographs of TiAl worn for 4 hours against:

a - Incoloy 800 counterface at room temperature
b - Incoloy 800 counterface at 750°C
c - Stellite 6 counterface at room temperature
d - Stellite 6 counterface at 750°C
e - Si_3N_4 counterface at room temperature
f - Si_3N_4 counterface at 750°C

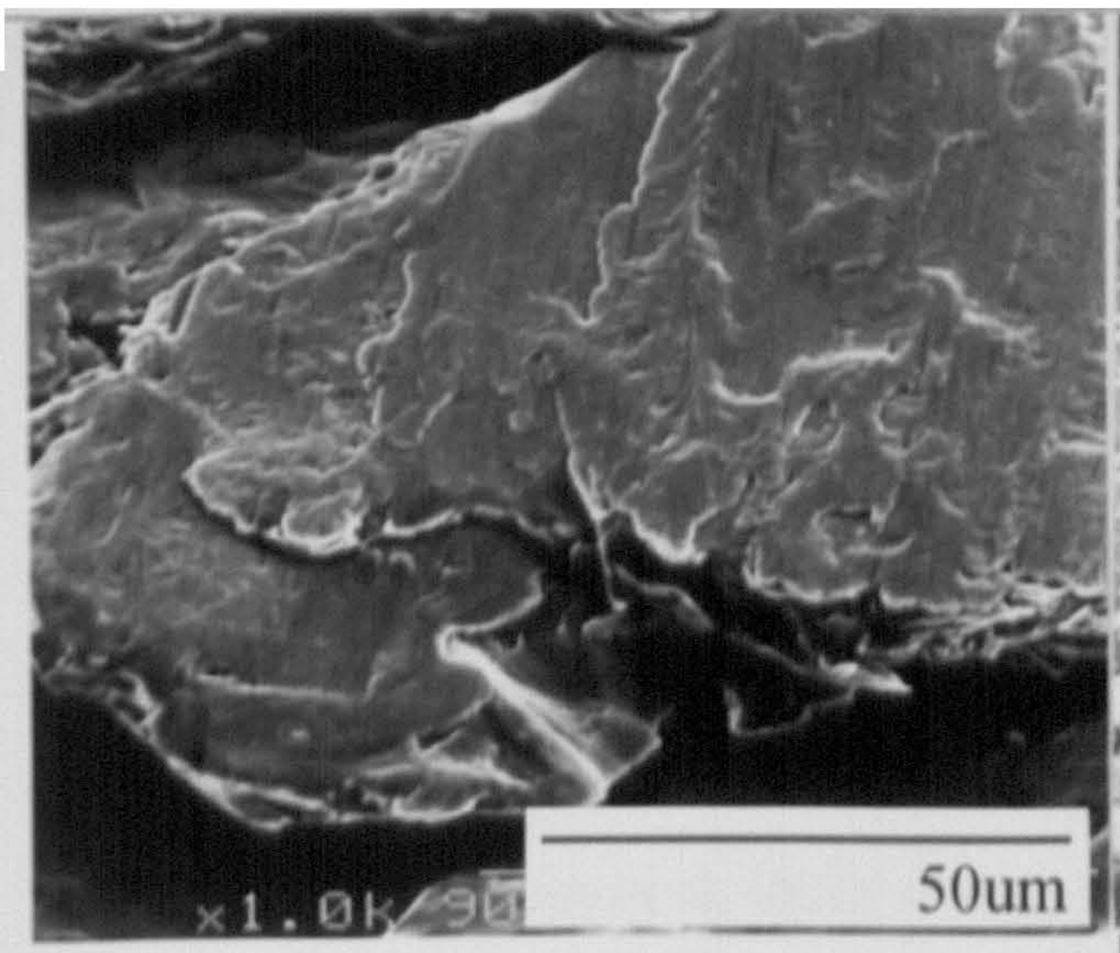

a

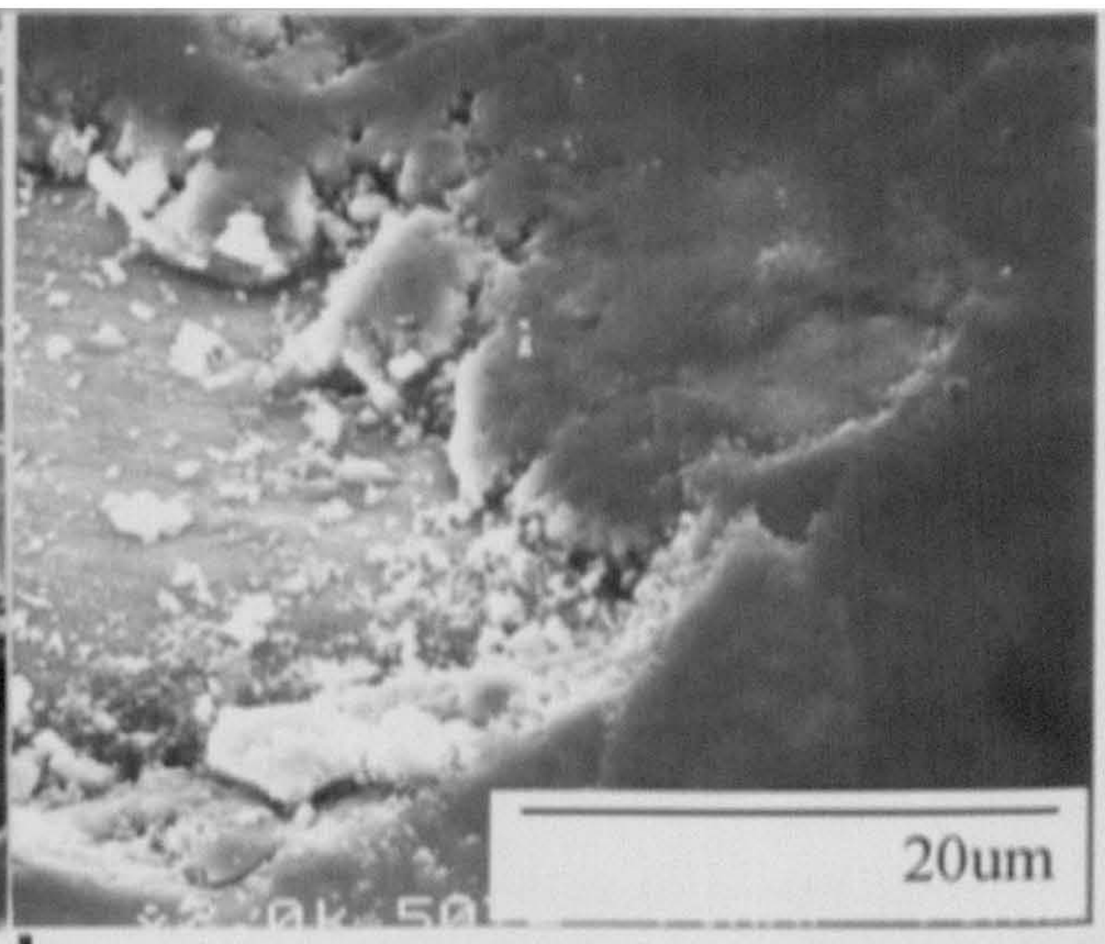

b

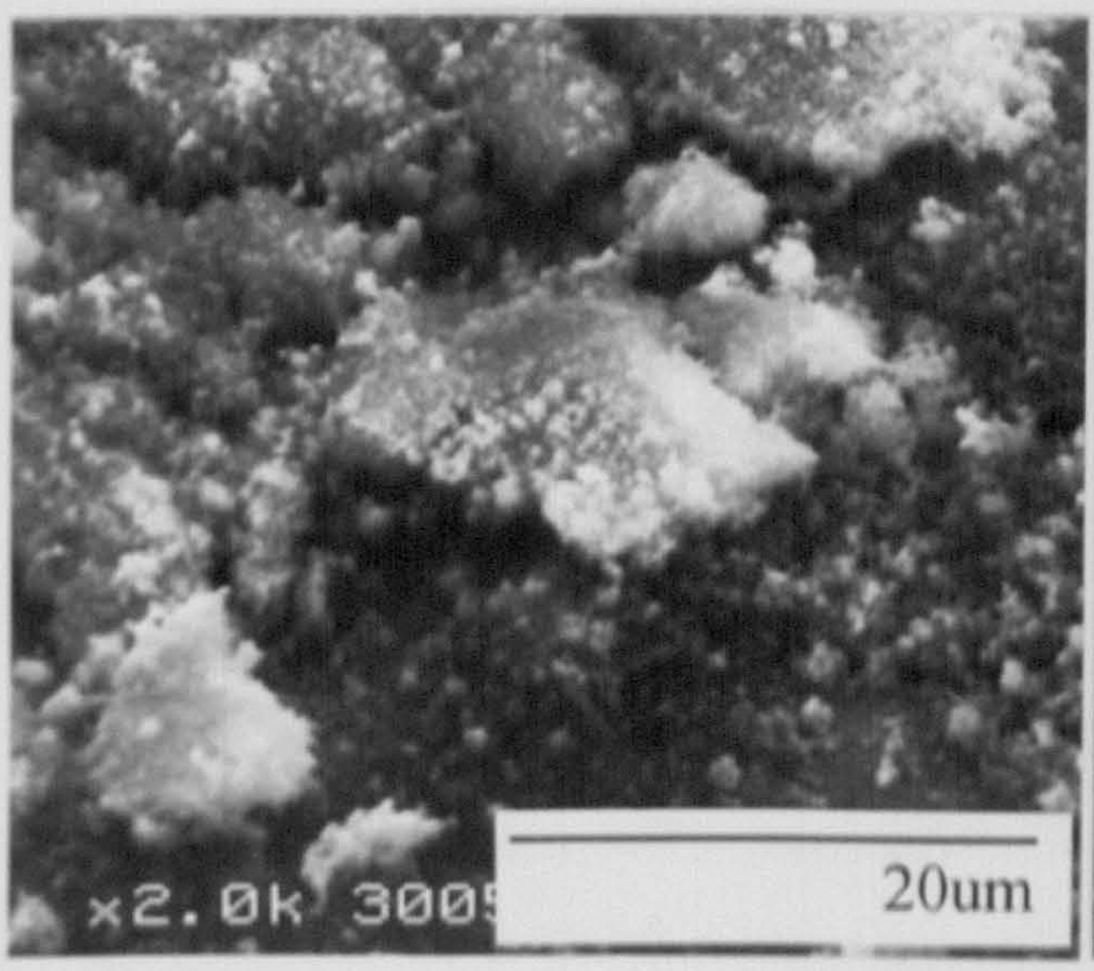

c

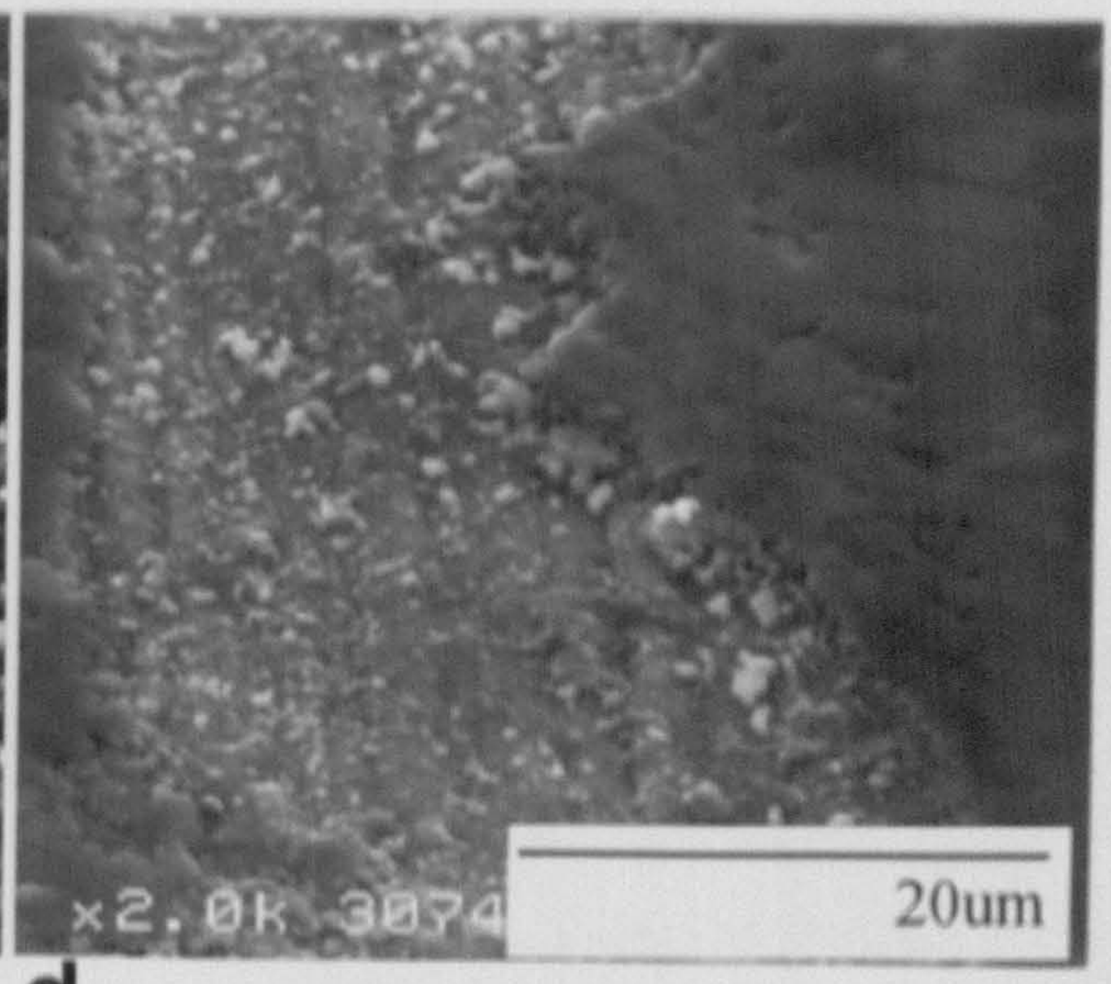

d

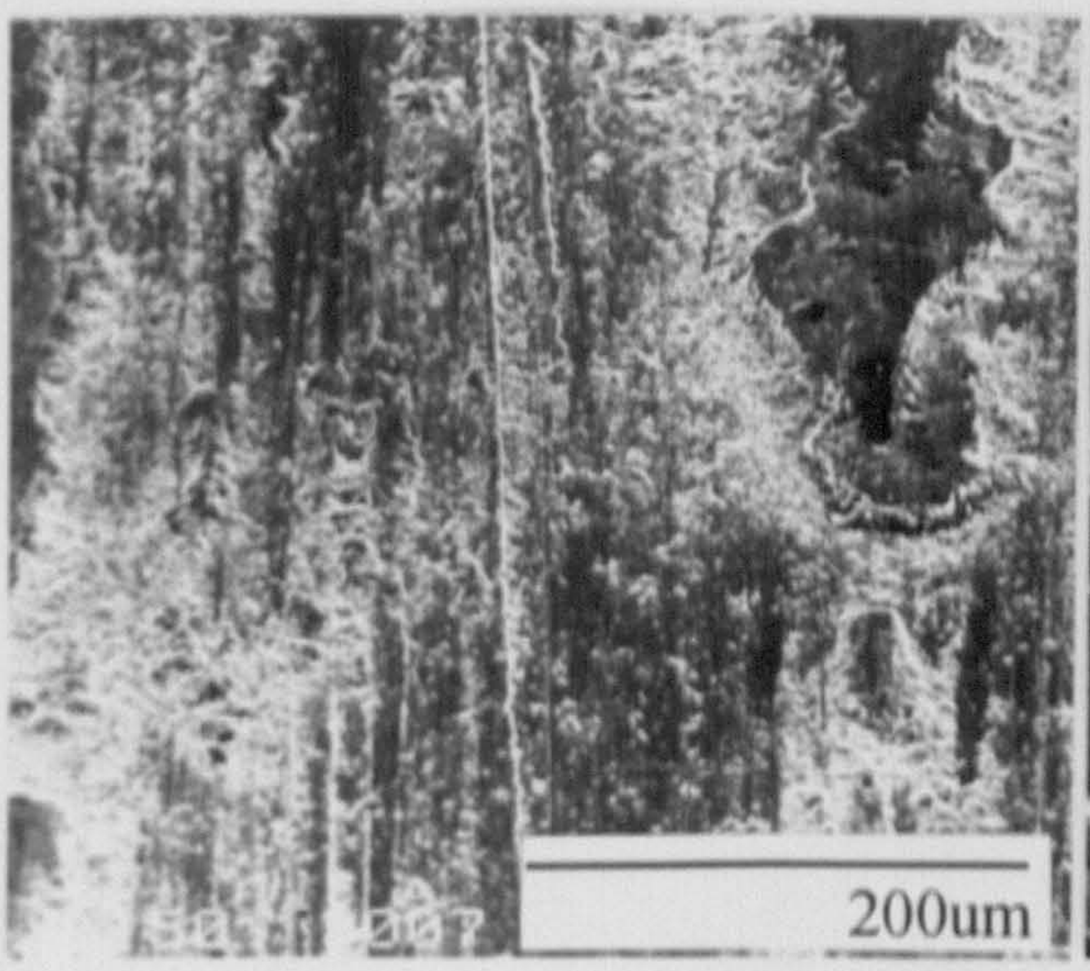

e

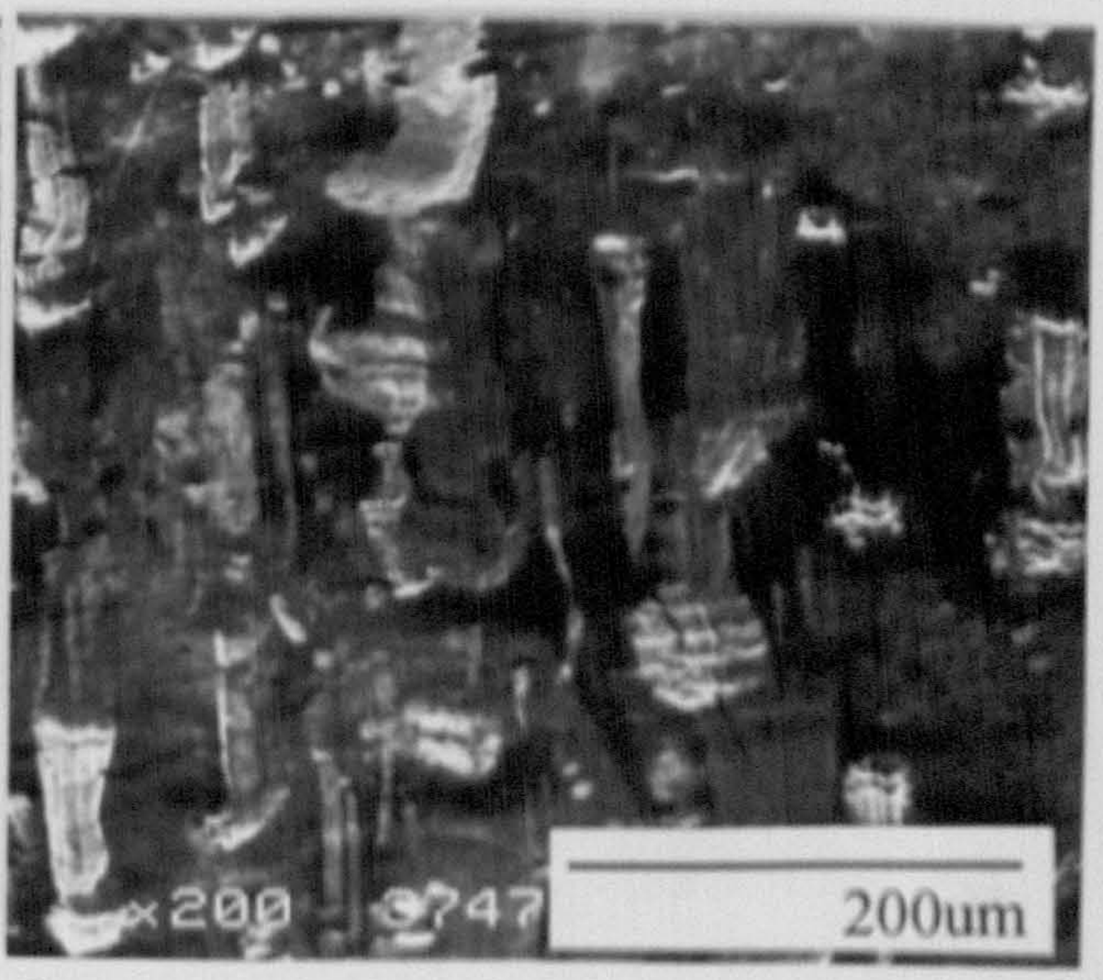

f

5.3.5 Hardness Testing

Table 5.6 displays room temperature hardness values of a selected group of the block alloys following wear tests against the various counterfaces at room temperature and 750°C. Hardness values could not be recorded for all of the worn block alloys as often the surfaces were too uneven to obtain reliable results. The hardness values that were taken were, wherever possible, measured on the plateaux/glazes that formed.

In all cases, the hardness values were higher, some considerably so, than the hardness of the unworn block alloys. The hardness of Ma956 was initially Hv303 but increased to Hv533 after wearing against Incoloy 800 at room temperature. An even higher hardness of Hv580 was achieved after Ma956 wore against Stellite 6 at 750°C. The only other worn Ma956 sample in which reliable hardness values could be recorded was the sample tested against Si_3N_4 at 750°C which gave a value of Hv470.

Nimonic 90 showed a hardness increase from an unworn value of Hv242 to a value of Hv563 and a considerably higher value of Hv1016 after wearing against Incoloy 800 at room temperature and 750°C respectively. Testing of Nimonic 90 after wearing against a Si_3N_4 counterface at 750°C revealed an increase in surface hardness to a value of Hv636.

The Nimonic 80A (cast) showed lower hardness increases than Nimonic 90 when tested against Incoloy 800. The initial hardness of Nimonic 80A (cast) was Hv223 which increased to Hv546 and Hv788 after testing against Incoloy 800 at room temperature and 750°C respectively.

It was possible to measure the hardness on all of the worn TiAl samples except on those tested against the Si_3N_4 counterface at room temperature. The hardness values of the worn TiAl ranged between Hv370 (Si_3N_4 counterface at 750°C) to Hv594 (Incoloy 800 at room temperature), all showing an increase from an unworn value of Hv345.

Table 5.6 Hardness values of block alloys prior to and after wearing against various counterfaces at room temperature and 750°C

Alloy	Hardness Hv 500g	Temp.	Hardness Hv 500g		
			Incoloy 800	Stellite 6	Si_3N_4
MA956	303	RT	533	Too uneven	Too uneven
		750°C	Too uneven	580	470
Nimonic 90	242	RT	563	Too uneven	Too uneven
		750°C	1016	Too uneven	636
Nimonic 80A (Cast)	223	RT	546	Too uneven	Too uneven
		750°C	788	Too uneven	Too uneven
TiAl	345	RT	594	563	Too uneven
		750°C	402	442	370

5.3.6 EDX Analysis

(a) Room Temperature

The information obtained from the EDX analyses of the block alloys worn at room temperature against different counterfaces is displayed in ***Table 5.7***. On all of the alloys worn against Incoloy 800 at room temperature, high amounts of Fe and Ni were detected indicating considerable material transfer from the counterface. The values of Fe/Ni varied from 43.3/30.1%wt (Nimonic 90 vs Incoloy 800) to 46.1/31.7%wt (Nimonic 80A cast vs Incoloy 800).

Material transfer onto the block material also occurred when the block alloys were worn against cobalt based Stellite 6. EDX analysis of Ma956, after wearing against Stellite 6, indicated a level of cobalt of 21.9%wt. For Nimonic 90 and Nimonic 80A (cast), worn under similar conditions, the values for cobalt were 44.5%wt and 16.1%wt respectively.

Analysis of the worn TiAl sample showed only a very small amount (1.6%wt) of cobalt present.

Analysis of block alloys worn against the Si_3N_4 counterface revealed only very small amounts of Si that had been transferred from the counterface. Silicon values varied from 0.4%wt for Nimonic 80A (cast) to a value of 5.1%wt for Nimonic 90.

Table 5.7 Composition of the surface of the block alloys after wearing against various counterfaces at room temperature

Alloy	Wheel	Composition %wt								
		Ni	Cr	Co	Fe	Ti	Mn	Al	O	Other
Ma956	In800	29.1	20.2	-	44.8	0.5	0.5	0.6	4.0	Si 0.3
Ma956	St 6	-	17.8	21.9	28.9	0.4	-	1.3	27.4	W 2.0
Ma956	Si_3N_4	-	19.3	-	71.6	0.4	-	2.8	4.1	Si 3.0
Nimonic 90	In800	30.1	17.9	-	43.3	0.5	1.0	0.4	3.4	
Nimonic 90	St 6	23.0	23.5	44.5	1.1	1.0	-	0.4	2.8	W 3.3
Nimonic 90	Si_3N_4	51.9	19.1	14.6	-	2.6	-	1.8	3.8	Si 5.1
N80A (Cast)	In800	31.7	21.7	-	46.1	0.4	0.9	0.4	-	
N80A (Cast)	St6	51.3	20.8	16.1	3.9	2.2	0.6	-	3.6	W 1.4
N80A(Cast)	Si_3N_4	74.6	18.2	-	0.9	2.4	-	1.2	2.9	Si 0.4
TiAl	In800	30.0	20.1	-	44.0	0.3	0.8	0.7	2.8	Si 0.5
TiAl	St 6	-	0.9	1.6	-	62.2	2.2	27.2	0.7	
TiAl	Si_3N_4	-	-	-	-	64.8	2.8	29.2	3.9	Si 0.6

(b) 750°C

Table 5.8 illustrates EDX analysis of the block alloys after wearing against various counterfaces at 750°C. EDX analysis of Ma956 tested against Incoloy 800 could not detect any nickel in the wear scar. Analysis of Nimonic 80A (cast) after wearing under the same conditions revealed only 0.8%wt of Fe present indicating only a very small amount, if any, of Incoloy 800 material on the surface. Higher values of Fe were recorded on Nimonic 90 (38.1%wt) and TiAl (37.5%wt) after wearing against Incoloy 800.

Table 5.8 Composition of the surface of the block alloys after wearing against various counterfaces at 750°C

Alloy	Wheel	Composition %wt								
		Ni	Cr	Co	Fe	Ti	Mn	Al	O	Other
Ma956	In800	-	12.8	-	52.1	0.2	-	2.8	bal.	Y 0.4
Ma956	St 6	0.2	14.9	7.4	40.0	0.4	-	2.1	bal.	W 0.8
Ma956	Si_3N_4	-	10.6	-	40.1	0.3	-	11.7	bal.	Si 1.3
Nimonic 90	In800	27.0	23.8	2.0	38.1	0.6	1.7	0.5	bal.	Si 0.7
Nimonic 90	St 6	25.5	11.6	13.8	0.5	1.0	-	0.5	bal.	W 0.6
Nimonic 90	Si_3N_4	64.0	12.3	9.3	1.2	1.1	-	0.7	bal.	Si 0.5
N80A (Cast)	In800	23.9	10.5	-	0.8	0.7	0.8	0.4	bal.	Si 0.3
N80A (Cast)	St6	55.5	15.9	7.3	4.4	1.3	0.9	0.7	bal.	-
N80A(Cast)	Si_3N_4	47.8	14.5	-	0.2	2.4	-	6.4	bal.	Si 0.6
TiAl	In800	19.3	12.9	-	37.5	0.8	-	0.4	bal.	Si 0.7
TiAl	St 6	-	3.3	3.9	0.4	50.0	1.8	21.8	bal.	W 0.6
TiAl	Si_3N_4	-	-	-	-	14.0	0.5	39.0	bal.	Si 0.9

Analysis of the block alloys after wearing against Stellite 6 revealed the presence of cobalt in the wear scar for all of the samples. The amount of Co was between 3.9%wt for worn TiAl up to 13.8%wt for worn Nimonic 90. Although the as-received Nimonic 90 does contain Co, the proportion compared to the nickel was higher in the worn sample indicating material transfer from the Stellite 6 counterface.

Very small amounts of Si were detected on the block alloys after wearing against the Si_3N_4 counterface at 750°C. These were similar to the amounts observed at room temperature. The levels of Si varied from between 0.5%wt (Nimonic 90) to 1.3%wt (Ma956).

5.3.7 Cross-sectional EDX of Block Alloys and EDX Analysis of Wear debris

A summary of the results of the cross-sectional EDX analysis of the worn block alloys and the analysis of the collected wear debris is shown in ***Tables 5.9-5.14***.

Overall, the block alloys showed a similar cross-sectional composition after wearing against Incoloy 800 at room temperature. The layer was comprised of a mainly unoxidised Ni/Fe/Cr and was 10-20μm thick as shown in **Fig.5.15a** and **Fig.5.17a**. The only exception was Nimonic 90 that contained two separate materials in the wear scar, one Fe/Cr/Ni material and the other Ni/Cr/Co material, as shown in **Fig.5.16a**. This layer was 15μm thick and unoxidised.

The wear debris produced from the wearing of the block alloys against Incoloy 800 at room temperature, was composed mainly of one type, as seen in **Fig.5.20c** and **Fig.5.20f**. This type of particle was flat and angular and between 300-500μm in diameter, containing Fe/Ni/Cr.

A similar composition of the wear scar was observed when the Nimonics and TiAl were worn against Incoloy 800 at 750°C, as shown in **Fig.5.16b** and **Fig.5.17b**. The wear scars were 10-15μm thick being composed of oxidised Fe/Cr/Ni. Wear debris collected was

also similar containing flat angular particles <500μm diameter and comprised of Fe/Ni/Cr. The wear scar observed on the ODS alloys, however, after wearing under the same conditions, was 8-15μm thick containing oxidised Fe/Cr/Al with a small amount of Ni also being detected (see **Fig.5.15b**). In addition, analysis revealed two types of particles to be present in the wear debris: flat angular particles (<200μm diameter) containing Fe/Cr/Ni and flat angular particles (<200μm diameter) comprised of Fe/Cr/Al.

Transferred Stellite 6 material could not be detected in the cross-section of the wear scar on the ODS alloys after wearing against Stellite 6 at room temperature. **Fig.5.18a**, shows the surface layer was 2μm thick and contained only oxidised Fe/Cr/Al. Wear debris analysis detected two types of particles. In both cases, the particles were <25μm diameter, containing mainly Fe/Cr with a small amount of Co. However, one type of particle was flat and angular and the other had a powder-like appearance.

Stellite 6 transfer, however, was detected in the wear scars produced on the Nimonic's after wearing against Stellite 6 at room temperature. The layer contained Ni/Cr with some Co and was oxidised only on the Nimonic 90 sample. This wear scar was thicker on Nimonic 80A (10μm) compared to the Nimonic 90 (2-5μm). Analysis of the wear debris produced during the Nimonic 90 test, revealed only powdery particles (<100μm diameter) to be present containing mainly Co/Cr/Ni with a little Fe (see **Fig.5.20d**). These were also observed after testing with Nimonic 80A (cast and HIPped) but with additional flat angular particles containing Ni/Cr with a little Fe/Co.

The wear scar on TiAl after wearing under the same conditions was comprised of mainly oxidised Co/Cr material 1-2μm thick. Wear debris collected showed only one type of powdery particle (<50μm diameter) to be present containing a mixture of Ti/Al/Cr/Co.

Cross-sectional analysis of the Nimonics after wearing against Stellite 6 at 750°C could not detect a mixed oxide layer. Wear debris analysis revealed flat angular particles had formed from mainly Ni/Cr but with a little Fe/Co. With the Nimonic 90 sample, flat angular particles containing only Co/Cr were also detected in the wear debris.

A wear scar 8-15μm thick was produced when the ODS alloys were worn against Stellite 6 at 750°C The layer contained a mixture of oxides containing Fe/Co/Al/Cr and included some internal oxidation, as shown in **Fig.5.18b**. Three types of wear debris particles were collected during the test, all being flat and angular (<200μm diameter). These particles contained Co/Cr, Co/Cr + little Fe and Fe/Cr + little Co.

A thin oxidised Co/Cr layer 1-2μm thick was detected on TiAl after wearing against Stellite 6 at 750°C. The test produced insufficient wear debris for analysis.

A mixed oxide layer was not detected on the Nimonic's after wearing against Si_3N_4 at room temperature. Wear debris particles collected were comprised of powdery particles (<100μm diameter) containing mainly Ni/Cr and a little Si (see **Fig.5.20a**.). Under the same wearing conditions, a layer 15μm thick was produced on the ODS alloys containing unoxidised Fe/Cr/Al/Si. Powdery particles <100μm in diameter were formed that contained mainly Fe/Cr + little Si. The wear scar of TiAl after wearing against Si_3N_4 at room temperature, as shown in **Fig.19a**., was comprised of an oxidised layer 2μm thick containing Ti/Al/Si/N. **Fig.5.20e**. shows the powdery particles produced during the wearing process that contained mainly Ti/Al/Si.

A very thin mixed oxide layer, 2μm thick, was formed on Ma956 during the wear with Si_3N_4 at 750°C. The layer contained a mixture of Fe/Al/Cr/Si/N and there was insufficient wear debris for analysis. An even thinner wear scar only 1μm thick was produced on Nimonic 80A (cast) after wearing under similar conditions made up of oxidised Si & N. In this experiment two types of wear debris were detected, one flat and angular (<200μm diameter) containing mainly Ni/Cr and the other being a powdery particle (<20μm diameter) comprised of mainly Si and a small amount of Ni (see **Fig.5.20b**.).

Cross-sectional analysis of Nimonic 90 after wearing against Si_3N_4 at 750°C revealed a heavily deformed region of Nimonic 90 5μm thick at the surface. On top was a thin oxide layer (<2μm thick) containing Ni/Cr/Co/Si/N. There was insufficient debris for analysis. A wear scar 4μm thick was produced on TiAl after wearing under similar

conditions as shown in **Fig.5.19b**. The oxidised layer was comprised of Si/Ti/Al/N and again there was insufficient debris for analysis.

Table 5.9 Cross-sectional EDX of the worn block alloys and analysis of the collected wear debris after testing against Incoloy 800 at room temperature

Alloy	Cross-section of wear scar	Wear debris
Ma956/PM2000/ PM2000SD	Wear scar 10-20μm thick- contained mainly unoxidised Ni/Cr/Fe (see **Fig.5.15a**)	Flat angular wear debris (~ 500μm diameter). Mainly one type that contained Ni/Cr/Fe (see **Fig.5.20f**).
Nimonic 80A (cast)/ Nimonic 80A (HIPped)	Wear scar 10-20μm thick- contained mainly unoxidised Ni/Cr/Fe	Flat angular wear debris (~ 500μm diameter). Mainly one type that contained Ni/Cr/Fe
Nimonic 90	Wear scar 15μm thick - contained two unoxidised materials - 1. Ni/Cr/Fe 2. Ni/Cr/Co (see **Fig.5.16a**)	Flat angular wear debris (range from ~300μm diameter and smaller). Mainly one type that contained Ni/Cr/Fe (see **Fig.5.20c**)
TiAl	Wear scar 15μm thick - contained partially oxidised Ni/Cr/Fe (see **Fig.5.17a**)	Flat angular wear debris (range from ~500μm diameter and smaller). Mainly one type that contained Ni/Cr/Fe

Table 5.10 Cross-sectional EDX analysis of the worn block alloys and analysis of the collected wear debris after testing against Incoloy 800 at 750°C

Alloy	Cross-section of wear scar	Wear debris
Ma956/PM2000/ PM2000SD	Wear scar 8-15μm thick - contained mainly oxidised Fe/Cr/Al and a very small amount of Ni (see **Fig.5.15b**)	Two types of particles: 1. Flat angular (<200μm) - mainly Fe/Cr/Ni 2. Flat angular (<200μm) - mainly Fe/Cr/Al
Nimonic 80A (Cast)/ Nimonic 80A (HIPped)	Wear scar 10μm thick - contained mainly oxidised Ni/Cr/Fe	Flat angular wear debris (<500μm). Mainly one type that contained Ni/Cr/Fe
Nimonic 90	Wear scar 10μm thick - contained mainly oxidised Ni/Cr/Fe (see **Fig.5.16b**)	Flat angular wear debris (<500μm). Mainly one type that contained Ni/Cr/Fe
TiAl	Wear scar 10-15μm thick - contained mainly oxidised Ni/Cr/Fe (see **Fig.5.17b**)	Flat angular wear debris (<500μm). Mainly one type that contained Ni/Cr/Fe

Table 5.11 Cross-sectional EDX analysis of the worn block alloys and analysis of the collected wear debris after testing against Stellite 6 at room temperature

Alloy	Cross-section of wear scar	Wear debris
Ma956/PM2000 /PM2000SD	Wear scar 2μm thick - contained oxidised Fe/Cr/Al (see **Fig.5.18a**)	Two type of particles: 1. Flat angular (<25μm) - mainly Fe/Cr but small amount Co 2. Powdery particle (<25μm) - mainly Fe/Cr/Co
Nimonic 80A (cast)/ Nimonic 80A (HIPped)	Wear scar 10μm thick - contained mainly unoxidised Ni/Cr with some small traces of Co	Two types of particles: 1. Flat angular (< 100μm)- mainly Ni/Cr but also small amount of Co/Fe 2. Powdery particle (<100μm) - mainly Co/Cr but also Ni/Fe
Nimonic 90	Wear scar 2-5μm thick - contained mainly oxidised Ni/Cr/Co	Powdery particles (<100μm)- mainly Co/Cr/Ni and a small amount of Fe (see **Fig.5.20d**)
TiAl	Wear scar 1-2μm thick - contained mainly oxidised Co/Cr	Powdery particles (<50μm)- mainly Ti/Al/Cr/Co

Table 5.12 Cross-sectional EDX analysis of the worn block alloys and analysis of the collected wear debris after testing against Stellite 6 at 750°C

Alloy	Cross-section of wear scar	Wear debris
Ma956/PM2000/ PM2000SD	Wear scar 8-15μm thick (including some internal oxidation) - comprised of Fe/Co/Al/Cr oxides (see **Fig.5.18b**)	3 types all flat angular & <200μm: 1. Co/Cr 2. Co/Cr and little Fe 3. Fe/Cr and little Co
Nimonic 80A (cast)/ Nimonic 80A (HIPped)	No mixed oxide layer detected	One type of flat angular particle (<100μm). Contained mainly Ni & Cr in addition to Fe & Co.
Nimonic 90	No mixed oxide layer detected	Two types (<100μm): 1. Co/Cr (powdery) 2. Ni/Cr/Co (flat/angular)
TiAl	Wear scar 1-2μm thick - contained oxidised Co/Cr	Insufficient wear debris for analysis

Table 5.13 Cross-sectional EDX analysis of the worn block alloys and analysis of the collected wear debris after testing against Si_3N_4 Wheel at room temperature

Alloy	Cross-section of wear scar	Wear debris
Ma956/PM2000 /PM2000SD	Wear scar 15μm thick - comprised of unoxidised Fe/Cr/Al/Si	One type of powdery particle (<100μm). Contained mainly Fe/Cr but small amount of Si
Nimonic 80A (cast)	No detected mixed oxide layer	One type of powdery particle (<100μm). Contained mainly Ni/Cr but small amount of Si (see **Fig.5.20a)**
Nimonic 90	No detected mixed oxide layer	One type of powdery particle (<100μm). Contained mainly Ni/Cr but small amount of Si
TiAl	Wear scar 2μm thick - comprised of oxidised layer of Si/Al/Ti/N (see **Fig.5.19a)**	One type of powdery particle (<100μm). Contained mainly Ti/Al/Si (see **Fig.5.20e)**.

Table 5.14 Cross-sectional EDX analysis of the worn block alloys and analysis of the collected wear debris after testing against Si_3N_4 at 750°C

Alloy	Cross-section of wear scar	Wear debris
Ma956	Mixed oxide layer (2μm thick) contained Fe/Al/Cr/Si/N	Insufficient wear debris for analysis
Nimonic 80A (cast)	Mixed oxide layer <1μm - comprised of Si/N	Two types of wear debris: 1. Flat angular debris (<200μm) - contained mainly Ni/Cr 2. Powdery particles (<20μm) - mainly Si but very small amount of Ni (see **Fig.5.20b**)
Nimonic 90	Heavily deformed oxidised substrate 5μm thick. On the surface of this layer an oxidised Ni/Cr/Co/Si/N layer was present (<2μm thick)	Insufficient debris for analysis
TiAl	Wear scar 4μm thick - oxidised layer comprised of Si/Ti/Al/N (see **Fig.5.19b**)	Insufficient debris for analysis

Fig.5.15 Cross-sectional EDX analysis of Ma956 worn against an Incoloy 800 counterface at:
a - room temperature
b - 750°C

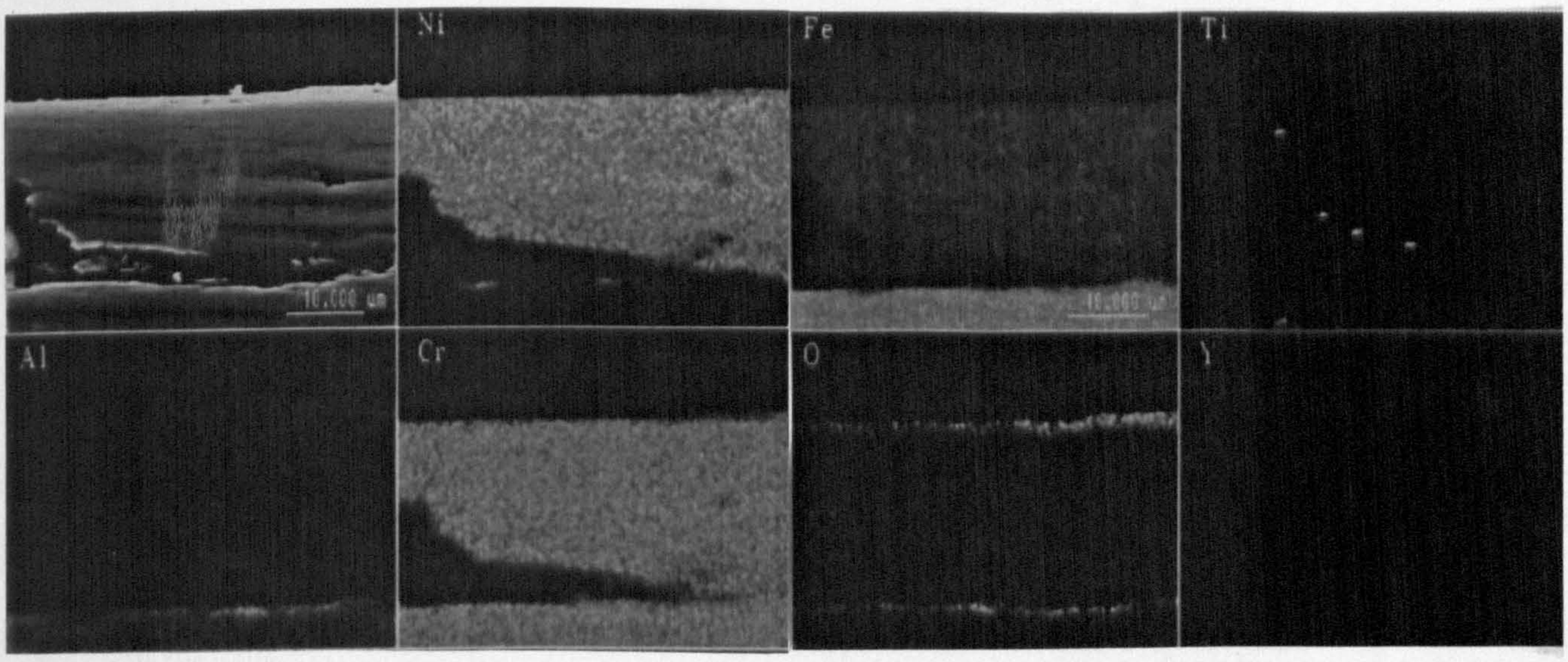
Ni
Fe
Ti
10.000 um
Al
Cr
O
Y

a

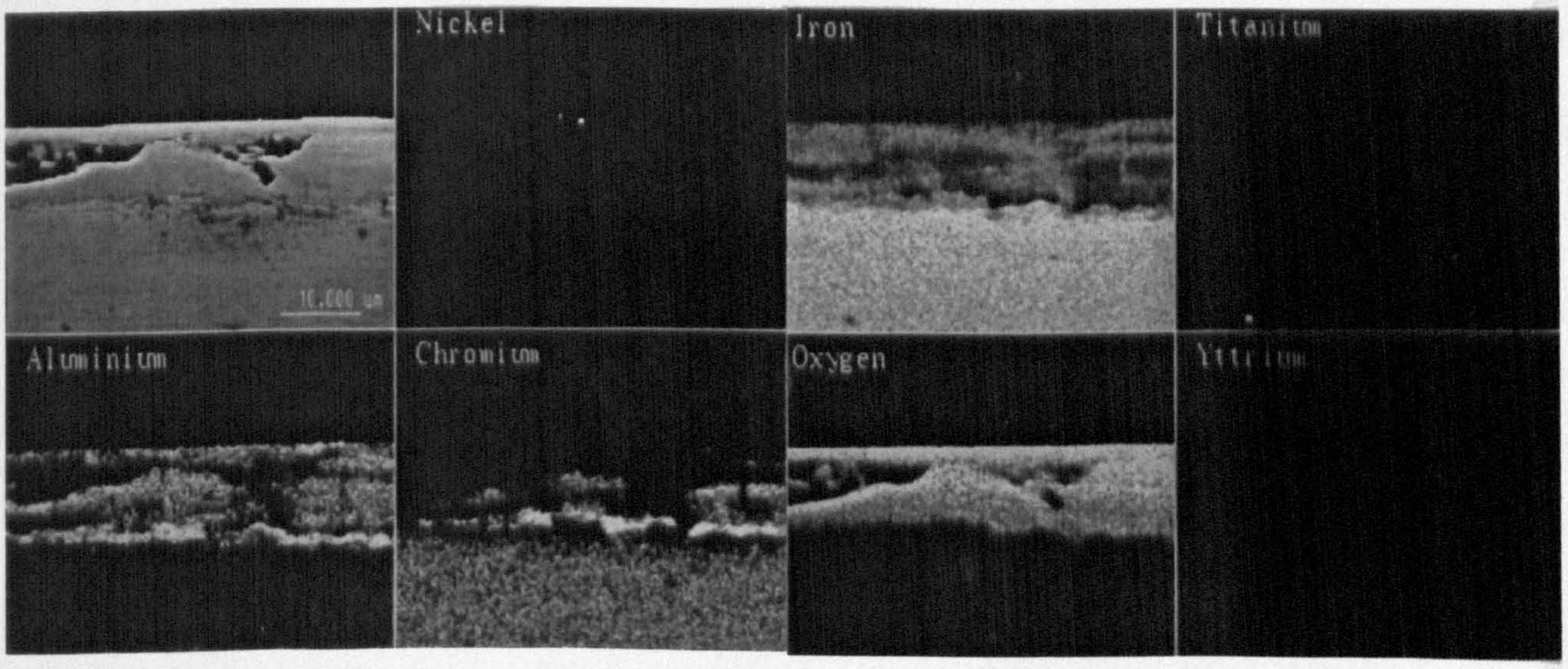
Nickel
Iron
Titanium
10.000 um
Aluminium
Chromium
Oxygen
Yttrium

b

Fig.5.16 Cross-sectional EDX analysis of Nimonic 90 worn against an Incoloy 800 counterface at:

a - room temperature

b - 750°C

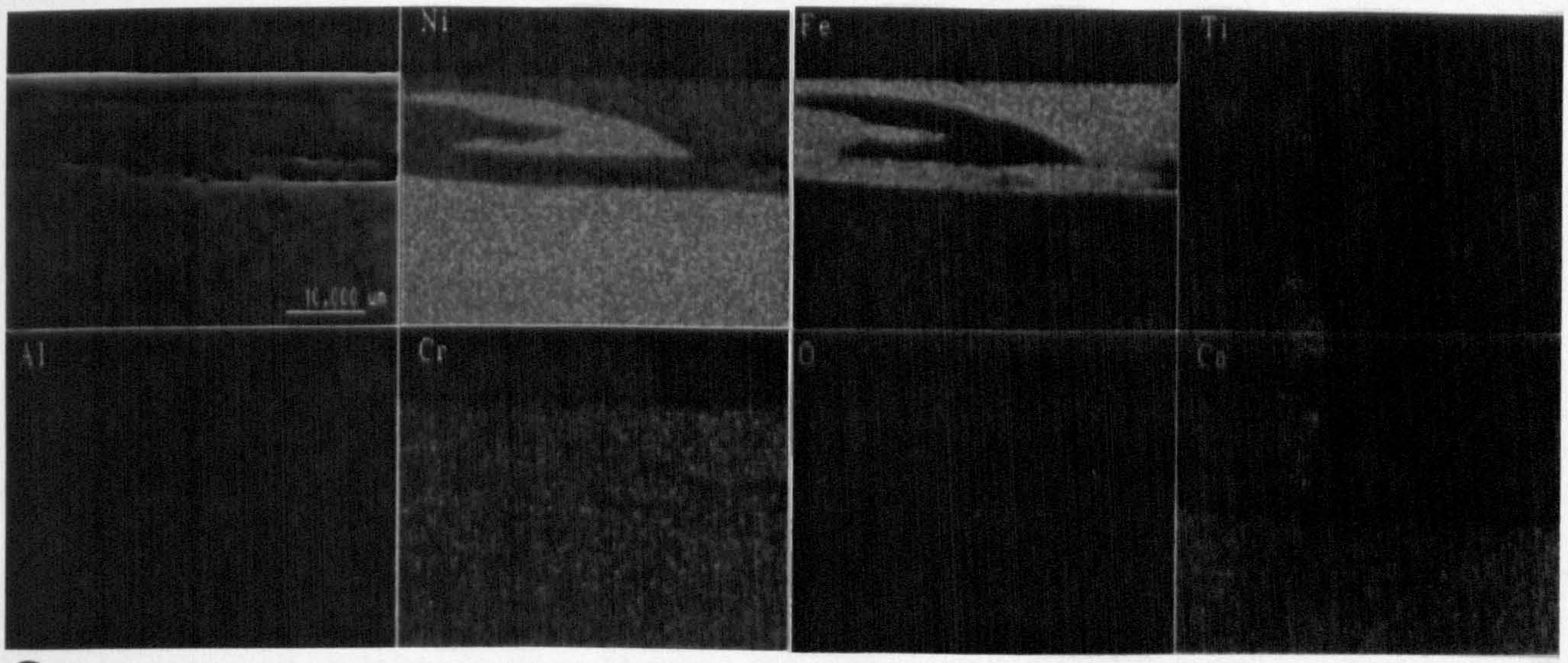

a

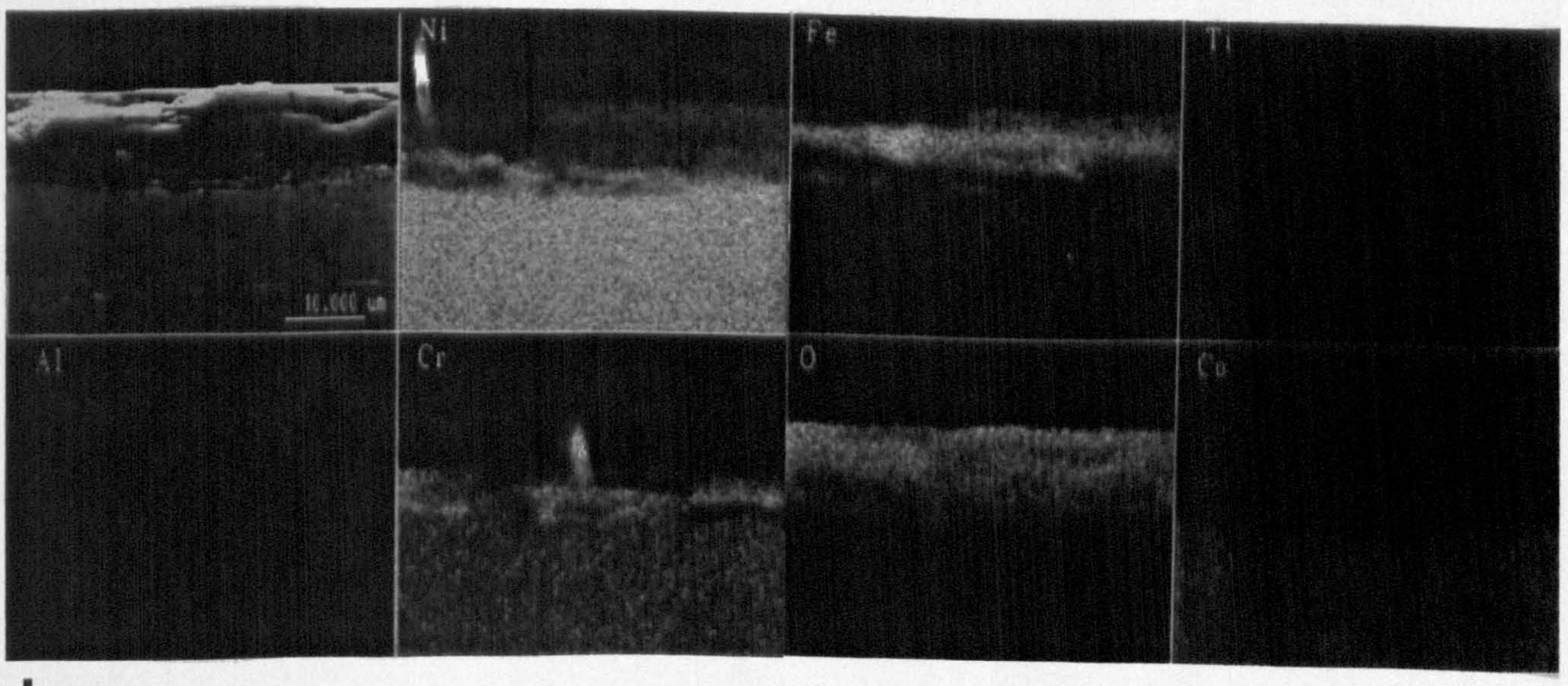

b

Fig.5.17 Cross-sectional EDX analysis of TiAl worn against an Incoloy 800 counterface at
a - room temperature
b - 750°C

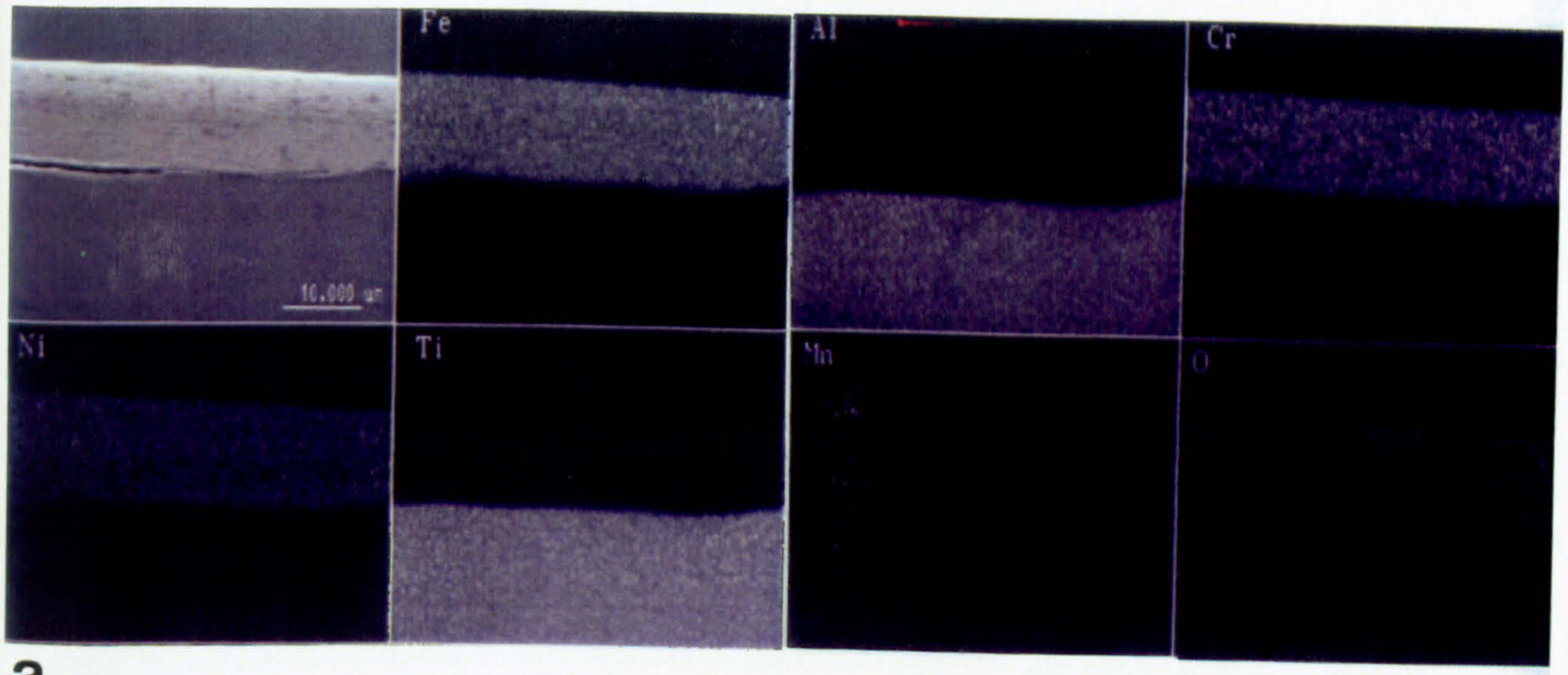
Fe
Al
Cr
10.000 um
Ni
Ti
Mn
O

a

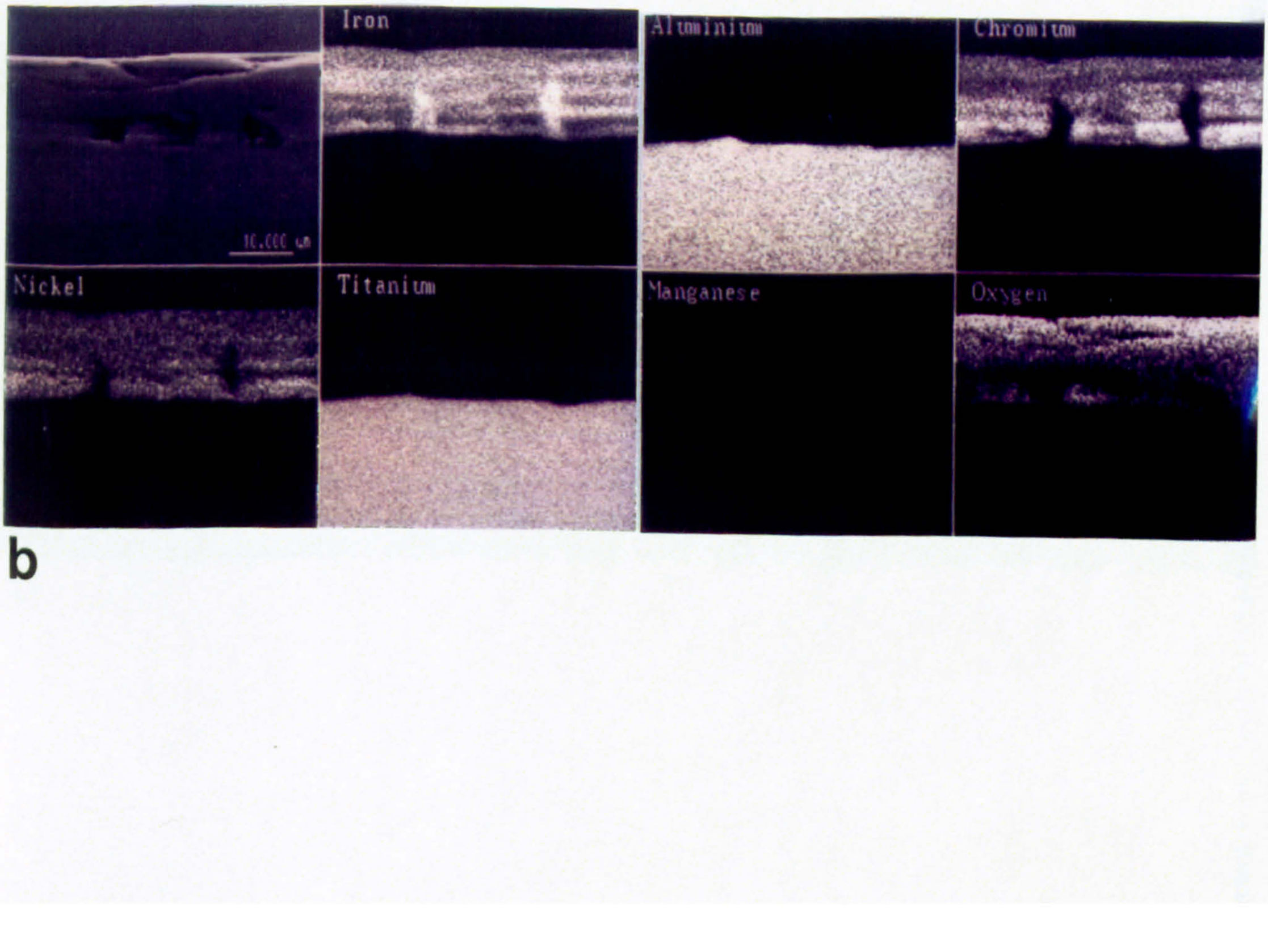
Iron
Aluminium
Chromium
10.000 um
Nickel
Titanium
Manganese
Oxygen

b

Fig.5.18 Cross-sectional EDX analysis of Ma956 worn against a Stellite 6 counterface at:

a - room temperature
b - 750°C

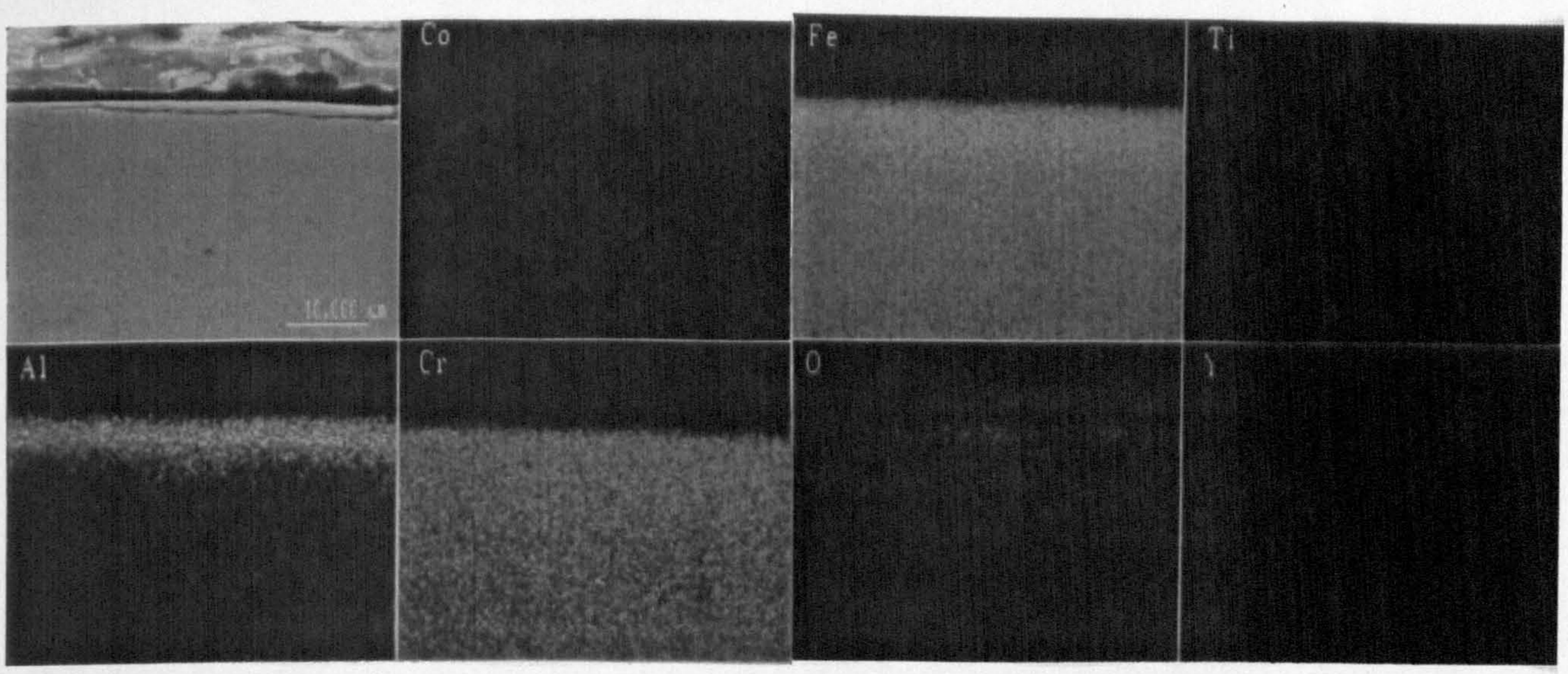

a

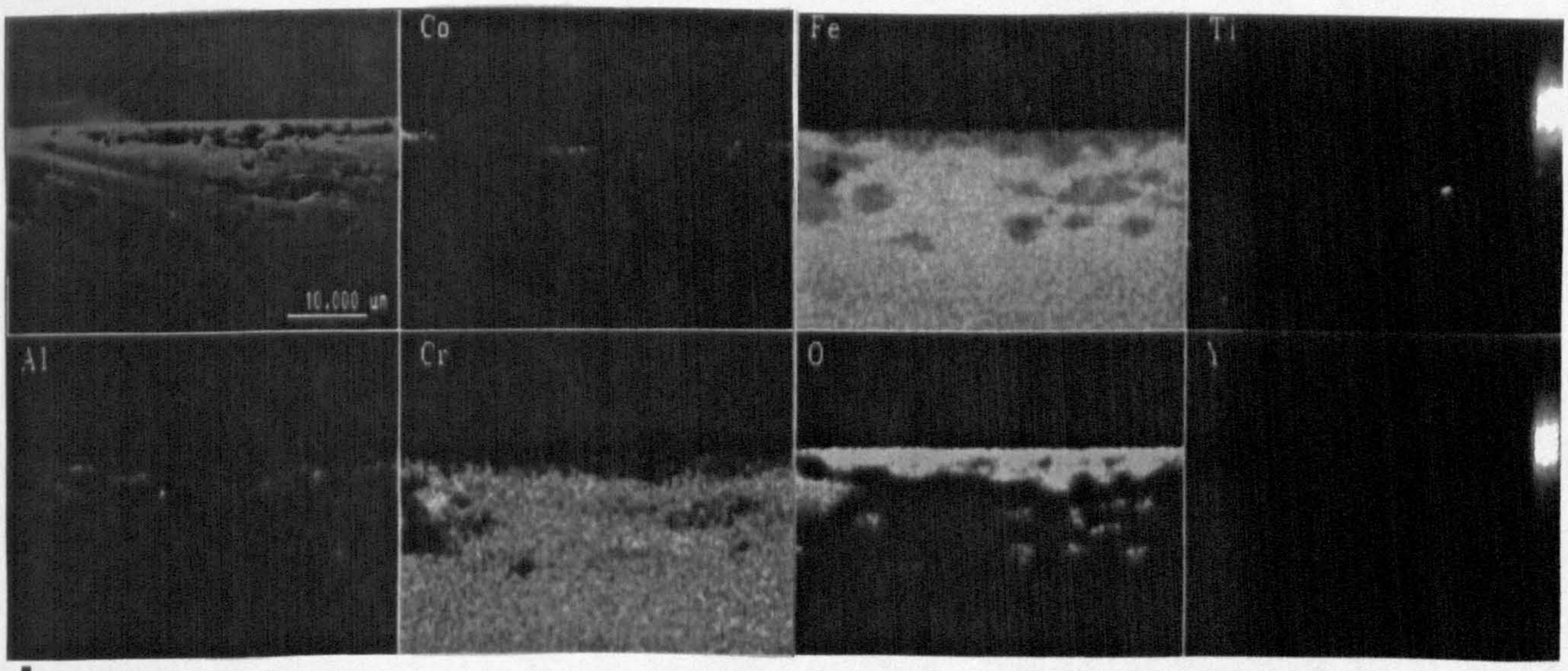

b

Fig.5.19 Cross-sectional EDX analysis of TiAl worn against a Si_3N_4 counterface at:

a - room temperature
b - 750°C

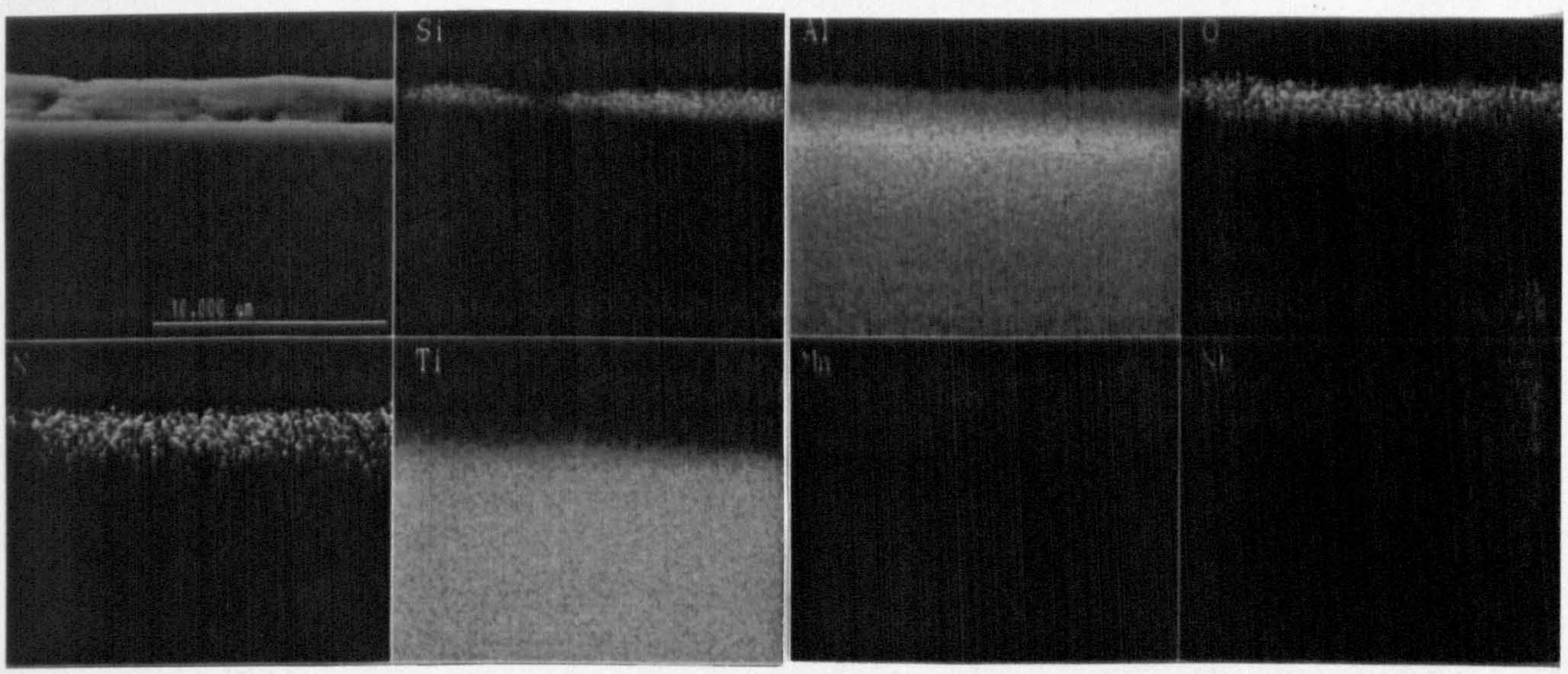

a

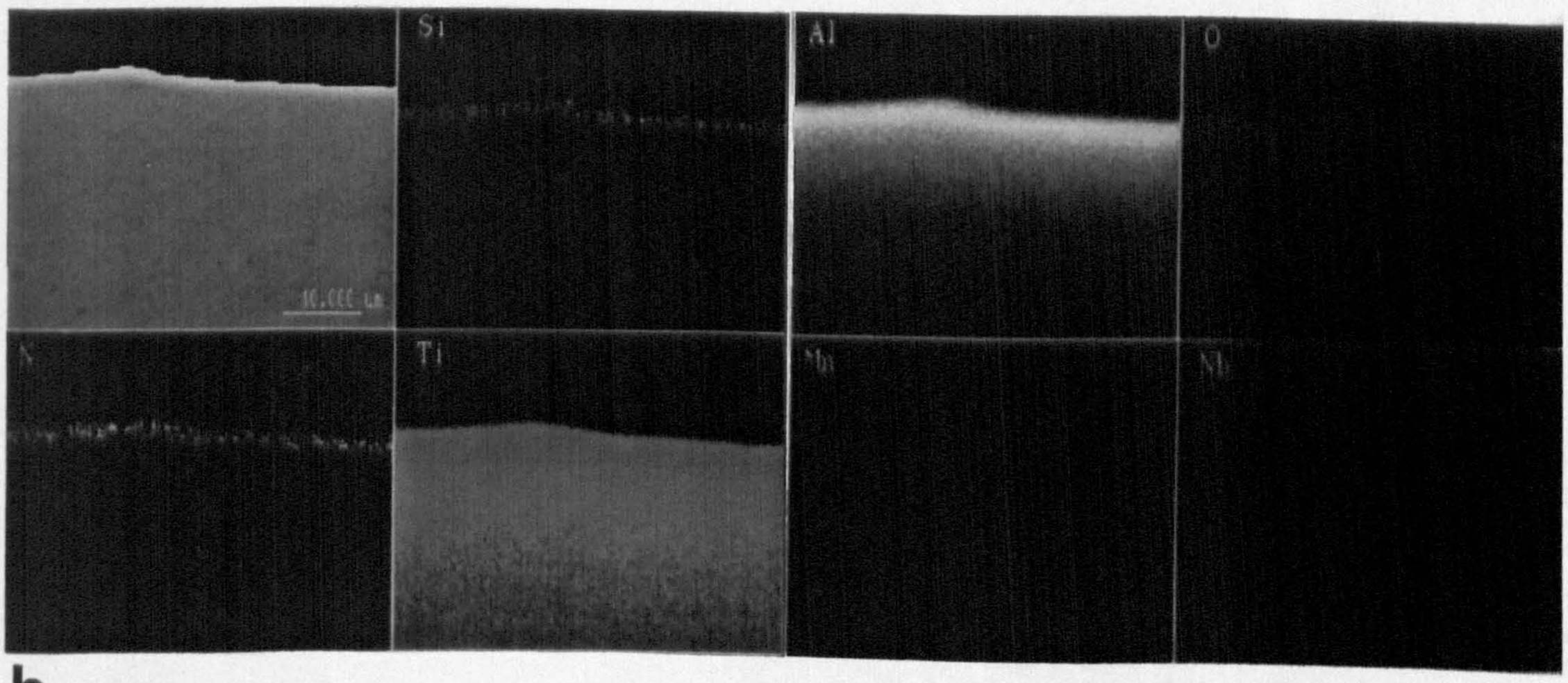

b

Fig.5.20 Selected SEM micrographs of wear debris from:
a - Nimonic 80A (cast) vs Si_3N_4 counterface at room temperature
b - Nimonic 80A (cast) vs Si_3N_4 counterface at 750°C
c - Nimonic 90 vs Incoloy 800 counterface at room temperature
d - Nimonic 90 vs Stellite 6 counterface at room temperature
e - TiAl vs Si_3N_4 counterface at room temperature
f - Ma956 vs Incoloy 800 counterface at room temperature

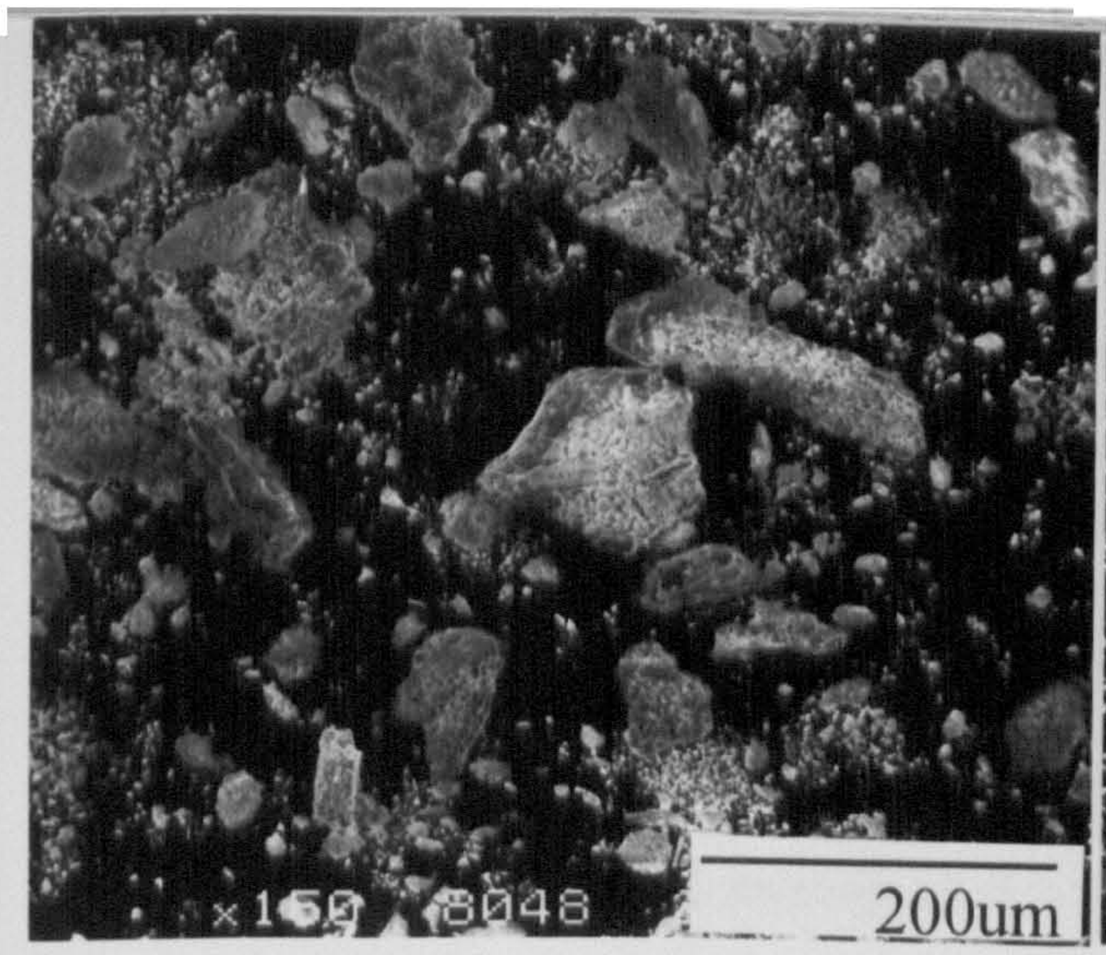
x150 8048
200um

a

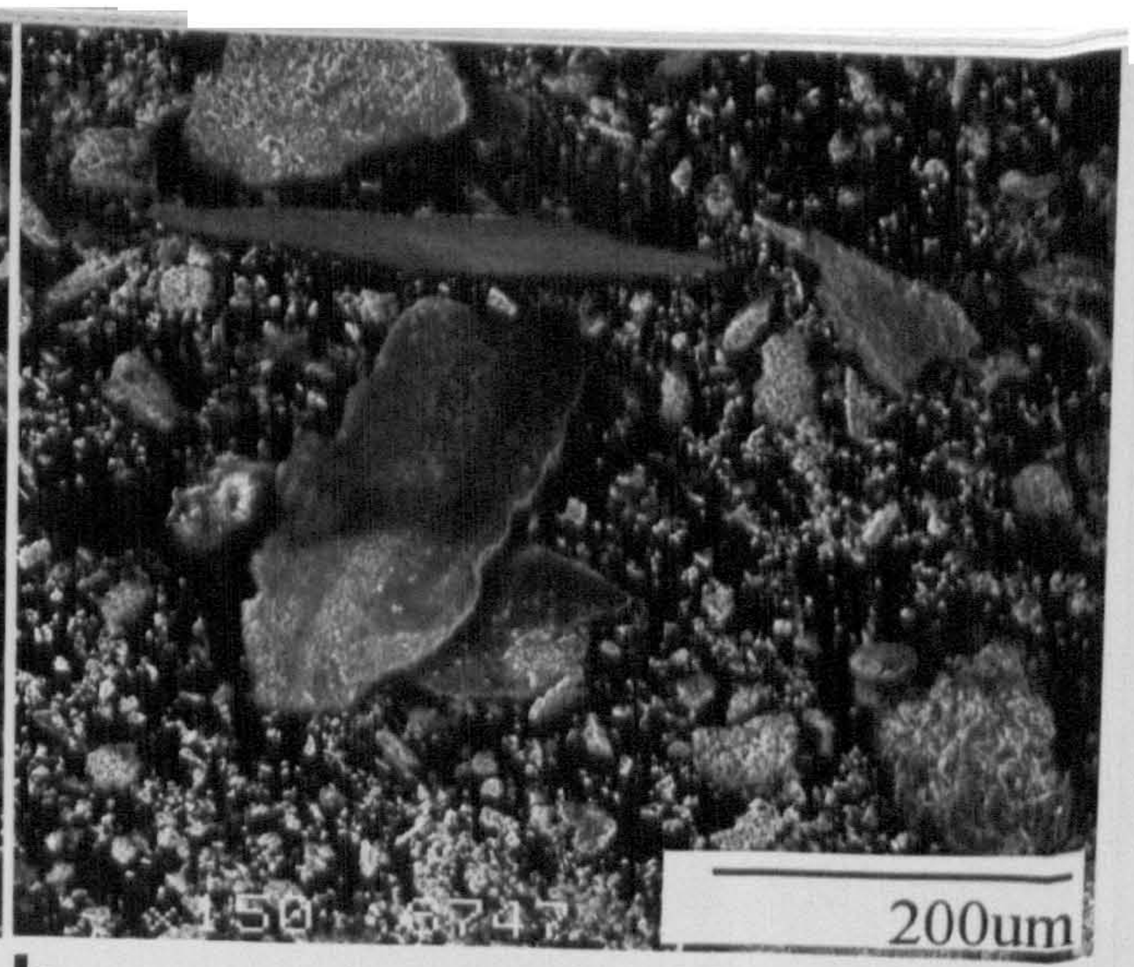
150 6747
200um

b

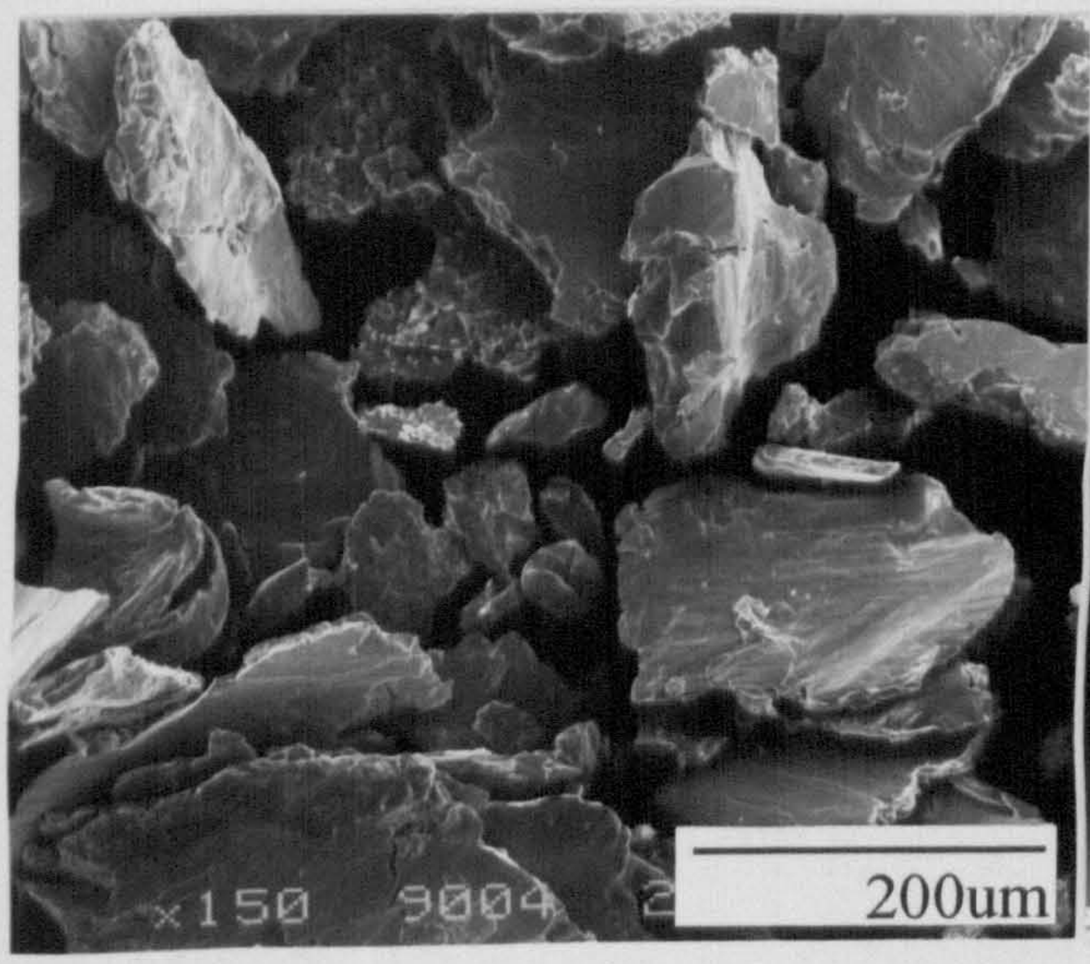
x150 9004
200um

c

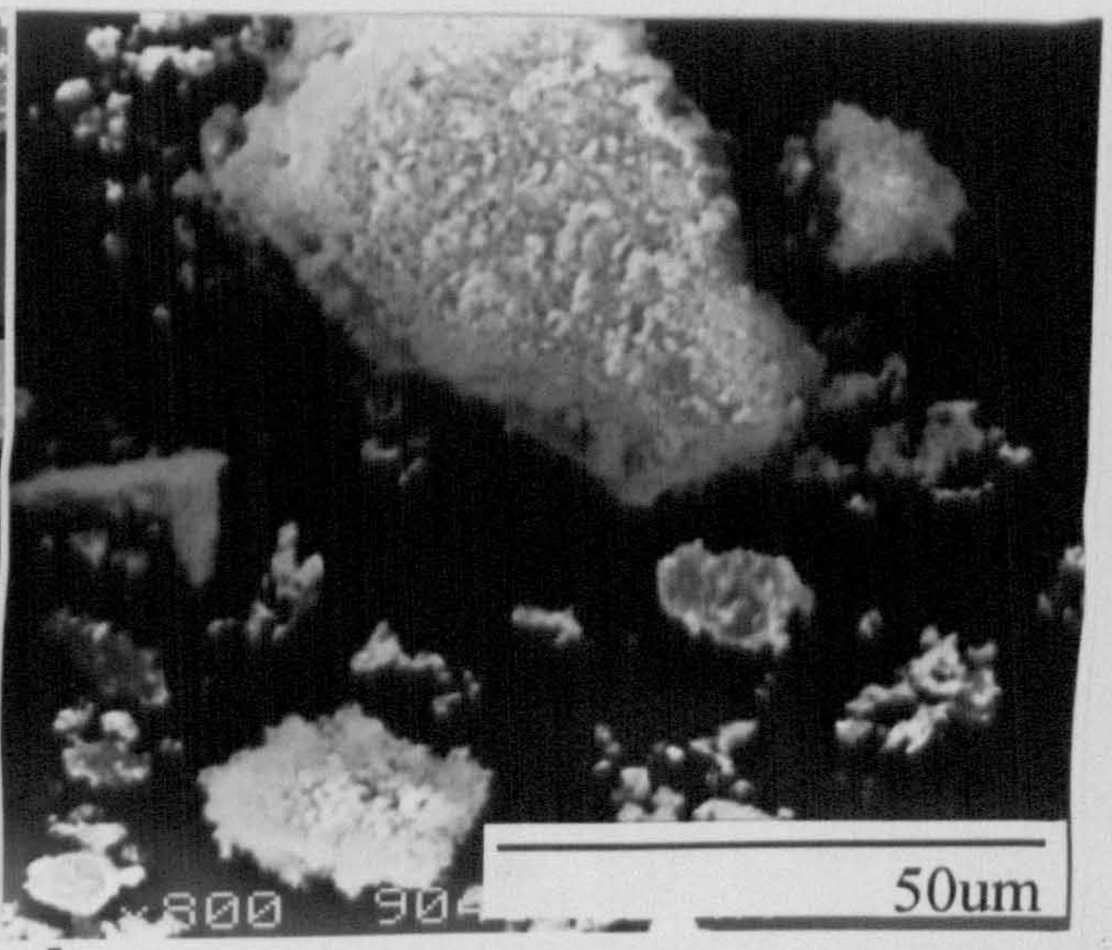
50um

d

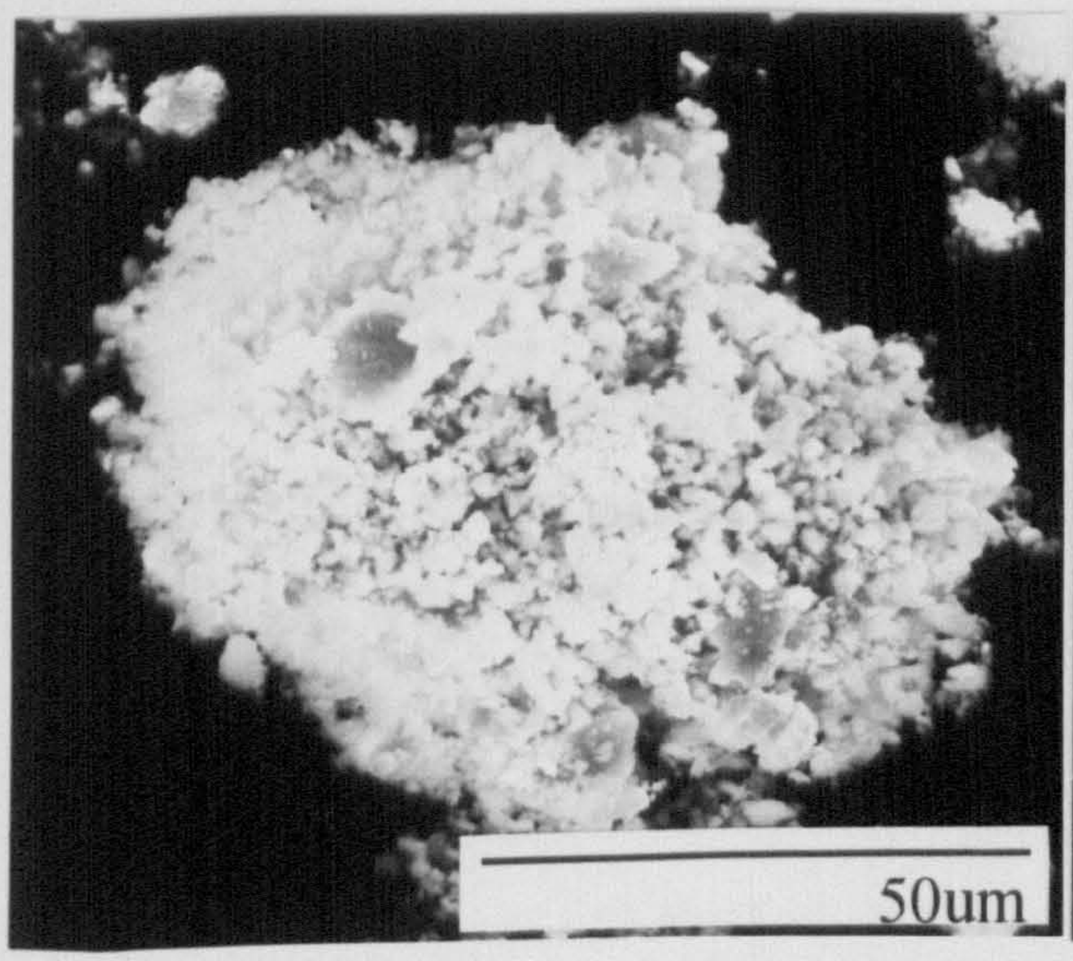
50um

e

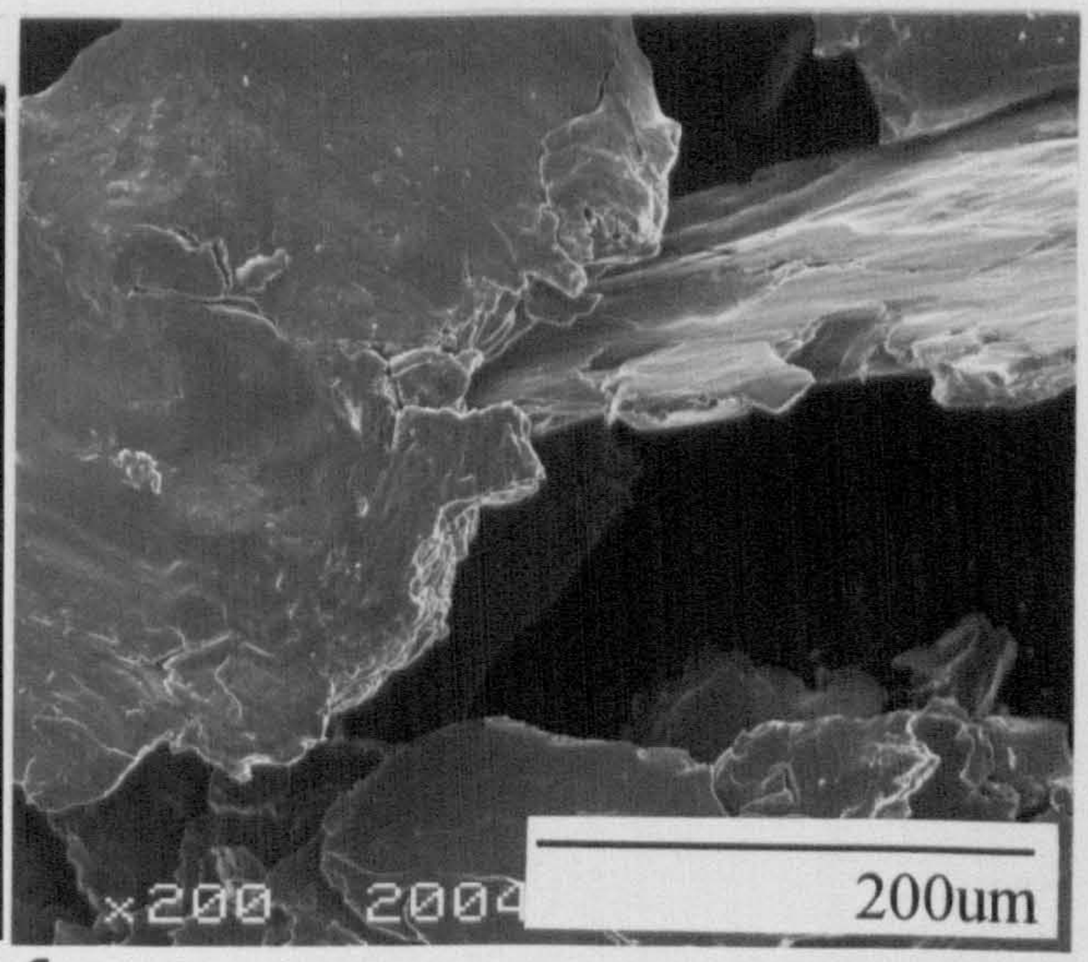
x200 2004
200um

f

5.4 Wear Studies of Nimonic 90 and Ma956 Worn against Incoloy 800 and Stellite 6 at 750°C for 2 Minutes to 1 Hour

5.4.1 Weight changes

Fig.5.21 displays weight changes for Ma956 and Nimonic 90 after wearing against Incoloy 800 at 750°C from 2 minutes to 4 hours. The Nimonic 90 sample showed a small weight increase throughout the test varying from +12.5mgcm^{-2} (after 2 minutes) to +18.5mgcm^{-2} (after 1 hour) after wearing against Incoloy 800. The Ma956 sample wearing against Incoloy 800 also showed a small weight increase of +1.2mgcm^{-2} after 10 minutes. However, after 20 minutes a weight loss of -69.9mgcm^{-2} was recorded rising to -354.1mgcm^{-2} after 1 hour.

The weight change of Ma956 and Nimonic 90 worn against Stellite 6 at 750°C for up to 4 hours is illustrated in **Fig.5.22**. Ma956 showed a small weight increase of +0.7mgcm^{-2} after 2 minutes but exhibited a steady weight loss after this time reaching a figure of -1.8mgcm^{-2} after 1 hour. Nimonic 90 also showed a small weight increase of +0.8mgcm-$^{-2}$ up to 10 minutes after wearing against Stellite 6. However, a small weight loss of -1.8mgcm^{-2} was recorded after 20 minutes which increased to -31.7mgcm^{-2} after 1 hour.

5.4.2 XRD Analysis

Table 5.15 shows the phases detected on the surface of Ma956 and Nimonic 90 worn against Incoloy 800 and Stellite 6 at 750°C. Initially (after 2 minutes), only the Fe-Cr substrate could be detected on Ma956 after wearing against Incoloy 800, but after 10 minutes Fe_2O_3 maghemite/$NiCr_2O_4$ was also identified. An additional phase of Cr_2O_3 eskolaite was observed after 20 minutes and 1 hour on the Ma956.

The Fe-Cr substrate was the only phase detected on Ma956 after wearing against Stellite 6 for 2 minutes and 10 minutes. However, on samples worn for 20 minutes and 1 hour, $Cr_{1.3}Fe_{0.70}O_{0.36}$ and $CoCr_2O_4/Fe_2O_3$ maghemite phases were also recognised.

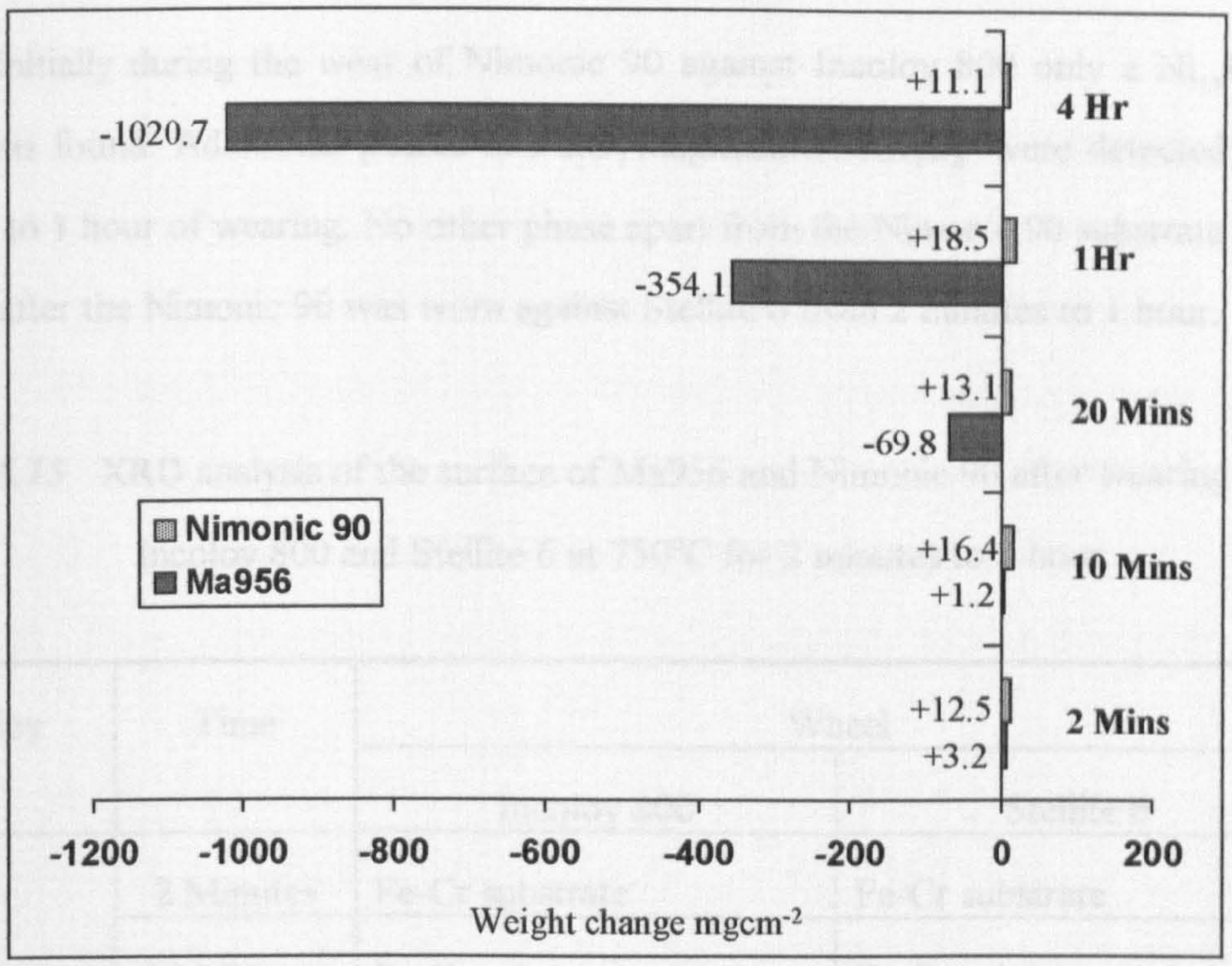

Fig.5.21 Weight changes of Nimonic 90 and Ma956 after wearing against Incoloy 800 at 750°C for 2 minutes to 4 hours

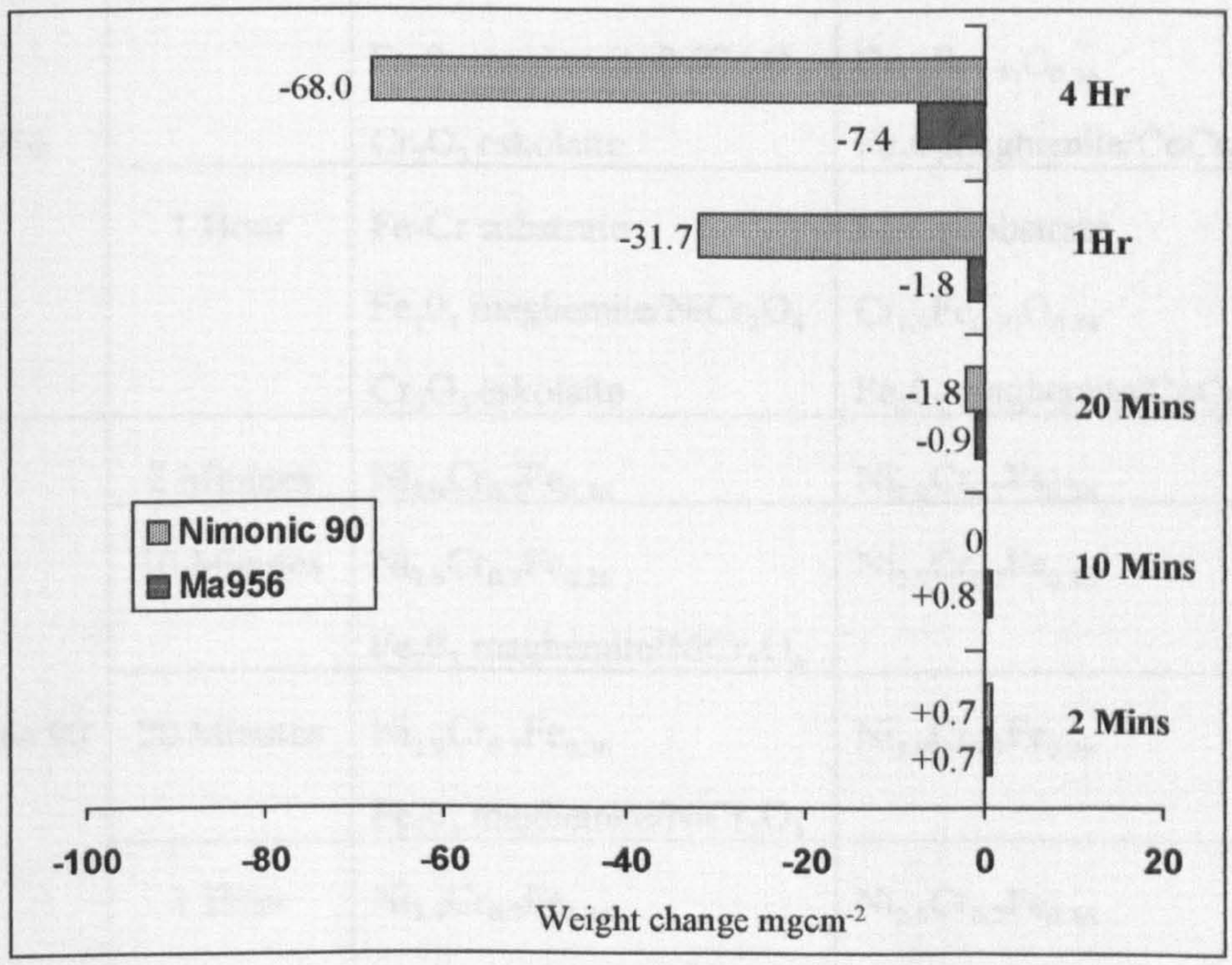

Fig.5.22 Weight changes of Nimonic 90 and Ma956 after wearing against Stellite 6 at 750°C for 2 minutes to 4 hours

Initially during the wear of Nimonic 90 against Incoloy 800 only a $Ni_{2.9}Cr_{0.7}Fe_{0.36}$ phase was found. Additional phases of Fe_2O_3 maghemite/$NiCr_2O_4$ were detected after 10 minutes to 1 hour of wearing. No other phase apart from the Nimonic 90 substrate could be located after the Nimonic 90 was worn against Stellite 6 from 2 minutes to 1 hour.

Table 5.15 XRD analysis of the surface of Ma956 and Nimonic 90 after wearing against Incoloy 800 and Stellite 6 at 750°C for 2 minutes to 1 hour

Alloy	Time	Wheel	
		Incoloy 800	Stellite 6
Ma956	2 Minutes	Fe-Cr substrate	Fe-Cr substrate
	10 Minutes	Fe-Cr substrate Fe_20_3 maghemite/$NiCr_2O_4$	Fe-Cr substrate
	20 Minutes	Fe-Cr substrate Fe_20_3 maghemite/$NiCr_2O_4$ Cr_2O_3 eskolaite	Fe-Cr substrate $Cr_{1.3}Fe_{0.70}O_{0.36}$ Fe_20_3maghemite/$CoCr_20_4$
	1 Hour	Fe-Cr substrate Fe_20_3 maghemite/$NiCr_2O_4$ Cr_2O_3 eskolaite	Fe-Cr substrate $Cr_{1.3}Fe_{0.70}O_{0.36}$ Fe_20_3 maghemite/$CoCr_20_4$
Nimonic 90	2 Minutes	$Ni_{2.9}Cr_{0.7}Fe_{0.36}$	$Ni_{2.9}Cr_{0.7}Fe_{0.36}$
	10 Minutes	$Ni_{2.9}Cr_{0.7}Fe_{0.36}$ Fe_20_3 maghemite/$NiCr_2O_4$	$Ni_{2.9}Cr_{0.7}Fe_{0.36}$
	20 Minutes	$Ni_{2.9}Cr_{0.7}Fe_{0.36}$ Fe_20_3 maghemite/$NiCr_2O_4$	$Ni_{2.9}Cr_{0.7}Fe_{0.36}$
	1 Hour	$Ni_{2.9}Cr_{0.7}Fe_{0.36}$ Fe_20_3 maghemite/$NiCr_2O_4$	$Ni_{2.9}Cr_{0.7}Fe_{0.36}$

5.4.3 SEM Morphological Analysis

The surface of Nimonic 90 after wearing against Incoloy 800 for 2 minutes was smeared with a thin layer of material from the counterface. The material did not fully cover the surface and some unaffected areas on Nimonic 90 surface could be observed as shown in **Fig.5.23a**. After 10 minutes of wear the Nimonic 90 surface was completely covered in the material layer (see **Fig.5.23b**). The micrographs obtained from Nimonic 90 after 20 minutes and 1 hour of wear against Incoloy 800 revealed glaze formation (**Fig.5.23c-Fig.5.23d**). These glazes were comprised of particles which became finer with increased wear time.

Plateaux composed of layered material were initially observed (2 minutes) on Nimonic 90 when it was worn against Stellite 6 (see **Fig.5.24a**). After 10 minutes, glaze formation occurred (see **Fig.5.24b**) but the size and coverage of the glaze started to decrease after 20 minutes (see **Fig.5.24c**). At 1 hour the wear surface on the Nimonic 90 was deeply grooved with only very small glazes (see **Fig.5.24d**) being present.

Fig.5.25a revealed the surface of Ma956 to be uneven and grooved after 2 minutes of wearing against Incoloy 800. However, after 10 minutes, shown in **Fig.5.25b,** the surface of the Ma956 was covered in large mounds (1mm length) which were slowly smoothed out with time (see **Fig.5.25c**) until they appeared as part of the Ma956 surface after 1 hour as shown in **Fig.5.25d**).

The Stellite 6 counterface produced a very different morphology on Ma956 from that observed with the Incoloy 800 counterface. After two minutes of testing against Stellite 6, small load-bearing plateaux developed on the surface of Ma956 comprised of layered material (**Fig.5.26a**). However, with increased wear time, glaze formation occurred (see **Fig.5.26b**) as shown by presence of coarse particles within the glaze which became finer with time, as shown in **Fig.5.26c-Fig.5.26d**.

Fig.5.23 SEM micrographs of Nimonic 90 worn against an Incoloy 800 counterface at 750°C for:

a - 2 minutes
b - 10 minutes
c - 20 minutes
d - 1 hour

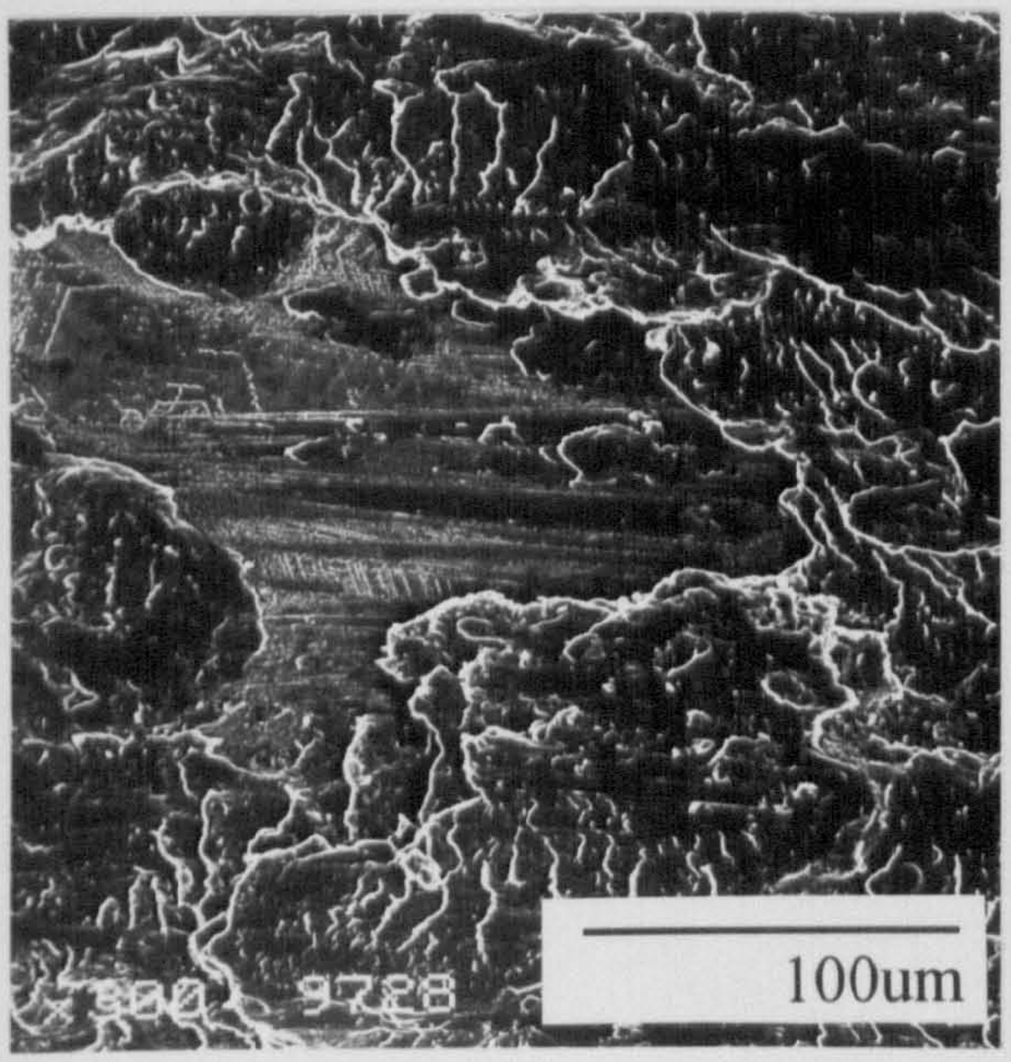

a

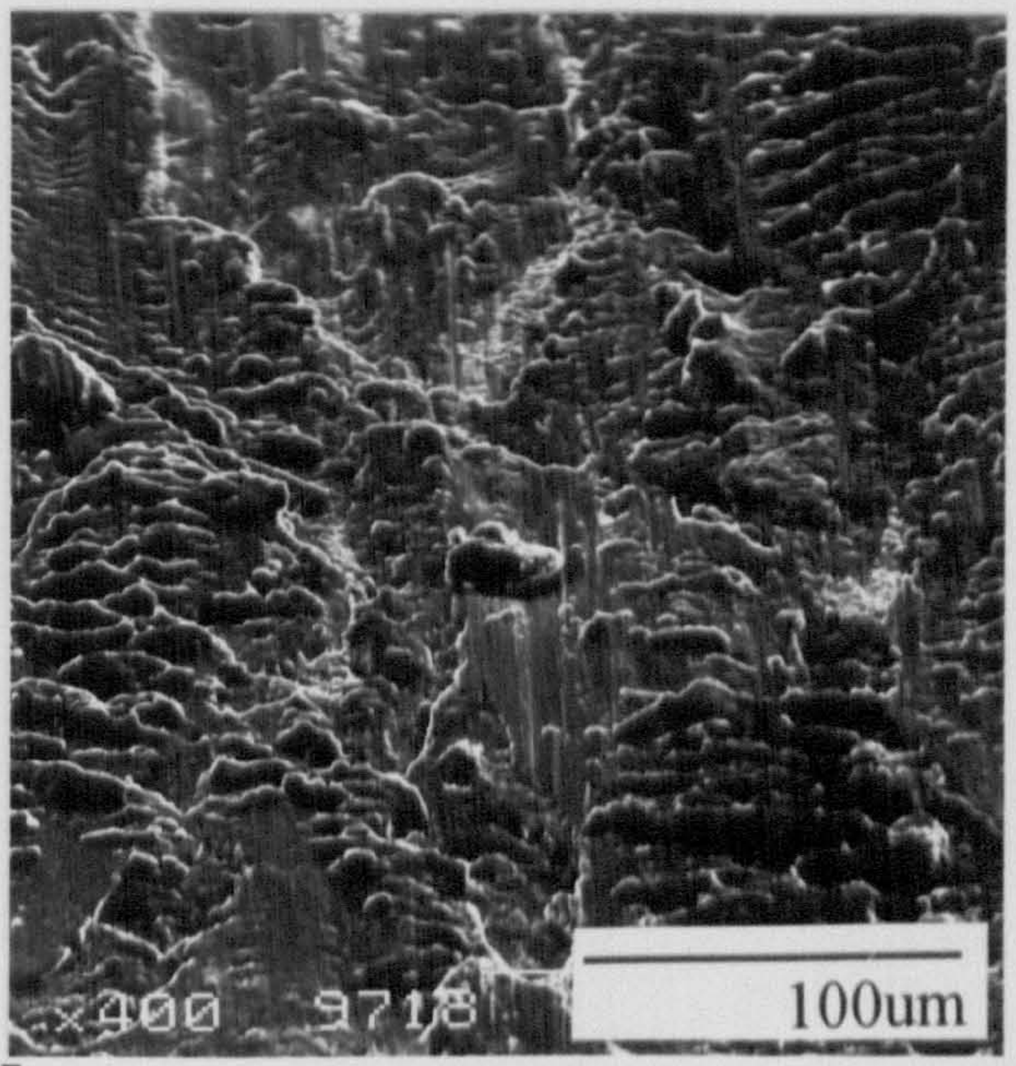

b

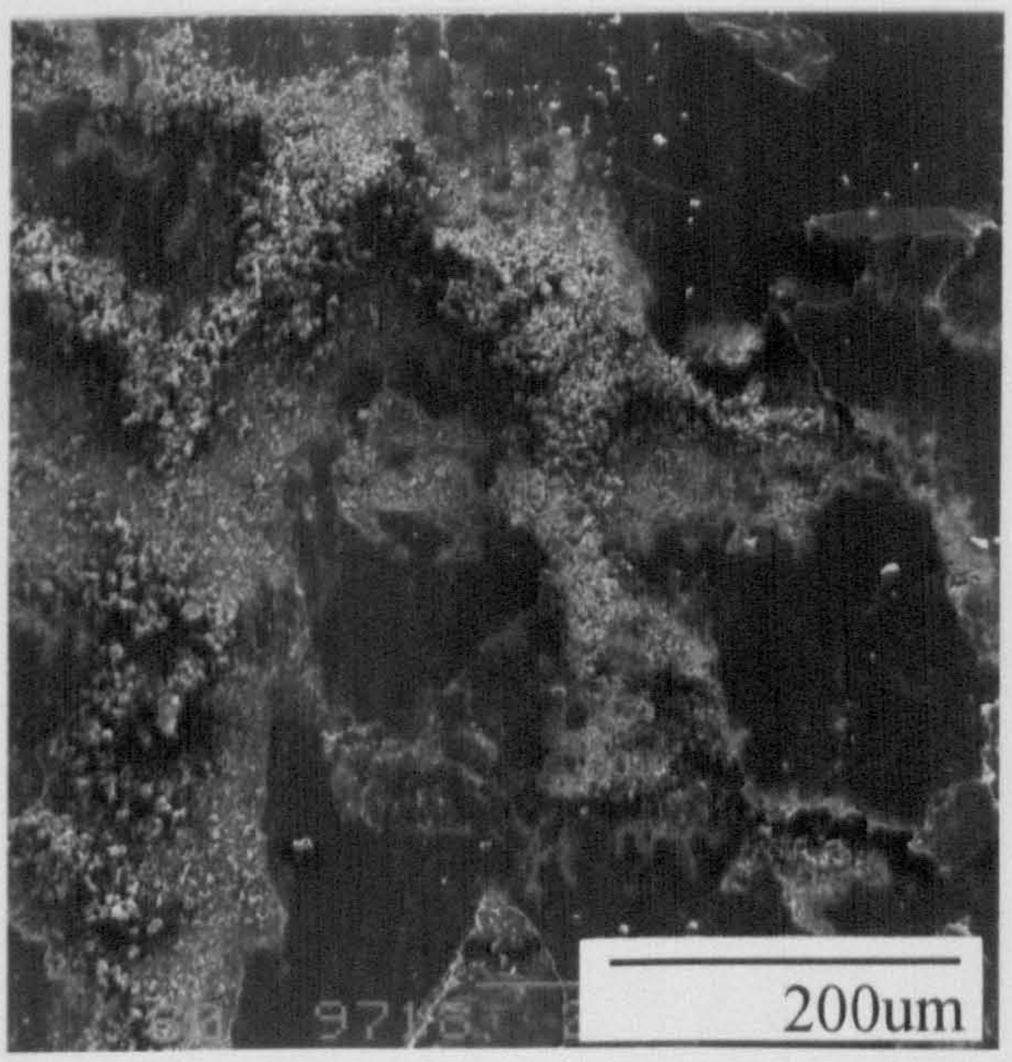

c

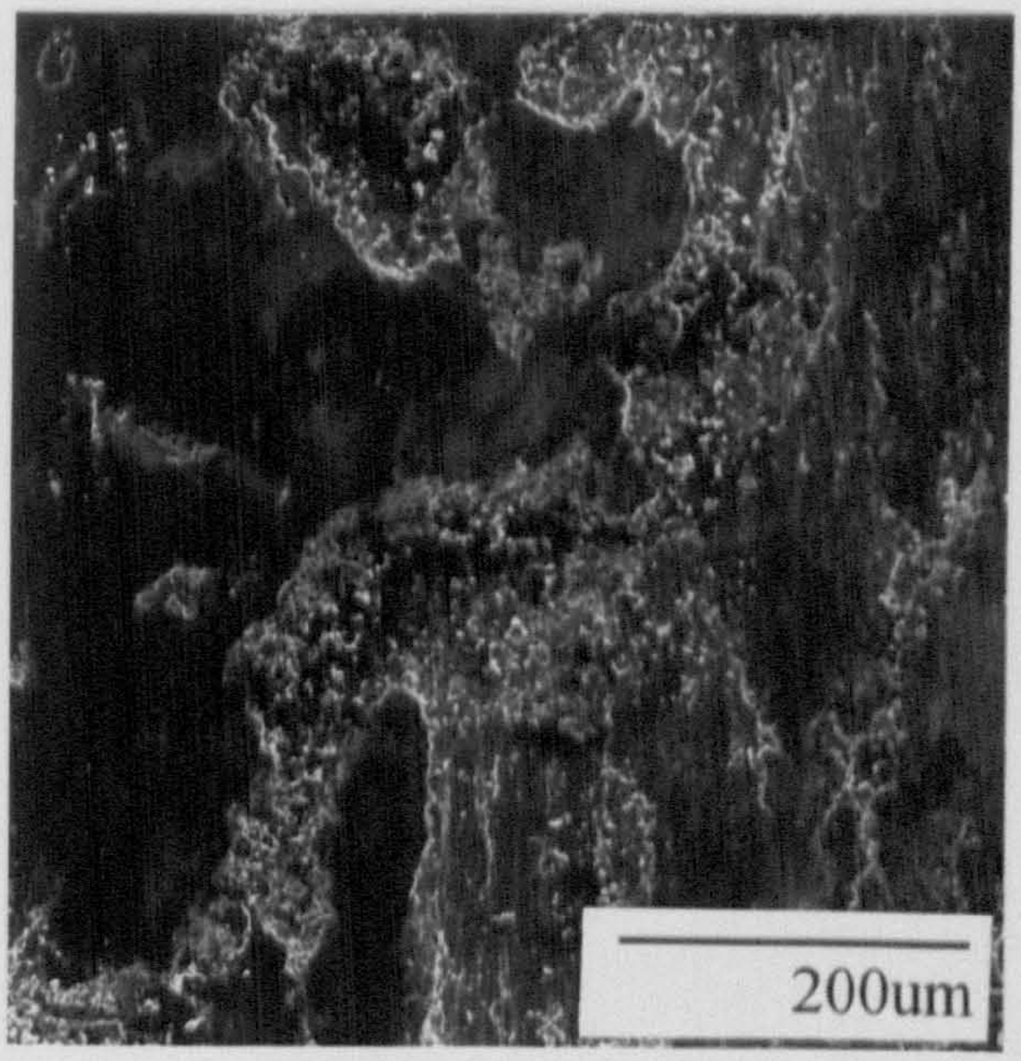

d

Fig.5.24 SEM micrographs of Nimonic 90 worn against a Stellite 6 counterface at 750°C for:

a - 2 minutes
b - 10 minutes
c - 20 minutes
d - 1 hour

a

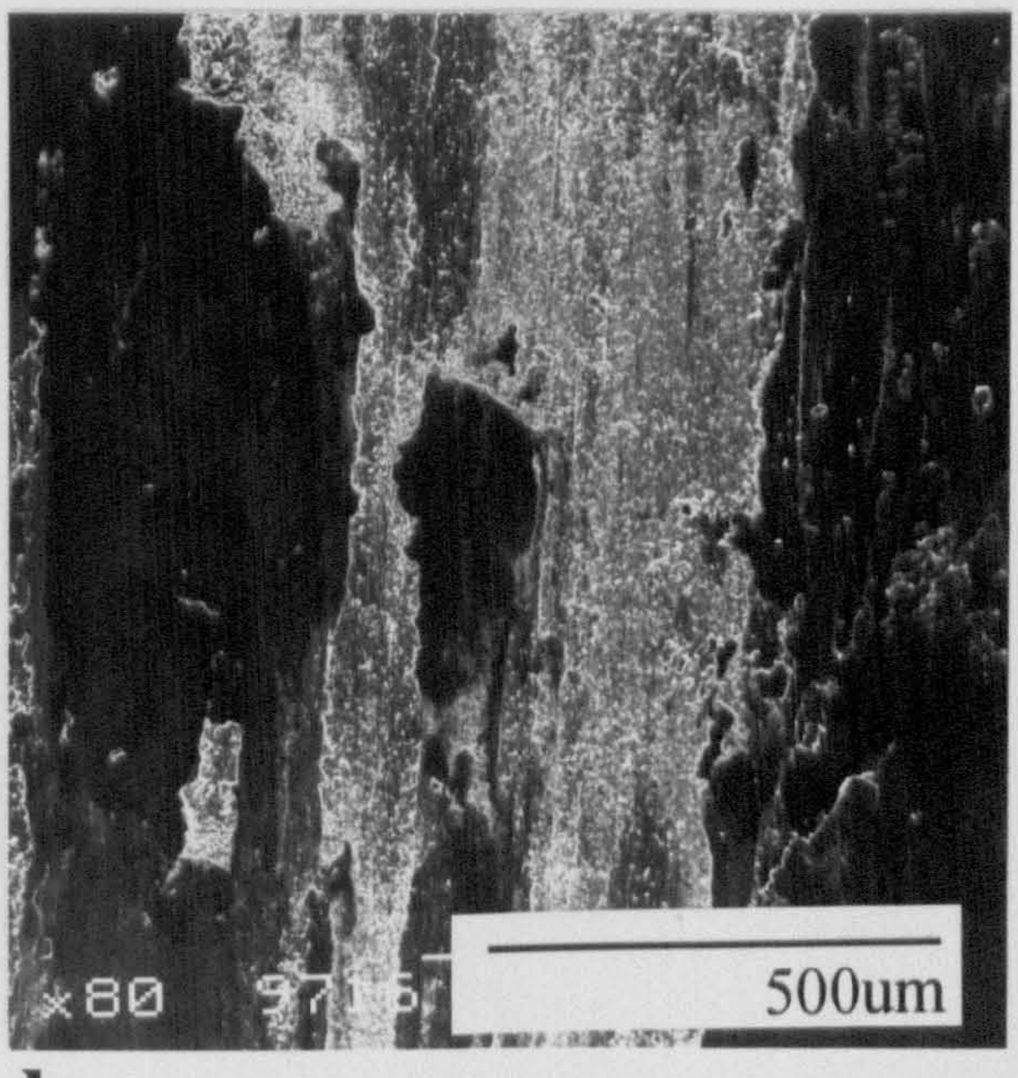

b

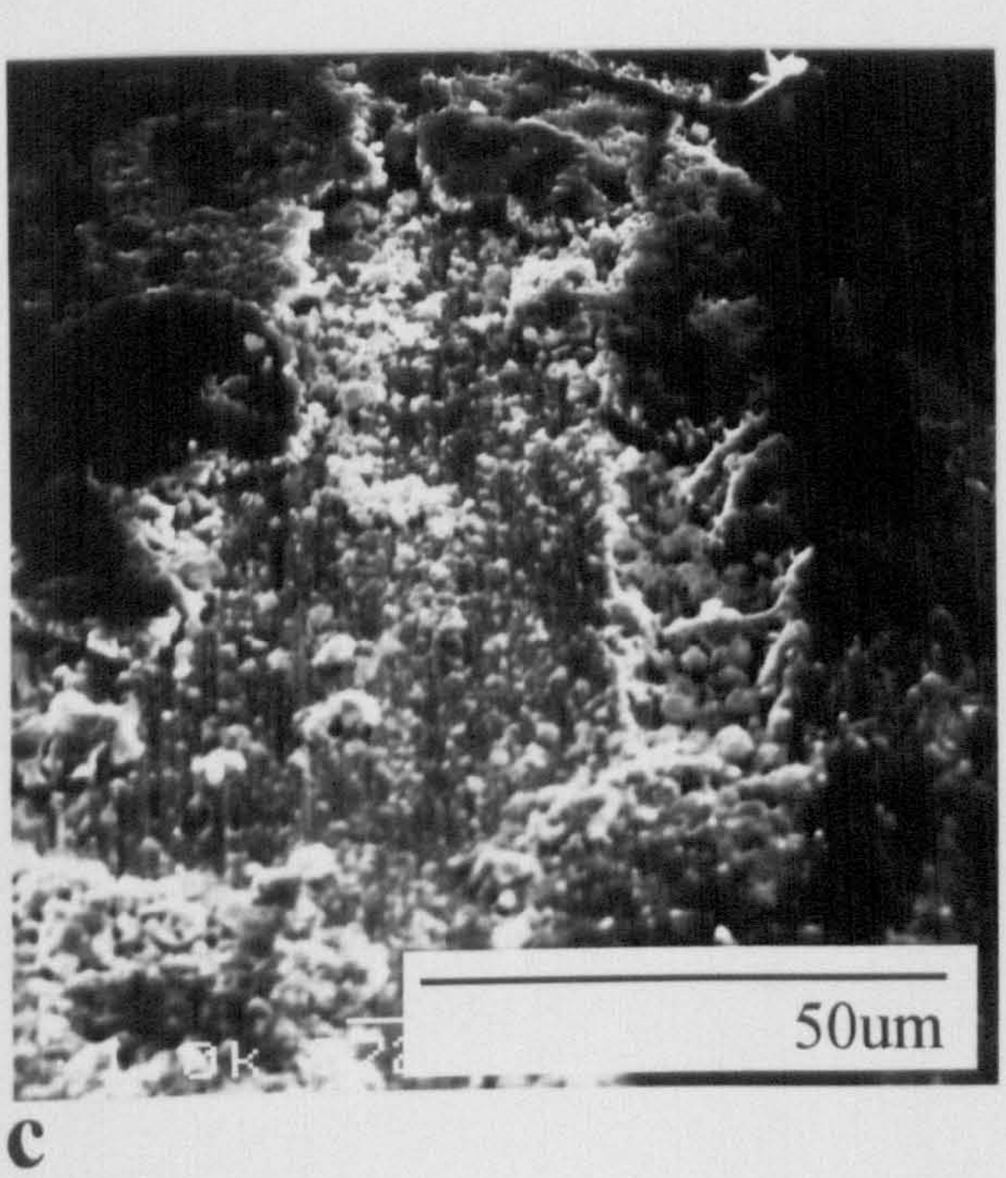

c

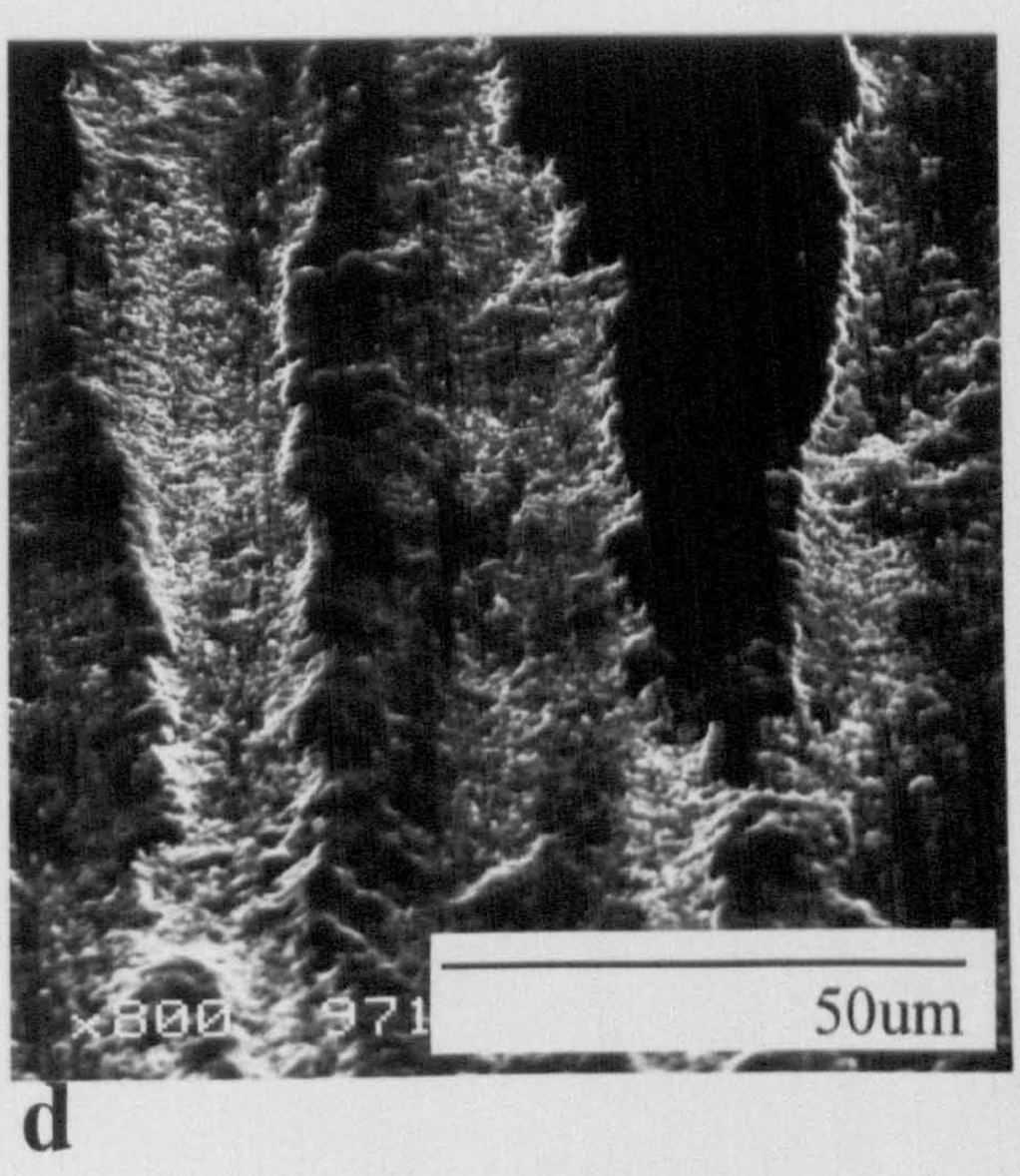

d

Fig.5.25 SEM micrographs of Ma956 worn against an Incoloy 800 counterface at 750°C for:

a - 2 minutes
b - 10 minutes
c - 20 minutes
d - 1 hour

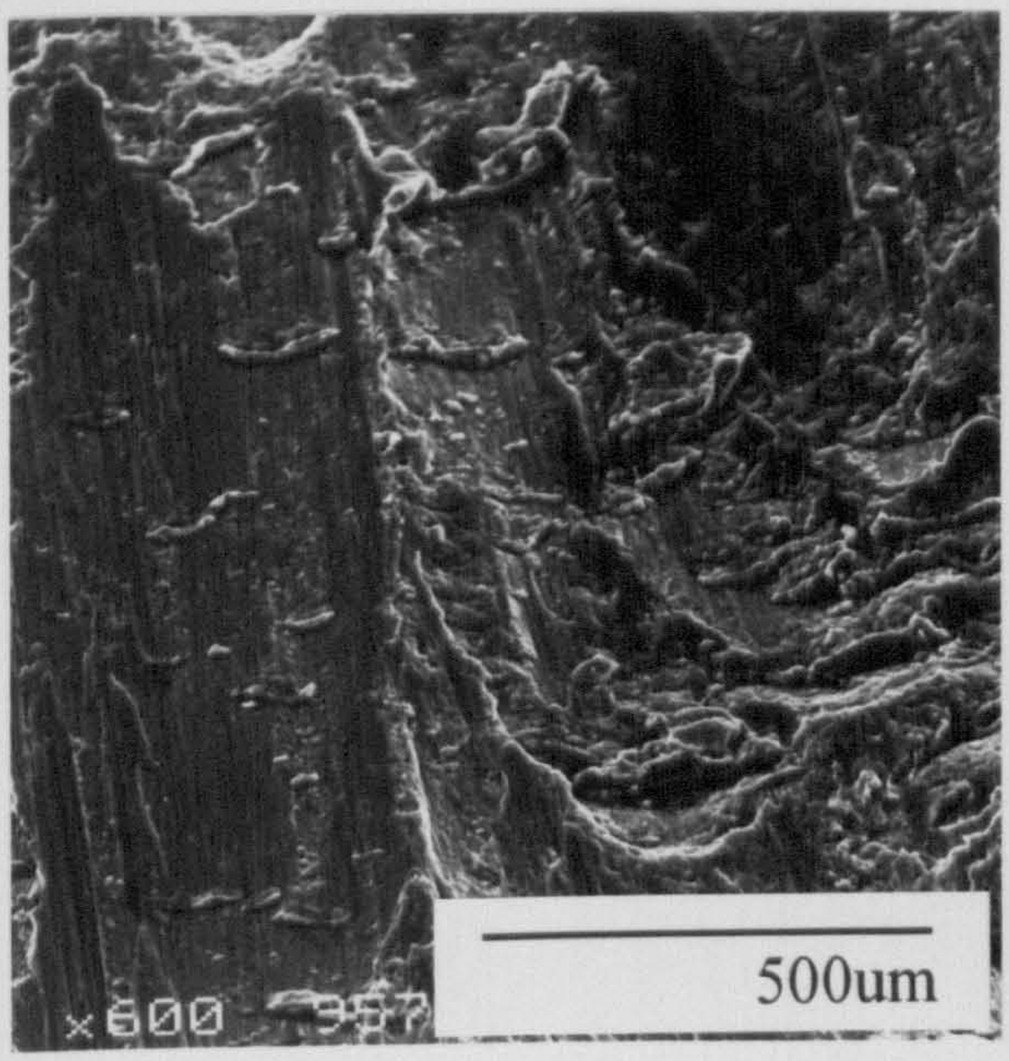

a

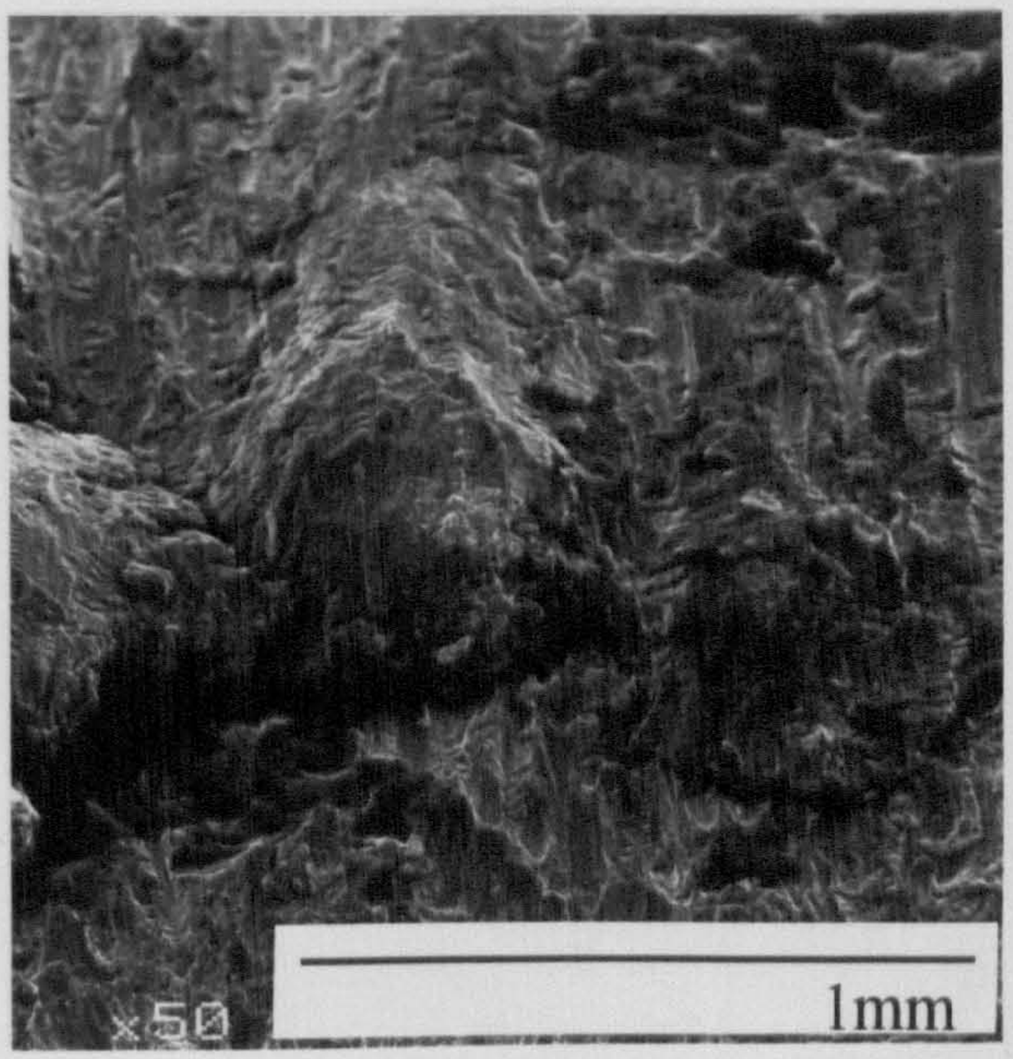

b

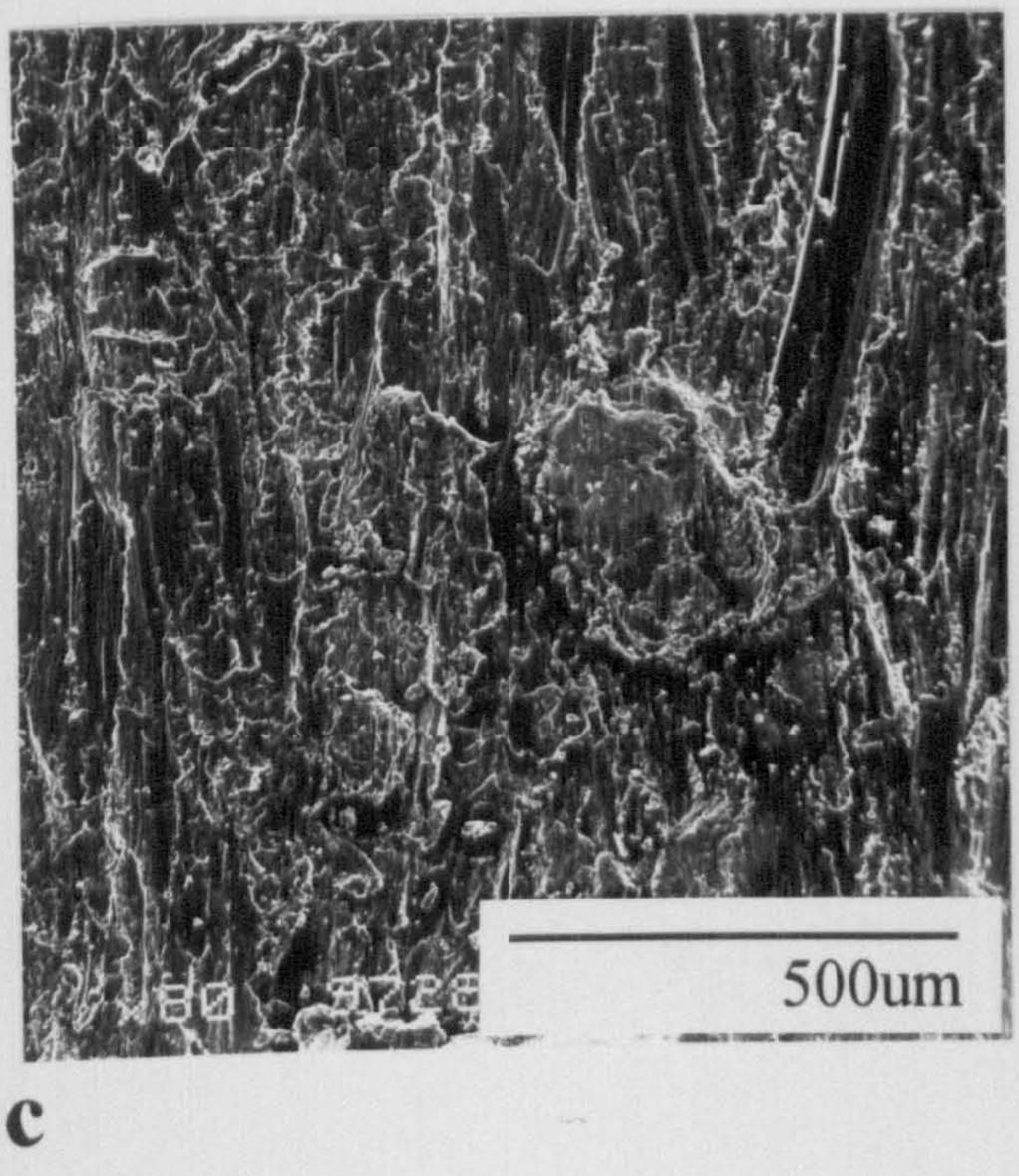

c

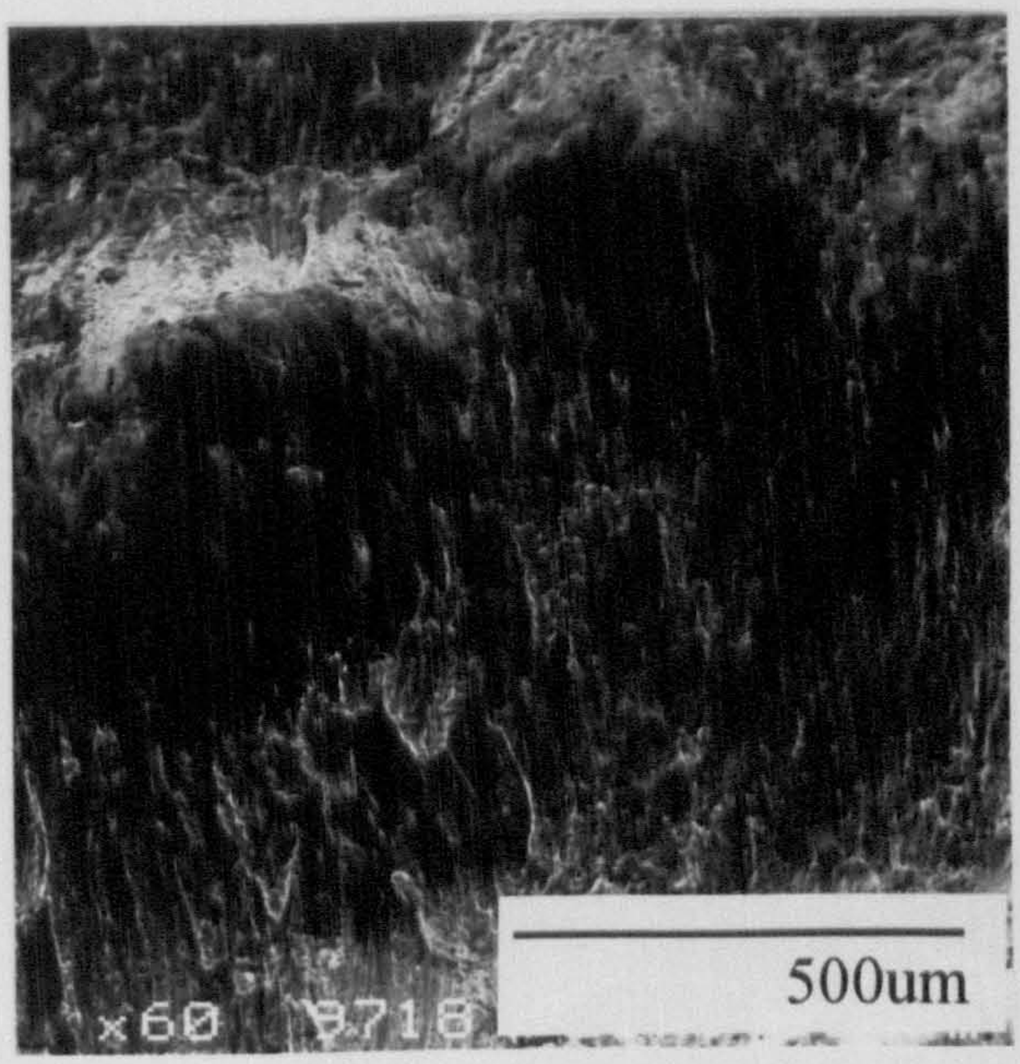

d

Fig.5.26 SEM micrographs of Ma956 worn against a Stellite 6 counterface at 750°C for:

a - 2 minutes
b - 10 minutes
c - 20 minutes
d - 1 hour

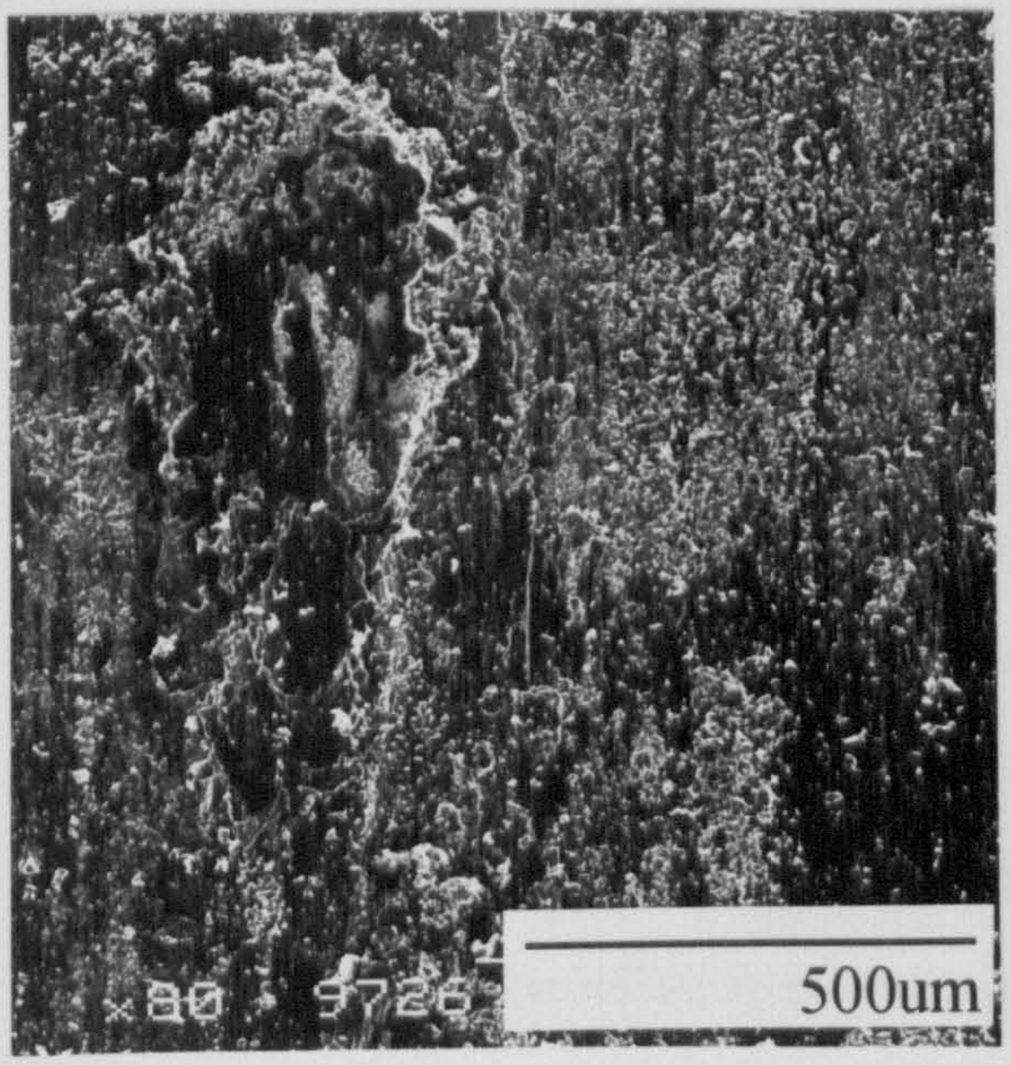

a

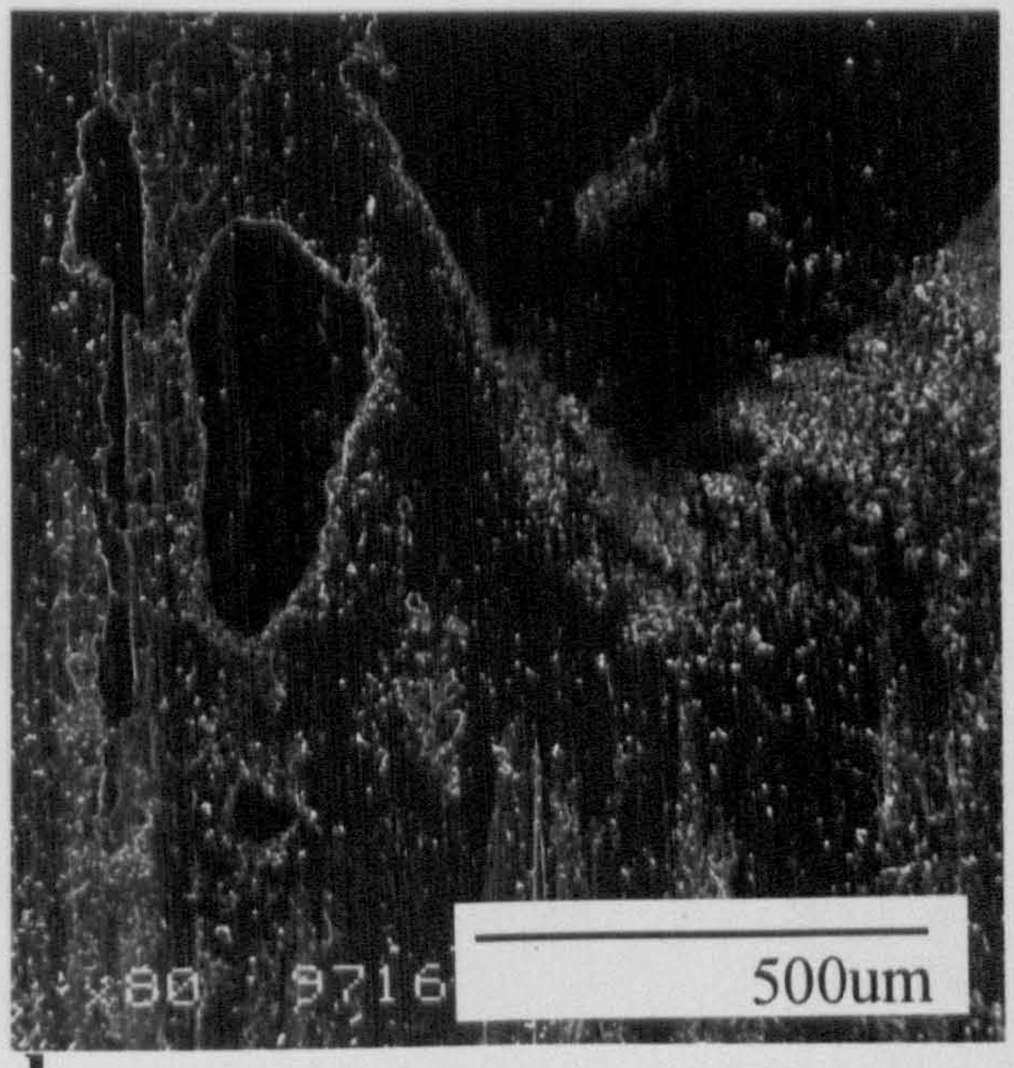

b

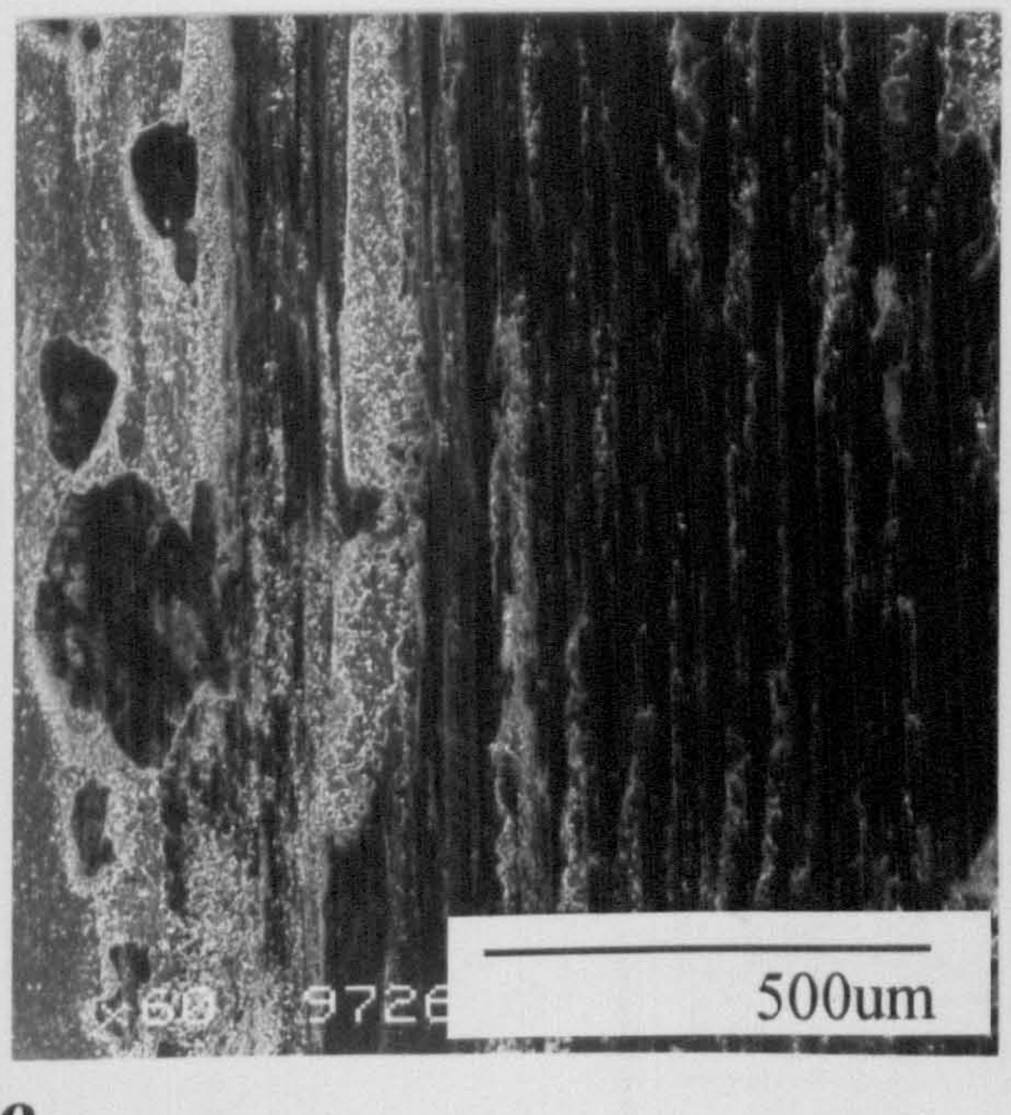

c

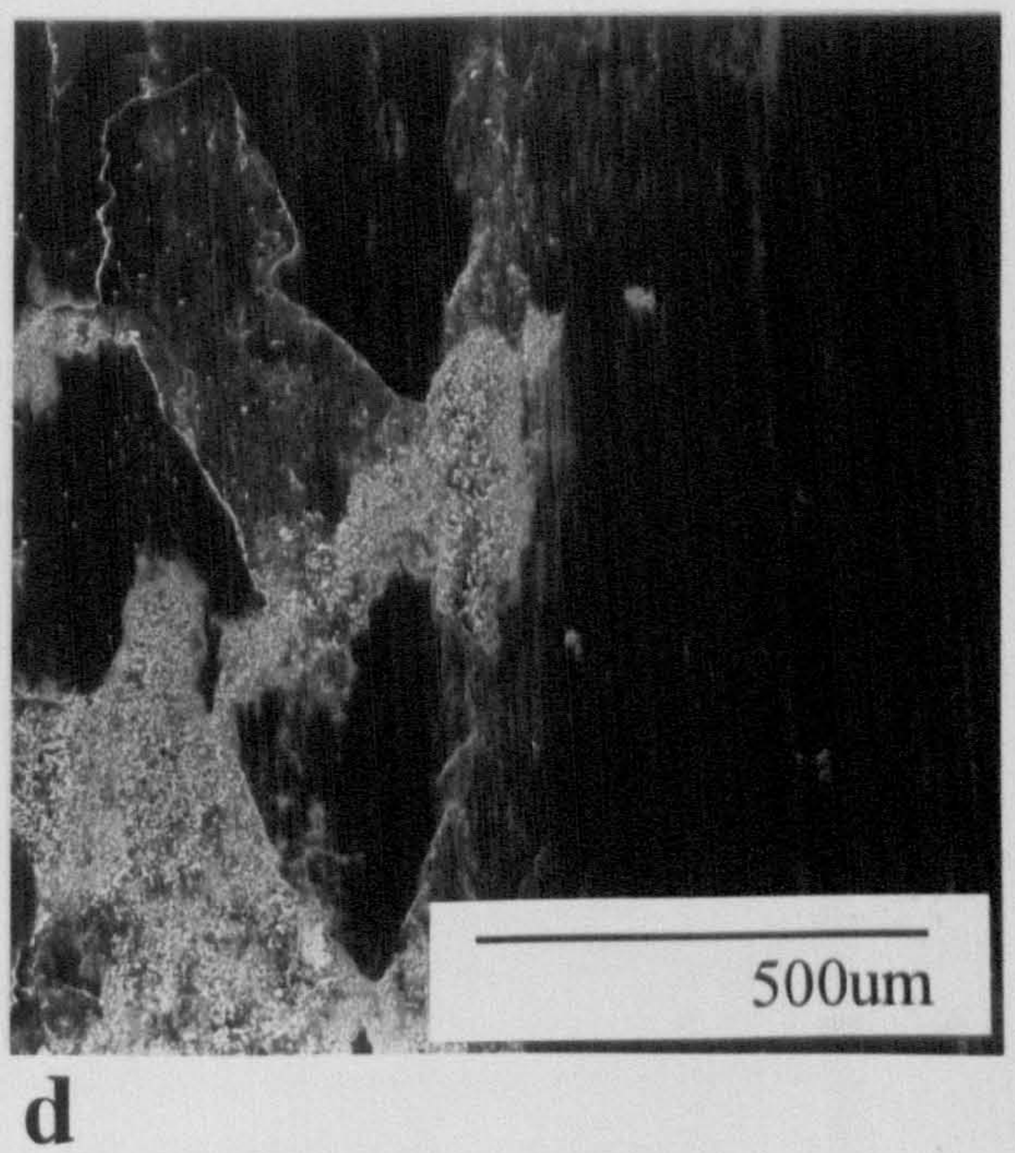

d

5.4.4 Hardness Testing

The hardness values determined on Ma956 and Nimonic 90 after wearing against Incoloy 800 and Stellite 6 at 750^{o}C are displayed in ***Table 5.16***. Reliable hardness values could not be recorded for any of the Ma956 samples worn against Incoloy 800 as the surface was too uneven. However, hardness values, measured on Ma956 after wearing against Stellite 6 showed an initial increase in hardness from an unworn value of Hv303 to Hv523 after 2 minutes. After 10 minutes the hardness of the worn Ma956 decreased to Hv368 but increased to a value of Hv533 after 1 hour.

Higher hardness values were measured on Nimonic 90 after wearing against Incoloy 800 and Stellite 6 than on Ma956. Values of Hv812 and Hv878 were recorded after 20 minutes and 1 hour respectively of wearing against Incoloy 800. Testing of the Nimonic 90 samples after wearing against Stellite 6 proved difficult as the plateaux formed during the early stages of wearing were either too small or cracked during hardness testing. Only one hardness value of Hv753 was recorded after 20 minutes.

Table 5.16 Hardness of Ma956 and Nimonic 90 after wearing against Incoloy 800 and Stellite 6 at 750°C for 2 minutes to 1 hour

Alloy	Duration (minutes)	Hardness Hv 500g	
		Incoloy 800	Stellite 6
MA956	2	Too uneven	523
	10	Too uneven	368
	20	Too uneven	502
	60	Too uneven	533
Nimonic 90	2	Too uneven	Too uneven
	10	Too uneven	Too uneven
	20	812	753
	60	878	Too uneven

5.4.5 Cross-Sectional EDX of Block Alloys/EDX Analysis of Counterface and EDX Analysis of Wear Debris

Tables 5.17-5.20 display a summary of various analysis made after Ma956 or Nimonic 90 was worn against Incoloy 800 or Stellite 6 at 750°C for 2 minutes to 1 hour.

Cross-sectional analysis of the wear scar on Nimonic 90 after wearing against Incoloy 800 for 2 minutes revealed a partially oxidised layer of Ni/Fe/Cr material present, 40μm thick. This layer was also detected at 10 minutes, 20 minutes and 1 hour, though an oxidised layer containing mainly Fe was seen to form at the very surface of the layer in the latter times (see **Fig.5.27c**). Observations of the Incoloy 800 counterface showed the presence of glazes after 20 minutes and 1 hour being composed of mainly Fe oxides as shown in **Fig.5.29b-Fig.5.29c.**. Analysis of the wear debris revealed similar wear particles produced throughout the test. These were flat angular particles <500μm in diameter and contained Fe/Cr/Ni (see **Fig.5.31a**).

An oxidised Co/Cr layer 15μm thick was detected on Nimonic 90 after wearing against Stellite 6 for 2 minutes as shown in **Fig.5.28a**. The Co/Cr layer increased in thickness to 30μm after 10 minutes and thin layers of Ni material were observed within it. At 20 minutes, cross-sectional analysis revealed the layer to be comprised of two separate materials (see **Fig.5.28b**). One material contained mainly Ni/Cr and other was composed of mainly Co/Cr. After 1 hour of wearing a mixed oxide layer could not be detected on the Nimonic 90. Glaze formation was observed on the Stellite 6 counterface after 10 minutes as shown in **Fig.5.30b**. The glazes were composed of mainly Co/Cr oxides but also consisted of some Ni oxides. The content of Co was seen to decrease with increasing wear time until after 1 hour the glazes on the Stellite 6 counterface contained mainly Ni/Cr with only a little Co (see **Fig.5.30c**). Collected wear analysis showed two types of wear particles were produced. One type was a Co/Cr powdery particle (<100μm diameter) and only appeared to be produced in the early stages of wearing while the second type, a flat angular particle containing Ni/Cr/Co (see **Fig.5.31b**), and was observed throughout the test.

Deformation and partial oxidation of Ma956 occurred after the alloy was worn against Incoloy 800 for 2 minutes (see **Fig.5.32a**). Small amounts of nickel were also detected in the deformed region. After 10 minutes wear, the wear scar of the Ma956 was 120μm thick and contained unoxidised Ni/Fe/Cr material. At 20 minutes the wear scar was comprised of two separate materials containing Ni/Fe/Cr and Fe/Cr/Al and was approximately 50μm thick as shown in **Fig.5.32b**. A very much thinner wear scar, less than 5μm, was observed on the Ma956 after 1 hour of wearing against the Incoloy 800 counterface, being composed of Ni/Cr (see **Fig.5.32c**). Glazes were seen to occur on the Incoloy 800 counterface after 20 minutes and 1 hour of wearing and were formed from mainly Fe/Cr oxides as shown in **Fig.5.34b** and **Fig.5.34c**. The formation of flat angular particles (<500μm diameter) containing Ni/Cr/Fe were observed during testing up to 1 hour. Additional flat angular particles (<500μm diameter) composed of Fe/Cr/Al were detected after 20 minutes and 1 hour (see **Fig.5.36a**).

Analysis of the surface of Ma956 after wearing against Stellite 6 for 2 minutes revealed the formation of an oxidised Co/Cr layer 3μm thick as shown in **Fig.5.33a**. However, after 10 minutes, subsequent analyses of the Ma956 showed the layer to be composed of Fe/Cr/Al/Co oxides varying from 5-10μm in thickness (see **Fig.5.33b** and **Fig.5.33c**). Glaze formation was observed on the Stellite 6 counterface after 10 minutes with the glazes consisting of oxides of Co/Cr and a little Fe (see **Fig.5.35b**). However, at 20 minutes and 1 hour a change in composition was observed with mainly oxides of Fe being detected with some Cr/Co as shown in **Fig.5.35c**. Three types of wear debris particles were observed to be produced during the wear of Ma956 with Stellite 6 all <50μm in diameter. Two types were flat and angular, one containing Co/Cr + little Fe and the other comprised of Fe/Cr + little Co. The third type of particle had a powdery structure that contained Co/Cr (see **Fig.5.36b**) and was only produced in the early stages of wearing (<10 minutes).

Table 5.17 Analysis of the wearing system: Nimonic 90 vs. Incoloy 800 for 2 minutes to 1 hour at 750°C

Duration	Nimonic 90 sample (SEM/cross sectional EDX)	In800 counterface (SEM/spot EDX)	Wear debris (SEM/spot EDX)
2 mins	Wear scar (40μm thick) contained partially oxidised Ni/Fe/Cr (see **Fig.5.27a**). Incomplete layer of smeared material on surface	Worn surface - no glazes, contained mainly oxidised Ni/Fe/Cr (see **Fig.5.29a**)	One type of flat angular debris (<200μm diameter) - contained Ni/Fe/Cr
10 mins	Wear scar (10μm thick) contained oxidised Ni/Fe/Cr. Surface covered in smeared layer	Worn surface - no glazes, contained mainly oxidised Ni/Fe/Cr	One type of flat angular debris (<500μm diameter). Contained Ni/Fe/Cr
20 mins	Wear scar (20μm thick) contained a mainly oxidised Fe layer on top of a Ni/Fe/Cr layer (see **Fig.5.27b**). Glaze formation	Glazed surface - contained mainly Fe (see **Fig.5.29b**)	One type of flat angular debris (<500μm diameter). Contained Ni/Fe/Cr
1 hour	Wear scar (12μm thick) contained a mainly oxidised Fe layer on top of a partially oxidised Ni/Fe/Cr layer (see **Fig.5.27c**). Glaze formation	Glazed surface - contained mainly Fe (see **Fig.5.29c**)	One type of flat angular debris (<500μm diameter). Contained Ni/Fe/Cr (see **Fig.5.31a**)

Table 5.18 Summary of the analysis of the wearing system: Nimonic 90 vs Stellite 6 for 2 minutes to 1 hour at 750°C

Duration	Nimonic 90 sample (SEM/cross-sectional EDX)	Stellite 6 counterface (SEM/spot EDX)	Wear debris (SEM/spot EDX)
2 mins	Wear scar (15μm thick) contained partially oxidised Co/Cr. (see **Fig.5.28a**). Plateaux present comprised of layered material	Worn surface - no glazes. Surface contained mainly Co/Cr oxides (see **Fig.5.30a**)	2 types (<100μm): 1. Co/Cr (powdery particles) 2. Co/Cr/Ni (flat angular)
10 mins	Wear scar (30μm thick) contained mainly oxidised Co/Cr and thin Ni oxide layers. Glaze formation	Glazed surface - consisted of mainly Co/Cr oxides but also some Ni oxides (see **Fig.5.30b**)	2 types (<100μm): 1. Co/Cr (powdery particles) 2. Co/Cr/Ni (flat angular)
20 mins	Wear scar (10μm thick) consisted of a partially oxidised layer of two materials: 1. Ni/Cr 2. Co/Cr (see **Fig.5.28b**). Glaze coverage decreased	Glazed surface - consisted of Co/Cr/Ni oxides	1 type (<100μm): Co/Cr/Ni (flat angular) - Co content decreases with time.
1 hour	No mixed oxide layer observed. (see **Fig.5.28c**). Very small glazes present on surface	Glazed surface - consisted of mainly Ni/Cr oxides and some Co oxides (see **Fig.5.30c**)	1 type (<100μm): Co/Cr/Ni (flat angular) (see **Fig.5.31b**)

Table 5.19 Summary of the analysis of the wearing system: Ma956 vs Incoloy 800 for 2 minutes -1 hour at 750°C

Duration	Ma956 sample (SEM/cross-sectional EDX)	In800 counterface (SEM/spot EDX)	Wear debris (SEM/spot EDX)
2 mins	Wear scar (10μm thick) comprised of deformed and partially oxidised Fe/Cr/Al and some Ni (see **Fig.5.32a**). Uneven and grooved surface	Worn surface - contained Ni/Fe/Cr (see **Fig.5.34a**)	Flat angular particles (<500μm diameter) contained mainly Ni/Fe/Cr
10 mins	Wear scar (120μm thick) contained unoxidised Ni/Fe/Cr. Large mounds on surface	Worn surface - contained mainly Ni/Cr but also small amount of Fe	Flat angular particles (<500μm diameter) contained mainly Ni/Fe/Cr
20 mins	Wear scar (50μm thick) contained two materials: 1. Ni/Fe/Cr 2. Fe/Cr/Al (see **Fig.5.32b**). Smoother mounds on surface	Glazed surface comprised of Fe/Cr oxides (see **Fig.5.34b**)	Two types of flat angular particles (<500μm diameter) contained: 1. Ni/Fe/Cr 2. Fe/Cr/Al
1 hour	Wear scar comprised of very thin Ni/Cr oxide layer <5μm. (see **Fig.5.32c**). Smooth mounds on surface	Glazed surface comprised of Fe/Cr oxides (see **Fig.5.34c**)	Two types of flat angular particles (<500μm diameter) contained: 1. mainly Ni/Cr/Fe 2. Fe/Cr/Al (see **Fig.5.36a**)

Table 5.20 Summary of the analysis of the wearing system: Ma956 vs Stellite 6 for 2 minutes -1 hour at 750°C

Duration	Ma956 sample (SEM/cross-sectional EDX)	St6 counterface (SEM/spot EDX)	Wear debris (SEM/spot EDX)
2 mins	Wear scar (3μm thick) comprised of an oxidised Co/Cr layer (see **Fig.5.33a**). Plateaux present composed of layered material	Worn surface - consisted of mainly Co/Cr with some Fe (see **Fig.5.35a**)	Three types (<50μm diameter): 1. Fe/Cr + little Co (flat angular) 2. Co/Cr (powdery particle) 3. Co/Cr + little Fe (flat angular)
10 mins	Wear scar (10μm thick) contained partially oxidised Fe/Cr/Al/Co layer (see **Fig.5.33b**). Glaze formation	Glazed surface - consisted of mainly Co/Cr and some Fe oxides (see **Fig.5.35b**)	Two types (<50μm diameter): 1. Fe/Cr + little Co (flat angular) 2. Co/Cr + little Fe (flat angular)
20 mins	Wear scar (10μm thick) comprised of partially oxidised layer of Fe/Cr/Al/Co oxides. Glaze formation	Glazed surface - consisted of mainly Fe but also some Cr/Co oxides	Two types (<50μm diameter): 1. Fe/Cr + little Co (flat angular) 2. Co/Cr + little Fe (flat angular)
1 hour	Wear scar (5μm thick) comprised of oxidised layer of mainly Fe/Cr/Al/Co (see **Fig.5.33c**). Glaze formation	Glazed surface - consisted of mainly Fe but also some Cr/Co oxides (see **Fig.5.35c**)	Two types (<50μm diameter): 1. Fe/Cr + little Co (flat angular) 2. Co/Cr + little Fe (flat angular) (see **Fig.5.36b**)

Fig.5.27 Cross-sectional EDX analysis of Nimonic 90 worn against an Incoloy 800 counterface at 750°C for:

a - 2 minutes
b - 20 minutes
c - 1 hour

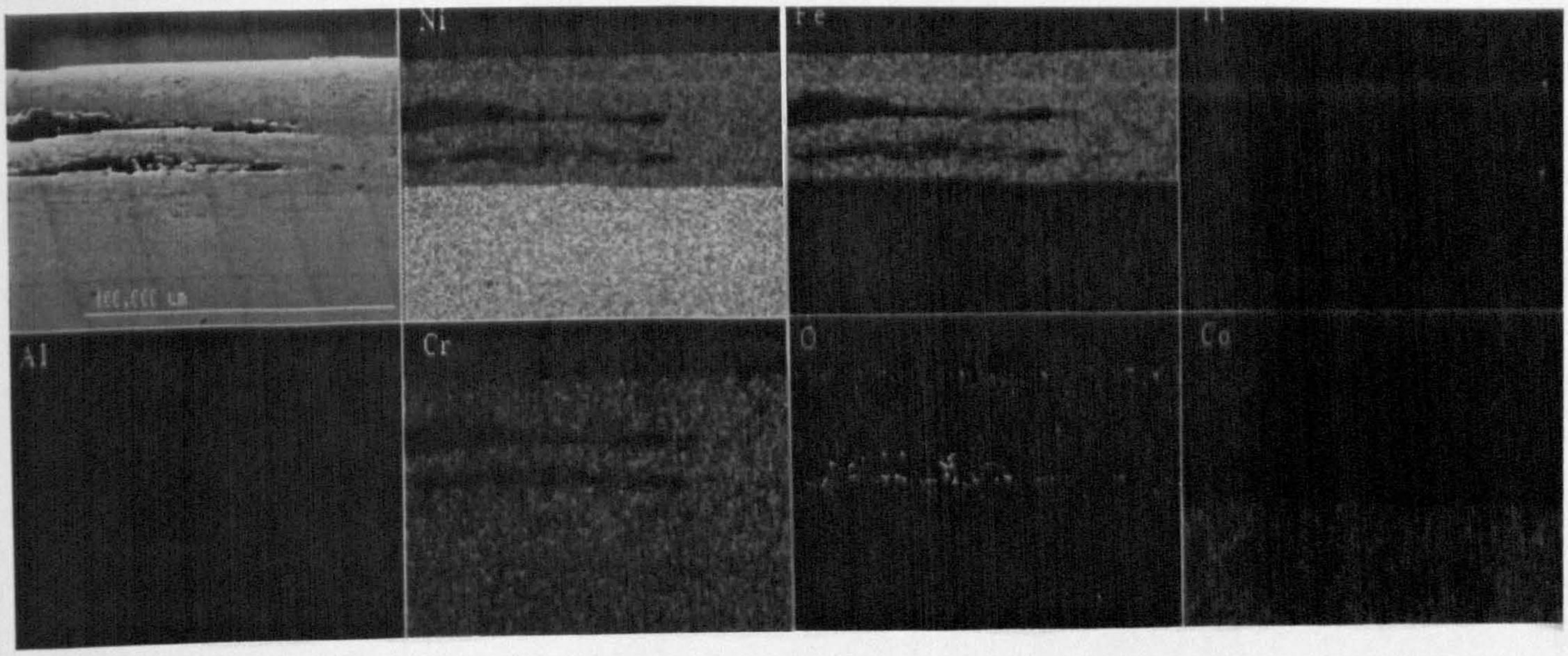

a

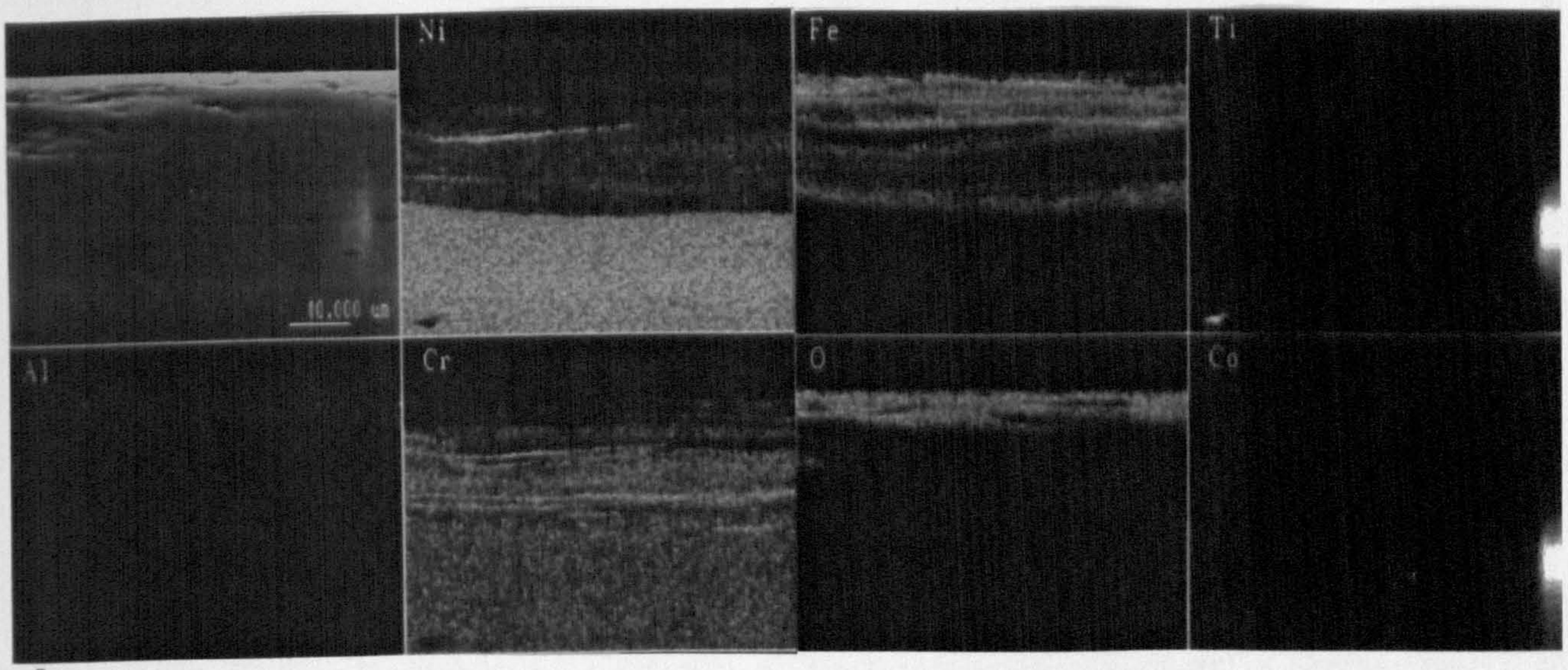

b

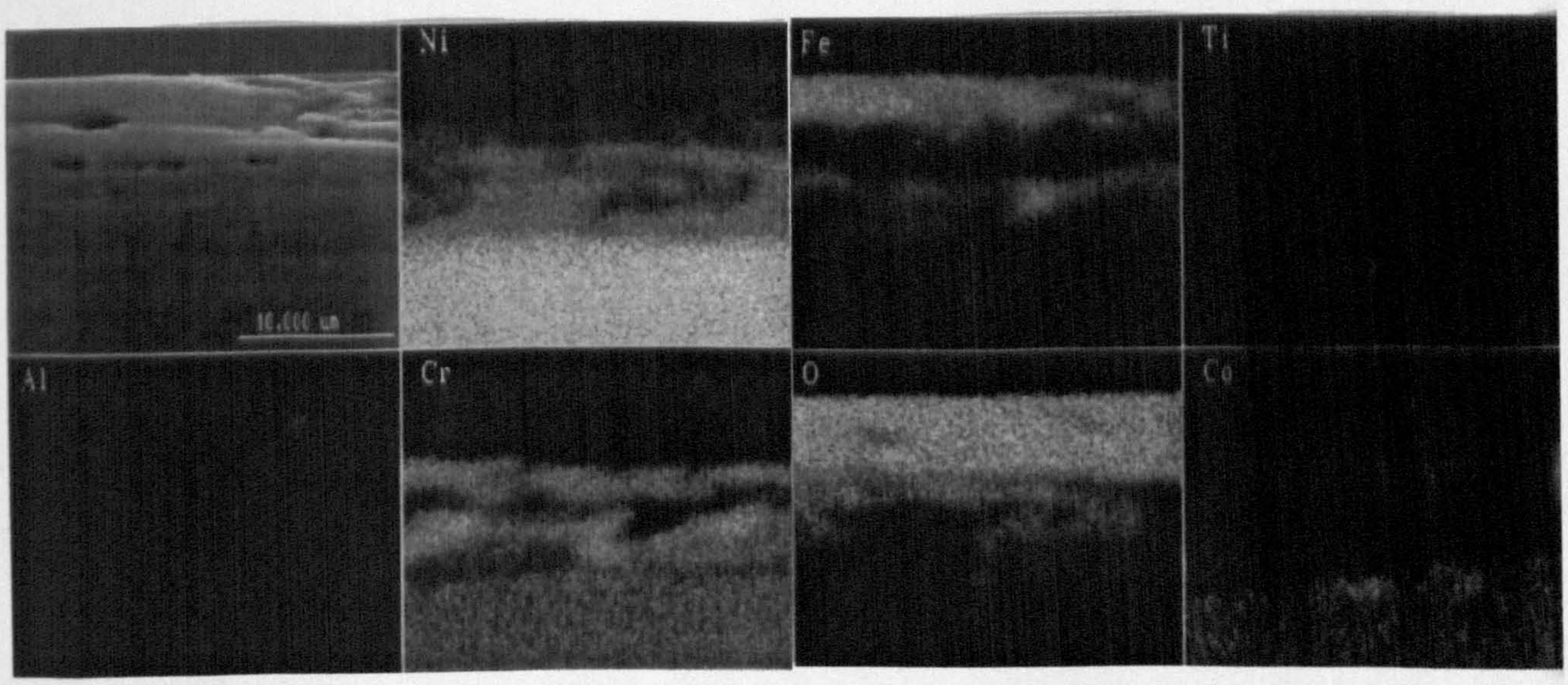

c

Fig.5.28 Cross-sectional EDX analysis of Nimonic 90 worn against a Stellite 6 counterface at 750°C for:

a - 2 minutes
b - 20 minutes
c - 1 hour

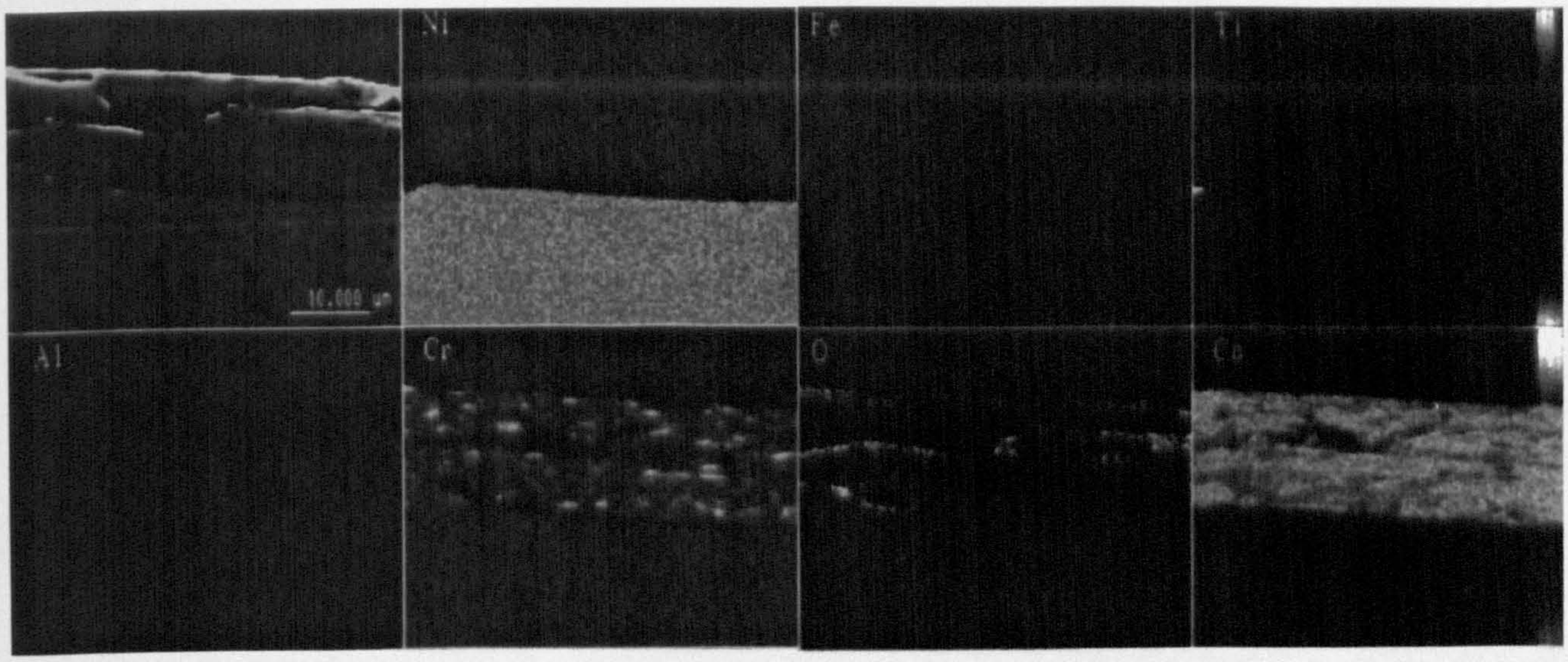

a

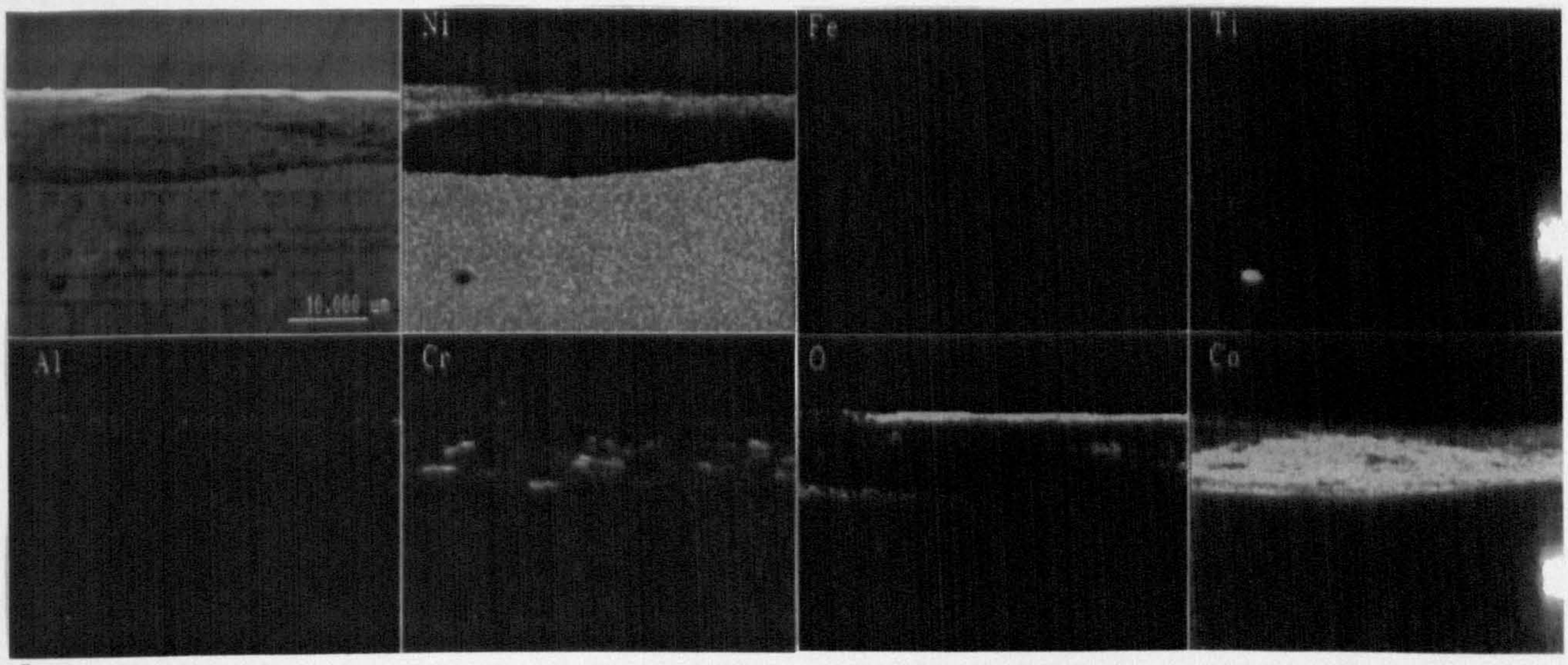

b

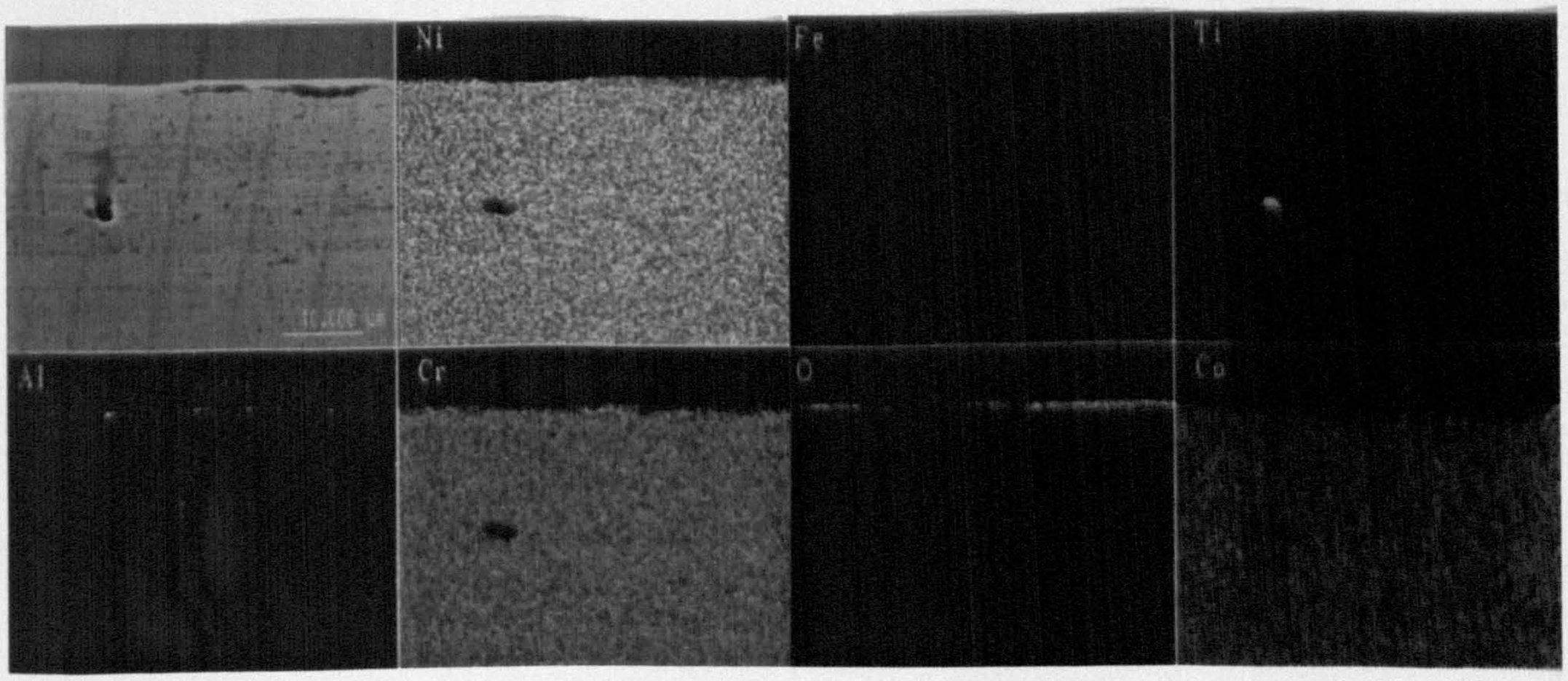

c

Fig.5.29 SEM micrographs and EDX analysis of an Incoloy 800 **counterface** after wearing against Nimonic 90 at 750°C for:

a - 2 minutes
b - 20 minutes (analysis of glaze)
c - 1 hour (analysis of glaze)

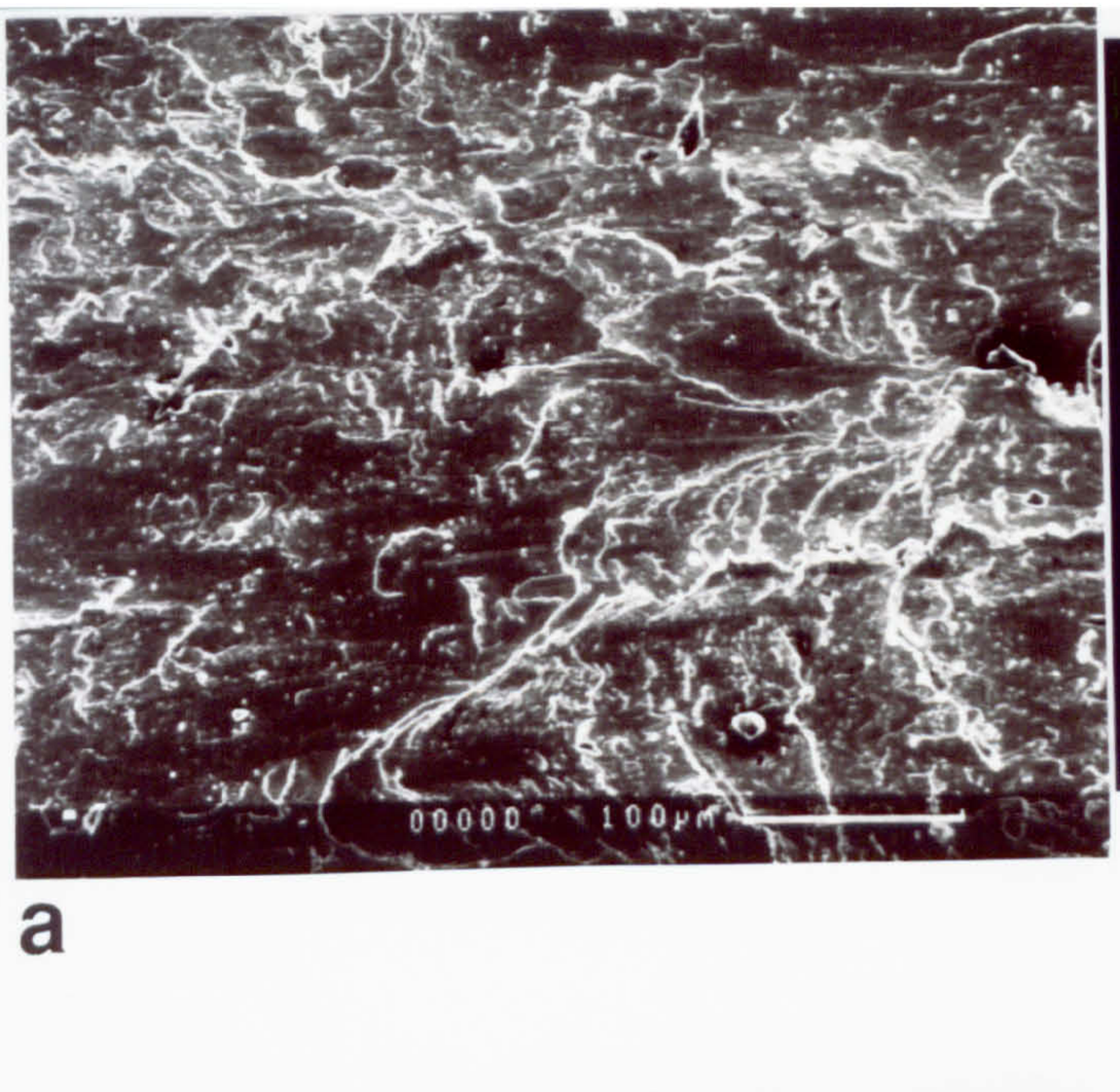
00000 100µm

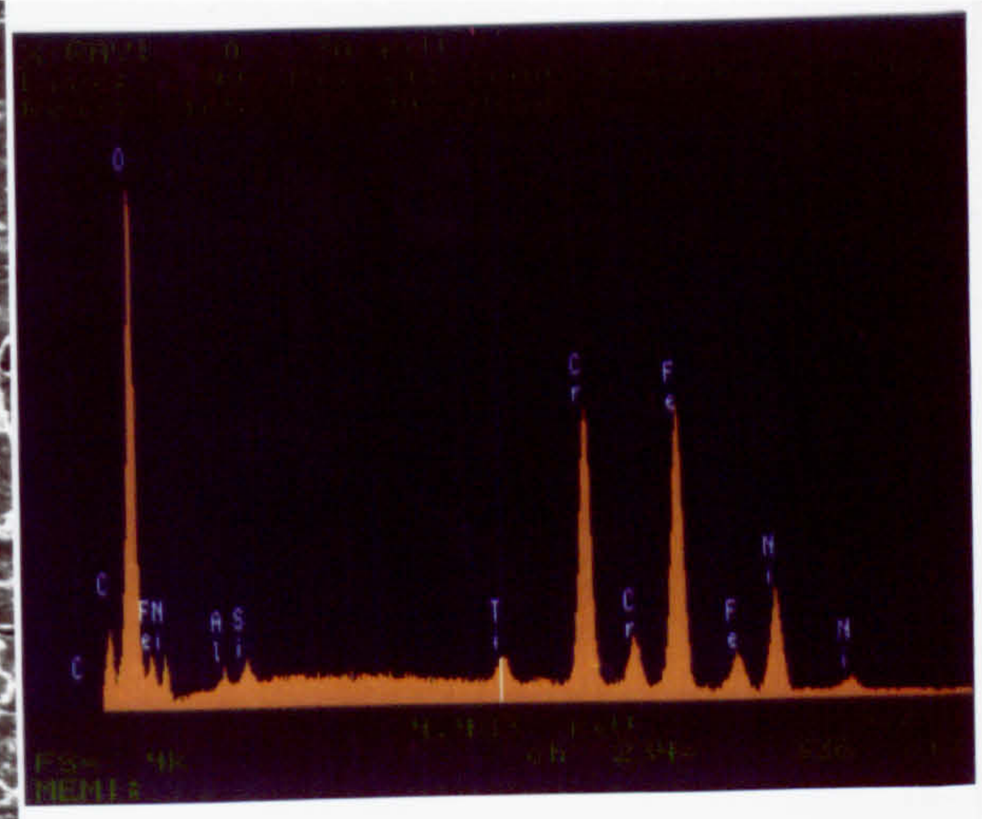
O
C
Cr
Fe
Ni
MEM1:

a

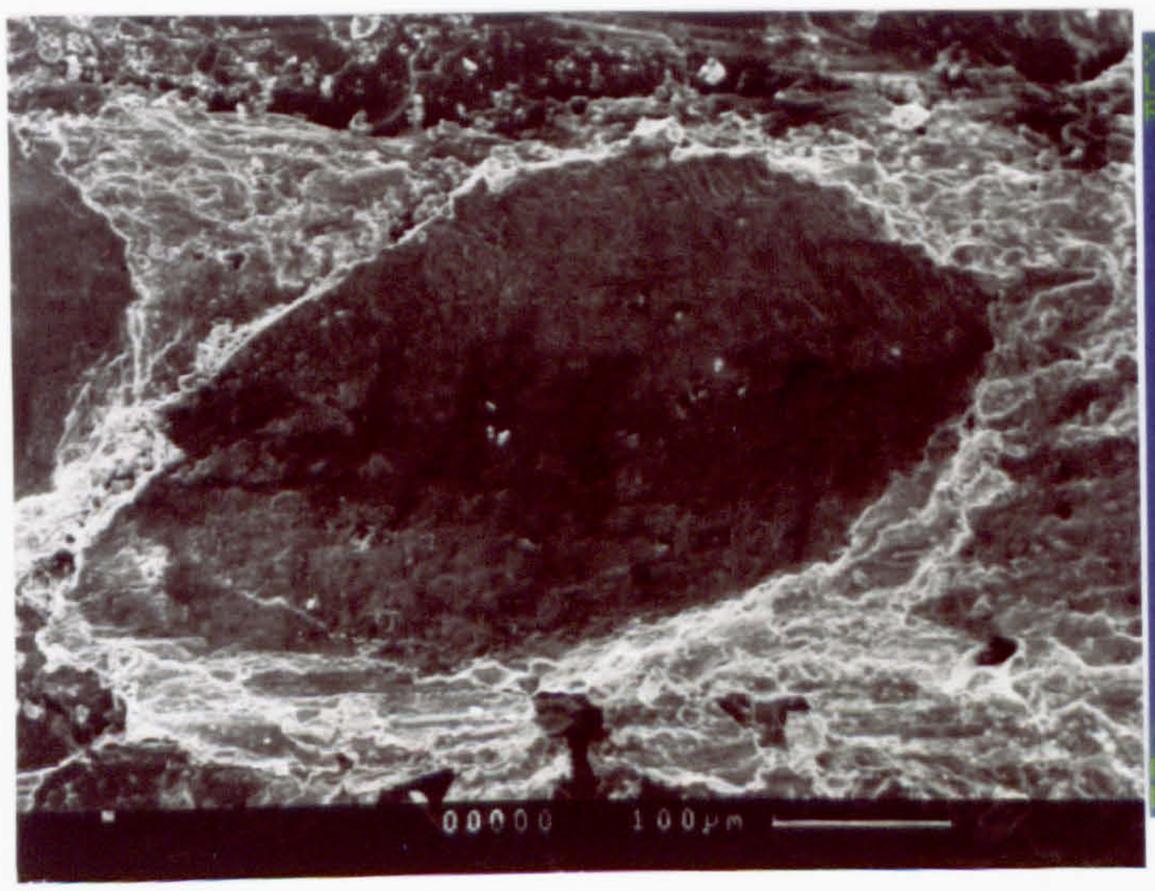
00000 100µm

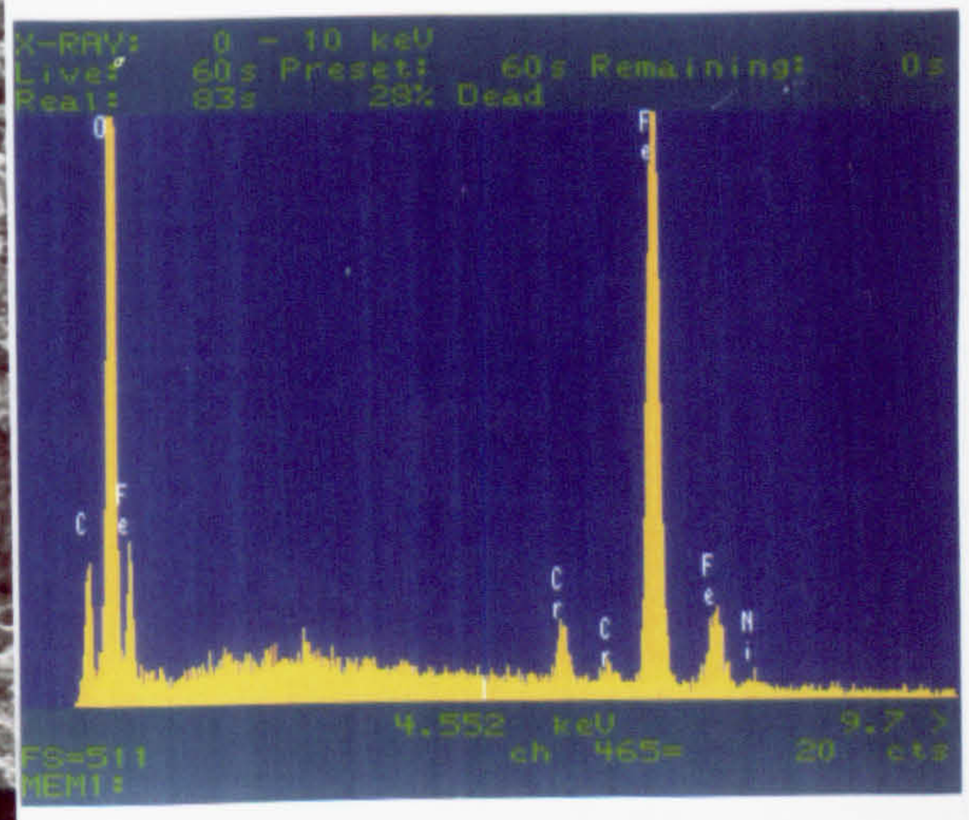
X-RAY: 0 - 10 keV
Live: 60s Preset: 60s Remaining: 0s
Real: 83s 28% Dead
O
C
Fe
Cr
Fe
Ni
4.552 keV 9.7 >
FS=511 ch 465= 20 cts
MEM1:

b

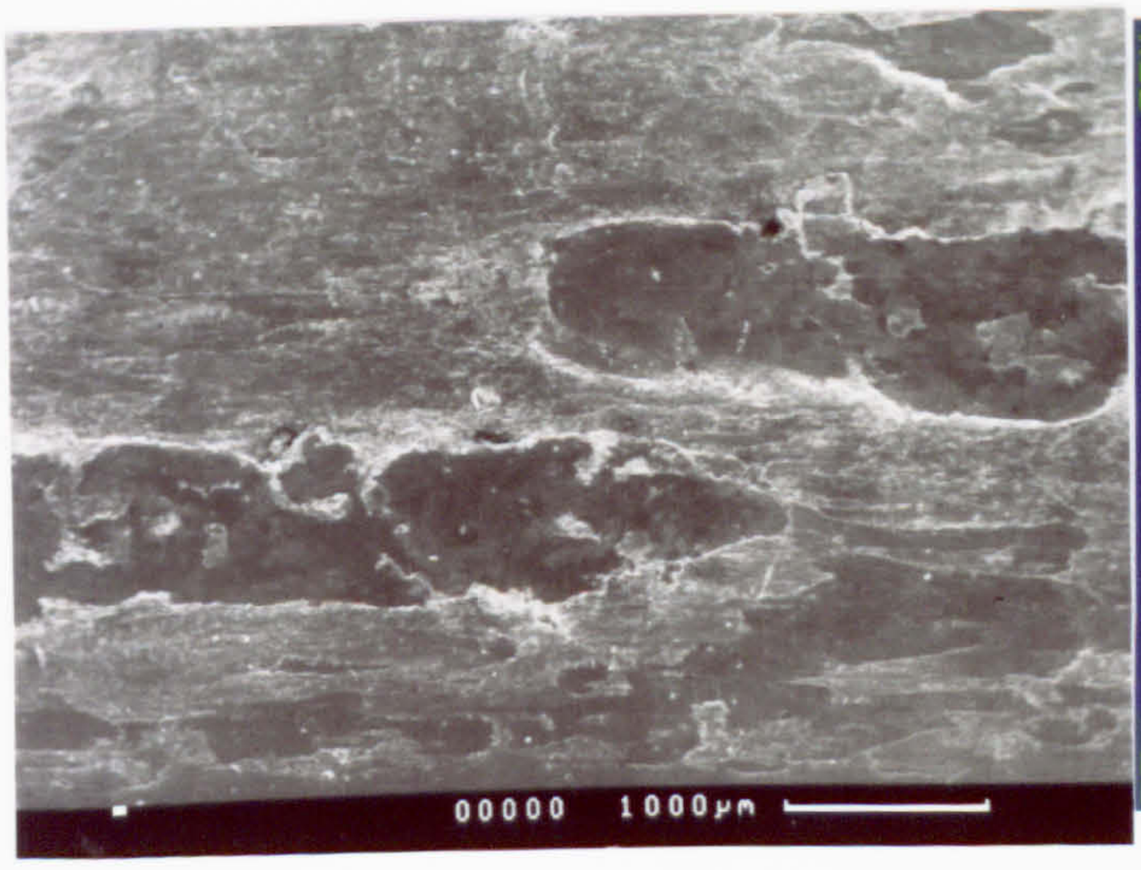
00000 1000µm

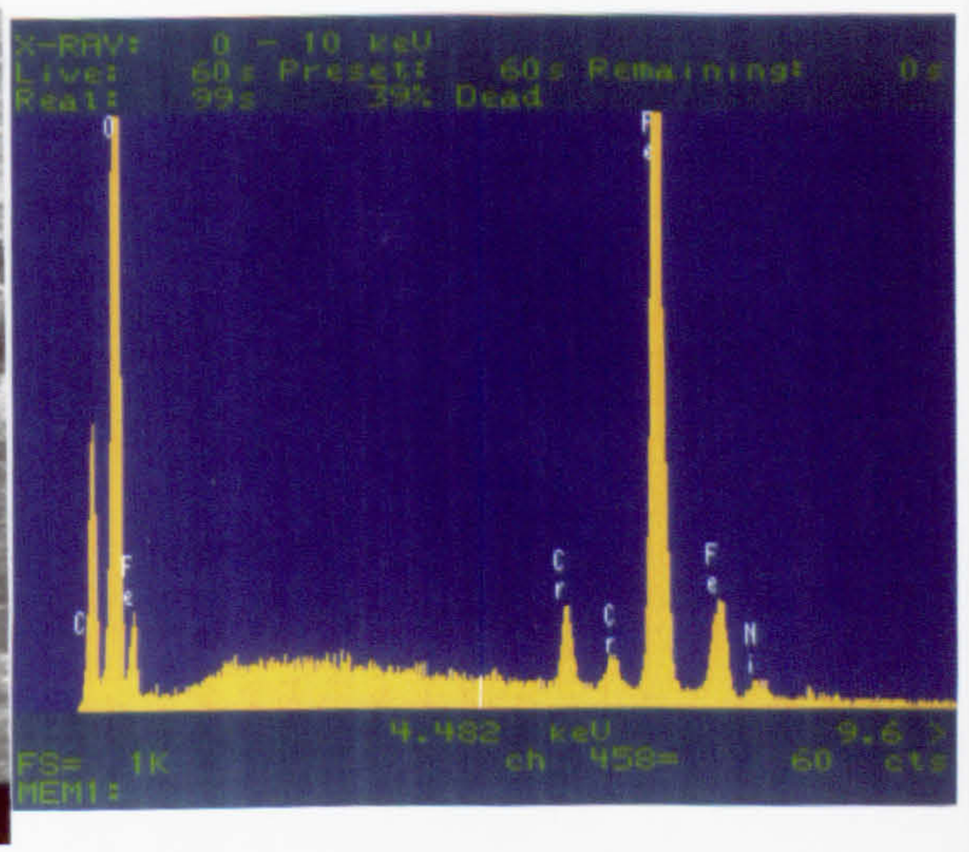
X-RAY: 0 - 10 keV
Live: 60s Preset: 60s Remaining: 0s
Real: 99s 39% Dead
O
C
Fe
Cr
Fe
Ni
4.482 keV 9.6 >
FS= 1K ch 458= 60 cts
MEM1:

c

Fig.5.30 SEM micrographs and EDX analysis of a Stellite 6 **counterface** after wearing against Nimonic 90 at 750°C for:

a - 2 minutes
b - 10 minutes (analysis of glaze)
c - 1 hour (analysis of glaze)

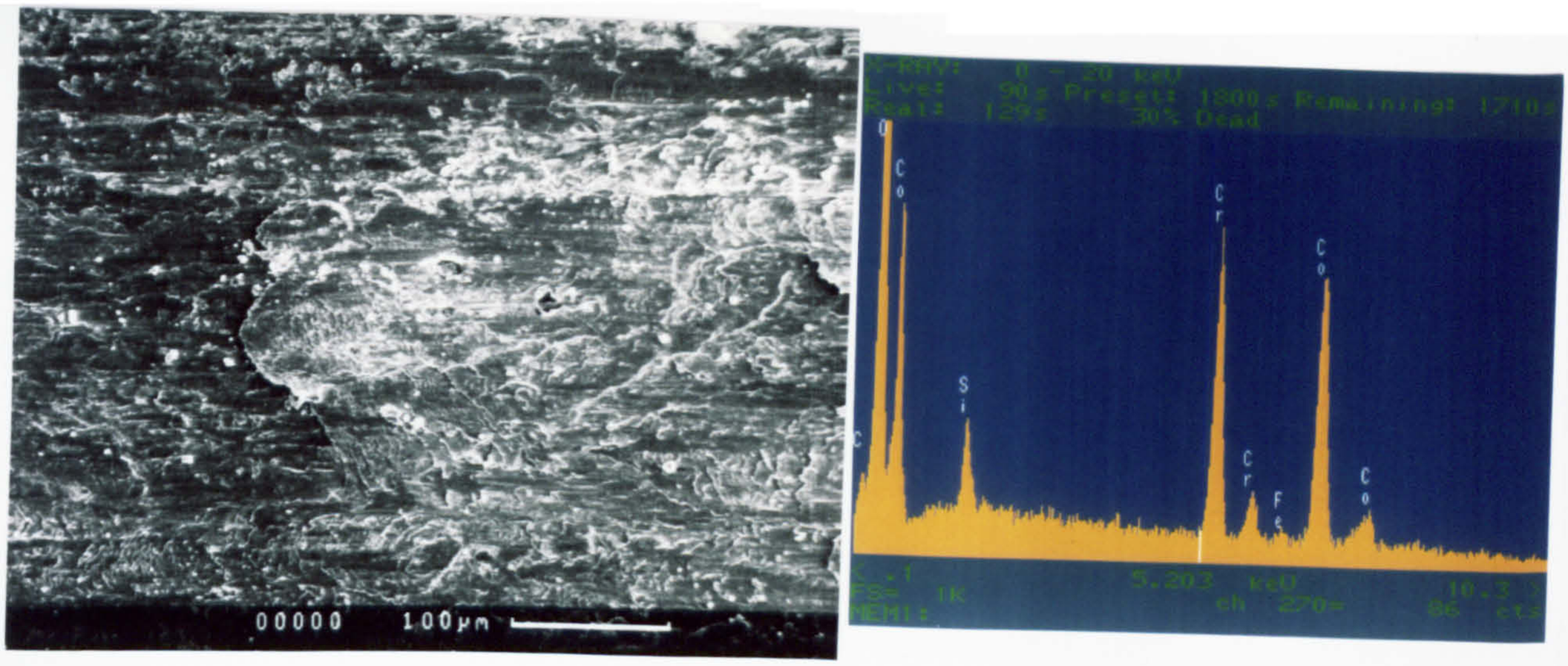
00000 100µm
X-RAY: 0 - 20 keV
Live: 90s Preset: 1800s Remaining: 1710s
Real: 129s 30% Dead
O
C o
S i
C r
C r
F e
C o
C o
C
5.203 keV
FS= 1K
MEM1:

a

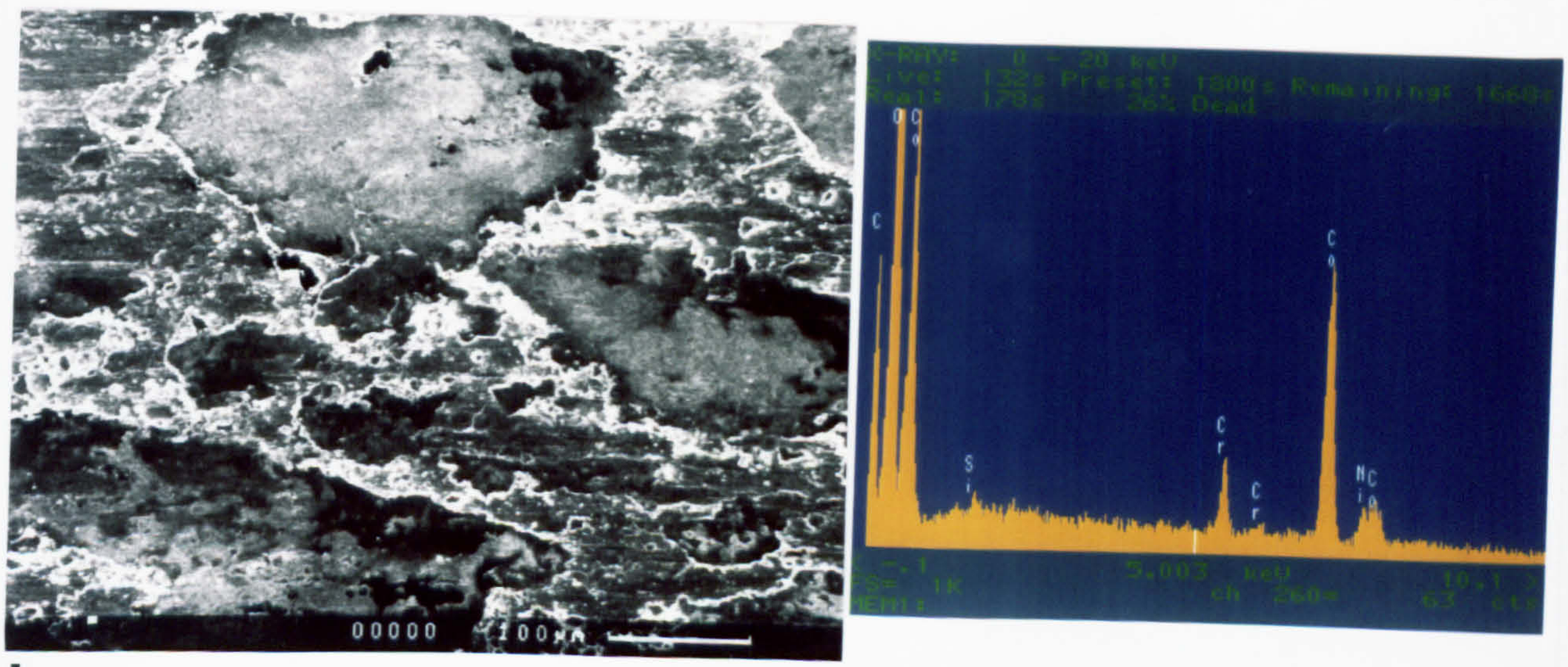
00000 100µm
X-RAY: 0 - 20 keV
Live: 132s Preset: 1800s Remaining: 1668s
Real: 178s 26% Dead
C
O
O
S i
C r
C r
C o
N i
C o
5.003 keV
FS= 1K
MEM1:

b

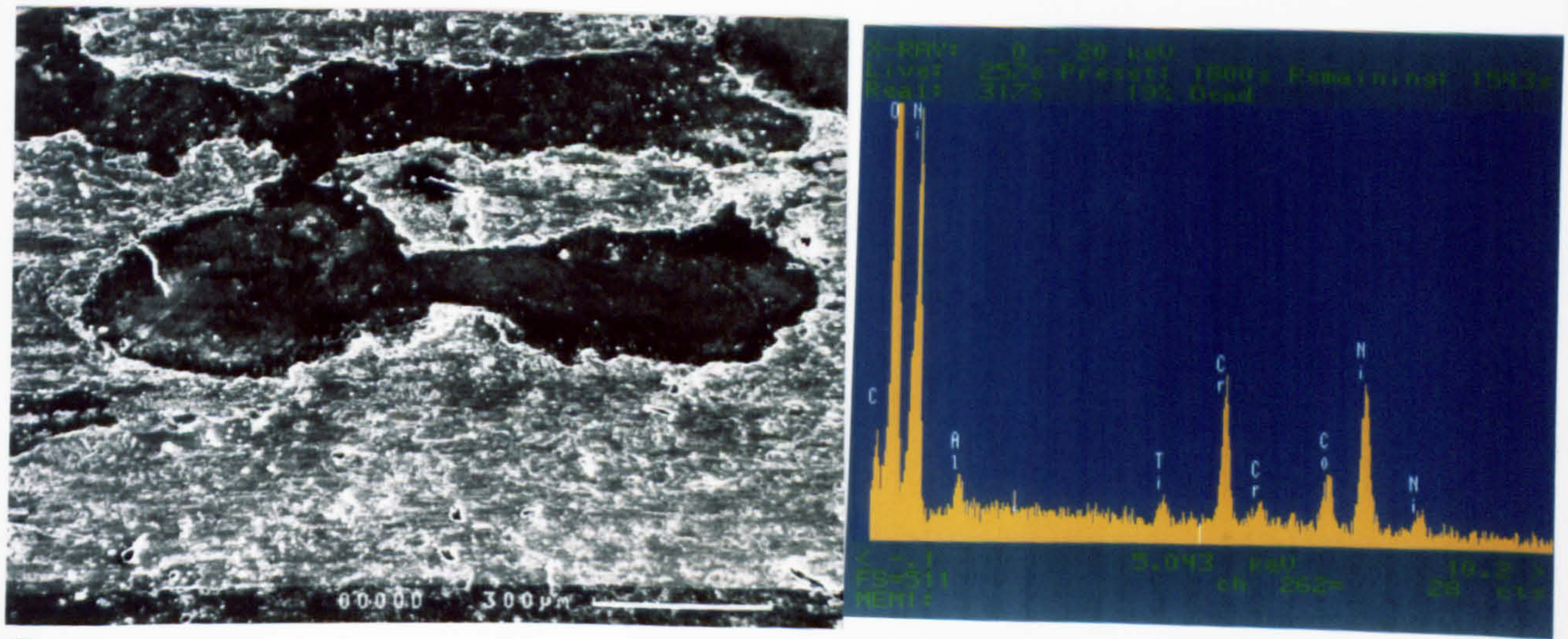
00000 300µm
X-RAY: 0 - 20 keV
Live: 252s Preset: 1800s Remaining: 1543s
Real: 317s 19% Dead
C
O
A l
T i
C r
C r
C o
N i
N i
5.043 keV
FS=511
MEM1:

C

Fig.5.31 SEM micrographs and EDX analysis of wear debris from :

a - Nimonic 90 vs Incoloy 800 counterface at 750°C (2 mins-1hr)
b - Nimonic 90 vs Stellite 6 counterface at 750°C (2 mins-1hr)

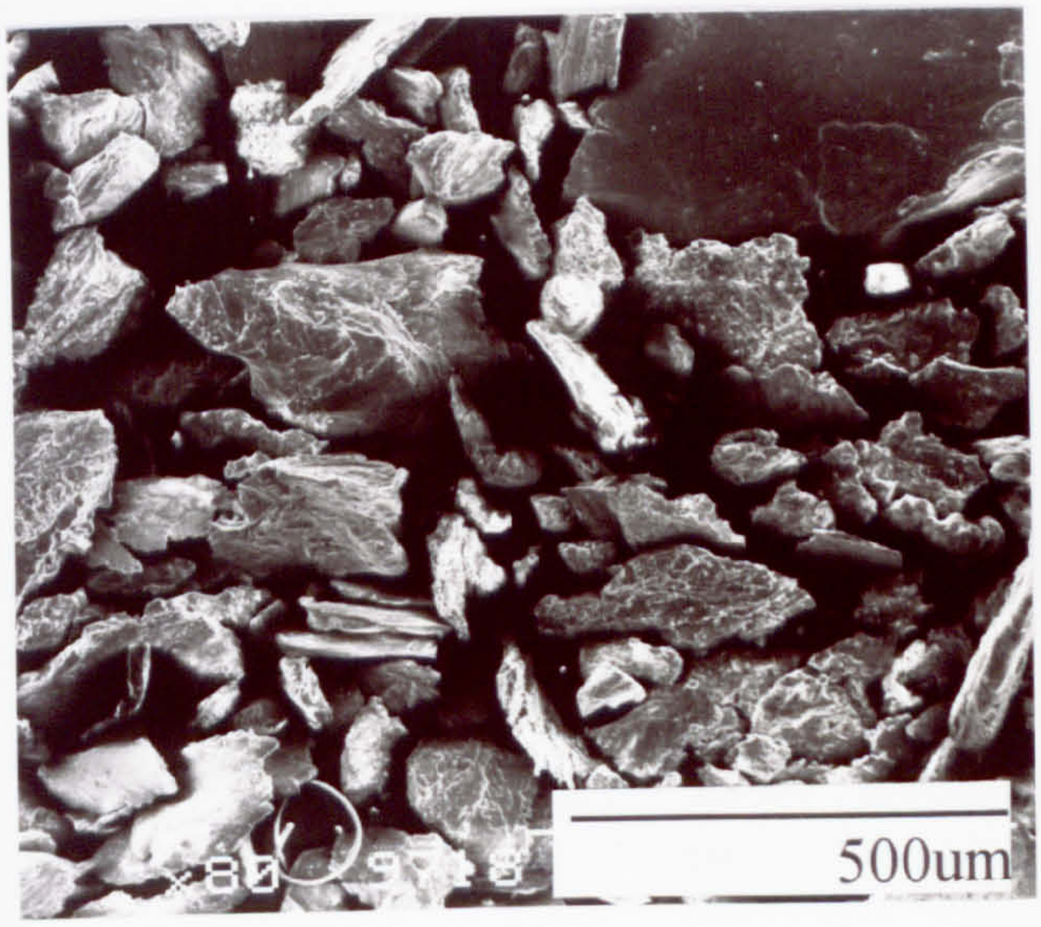
500um

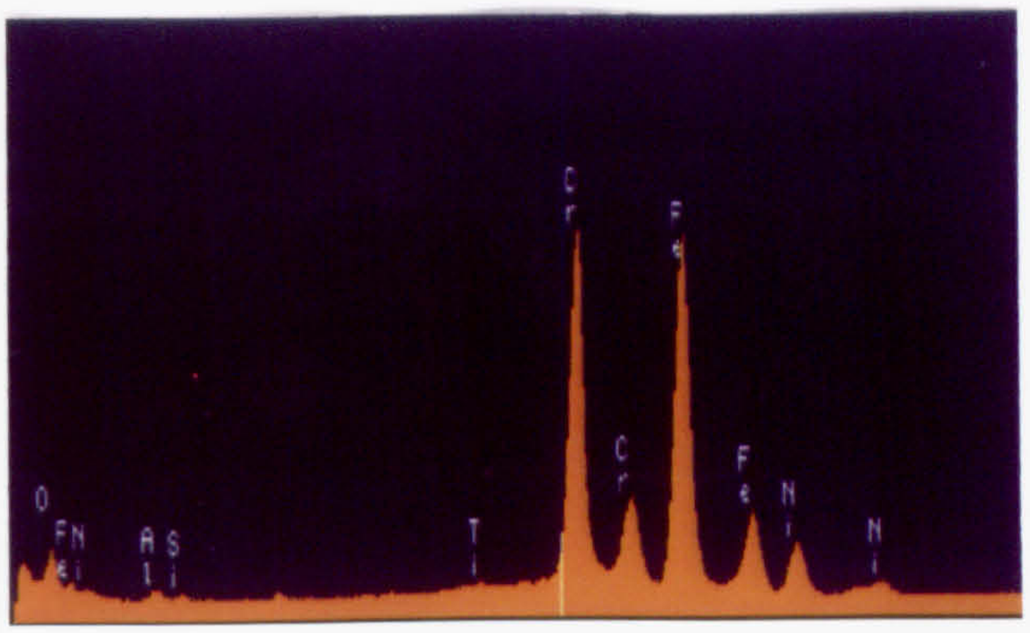
O
FN
Si
Al
Si
Ti
Cr
Cr
Fe
Fe
Ni
Ni

a


500um

O
N
Al
Si
Ti
Cr
Cr
Fe
Fe
Co
Ni
Ni

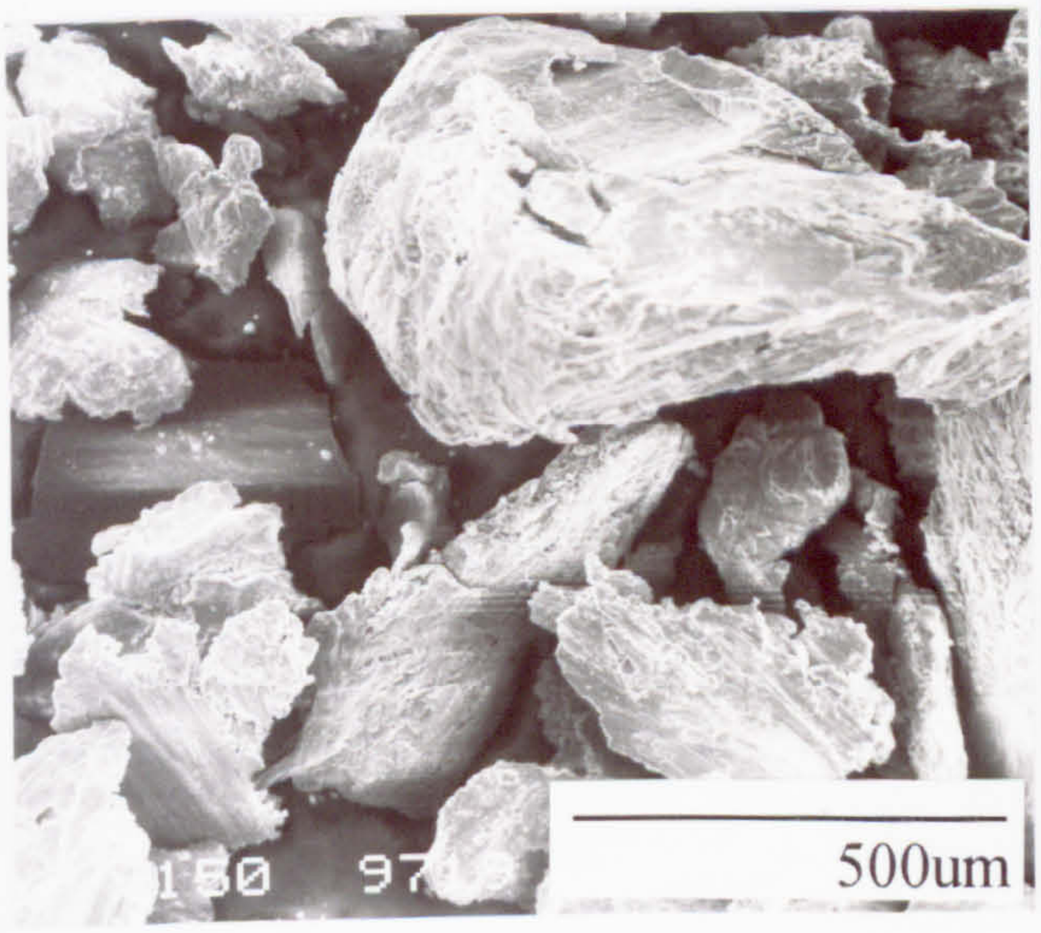
500um

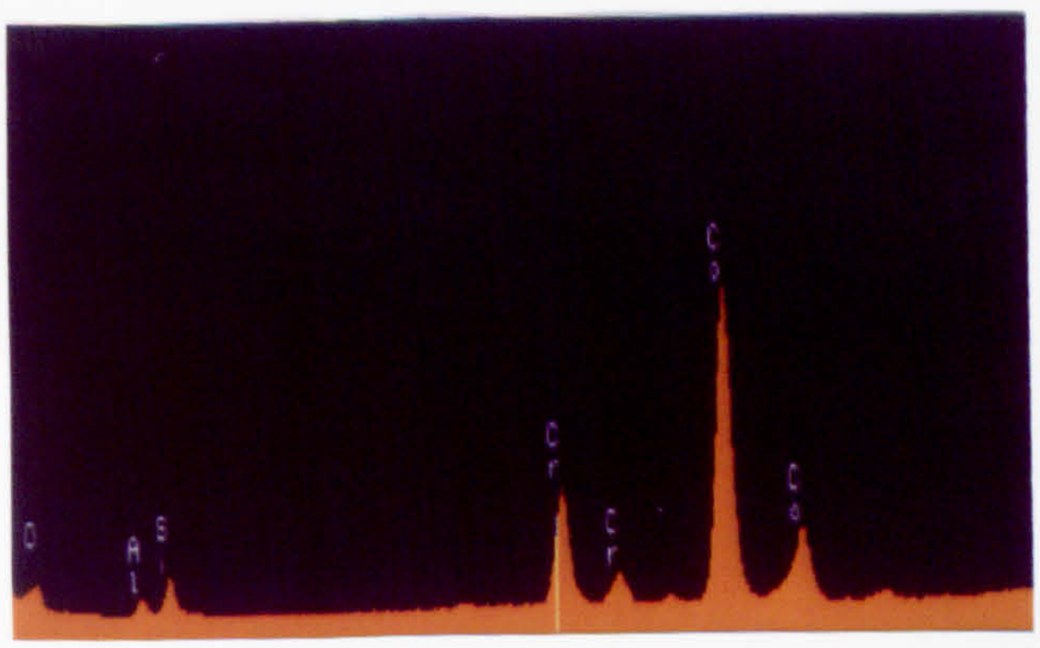
O
Al
Si
Cr
Cr
Co
Co

b

Fig.5.32 Cross-sectional EDX analysis of Ma956 worn against an **Incoloy** 800 counterface at 750°C for:

a - 2 minutes
b - 20 minutes
c - 1 hour

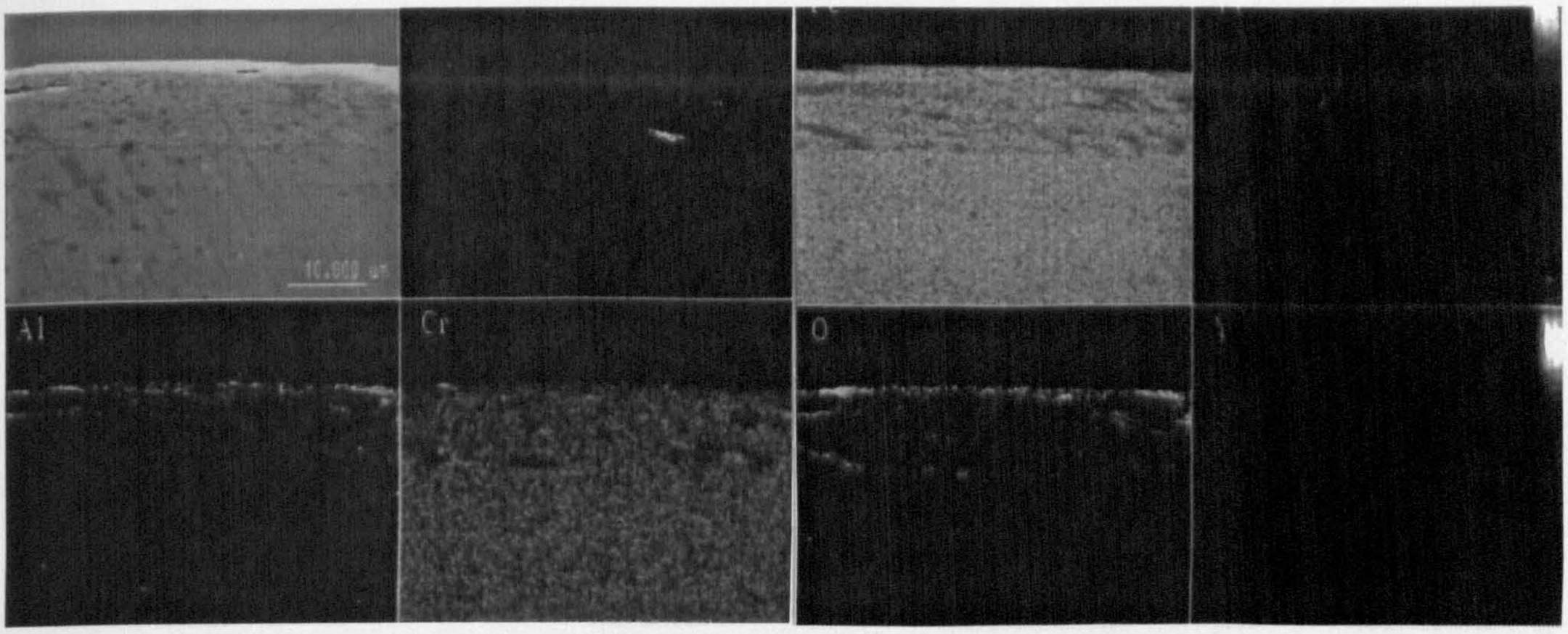

a

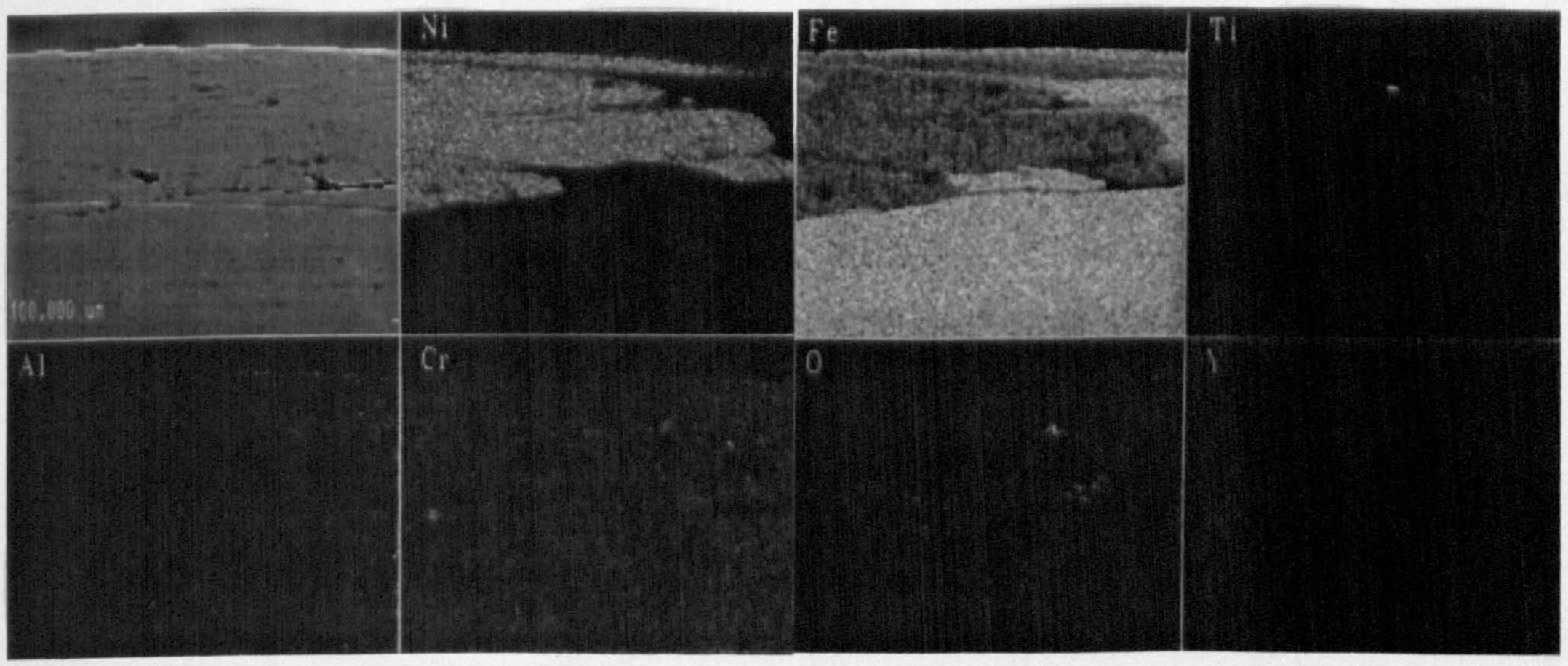

b

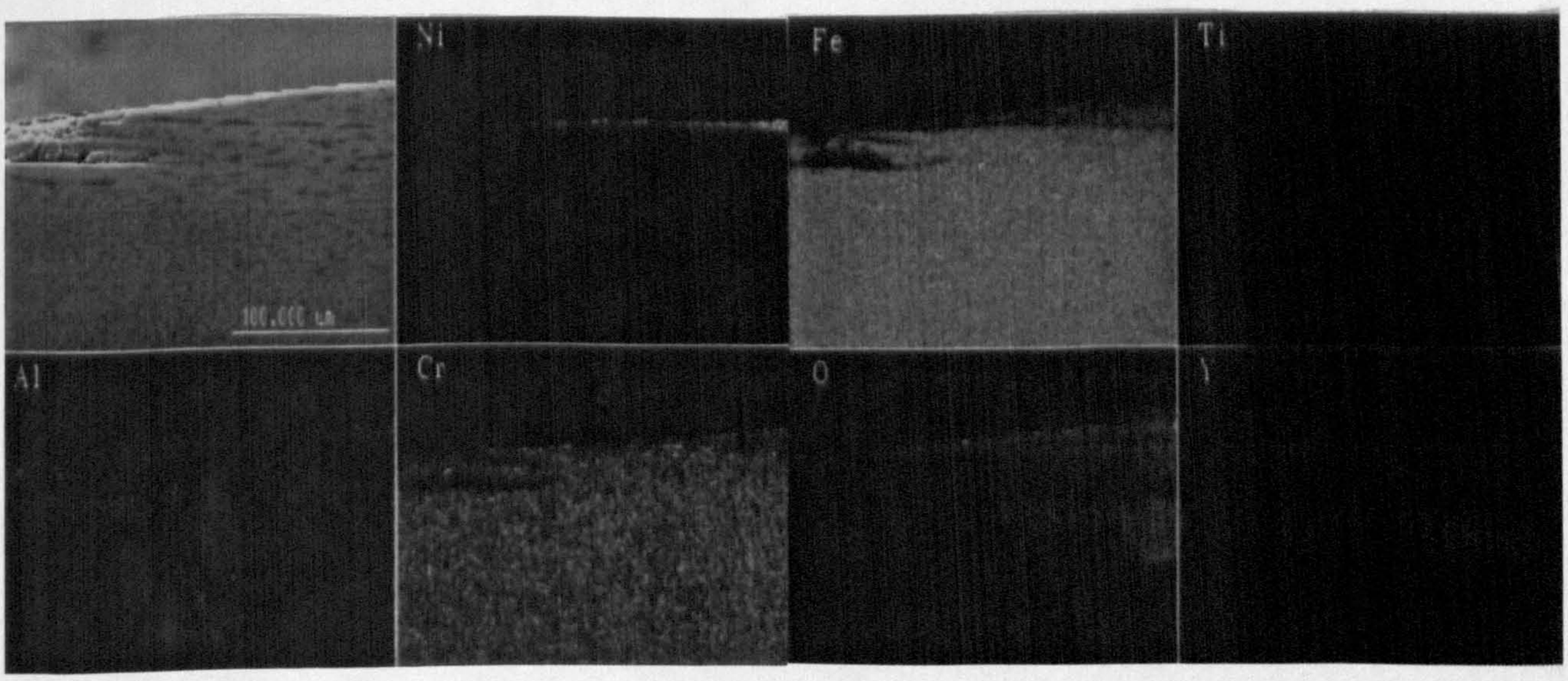

c

Fig.5.33 Cross-sectional EDX analysis of Ma956 worn against a **Stellite 6** counterface at 750°C for:

a - 2 minutes
b - 10 minutes
c - 1 hour

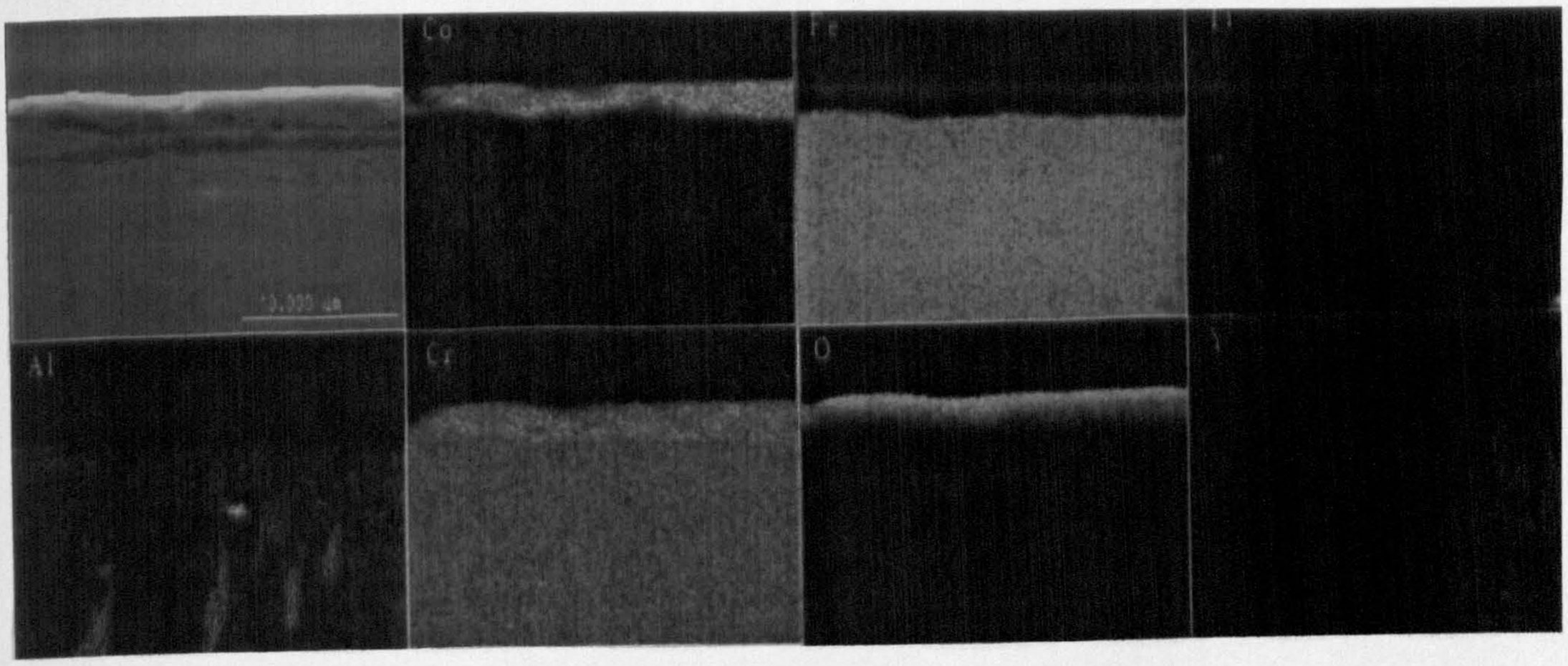

a

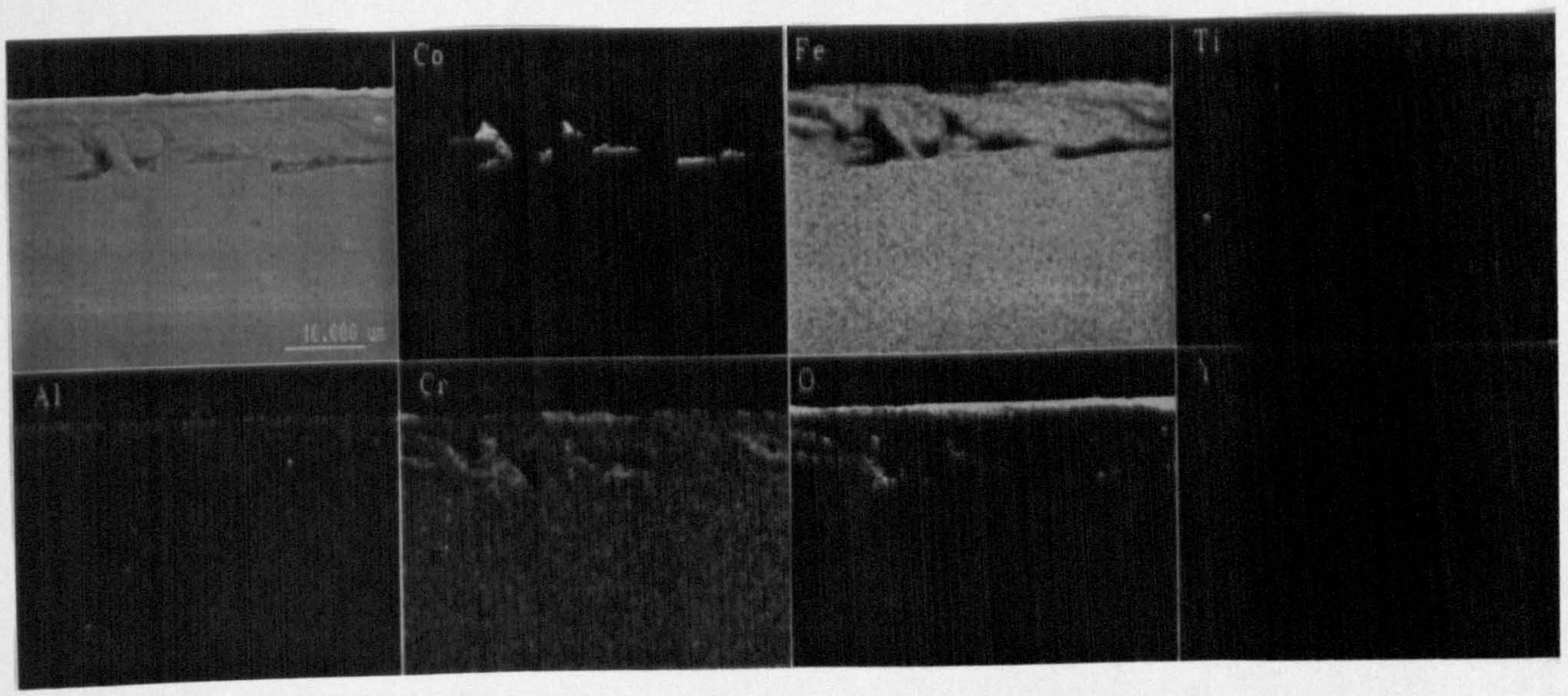

b

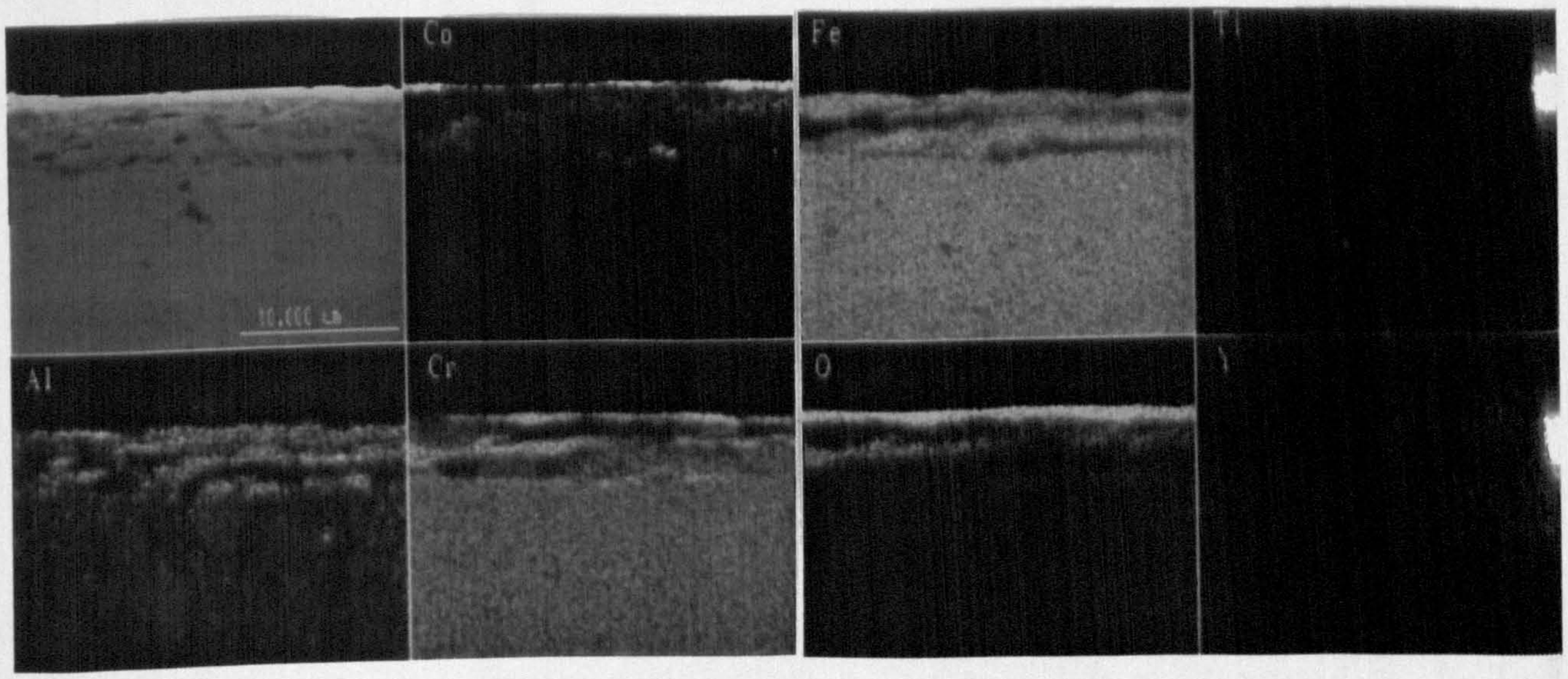

C

Fig.5.34 SEM micrographs and EDX analysis of an Incoloy 800 **counterface** after wearing against Ma956 at 750°C for:

a - 2 minutes
b - 20 minutes (analysis of glaze)
c - 1 hour (analysis of glaze)

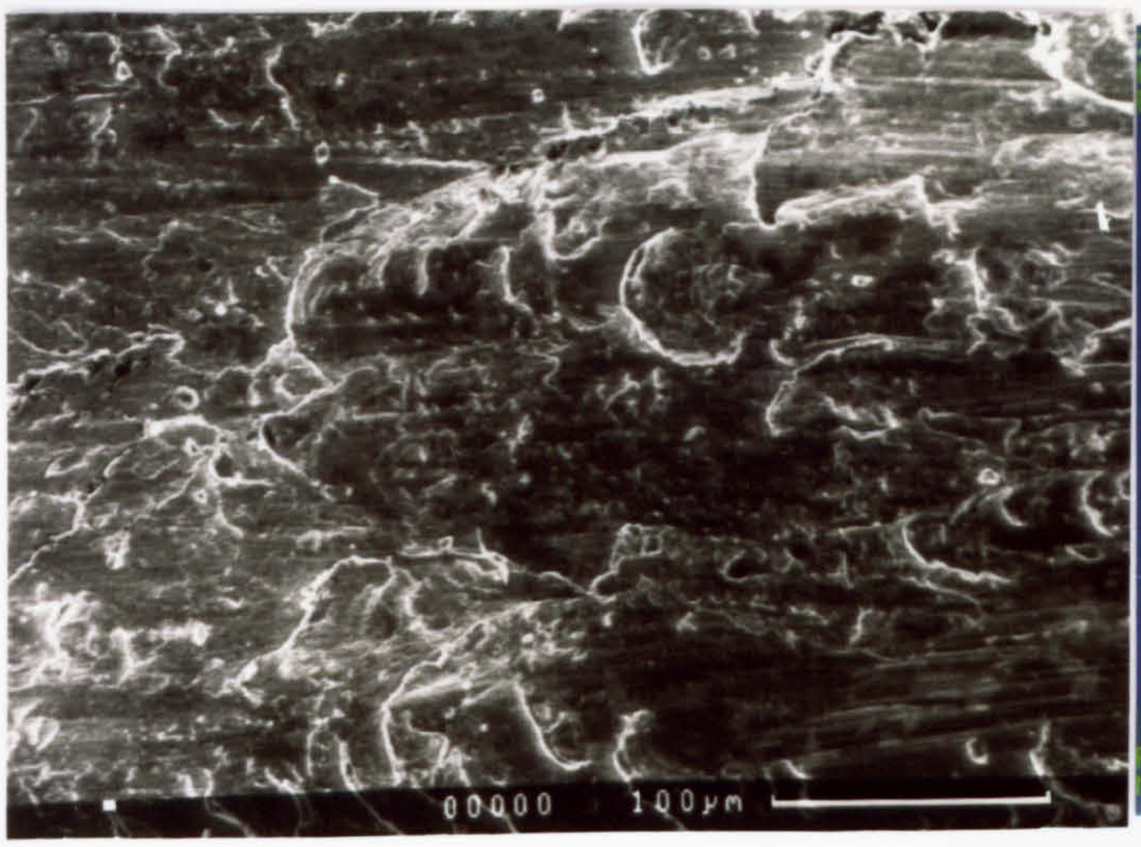
00000 100µm

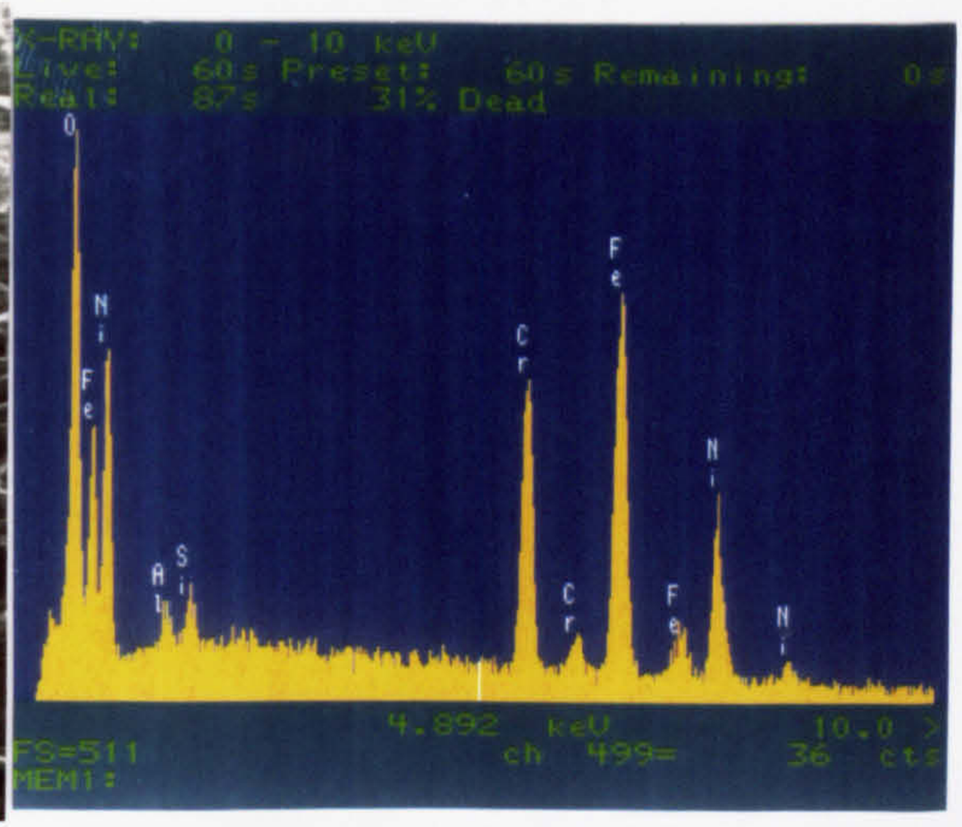
X-RAY: 0 - 10 keV
Live: 60s Preset: 60s Remaining: 0s
Real: 87s 31% Dead
O
Fe
Ni
Al
Si
Cr
Cr
Fe
Fe
Ni
Ni
4.892 keV 10.0 >
FS=511 ch 499= 36 cts
MEM1:

a

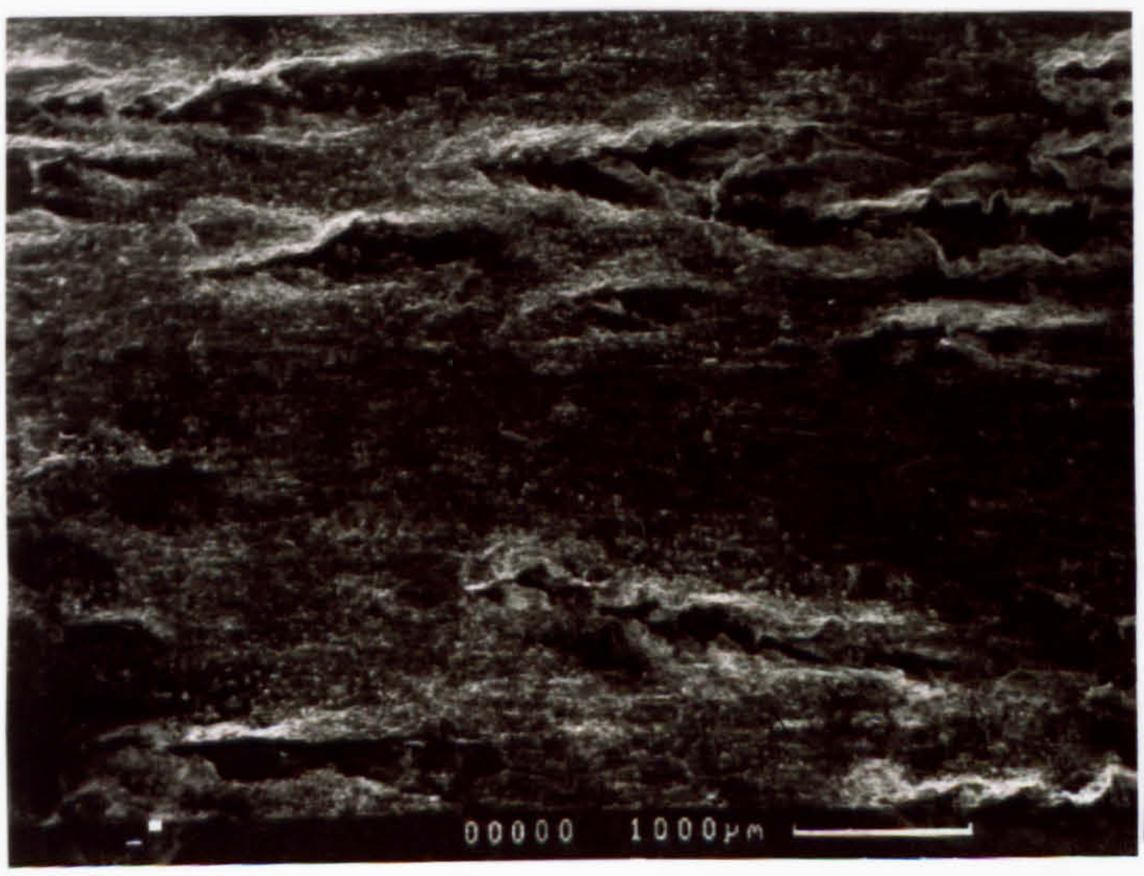
00000 1000µm

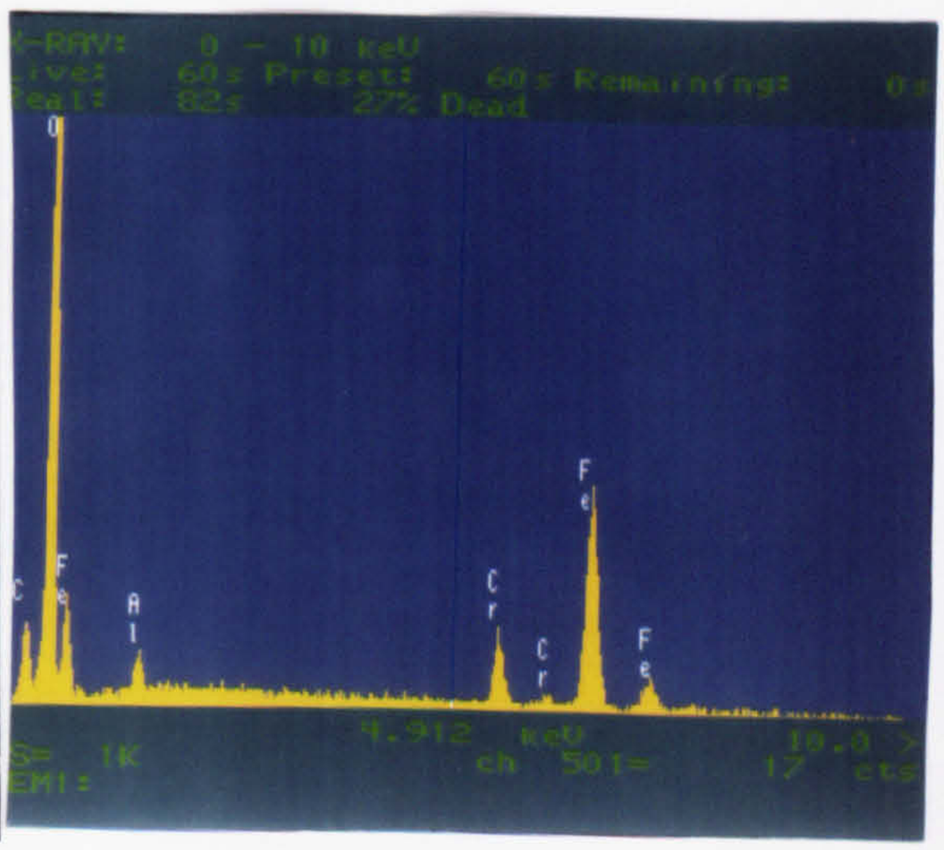
X-RAY: 0 - 10 keV
Live: 60s Preset: 60s Remaining: 0s
Real: 82s 27% Dead
O
C
Fe
Al
Cr
Cr
Fe
Fe
4.912 keV 10.0 >
FS= 1K ch 501= 17 cts
MEM1:

b

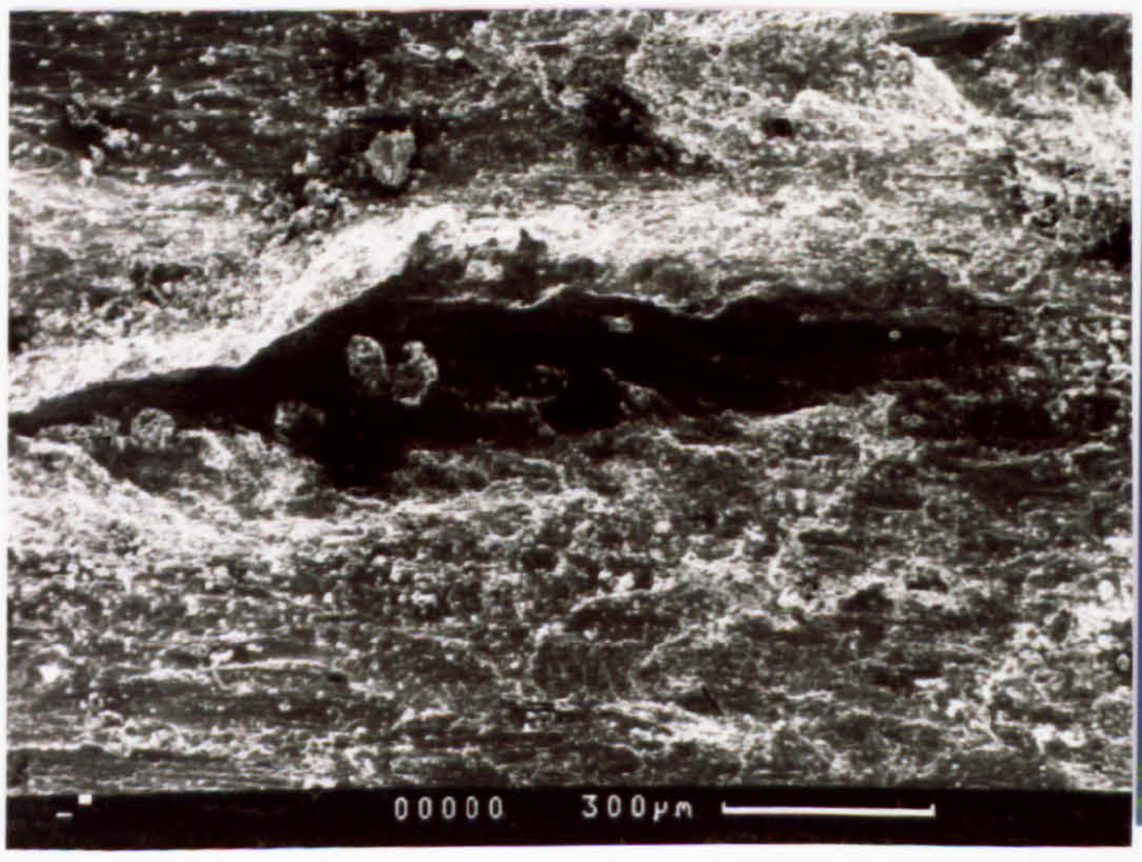
00000 300µm

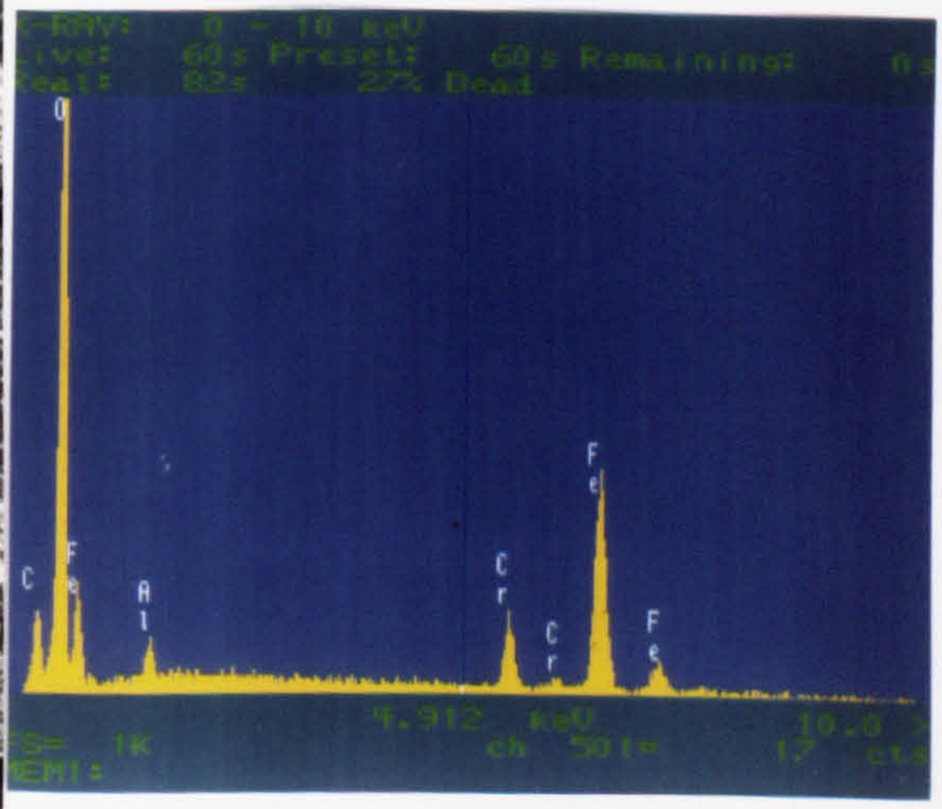
X-RAY: 0 - 10 keV
Live: 60s Preset: 60s Remaining: 0s
Real: 82s 27% Dead
O
C
Fe
Al
Cr
Cr
Fe
Fe
4.912 keV 10.0 >
FS= 1K ch 501= 17 cts
MEM1:

C

Fig.5.35 SEM micrographs and EDX analysis of a Stellite 6 **counterface** after wearing against Ma956 at 750°C for:

a - 2 minutes
b - 10 minutes (analysis of glaze)
c - 1 hour (analysis of glaze)

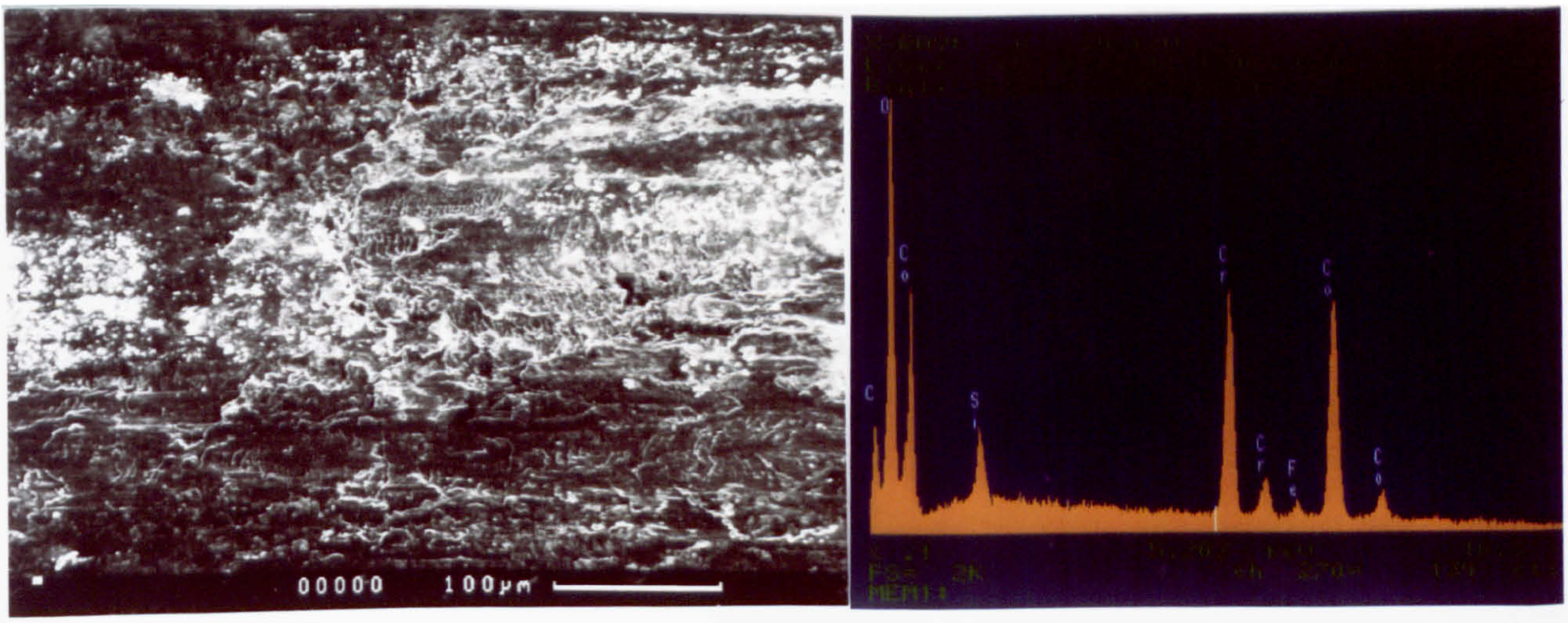
00000 100µm
O
C o
C
S i
C r
F e
C o
C o
FS= 2K
MEM1:

a

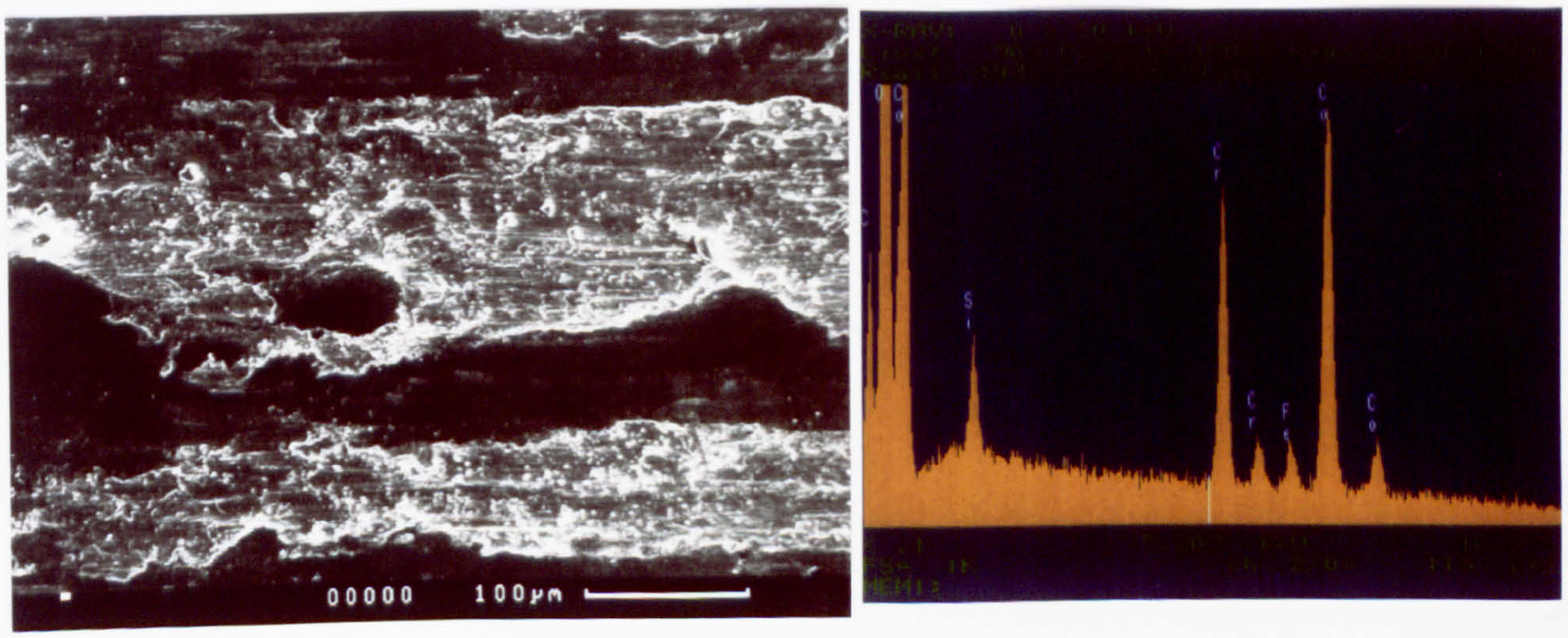
00000 100µm
O
C o
C
S i
C r
F e
C o
C o

b

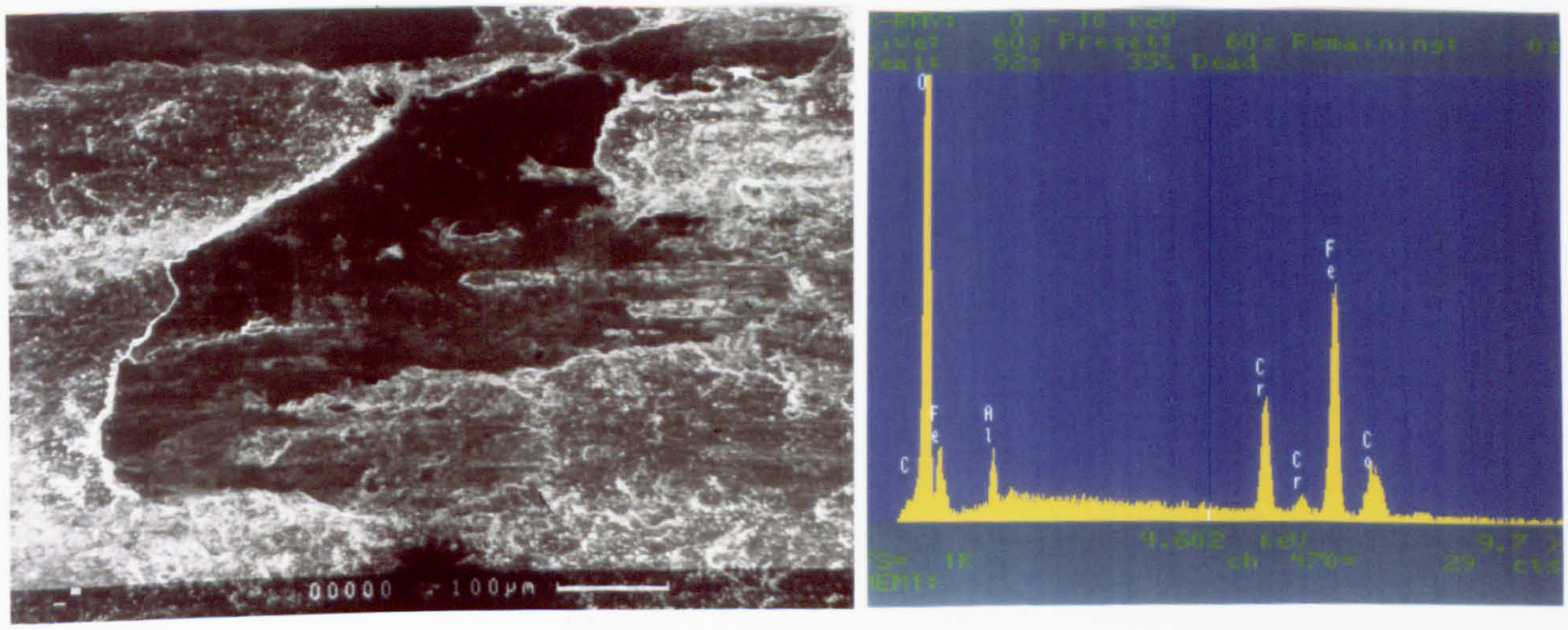
00000 100µm
-PHYS 0 - 10 keV
ive: 60s Preset: 60s Remaining: 0s
ent: 92s 35% Dead
O
F e
A l
C
C r
C r
C o
4.602 keV 9.7 >
FS= 1K ch 470= 29 cts
MEM1:

C

Fig.5.36 SEM micrographs and EDX analysis of wear debris from :

a - Ma956 vs Incoloy 800 counterface at 750°C (2 mins-1hr)
b - Ma956 vs Stellite 6 counterface at 750°C (2 mins-1hr)

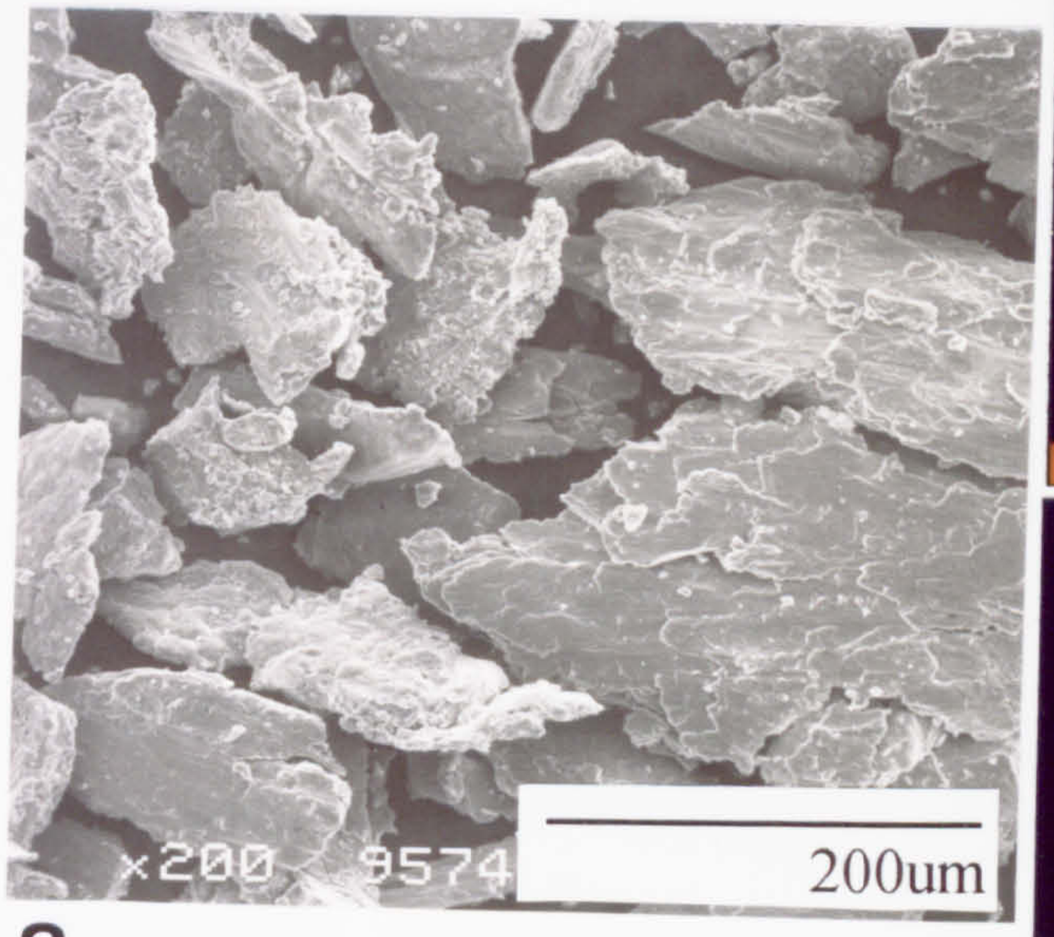
×200 9574
200um

a

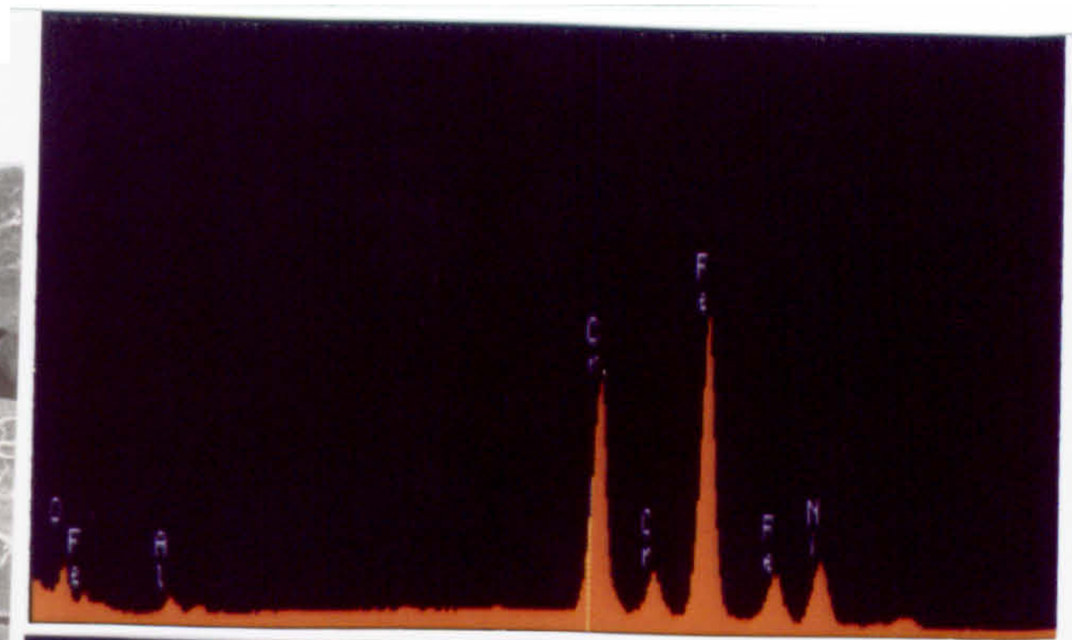
O
Fe
Al
Cr
Fe
Fe
Ni

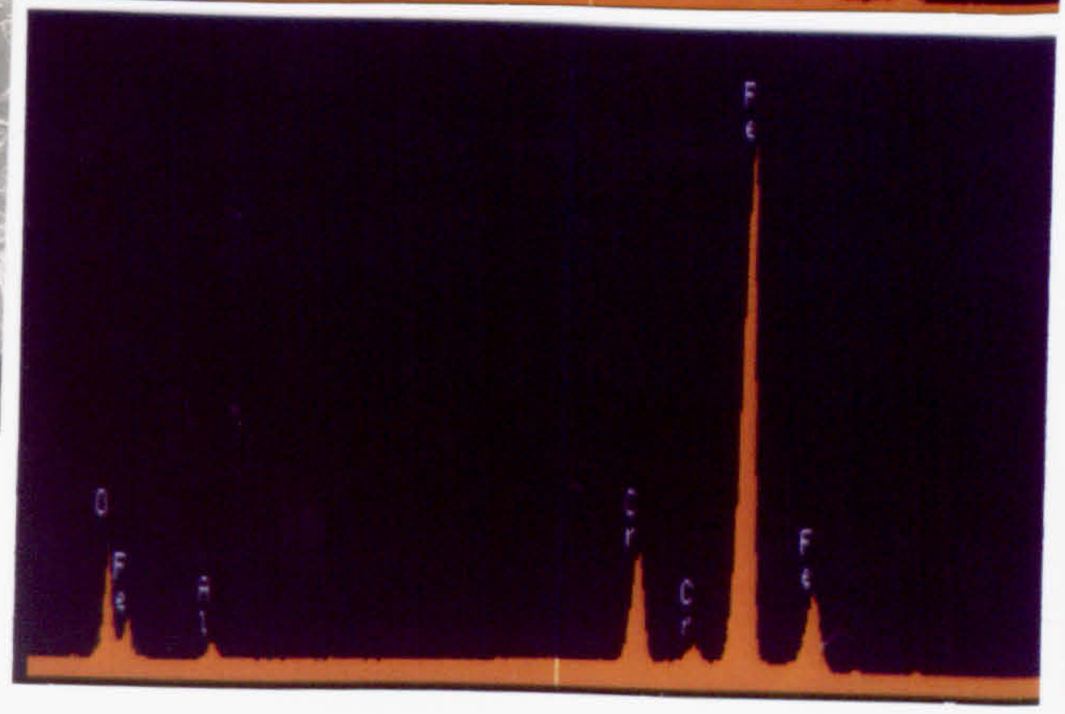
Fe
O
Fe
Al
Cr
Cr
Fe

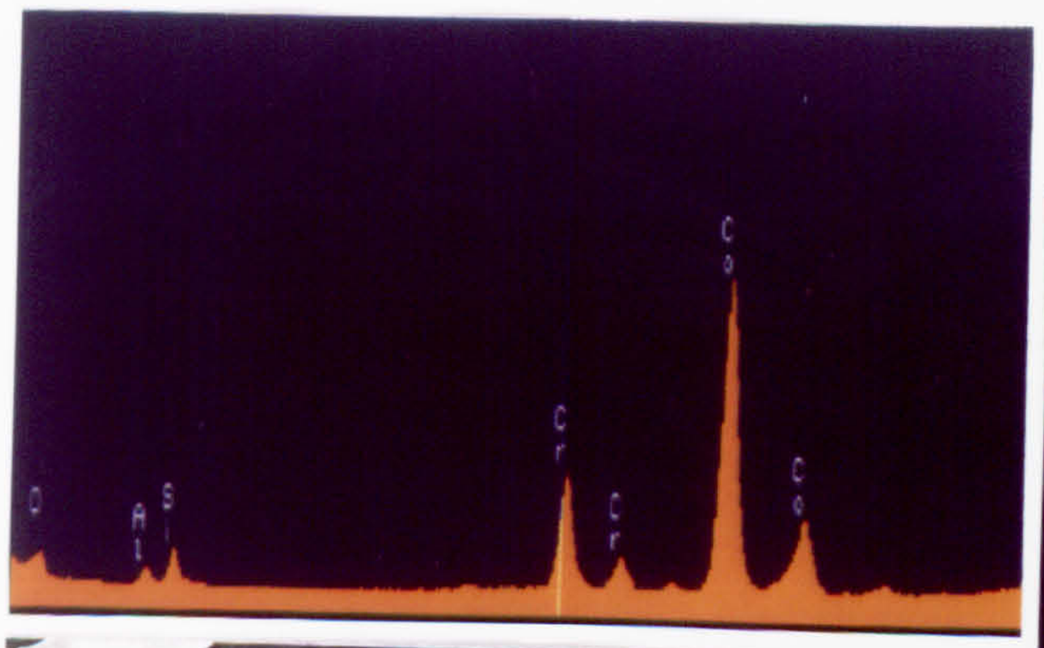
C
O
Al
Si
Cr
Cr
Co
Co

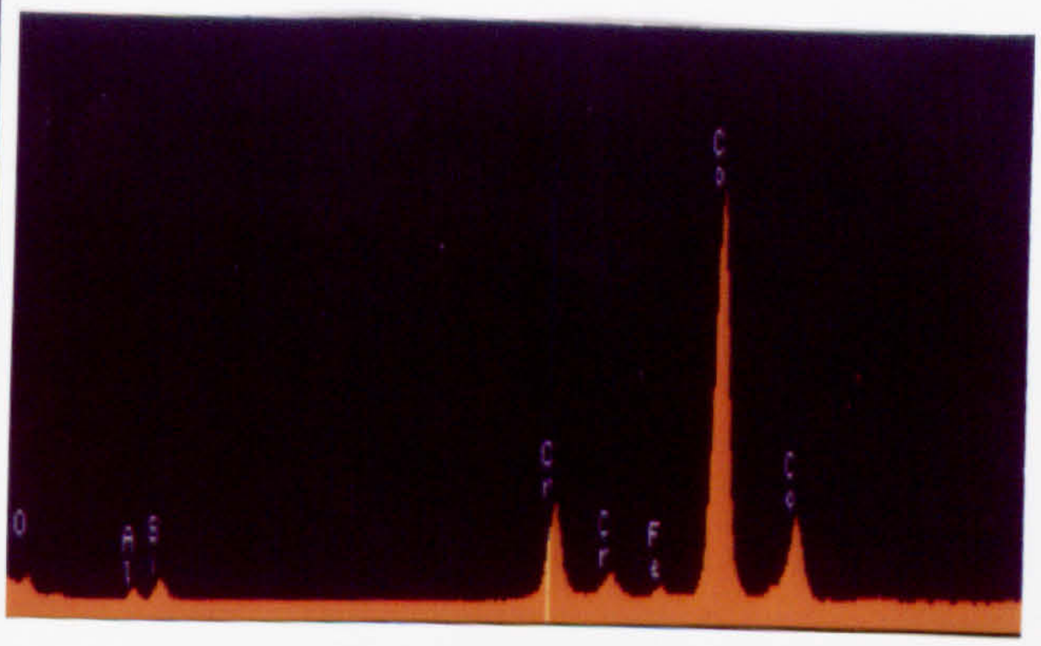
Co
O
Al
Si
Cr
Cr
Fe
Co

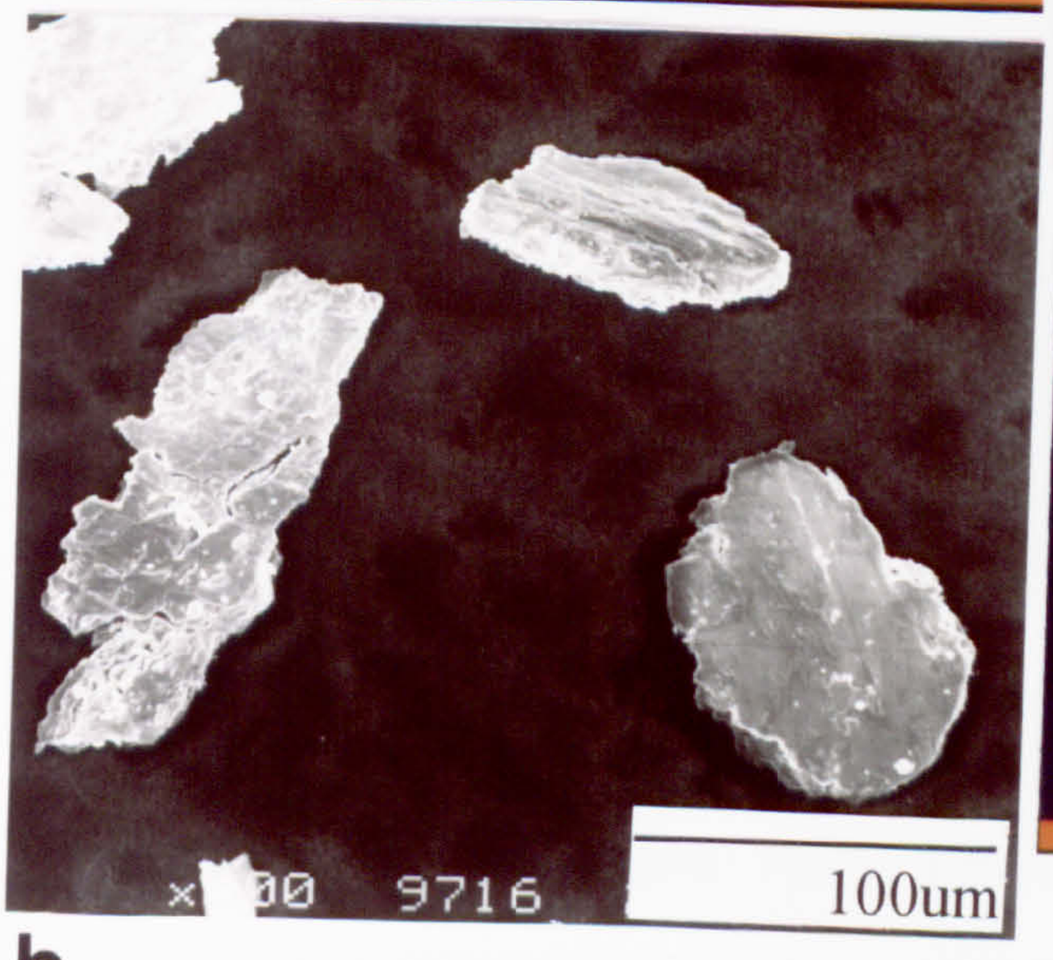
×200 9716
100um

b

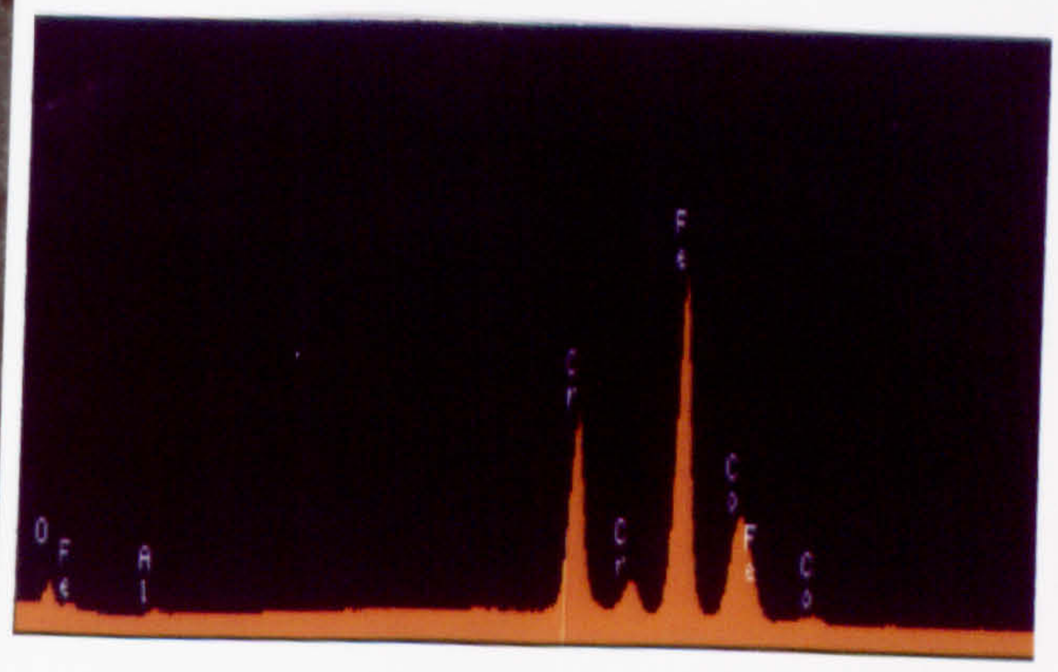
Fe
O
Fe
Al
Cr
Cr
Fe
Co
Co

5.5 Effect of Temperature on the Wear Resistance of Ma956 Wearing Against Stellite 6

5.5.1 Weight Changes

Weight changes of Ma956 after wearing against Stellite 6 for 4 hours at room temperature, 350°C, 550°C and 750°C are displayed in **Fig.5.37**. The results illustrate a fairly similar weight loss for all of the temperatures, ranging between -7.4mgcm^{-2} at 750°C to -18.1mgcm^{-2} at 550°C.

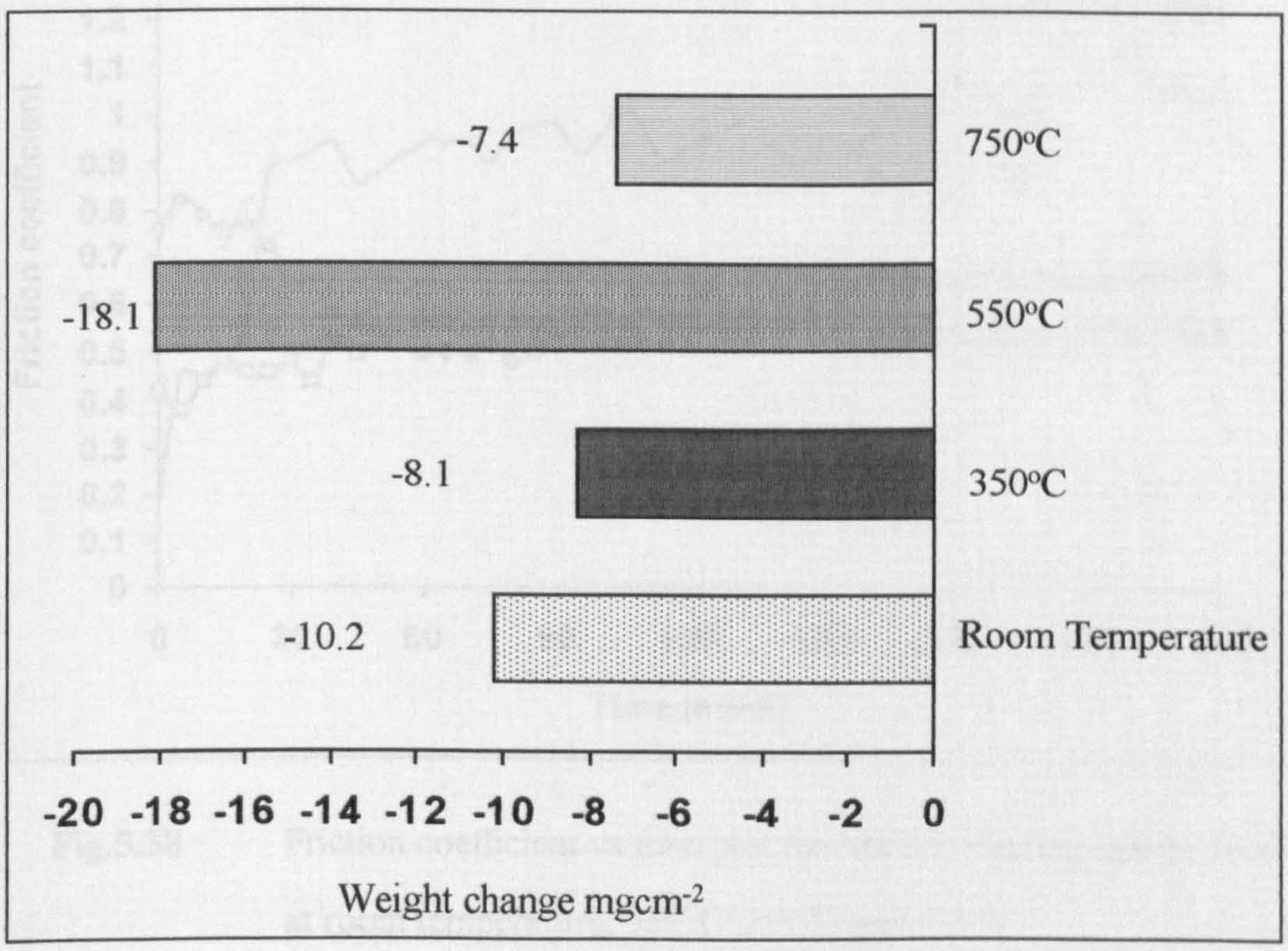

Fig.5.37 Weight change of Ma956 after wearing against Stellite 6 at room temperature, 350°C, 550°C and 750°C

5.5.2 Friction coefficient

Fig.5.38 presents friction coefficient vs time plots for Ma956 wearing against Stellite 6 at room temperature, 350°C, 550°C and 750°C. The plot at room temperature showed a steep increase from an initial value of 0.2 to a value ~0.9 after about 30 minutes.

The readings then oscillated for the rest of the test between 0.9-1.1. However, at 350°C, the initial friction coefficient reading was ~ 0.4 which increased slowly during the test reaching a maximum around 0.7. Results obtained at 550°C and 750°C showed a similar trend, with the friction coefficient decreasing from 0.8, to a value ~ 0.6 after 30 minutes.

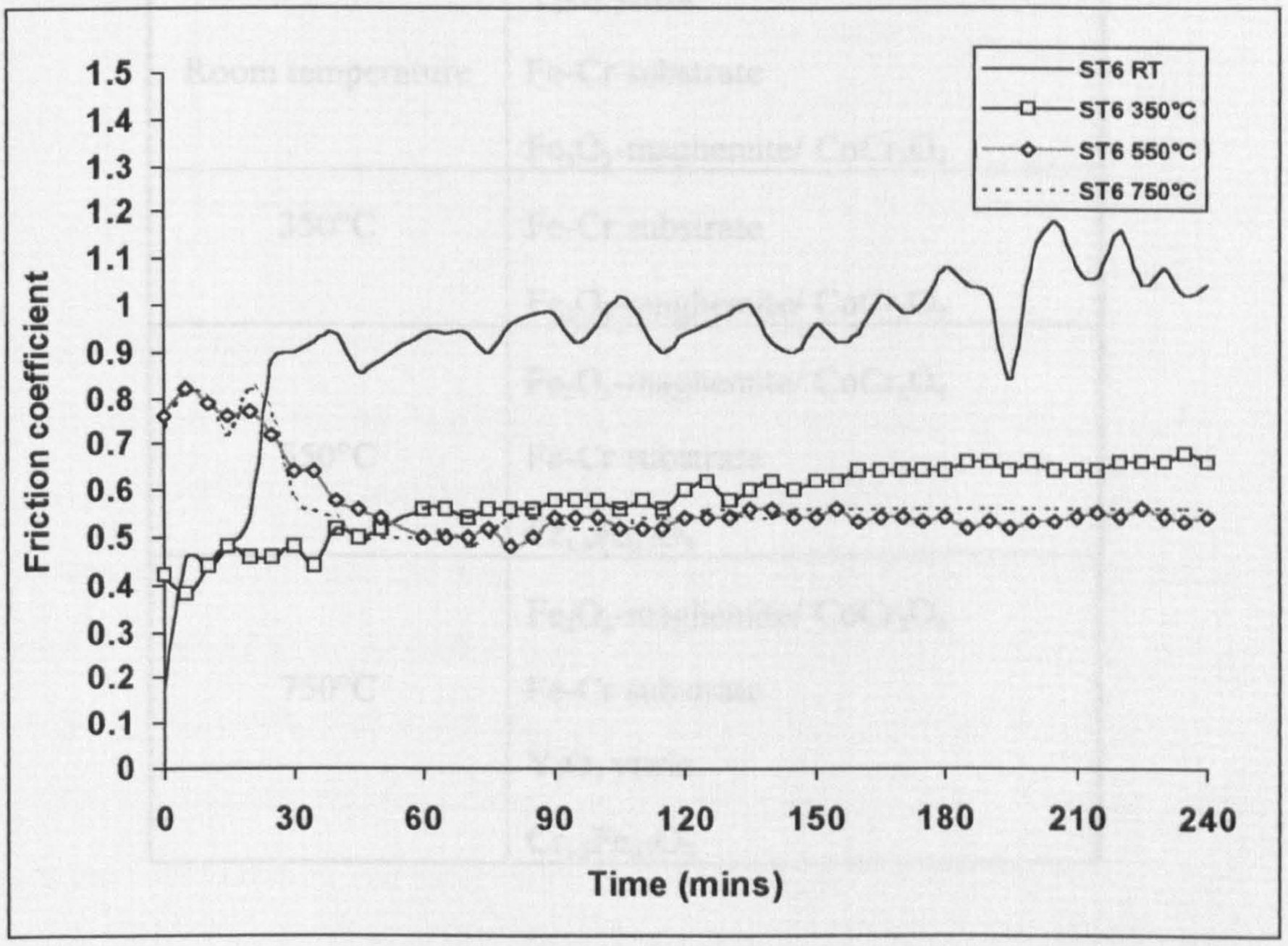

Fig.5.38 Friction coefficient vs time plot for Ma956 wearing against Stellite 6 at room temperature, 350°C ,550°C and 750°C

5.5.3 XRD Analysis

The phases detected by XRD analysis on Ma956 after wearing against Stellite 6 at room temperature, 350°C, 550°C and 750°C are shown in ***Table 5.21***. At all temperatures the Fe-Cr substrate and Fe_2O_3-maghemite/$CoCr_2O_4$ were detected. A Y_2O_3 phase was also identified at room temperature and 750°C and $Cr_{1.3}Fe_{0.7}O_3$ was observed at 550°C and 750°C.

Table 5.21 XRD analysis of the surface of Ma956 after wearing against Stellite 6 at different temperatures

Temperature	Phase detected by XRD
Room temperature	Y_2O_3 yttria Fe-Cr substrate Fe_2O_3-maghemite/ $CoCr_2O_4$
350°C	Fe-Cr substrate Fe_2O_3-maghemite/ $CoCr_2O_4$
550°C	Fe_2O_3-maghemite/ $CoCr_2O_4$ Fe-Cr substrate $Cr_{1.3}Fe_{0.7}O_3$
750°C	Fe_2O_3-maghemite/ $CoCr_2O_4$ Fe-Cr substrate Y_2O_3 yttria $Cr_{1.3}Fe_{0.7}O_3$

5.5.4 Hardness Testing

A higher hardness value of Hv580 was recorded on Ma956 after wearing against Stellite 6 at 750°C compared to a value of Hv486 when the alloy was worn at 550°C, as shown in ***Table 5.22.***. Hardness results could not be obtained for room temperature and 350°C tests because the surface was too rough or the plateaux too small for testing.

Table 5.22 Hardness of Ma956 after wearing against Stellite 6 at room temperature, 350°C, 550°C and 750°C

Temperature	Hardness Hv 500g
Room temp.	Too uneven
350°C	Too uneven
550°C	486
750°C	580

5.5.5 SEM/Cross-sectional EDX of Ma956 and EDX Analysis of Wear Debris

A summary of analysis carried out after Ma956 was worn against Stellite 6 at room temperature, 350°C, 550°C and 750°C is shown in ***Table 5.23*** .

At room temperature the wear scar produced on the Ma956 was characterised by a powder-like film and glaze formation was not observed. Cross sectional analysis revealed a 2μm wear scar comprised of an oxidised layer of Fe/Cr/Al. No cobalt was detected in the wear scar. Wear debris particles collected during the test showed two types of particles being produced. One type was flat angular (<25μm diameter) containing Fe/Cr + little Co. The second type was a powdery particle (<25μm diameter) comprised of Fe/Cr/Co.

The surface of Ma956 was covered in small plateaux typically 150μm in length after wearing against Stellite 6 at 350°C, though the plateaux did not have a shiny appearance (see **Fig.5.39a**). The wear scar was 8μm thick and contained oxidised Co/Cr. Wear debris analysis again revealed two types of particles both <100μm. Type 1 was flat angular and contained Fe/Cr/Co. Type 2 was a powder-like particle containing mainly Co/Cr with a little Fe.

Glaze formation was observed on Ma956 after testing at 550°C with the glazes being >500μm in length as shown in **Fig.5.39b**. Cross-sectional analysis revealed the wear scar on Ma956 to be 5μm thick and contain an oxidised layer of Fe/Cr/Al/Co. Two types of

flat angular wear debris particles were produced (<150μm diameter) that contained either Fe/Cr + little Co or Co/Cr + little Fe.

Testing at 750°C revealed a similar pattern of results to that observed at 550°C. Glaze formation was observed on Ma956 and the wear scar was composed of mixed oxides of Fe/Cr/Al/Co. 3 types of wear debris particles were detected all being flat angular and <200μm diameter. Two types contained Co/Cr/Fe with varying compositions and the third type contained only Co/Cr.

Table 5.23 Summary of analysis of selected features after the wearing of Ma956 against Stellite 6 between room temperature and 750°C

Temperature	Analysis of Ma956	EDX analysis of wear debris
Room temperature	Surface covered in powder-like film - no glaze formation. Cross-sectional analysis detected a 2μm wear scar containing oxidised Fe/Cr/Al	Two types of particles: 1. Flat angular (<25μm diameter) - contained Fe/Cr + little Co 2. Powdery particles (<25μm diameter)- mainly Fe/Cr/Co
350°C	Surface covered in small plateaux typically 150μm in length. Wear scar (8μm thick) contained unoxidised Co/Cr (see **Fig.5.39a** and **Fig.5.39c**)	Two types of debris both <100μm diameter: 1. Flat angular - contained Fe/Cr/Co 2. Powdery particles - contained mainly Co/Cr + little Fe
550°C	Surface covered in large glazes >500μm in length. Wear scar (5μm thick) contained Fe/Al/Cr/Co oxides (see **Fig.5.39b** and **Fig.5.39d**).	Two types of flat angular debris (<150μm diameter): 1. Fe/Cr + little Co 2. Co/Cr + little Fe
750°C	Surface covered in large glazes. Wear scar 8-15μm thick (including some internal oxidation) - comprised Fe/Co/Al/Cr oxide	3 types all flat angular & <200μm: 1. Co/Cr 2. Co/Cr + little Fe 3. Fe/Cr + little Co

Fig.5.39 a - SEM micrograph of Ma956 worn against a Stellite 6 counterface at 350°C for 4 hours
b - SEM micrograph of Ma956 worn against a Stellite 6 counterface at 550°C for 4 hours
c - Cross-sectional EDX of Ma956 worn against a Stellite 6 counterface at 350°C for 4 hours
d - Cross-sectional EDX of Ma956 worn against a Stellite 6 counterface at 550°C for 4 hours

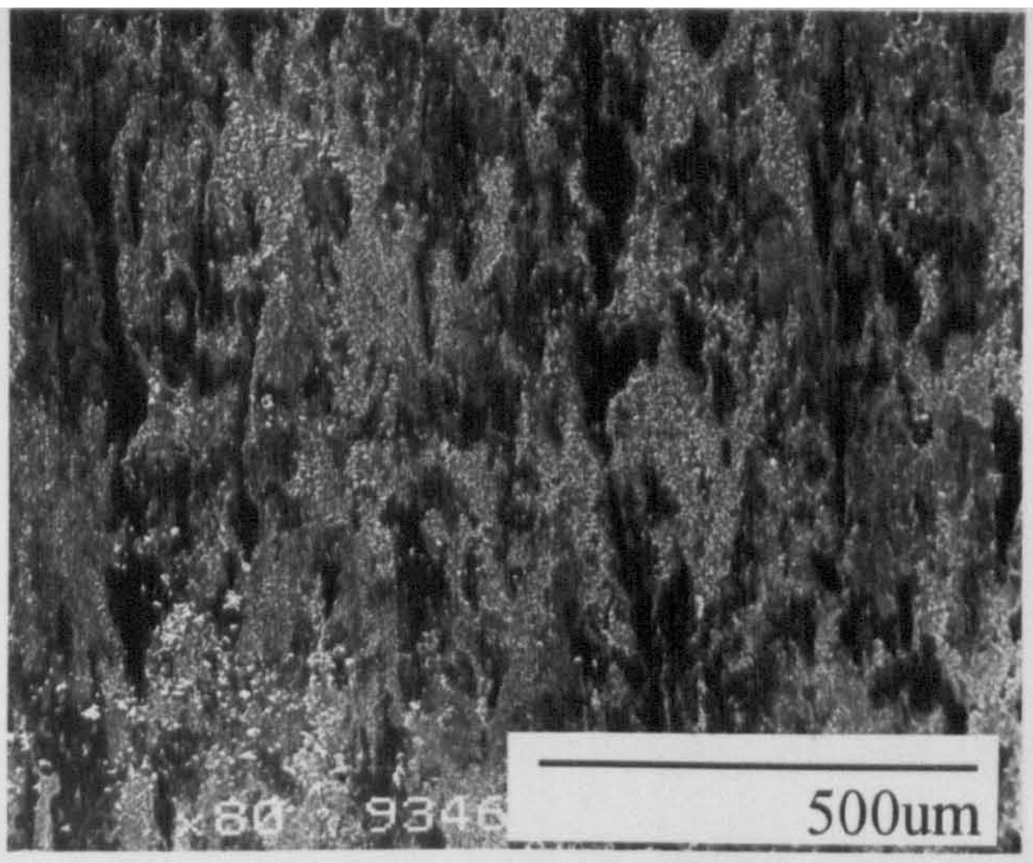

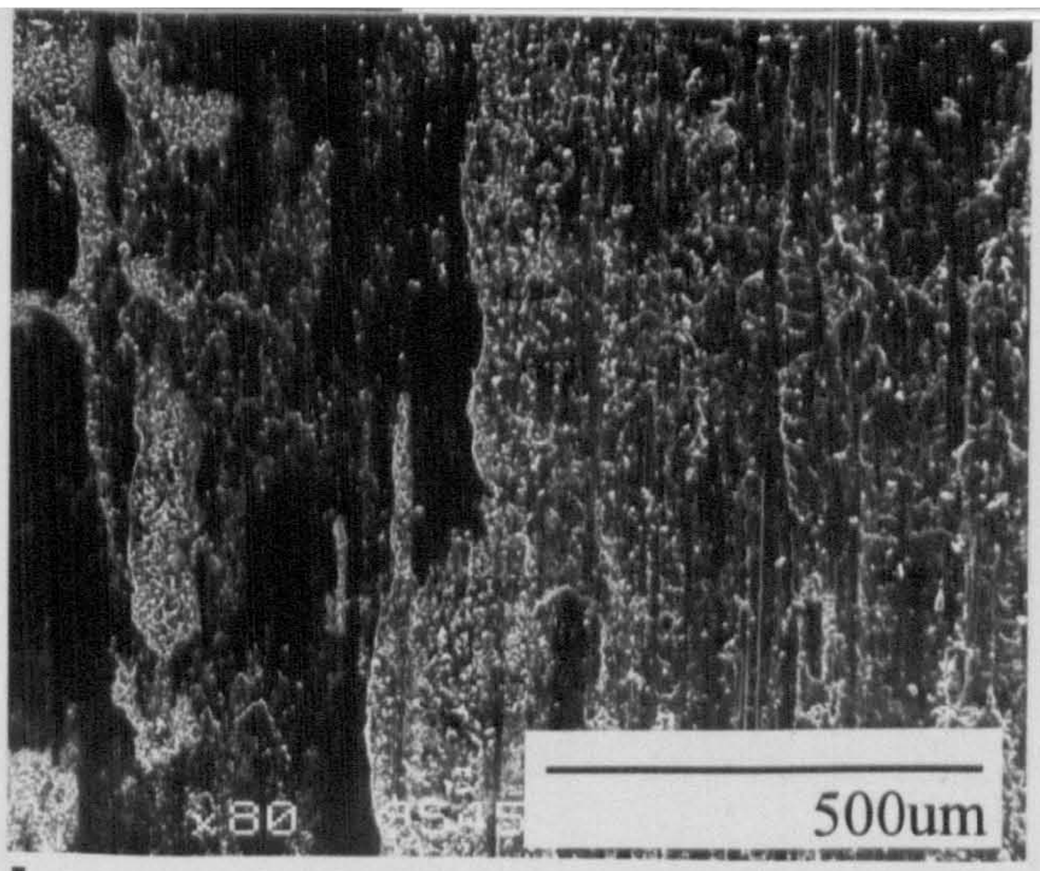

a

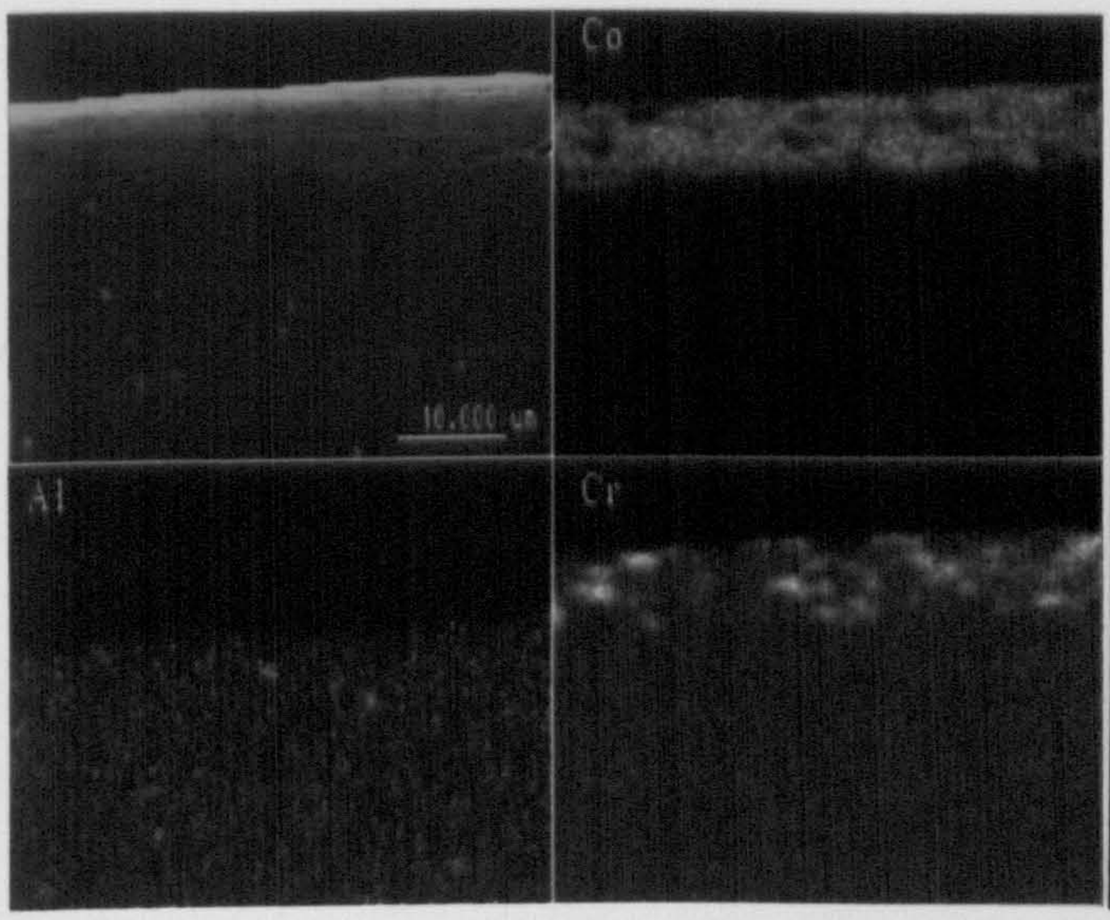

b

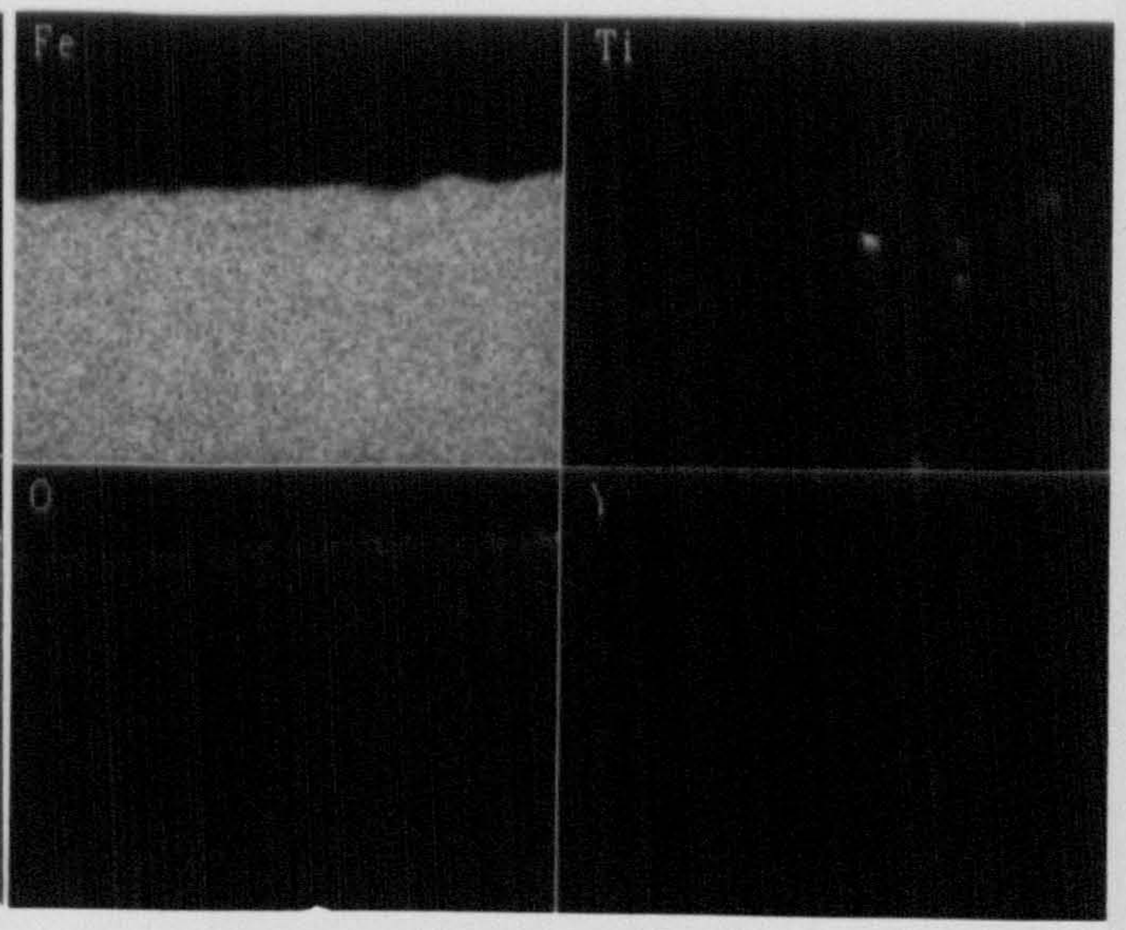

c

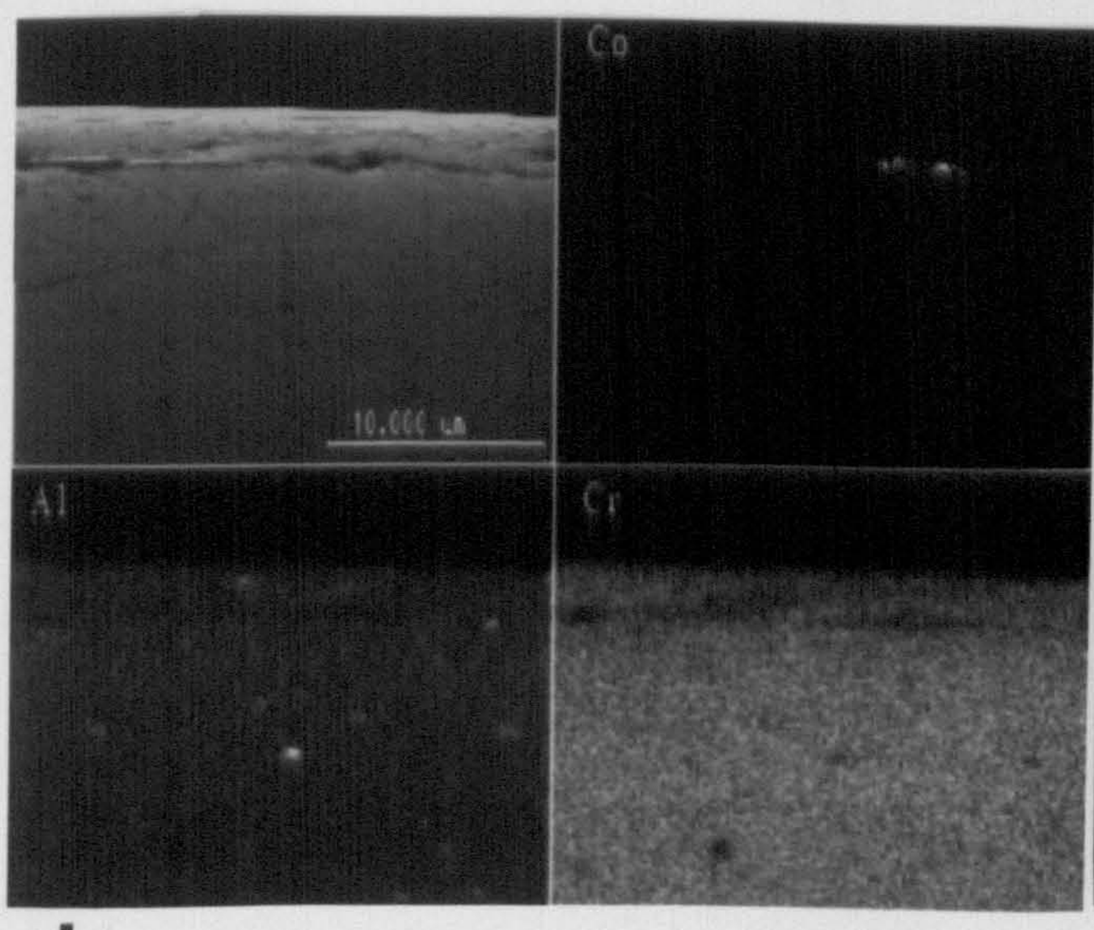

d

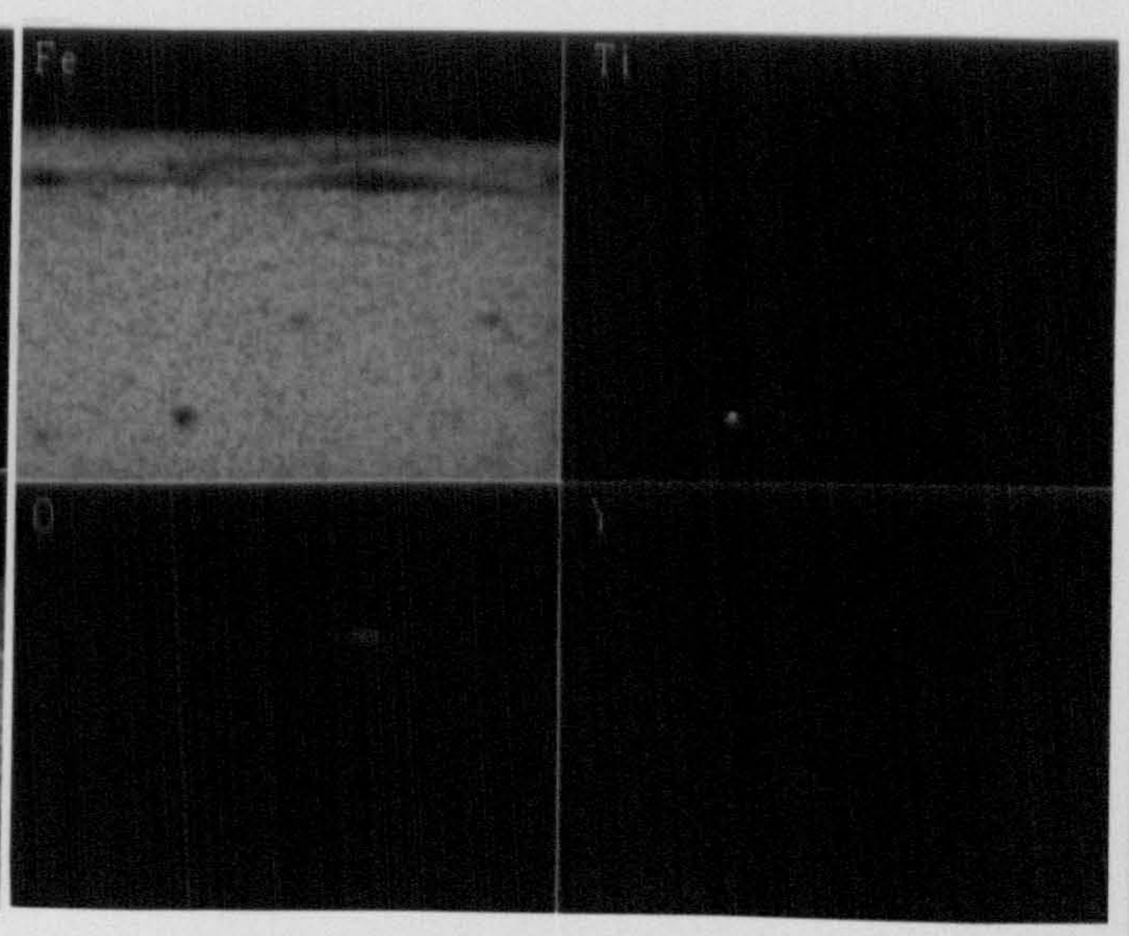

5.6 Effect of Preoxidation on the Wear Resistance of ODS Alloys Wearing Against Incoloy 800 Counterface at 750°C

5.6.1 Weight Changes

The values of weight changes shown by preoxidised Ma956, PM2000 and PM2000SD after wearing against Incoloy 800 at 750°C are displayed in **Fig.5.40**. The ODS alloys preoxidised for 1 hour showed a large variation in weight loss. A weight loss for preoxidised PM2000SD was -250mgcm^{-2} while the value for Ma956 and PM2000 (preoxidised in the same way) was -788.1mgcm^{-2} and -1056.4mgcm^{-2} respectively. The alloy Ma956, preoxidised at various exposure times and worn against Incoloy 800, showed a lowering of the weight loss with increased preoxidation time. For example the weight loss of Ma956 preoxidised for 1 hour was -788.1mgcm^{-2} compared to -475.3mgcm^{-2} for 10 hours preoxidation and -440.5mgcm^{-2} after 100 hours preoxidation.

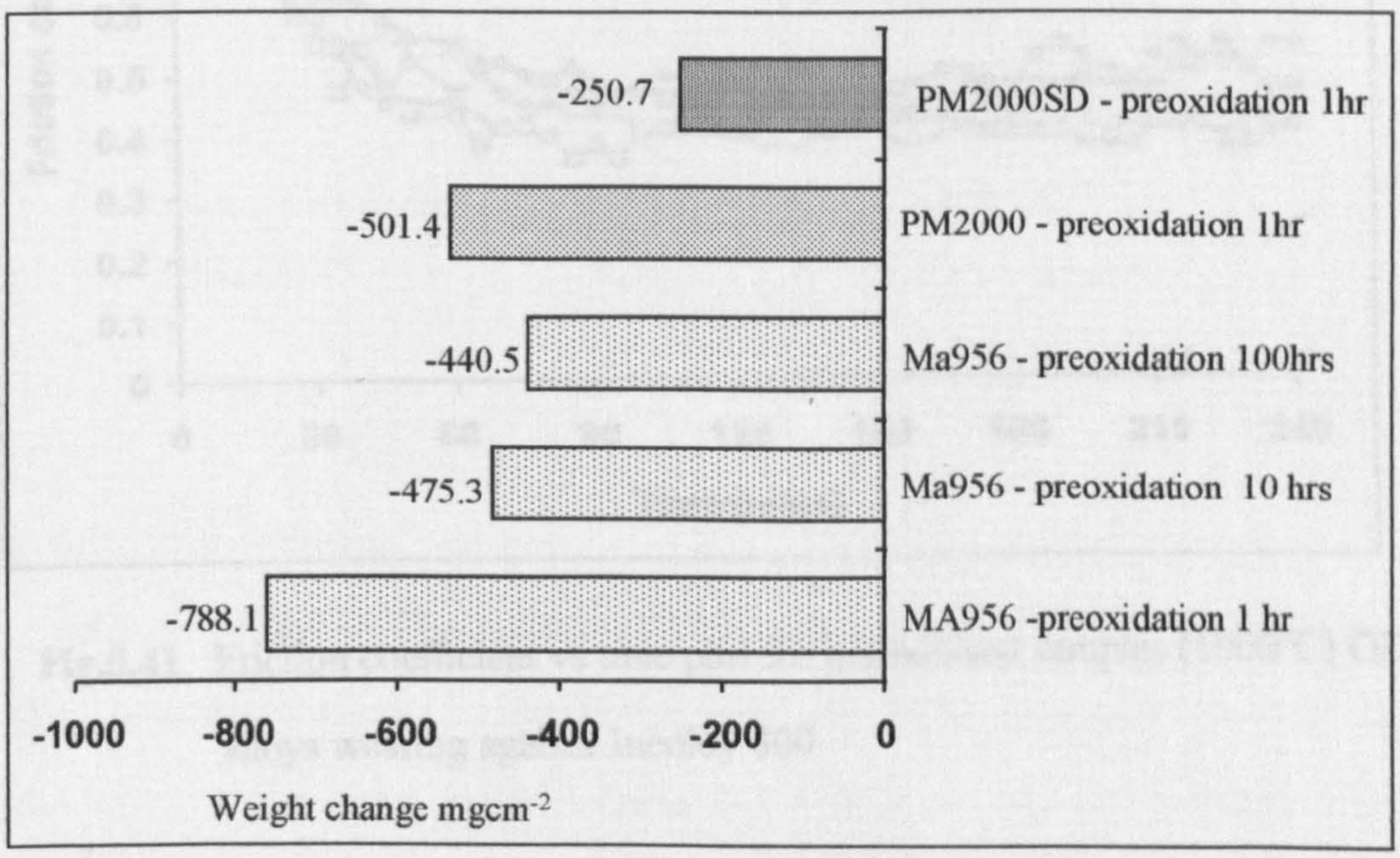

Fig.5.40 Weight change of the preoxidised ODS alloys after wearing against Incoloy 800 at 750°C

5.6.2 Friction Coefficient

The friction coefficient vs time plots for preoxidised Ma956, PM2000 and PM2000SD wearing against Incoloy 800 at 750°C are displayed in **Fig.5.41**. The results indicated very little difference in friction coefficients between the different alloys or between Ma956 that had been preoxidised for different times. Initial values of the friction coefficient for all the samples were between 0.9-1.1 dropping slowly until a value of 0.4-0.5 was reached after about 60 minutes.

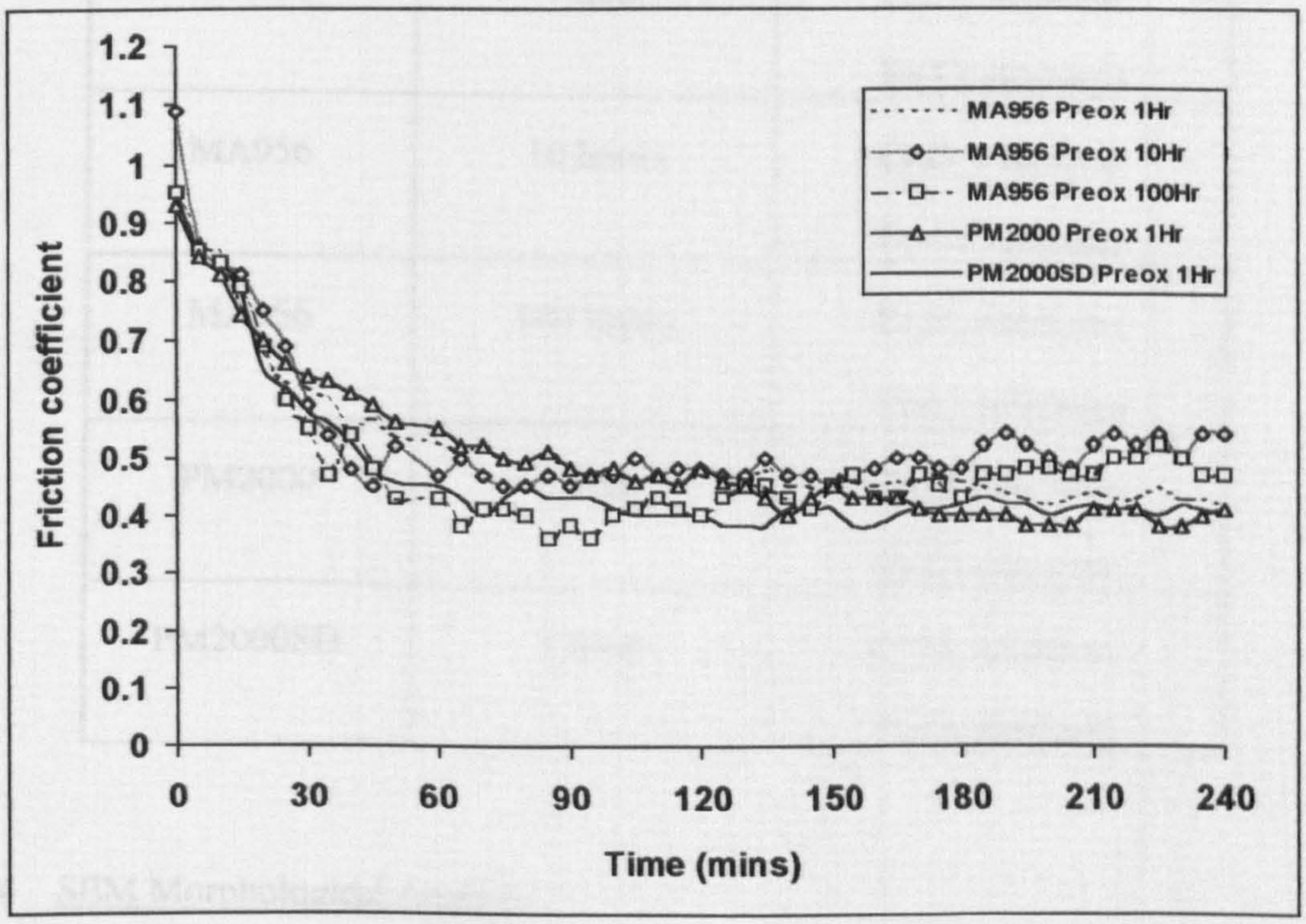

Fig.5.41 Friction coefficient vs time plot for preoxidised samples (1000°C) ODS alloys wearing against Incoloy 800

5.6.3 XRD Analysis

Phases detected by XRD on the surface of preoxidised Ma956, PM2000 and PM2000SD after wearing against Incoloy 800 are presented in ***Table 5.24***. It can be seen

from the results that the same phase of Cr_2O_3 eskolaite in addition to the Fe-Cr substrate were detected on all of the samples.

Table 5.24 XRD analysis of the surface of preoxidised ODS alloys after wearing against Incoloy 800 at 750°C

Alloy	Preoxidation time	Phase detected by XRD
MA956	1 hour	Cr_2O_3 eskolaite, Fe-Cr substrate
MA956	10 hours	Cr_2O_3 eskolaite, Fe-Cr substrate
MA956	100 hours	Cr_2O_3 eskolaite, Fe-Cr substrate
PM2000	1 hour	Cr_2O_3 eskolaite, Fe-Cr substrate
PM2000SD	1 hour	Cr_2O_3 eskolaite, Fe-Cr substrate

5.6.4 SEM Morphological Analysis

Analysis of Ma956, PM2000 and PM2000SD, that had been preoxidised for 1 hour and worn against Incoloy 800, showed the wear scar to be comprised of a very smooth surface that had cracked and spalled in places. A similar morphology, shown in **Fig.5.42**., was also observed on Ma956 preoxidised for various times (1hr to 100hrs) and worn under the same conditions.

Fig.5.42 SEM micrographs of preoxidised Ma956 worn against an Incoloy 800 counterface for 4 hours at 750°C

a - 1 hour preoxidation
b - 10 hours preoxidation
c - 100 hours preoxidation

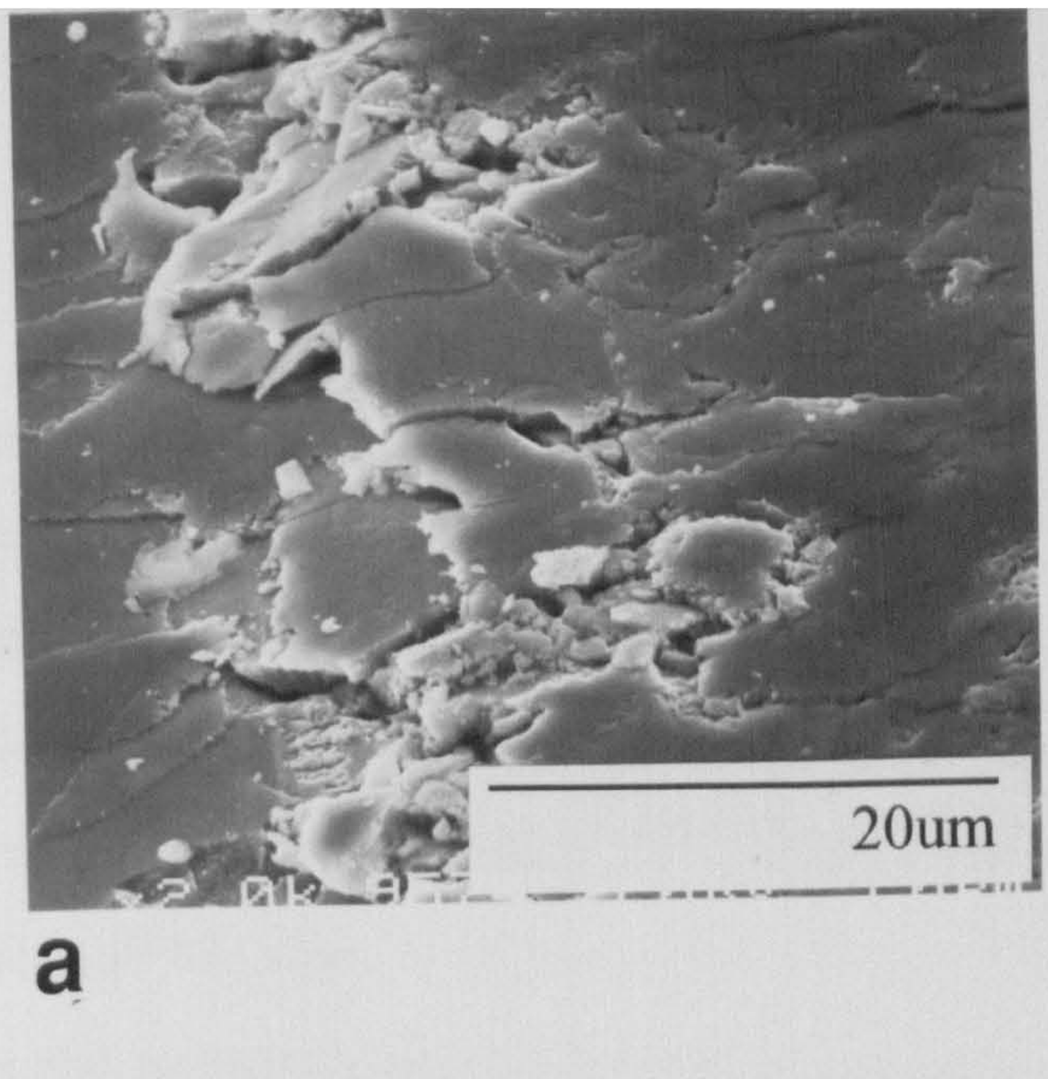

a

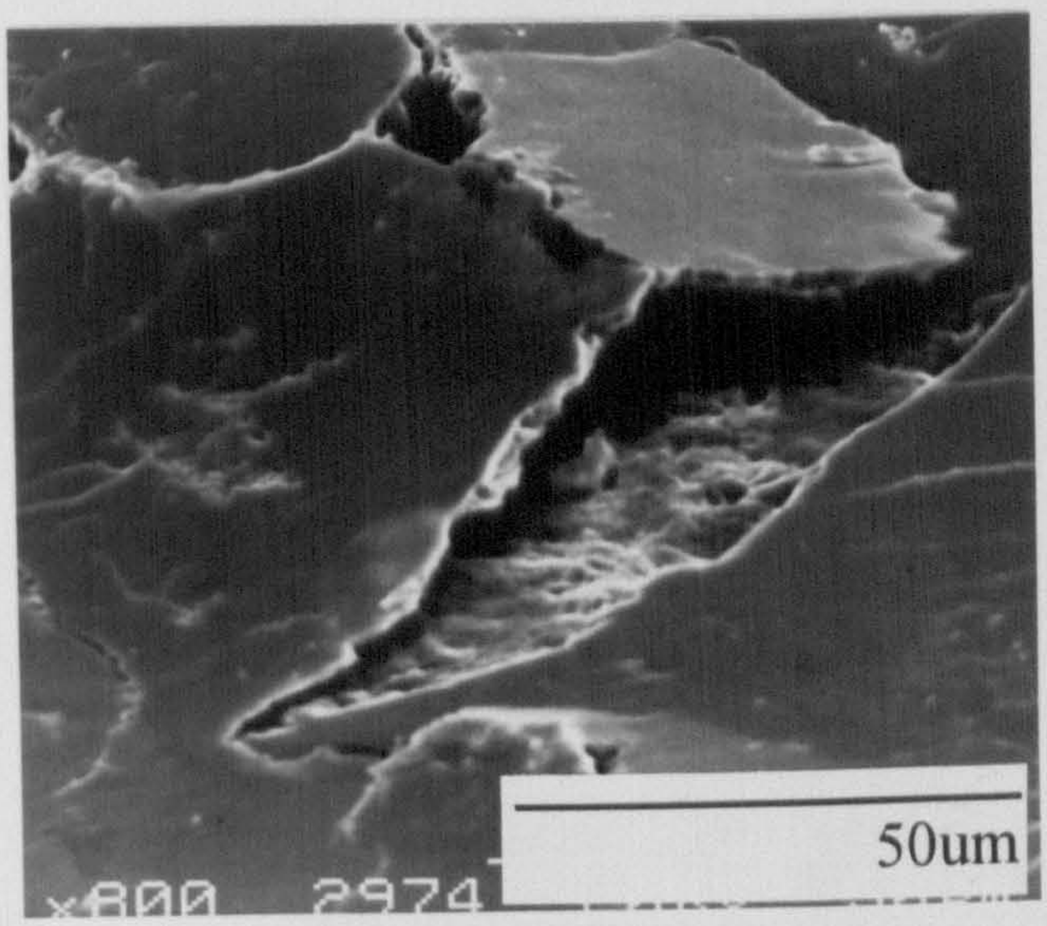

b

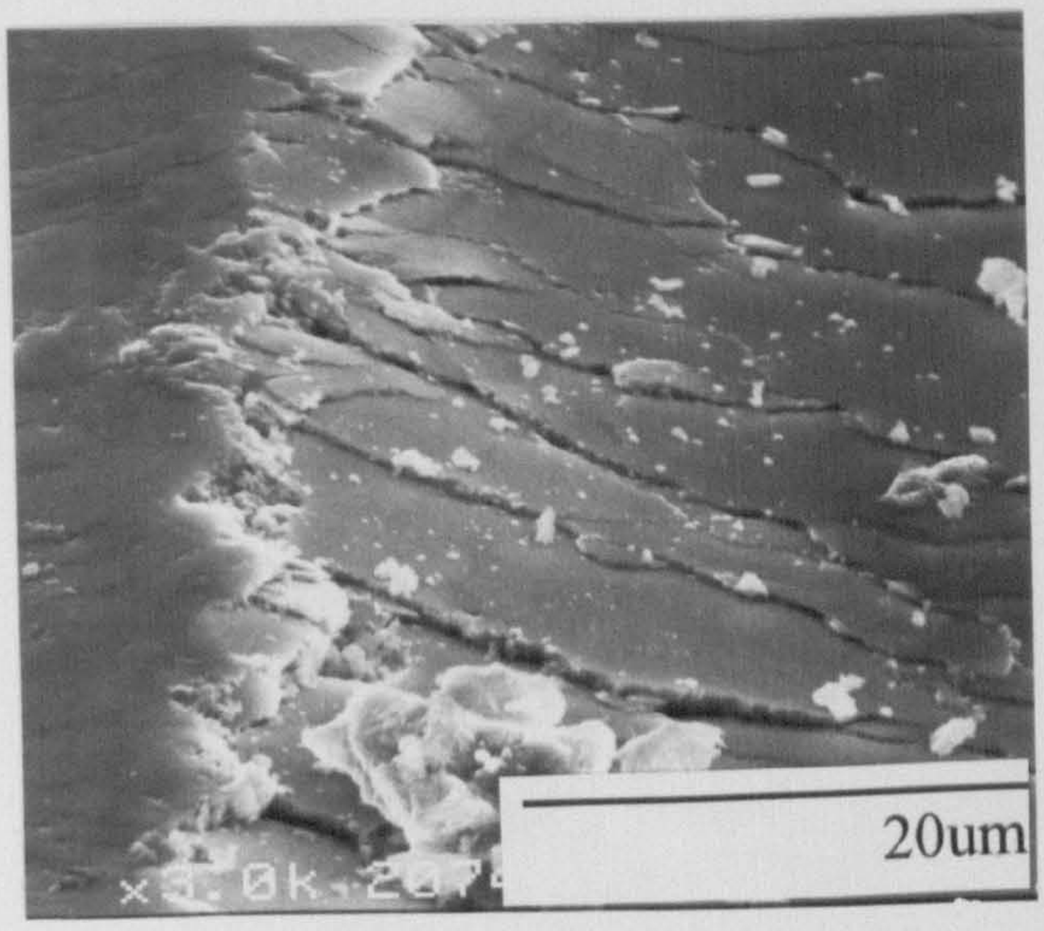

c

5.6.5 Cross-sectional EDX of Preoxidised ODS Alloys and EDX analysis of Wear Debris

Table 5.25 records a summary of cross-sectional EDX analysis of preoxidised Ma956 and EDX analysis of the wear debris after the alloy was worn against Incoloy 800 at 750°C. The thickness of the preformed oxide film, found to be Al_2O_3, is also shown.

For all of the preoxidised alloys similar observations were made during analysis. The cross-section of the worn ODS alloy was around 10-15μm thick comprised of Fe/Cr/Al oxides with a small amount of Ni also being detected. 2 types of flat angular wear debris were produced (<200μm) containing either Fe/Cr/Al or Ni/Fe/Cr. Thickness measurements of the preformed oxide film on the ODS alloys before wearing showed the thickness to around 0.5μm after 1 hour's oxidation at 1000°C. This increased to 1μm after 10 hours oxidation of Ma956 but no further increases were seen after 100 hours.

Table 5.25 Summary of analysis of the preoxidised ODS alloys worn against Incoloy 800

Alloy	Preformed film thickness	Cross-section of wear scar on the ODS Alloy	Wear debris
Ma956 PM2000 PM2000SD 1 Hr preox.	0.5μm	Wear scar 10-15μm thick - contained oxidised Fe/Al/Cr and very small amount of Ni	Two types of flat angular particles (<200μm): 1. Ni/Fe/Cr 2. Fe/Cr/Al
Ma956 10 Hrs preox.	1μm	Wear scar 12μm thick - contained oxidised Fe/Cr/Al and very small amount of Ni	Two types of flat angular particles (<200μm): 1. Ni/Fe/Cr 2. Fe/Cr/Al
Ma956 100 Hrs preox.	1μm	Wear scar 10μm thick - contained oxidised Fe/Cr/Al and very small amount of Ni	Two types of flat angular particles (<200μm): 1. Ni/Fe/Cr 2. Fe/Cr/Al

CHAPTER 6

DISCUSSION

6. DISCUSSION

This Chapter is presented in four major subsections: (1) wear studies using different counterfaces for 4 hours at room temperature and 750°C, (2) wear testing of Ma956 and Nimonic 90 for 2 minutes to 4 hours at 750°C, (3) effect of temperature on the wear resistance of Ma956 wearing against Stellite 6, and (4) effect of preoxidation on the wear resistance of the ODS alloys.

It is important to point out that in the following discussion, the whole wear resistant plateau on the surface of the wear scar was referred to as the glaze. In fact, glazes, as discussed previously in ***Chapter 2***, are actually only a very thin homogeneous layer of very small particles (10-50nm) at the very surface of the plateaux. However, studies [12] have shown that glazes have a similar composition to the underlying plateau. Therefore in the discussion it was assumed that the composition of the actual glaze was similar to the composition of the plateau supporting it as it was not possible to distinguish the glaze from the underlying oxide during cross-sectional analysis.

In addition, it has always been assumed that glaze formation will occur at elevated temperature and therefore only reasons why glazes were not formed will be discussed.

6.1 Wear Studies Using Different Counterfaces at Room Temperature and 750°C for 4 Hours

6.1.1 ODS Alloys vs Different Counterfaces

(a) ODS Alloy vs Incoloy 800 - RT and 750°C

The wear of the ODS alloys against Incoloy 800 at room temperature was accompanied by the transfer of Incoloy 800 material onto the surface of the ODS alloys. This material on the surface was then compacted into plateaux (see **Fig.5.11a**) and under the process of wear underwent work-hardening as indicated by the high hardness of the plateaux (Hv533 cf. to Hv183 for unworn Incoloy 800). This provided a wear resistant surface and therefore only small weight losses of the ODS alloys of between -9.4mgcm^{-2} to

-0.7mgcm^{-2} were observed. The work-hardening also probably prevented the occurrence of high friction coefficients and high wear rates usually associated with like-on-like sliding. Glaze formation was assumed not to have occurred as the plateaux were comprised of flat layers and not the small particles (<1μm) usually associated with glaze formation. In addition, the friction coefficient during the test did not show a significant decrease, again indicating the absence of glaze formation. The reason for the absence of glaze formation was probably due to the temperature being insufficient to produce either enough oxidised wear debris or an oxide film thick enough for to form glazes.

Analysis of the wear debris detected only Ni/Fe/Cr particles from the Incoloy 800 counterface and therefore any ODS material removed must have been detached with the Incoloy 800 material.

XRD analysis of the worn ODS alloys detected FeO, in addition to $NiCr_2O_4$/Fe_2O_3 and the Fe-Cr substrate. FeO is an oxide that forms at temperatures greater than 570°C indicating high flash temperatures during the wear test. However, this temperature was not sustained to facilitate glaze formation.

ODS materials wearing against Incoloy 800 at 750°C showed much higher weight losses than those observed at room temperature with values ranging between -280.3mgcm^{-2} for PM2000SD to -1020.7mgcm^{-2} for Ma956. The mechanism of the wear of Ma956 against Incoloy 800 at 750°C is discussed in more detail in ***Section 6.2.3*** and therefore will not be dwelled upon here. It is likely that a similar mechanism of wear also occurred for PM2000 and PM2000SD. However, it is important to discuss the reasons for the difference between results obtained at room temperature and at 750°C. One reason could be that the Ma956 was more vulnerable to deformation at 750°C than at room temperature. At room temperature, the Ma956 provided a substrate of sufficient strength for the transferred Incoloy 800 material to form wear-resistant plateaux which protected the surface of Ma956. However, at 750°C, deformation of the Ma956 occurred. It is known that the strength of the Ma956 diminishes substantially above 500°C [107]. The surface was

incapable of supporting the Incoloy 800 plateaux formation. A second reason could be that glaze formation occurring on the Incoloy 800 counterface at 750°C, caused a considerable reduction in the amount of Incoloy 800 transfer. At room temperature, glaze formation on Incoloy 800 is unlikely to have happened and therefore a steady supply of Incoloy 800 would have been transferred to the Ma956 surface creating wear-resistant plateaux.

(b) ODS Alloys vs Stellite 6 - RT and 750°C

A high and fluctuating friction coefficient between 0.8 to 1.1 was observed when the ODS alloys were worn against Stellite 6 at room temperature indicating high adhesion forces. This occurred due to the continued removal and transfer of Stellite 6 from the counterface onto the ODS alloy leading to like-on-like sliding. This increase in the friction coefficient attributed to material transfer, has also been observed by other researchers [112]. The Stellite 6 material could be seen on the surface of the ODS alloy as a powder-like film with no definable load-bearing plateaux. Surface analysis, as shown in ***Table 5.4***, revealed the cobalt may have been present as cochromite $CoCr_2O_4$. The poor film/substrate adhesion was indicated by the removal of the film following cross-sectional polishing of the alloys. This prevented detection by cross-sectional EDX analysis even though EDX analysis of the surface had revealed a high content of cobalt (21.9%wt for Ma956) prior to polishing. The reason why a more adherent cobalt-containing layer did not form probably stems from the high hardness of the Stellite 6 (Hv464 cf. to Hv183 for Incoloy 800). This prevented the removal and transfer of Stellite 6 in large coherent layers. Instead, small particles got detached from the Stellite 6 surface and transferred to the surface of the ODS alloy. The transfer of material in particulate form prevented the formation of wear-resistant plateaux and consequently fairly high weight losses were observed ranging between -10.2mgcm^{-2} for Ma956 to -22.8mgcm^{-2} for PM2000. Analysis of the wear debris revealed the presence of ODS material particles mixed with Stellite 6 material.

Glaze formation on the ODS alloys was observed when worn against Stellite 6 at 750°C. Consequently very low weight losses were observed of between -1.4mgcm^{-2} for PM2000 to -7.4 mgcm^{-2} for Ma956. A higher temperature of 750°C encouraged the formation of oxidised wear debris which facilitated in the formation of glazes. The mechanism for the wear of Ma956 against Stellite 6 at 750°C is described later in ***Section 6.2.4*** and it is assumed that PM2000 and PM2000SD followed a similar mechanism.

(c) ODS Alloys vs Si_3N_4 - RT and 750°C

An increase in the friction coefficient from ~ 0.3 to 0.9 was observed when the ODS alloys were worn against Si_3N_4 at room temperature. This again indicated like-on-like sliding. However, surface analysis of the ODS alloys detected only a very small amount of silicon (e.g. 1.3%wt for Ma956) and a Si-containing phase was not revealed by XRD. Limited material transfer from the counterface was observed because of the very high hardness of the Si_3N_4 , i.e. Hv1301. Therefore, it is suggested that like-on-like sliding occurred by the transfer of the ODS alloy to the Si_3N_4 counterface, and the ODS alloy was in fact wearing against itself. The absence of wild variation of friction coefficients during the test indicates that here the process of wear was not accompanied by a continuous transfer and removal process of materials between the two wearing surfaces. Observations of Ma956, as shown in **Fig.5.11e**, showed small plateaux present on the surface. In addition, cross-sectional analysis of the Ma956 revealed a mixed oxide layer present containing mainly Fe, Al and Cr with some Si, even after cross-sectional polishing. It appears that the adherent plateaux on the surface provided protection for PM2000 and PM2000SD resulting in very low weight losses of -2.4mgcm^{-2} and -1.5mgcm^{-2} respectively. Ma956 showed a larger weight loss of -95.3mgcm^{-2}. Only one type of wear debris particle was detected containing Fe/Cr/Si. This indicated that the removal of the ODS alloy occurred only after some degree of mixing with the counterface material. This happened on either the surface of the Ma956 and/or surface of the counterface.

Testing of the ODS alloys against Si_3N_4 at 750°C was limited only to Ma956 due to cracking of the ceramic counterface. The Ma956 showed a very low weight loss of only -1.4mgcm^{-2} in addition to a low friction coefficient of ~ 0.2. The surface of the Ma956 did not exhibit the normal plateaux glaze formation but an incomplete layer of material was observed on the surface. Surface analysis by XRD could not detect this film as shown in ***Table 5.5***. This layer was very thin (2μm thick) and comprised of Si and N transferred from the counterface in addition to Fe, Cr and Al from the Ma956. A grooved Ma956 surface could be seen beneath the surface film indicating the initial wear of the surface. Subsequently, the wear debris produced appears to have combined with the material transferred from the Si_3N_4 counterface to produce a wear resistant film with a very low friction coefficient signifying glaze formation.

The results of the wear tests with Ma956, PM2000 and PM2000SD, did show a similar variation in weight change when worn at different temperatures and against different counterfaces. However, comparing the behaviour of the ODS alloys tested, generally PM2000SD showed the lowest weight losses followed by PM2000 and then MA956. This can be related to the hardness values of the alloys which increased in the following order: Ma956 (Hv303), PM2000 (Hv311) and PM2000SD (Hv363). In various investigations [47-48] it has been observed that wear resistance can be related to hardness but only within the same group of materials as here with the ODS alloys.

6.1.2 Nimonics vs Different Counterfaces

(a) Nimonics vs Incoloy 800 - RT and 750°C

Nimonic 80A (cast and HIPped) showed a similar wear mechanism to the ODS alloys when worn against Incoloy 800 at room temperature. Large quantities of Incoloy 800 were transferred onto the surface of the Nimonic 80A which underwent work-hardening to provide a wear resistant surface. Consequently weight changes were very low, ranging between -3.2mgcm^{-2} for Nimonic 80A (HIPped) to +9.4 mgcm^{-2} for Nimonic 80A (cast). The hardness of the surface plateaux on Nimonic 80A (cast) was Hv563, which was similar to the value of Hv533 recorded for Ma956 wearing under the same conditions. The Nimonic 80A (cast and HIPped) surface for both alloys consisted of plateaux comprised of layers of flat material with no loose wear debris particles being observed. This is very different to the observations of Jiang et al. [64] who reported a surface of loosely compacted wear debris particles during like-on-like wear of Nimonic 80A. This difference was probably due to the change in the counterface or the change of sample geometry of the wear rigs. Testing conducting by Jiang et al. was carried out in a horizontal pin-on-disc rig in which wear debris retention could occur. However, in the present investigation the wear surface of the Nimonic 80A sample was facing downwards and with the reciprocation movement, the block alloy was out of contact with the counterface for a period of time discouraging debris retention.

Nimonic 90 showed in general a similar wearing pattern at room temperature to the Nimonic 80A samples. However, differences in the composition of the surface plateaux on Nimonic 90 and the friction coefficient were recorded. Cross-sectional analysis of the Nimonic 90 revealed the presence of Nimonic 90 in addition to the Incoloy 800 in the plateaux as shown in **Fig.5.16a**. The two materials did not undergo mechanical mixing but were present as two separate alloys. This may have just been an anomaly as the properties of the plateaux on the Nimonic 90 i.e. hardness (Hv563) and wear resistance (weight loss of Nimonic 90 was -2.0mgcm^{-2}) were similar to those observed on the worn Nimonic 80A

surfaces. A loose particle of Nimonic 90 may have been detached from the surface and incased in the Incoloy 800 material during material transfer from the counterface. However, there were differences in the friction coefficient values observed for Nimonic 90 and Nimonic 80A. For Nimonic 90, the friction coefficient increased from 0.3 to 0.7, while for Nimonic 80A (cast and HIPped) the value remained unchanged around 0.9. In all of the tests with the Nimonics only Ni/Fe/Cr containing wear debris was detected indicating any loss of the Nimonic was through detachment with Incoloy 800 material. This was assumed as the Fe content of the particles was far higher than the level in the as-received Nimonics.

FeO was detected on the surface of the worn Nimonic 90 again indicating high flash points. However, the phase was not detected on Nimonic 80A (cast and hipped).

Glaze formation was observed on all three of the Nimonics when tested against Incoloy 800 at 750°C. Consequently very low weight changes were observed ranging between -1.3mgcm^{-2} for Nimonic 80A (cast) to +11.1mgcm^{-2} for Nimonic 90. The mechanisms of wear of Nimonic 90 against Incoloy 800 at 750°C are described later in ***Section 6.2.1*** and it is likely that the two Nimonic 80A alloys follow a similar mechanism.

(b) Nimonics vs Stellite 6 - RT and 750°C

Stellite 6 transfer and subsequent like-on-like sliding also occurred during the wear of the Nimonics against Stellite 6 at room temperature. Friction coefficients were seen to increase and fluctuate considerably as shown in **Figs.5.7-5.9**. The surface morphology of the tested Nimonics had a powder-like appearance made up of mainly Stellite 6 material transferred from the counterface. This was indicated by the high content of Co (16.1-44.5%wt) on the surface, though a cobalt-containing phase was not detected. This provided little protection for the surface of the Nimonics and consequently weight losses of between -6.4mgcm^{-2} to -20.5mgcm^{-2} were observed, higher than values obtained with the Incoloy 800 counterface at room temperature (-3.2mgcm^{-2} to +9.4mgcm^{-2}). Nimonic material could not be detected in the wear debris, indicating that the Nimonic was removed

in combination with the Stellite 6 material. This was even the case for wear debris produced during the wear of Nimonic 90 which showed higher cobalt contents that would be expected only from Nimonic 90 material.

High weight losses were observed when the Nimonics were tested against Stellite 6 at 750°C. These values ranged between -68.0mgcm^{-2} for Nimonic 90 to -113.6mgcm^{-2} for Nimonic 80A (HIPped). The reason for the high weight losses was due to the formation of glazes that had poor adherence to the substrate and is explained in more detail later in ***Section 6.2.2***.

(c) Nimonics vs Si_3N_4 - RT and 750°C

Friction coefficient increases were again observed when Nimonic 90 and Nimonic 80A (cast) were worn against Si_3N_4 at room temperature indicating like-on-like sliding. Surface analysis revealed only small quantities of silicon on Nimonic 90 (5.1%wt) and Nimonic 80A (cast) (0.4%wt) and a Si-containing phase was not detected. Therefore, Nimonic material was transferred onto the Si_3N_4 wheel during the test causing Nimonic/Nimonic wearing. The wear debris was mainly composed of powdery particles containing Ni/Cr and a small amount of silicon, as shown in ***Table 5.13***, for both Nimonic 90 and Nimonic 80A (cast). This indicated the mixing and subsequent removal of Si_3N_4 material and Nimonic material during the process of wear. The surface of the Nimonics were composed of a powder-like film but this film was not adherent and could be removed by cross-sectional polishing. The poor adherence was also shown in the fairly high weight losses recorded for Nimonic 90 (-40.0mgcm^{-2}) and Nimonic 80A (cast) (-24.2mgcm^{-2}).

Two very different results were observed when Nimonic 80A (cast) and Nimonic 90 were worn against Si_3N_4 at 750°C. On the Nimonic 90 surface, small wear resistant glazes were formed composed of mainly Nimonic 90 material but also some counterface material indicated by the presence of Si (0.5%wt). These glazes had a fairly high hardness of Hv636 and enabled the surface of the Nimonic 90 to be protected leading to only a very

small weight loss of -2.4mgcm^{-2}. The friction coefficient decreased from just under 0.7 to a stable value ~ 0.2 after 5 minutes indicating a rapid formation of the glaze.

Glaze formation was not observed on the surface of Nimonic 80A (cast) and therefore a high weight loss of -73.3mgcm^{-2} was observed after it had worn against Si_3N_4 at 750°C. Friction coefficient measurements showed very high initial values ~ 1.3 which decreased to a more stable value after 20 minutes of ~ 0.6. However, this was still 3 times the value of the friction coefficient for Nimonic 90. The surface of the Nimonic 80A (cast) was deeply grooved with particles of wear debris present. Cross-sectional analysis revealed only a very thin Si/N oxide film present on the Nimonic 80A (cast) and a deformed layer could not be detected beneath it. Dissimilar wear performance can result from the differences in mechanical properties of the alloys. ***Table 6.1*** displays a comparison of mechanical properties of Nimonic 90 and Nimonic 80A.

Table 6.1 Comparison of the mechanical properties of Nimonic 90 and Nimonic 80A [107]

Property at 750°C	Alloy	
	Nimonic 90	Nimonic 80A
Rupture strength (1000h)	260 MPa	245 MPa
Tensile strength	800 MPa	820 MPa
Yield strength	600 MPa	660 MPa

As can be seen from ***Table 6.1***, the mechanical properties of Nimonic 90 and Nimonic 80A are very similar. However, the compositions of the two alloys are very different and were probably responsible for the differences in wear behaviour of these alloys. It is suggested that the presence of cobalt in Nimonic 90 facilitates the development of glazes and improves the adhesion and strength properties of these glazes. However, at present the way cobalt influences the formation of adherent glazes is not clear.

The processing route of an alloy has been seen by some investigators [62] to have an important influence on the wear resistance. In the present investigation the wear resistance of Nimonic 80A (cast) and Nimonic 80A (HIPped) have been compared but no significant difference has been observed. In three out of the four wear tests the Nimonic 80A (cast) was seen to have improved wear resistance over Nimonic 80A (HIPped). If all four test results showed this relationship then more confidence could be given to a determining effect of the processing route on the wear resistance. Longer tests and higher loads to give higher weight losses would need to be conducted before any definite conclusions could be made.

6.1.3 TiAl vs Different Counterfaces

(a) TiAl vs Incoloy 800 - RT and 750°C

TiAl showed a similar wear pattern to the ODS alloys and Nimonics when worn against Incoloy 800 at room temperature involving the same mechanism - the transfer of Incoloy 800 to TiAl surface → work hardening of the transferred material (Hv594) → formation of wear-resistant plateaux. Therefore, the TiAl showed a small weight increase of +3.2mgcm^{-2}. The transfer of material was indicated by XRD analysis of the worn sample which detected $NiCr_2O_4/Fe_2O_3$. The friction coefficient remained at a fairly steady value throughout the test of around 0.7 again suggesting the absence of glaze formation. The only wear particles detected were Ni/Fe/Cr platelets removed from either the Incoloy 800 counterface or transferred Incoloy 800 material on the TiAl surface.

Glaze formation was observed when TiAl was worn against Incoloy 800 at 750°C with the TiAl showing a small weight gain of +2.2mgcm^{-2}. Friction coefficient readings revealed a drop from an initial reading of just under 0.9 to a stable value of 0.6 after 25 minutes indicating glaze formation occurred in this period. Cross-sectional analysis, as shown in **Fig.5.17b** , revealed the glaze to be composed of oxidised Fe/Ni/Cr material from

the Incoloy 800 with titanium and aluminium not being detected. In addition deformation was not detected in the TiAl substrate. Surface analysis of the TiAl, as displayed in ***Table 5.8***, did identify small quantities of Ti (0.8%wt) and Al (0.4%wt) but these signals may have originated from the TiAl substrate. These results are not in line with those in the literature [12] which showed that glazes contain the elements in the same composition as the substrate alloy. In this particular case very little, if any, substrate alloy material was found to be present in the glaze and all of the wear debris originated from the Incoloy 800 counterface. The role played by TiAl in glaze formation was to provide a deformation-resistant and wear-resistant substrate for the glaze to form on and be sustained. This stems from the highly ordered structure of the intermetallic giving rise to different deformation mode and strengthening mechanisms compared to those operative in Nimonics and ODS alloys. One important point to note was that the hardness of the glaze on the TiAl was only Hv402 which was low compared to other glaze hardnesses, as shown in ***Table 5.6***. This indicates a low hardness of the glaze does not necessarily mean a higher wear rate of the underlying alloy. It can be concluded that although hardness is important, it is only one of the parameters that govern the formation of very wear-resistant glazes.

(b) TiAl vs Stellite 6 - RT and 750°C

A weight loss of 2.7mgcm^{-2} was observed when TiAl was worn against Stellite 6 at room temperature. The friction coefficient increased from 0.3 and fluctuated around 1.0 indicating like-on-like sliding. Cobalt (1.6%wt) was detected on the surface of TiAl in addition to $CoCr_2O_4$ indicating the transfer of Stellite 6. The Stellite/Stellite wearing produced the observed fluctuations in the friction coefficient. This was confirmed through cross-sectional analysis of the TiAl indicating a thin oxidised Co/Cr, i.e. Stellite 6 layer on the surface. This layer was not very adherent judging from observed weight loss of TiAl and the powder-like morphology on the TiAl. The low content of cobalt on the surface (1.6%wt) was again probably due to the very thin nature of the surface film (1-2μm) which

allowed the electron beam to pass through it during analysis. Analysis of the wear debris could only detect powder-like particles containing mainly Ti/Al/Cr/Co. Therefore the Stellite 6 layer must have been removed with TiAl material mainly from the surface of the block alloy.

Glaze formation was again observed on TiAl when worn against Stellite 6 at 750°C and a weight gain of $+0.8 mgcm^{-2}$ was recorded. Friction coefficient measurements did show a slow drop from an initial value of 0.9 to around 0.7 after 30 minutes indicating glaze formation in this period. In previous investigations it is has been observed [41] that a sudden drop in the friction coefficient occurs during glaze formation. In this investigation a fast change was hindered by the fact that the TiAl was reciprocating and only a small part of it was in contact with the counterface at any one time. The glaze was comprised a very thin oxidised layer of Co/Cr transferred from the Stellite 6 counterface with a hardness of only Hv402. Surface analysis of the glaze did reveal high contents of aluminium (21.8%wt) and titanium (50.0%wt) though $CoCr_2O_4$ was detected. This was again due to the very thin nature of the glaze and the penetration of the substrate during analysis. This glaze was much thinner (1-2μm) than the glaze observed on the TiAl sample worn against Incoloy 800 sample (10-15μm). The TiAl, as in other tests, only seemed to provide a wear- and deformation-resistant substrate for glaze formation to occur upon.

(c) TiAl vs Si_3N_4 - RT and 750°C

The TiAl samples showed very good wear resistance against all of the counterfaces at both room temperature and 750°C, apart from when worn against Si_3N_4 at room temperature. Under these wearing conditions, the TiAl showed a very high weight loss of $-210.4 mgcm^{-2}$ which is a very large volume loss when the low density of TiAl ($3.7 gcm^{-3}$) is taken into consideration. XRD analysis of the worn TiAl sample could only detect the presence of the substrate phases of TiAl. The friction coefficient fluctuated throughout the test between 0.6-0.7 indicating removal and formation of some type of film. Small plateaux

comprised of coarse wear debris were observed on the surface of the TiAl - these plateaux contained mixed oxides of Ti/Al/Si/N. Only one type of particle was detected in the wear debris which had the same composition as the plateaux on the TiAl. Obviously, material from the counterface was being transferred onto the TiAl which combined with wear debris from the TiAl itself to form mixed oxide plateaux. These were continually formed and removed which accounted for the fluctuations in the friction coefficient observed. However, the question still remains why the TiAl was so prone to wear with the Si_3N_4 counterface at room temperature. The TiAl susceptibility to wear must be due to the Si_3N_4 counterface material interfering with the ordered structure of the intermetallic. The reason for this may be due to the small nature of the atomic and covalent radii of silicon and nitrogen . These are displayed in ***Table 6.2*** with the atomic radius of other elements.

Table 6.2 Atomic radius and selected covalent radius of certain elements

Element	Atomic radius Å	Covalent radius Å
Silicon	1.46	1.11
Nitrogen	0.75	0.75
Chromium	1.85	-
Iron	1.72	-
Cobalt	1.67	-
Nickel	1.62	-

Table 6.2 shows that silicon and nitrogen have very small radii compared to elements present in other counterfaces. This might enable silicon and nitrogen to enter the ordered TiAl lattice more easily than the other elements and therefore disrupt the lattice increasing its susceptibility to wear. Razavizadeh and Eyre [113] observed that Fe transferred from a steel counterface into aluminium silicon pins (Al-16%Si and Al-16%Si-

1%Cu) improved the wear resistance of the pins. They concluded from TEM analysis that Fe had transferred and diffused into the aluminium-silicon pins and caused greater blockage of the dislocations leading to the improved wear resistance observed. Therefore, if transferred material can have a positive effect on the wear resistance then a negative effect may also be observed.

However, when TiAl was worn against Si_3N_4 at 750°C a small weight increase of $+0.5mgcm^{-2}$ was observed. Friction coefficients recorded throughout the test showed a small drop from just under 0.3 to around 0.2 indicating the possible formation of a glaze. Observations of the surface of the worn TiAl, as shown in **Fig.5.14f**, revealed the presence of a surface coating which was slightly scuffed in places. Obviously, this film was wear-resistant and a glaze may have been formed at the very surface of the film, though surface analysis could only detect substrate phases. Cross-sectional analysis revealed the film had developed from a mixture of material from the TiAl and transferred Si/N material from the counterface. Even though the film was wear-resistant, its hardness was only Hv370 compared to an unworn hardness of Hv345 for TiAl. This again shows that the hardness of the mixed oxide film/glaze does not always relate to its wear resistance. The reason why high weight losses were not observed was due to the formation of oxidised wear debris which quickly combined forming a wear-resistant film on the surface of the TiAl.

6.2 Wear Testing of Nimonic 90 and Ma956 Against Incoloy 800 and Stellite 6 at 750°C (2 Minutes - 4 Hours)

6.2.1. Nimonic 90 vs Incoloy 800 at 750°C

Figs.6.1-6.2 displays a schematic of the wearing of Nimonic 90 against Incoloy 800 from 2 minutes to 4 hours. An incomplete layer of Incoloy 800 was transferred on to the Nimonic 90 surface during the first two minutes of wearing causing the Nimonic 90 to show a weight gain of $+12.5 mgcm^{-2}$. Micrographs, as shown in **Fig.5.23a**, and cross-sectional analysis (see **Fig.5.27a**) showed the Nimonic 90 surface had remained relatively unaffected during the transfer. Observations of the counterface revealed no glaze formation and the Incoloy 800 surface remained unchanged in composition. Ni/Fe/Cr platelets were detected in the wear debris which came from the Incoloy 800 counterface or from Incoloy 800 smeared onto the surface of the Nimonic 90 sample.

After 10 minutes of wearing a complete layer of transferred Incoloy 800 material was observed on the Nimonic 90 surface leading to a weight gain of $+16.4 mgcm^{-2}$ for Nimonic 90. This layer was also detected through XRD analysis which indicated a new phase of Fe_2O_3 maghemite/$NiCr_2O_4$ to be present. Observations of the Incoloy 800 surface revealed the absence of glaze formation and the composition of the layer was still the same as that of the as-received Incoloy 800. Wear debris analysis again only detected the presence of Ni/Fe/Cr platelets originating either from the Incoloy 800 counterface or from the Nimonic 90 surface.

Glaze formation was observed both on the Incoloy 800 counterface and Nimonic 90 after 20 minutes of wear with the Nimonic 90 showing a weight increase of $13.1 mgcm^{-2}$. The glazes on the Incoloy 800 counterface contained mainly Fe with some Cr, with Ni not being detected. This indicated that the wear debris used to produce the glaze came mainly from the Incoloy 800 counterface.

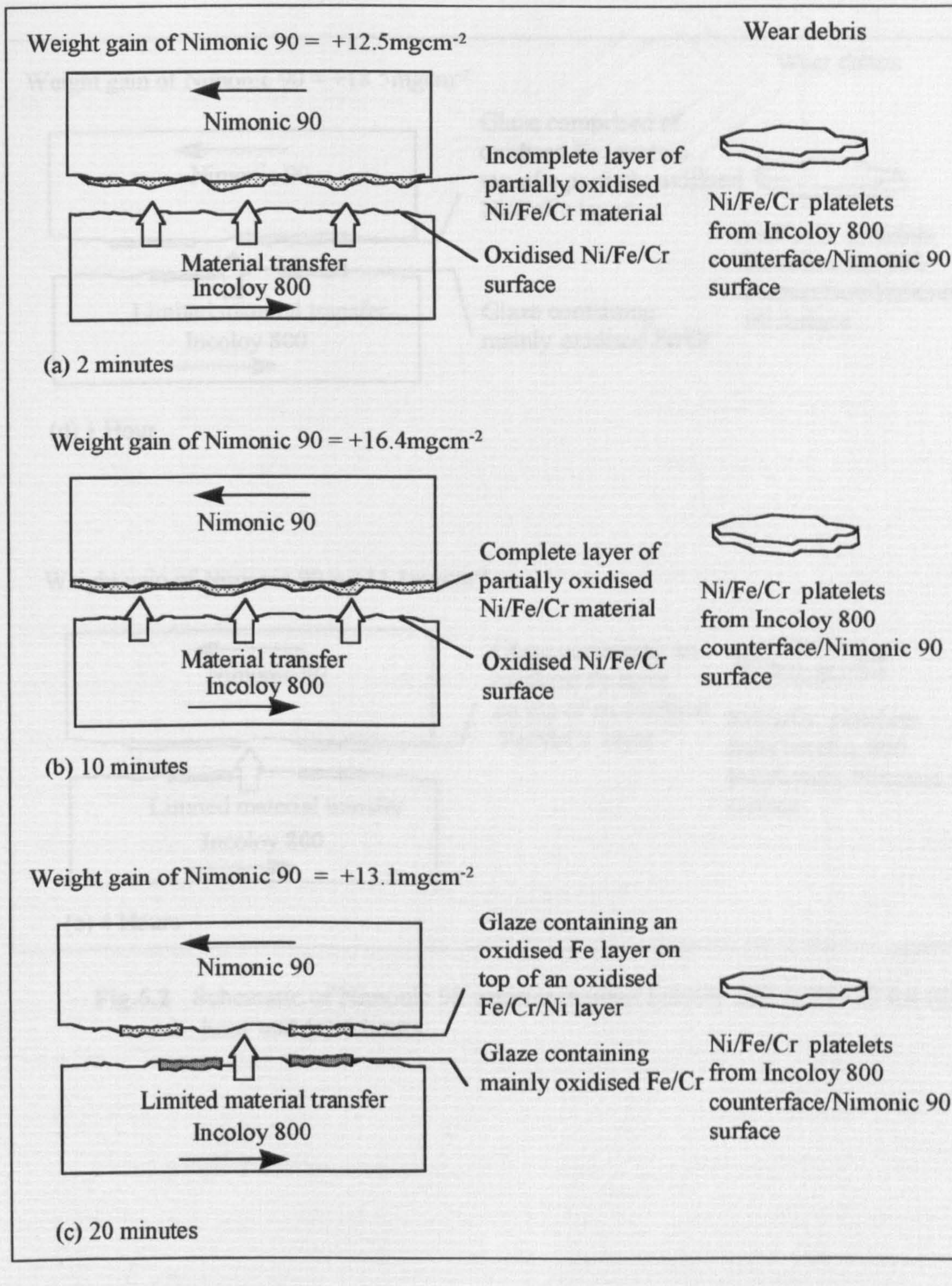

Fig.6.1 Schematic of Nimonic 90 wearing against Incoloy 800 at 750°C for (a) 2 minutes, (b) 10 minutes and (c) 20 minutes

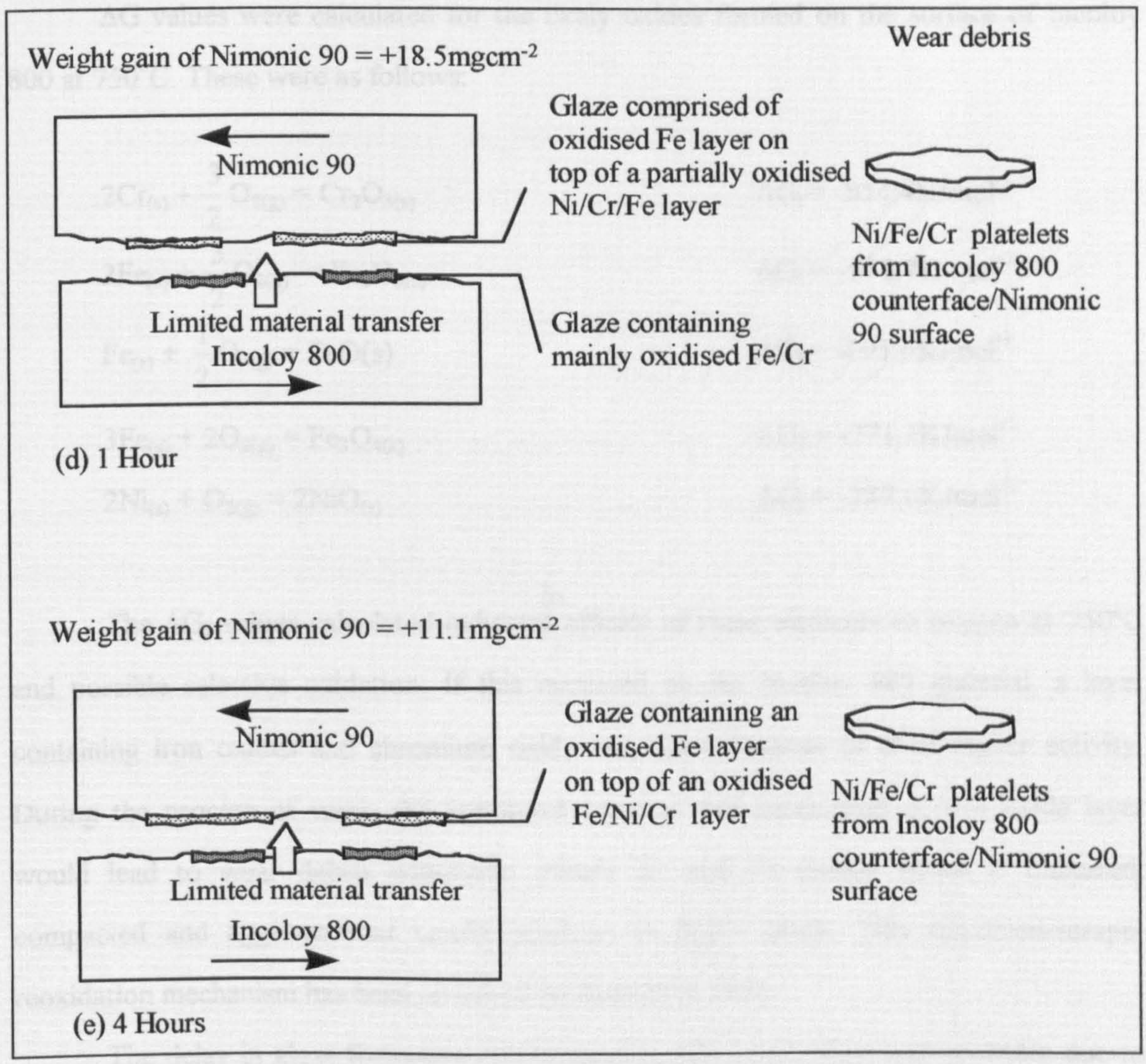

Fig.6.2 Schematic of Nimonic 90 wearing against Incoloy 800 at 750°C for (d) 1 hour and (e) 4 hours

ΔG values were calculated for the likely oxides formed on the surface of Incoloy 800 at 750°C. These were as follows:

$$2Cr_{(s)} + \frac{3}{2}O_{2(g)} = Cr_2O_{3(s)} \qquad \Delta G_f = -854.4 KJmol^{-1}$$

$$2Fe_{(s)} + \frac{3}{2}O_{2(g)} = Fe_2O_{3(s)} \qquad \Delta G_f = -550.7 KJmol^{-1}$$

$$Fe_{(s)} + \frac{1}{2}O_{2(g)} = FeO(s) \qquad \Delta G_f = -195.6 KJmol^{-1}$$

$$3Fe_{(s)} + 2O_{2(g)} = Fe_3O_{4(s)} \qquad \Delta G_f = -771.1 KJmol^{-1}$$

$$2Ni_{(s)} + O_{2(g)} = 2NiO_{(s)} \qquad \Delta G_f = -287.6 KJmol^{-1}$$

The ΔG_f values calculated indicates affinity of these elements to oxygen at 750°C and possible selective oxidation. If this occurred on the Incoloy 800 material, a layer containing iron oxides and chromium oxide may form because of their higher activity. During the process of wear, the continued removal and production of this oxide layer would lead to wear debris containing mainly Fe and Cr oxides which if fractured, compacted and agglomerated would produce an Fe/Cr glaze. This oxidation-scrape-reoxidation mechanism has been observed by Stott et al. [45].

The delay in glaze formation on the Incoloy 800 counterface was probably due to the initial lack of a sufficient amount of wear debris which is a major influence on glaze formation. The rig geometry used here did not encourage retention of wear debris on the rotating counterface.

Cross-sectional analysis through the Nimonic 90 sample worn for 20 minutes revealed the wear scar to be comprised of two layers, an oxidised Fe layer (Fe_2O_3) on top of a Ni/Cr/Fe layer. Earlier work showed that glazes [12] contain homogenous material and different oxide layers should not exist. Hence, it can be argued that the oxidised Fe layer was probably part of the glaze whilst the Ni/Cr/Fe material was deformed Incoloy 800 material that provided a substrate to sustain the glaze. The oxidised Fe layer on top of the

Fe/Cr/Ni layer in the glaze was probably due to the transfer of Fe material from the Incoloy 800 glazes.

Hardness measurements of the glaze formed on the Nimonic 90 after 20 minutes indicated a very high hardness of Hv812 compared to the as-received hardness value of Hv242. Wear debris analysis once again revealed the formation of Ni/Fe/Cr platelets produced from the Incoloy 800 counterface/ Nimonic 90 surface.

Nimonic 90 showed a weight gain of $+18.5 mgcm^{-2}$ after wearing against Incoloy 800 for 1 hour. Once again a mainly oxidised Fe/Cr glaze was observed on the Incoloy 800 counterface whilst on the Nimonic 90 surface the glaze consisted of fine Fe oxides particles on top of a partially oxidised Ni/Cr/Fe layer. The hardness of the glazes on the Nimonic 90 showed a small increase to Hv878 from Hv812 (recorded after 20 minutes of wearing). This increase was due to the increased compaction of the particles in the glaze because of their smaller size. Wear debris analysis revealed the production of mainly Ni/Fe/Cr platelets from the Incoloy 800 counterface/Nimonic 90 surface.

The Nimonic 90 sample still did not show a weight loss after 4 hours of wearing against Incoloy 800, instead a weight gain of $+11.1 mgcm^{-2}$ was recorded. Analysis of the glaze on the Nimonic 90 showed a mainly oxidised Fe layer present on top of an oxidised Fe/Ni/Cr layer. Micrographs of the glaze, displayed in **Fig.5.13b**, showed them to consist of very fine particles and consequently, due to the better compaction, a hardness of Hv1016 was recorded. Again, analysis of the wear debris revealed mainly the production of Ni/Cr/Fe platelets being removed from the Incoloy 800 counterface/Nimonic 90 surface.

During the 4 hour test the retention of Incoloy 800 wear debris on the Nimonic 90 surface was extremely good. The majority of the Incoloy 800 material transfer must have occurred during the first 10 minutes of the wear test. This was because, after 20 minutes of wearing, glaze formation occurred on the Incoloy 800 counterface thereby preventing large quantities of material transfer. However, the weight change of the Nimonic 90 remained

relatively unchanged throughout the test varying from +16.4mgcm^{-2} after 10 minutes to +11.1mgcm^{-2} after 4 hours.

Friction coefficient measurements recorded throughout the test revealed a large drop from an initial value of 1.1 to a largely stable value around 0.45 after 20 minutes by which time glazes had formed on both surfaces. The decrease in friction coefficient is generally accompanied by the formation of glazes. The early drop in friction coefficient indicates the formation of a thin layer of glaze not identified.

6.2.2 Nimonic 90 vs Stellite 6 Counterface at 750°C

A schematic of the stages of wear between Nimonic 90 and Stellite 6 for 2 minutes to 4 hours is shown in **Fig.6.3-6.4**. The Nimonic 90 initially showed a weight gain of +0.7mgcm^{-2} after wearing against Stellite 6 for 2 minutes. The small weight gain was due to Stellite 6 transferred to the surface of the Nimonic 90 as small load-bearing plateaux. It was unclear if these were glazes as Stellite 6 is a wear resistant alloy. However, the plateaux were composed of layered material and not small oxide particles indicating that glaze formation had not occurred. Analysis of the Stellite 6 counterface could not detect any transfer from the Nimonic 90 sample and glaze formation was not observed. Two types of wear debris were identified. One type was a powder-like particle containing mainly Co and Cr which became detached from the Stellite 6 counterface. The second type were platelets containing Ni, Cr and Co detached from the Nimonic 90 surface indicating the wearing of the Nimonic 90 surface. The wearing away of the Nimonic 90, did not occur with the Incoloy 800. The difference was probably due to the more abrasive nature of the Stellite 6 counterface which contained very hard Cr_7C_3 particles.

After 10 minutes of wearing the Nimonic 90 sample showed an unchanged weight. Glaze formation was observed on the Nimonic 90 as large plateaux comprised of small particles were present. In addition, cross-sectional analysis revealed the glazes to be

composed of a mixture of oxidised Stellite 6 material and thin layers of oxidised Ni material. A glaze was also observed on the Stellite 6 counterface which contained oxidised Stellite 6 debris with a small amount of Ni material transferred from the Nimonic 90 sample. Ni/Co/Cr platelets, detached from the Nimonic 90 surface were once again observed with particles of Stellite 6 material in the wear debris.

The glaze coverage decreased on the Nimonic 90 surface after 20 minutes of wearing. This was also confirmed in the slight weight loss of Nimonic 90 of -2.0mgcm^{-2} indicating the removal of the glaze. The remaining glazes on the Nimonic 90 sample consisted of an oxidised Ni/Cr layer on top of a Co/Cr layer. Hardness measurements of the glaze showed a value ~ Hv753 indicating that the glaze was strong but the lack of adhesion with the substrate was probably the main reason for its removal.

The glaze on the Stellite 6 counterface contained a higher proportion of Ni than that was observed previously. This indicated the presence of more nickel-containing wear debris produced due to the removal of the protective glazes on the Nimonic 90 sample. The glaze on the counterface also provided protection against wear for the Stellite 6 surface and, therefore little, if any, new Stellite 6 debris was produced. The main type of newly produced wear debris detected was again the Ni/Cr/Co platelets from the Stellite 6/Nimonic 90 surface.

Cross-sectional EDX analysis of the Nimonic 90 could not detect a mixed oxide layer after 1 hour of wearing (see **Fig.5.28c**). Small glazes were present on the Nimonic 90 surface but these provided little protection for the surface which accounted for the high recorded weight loss of -31.7mgcm^{-2}. Glazes on the Stellite 6 counterface, however, were still present containing mainly oxidised Ni/Cr/Co.

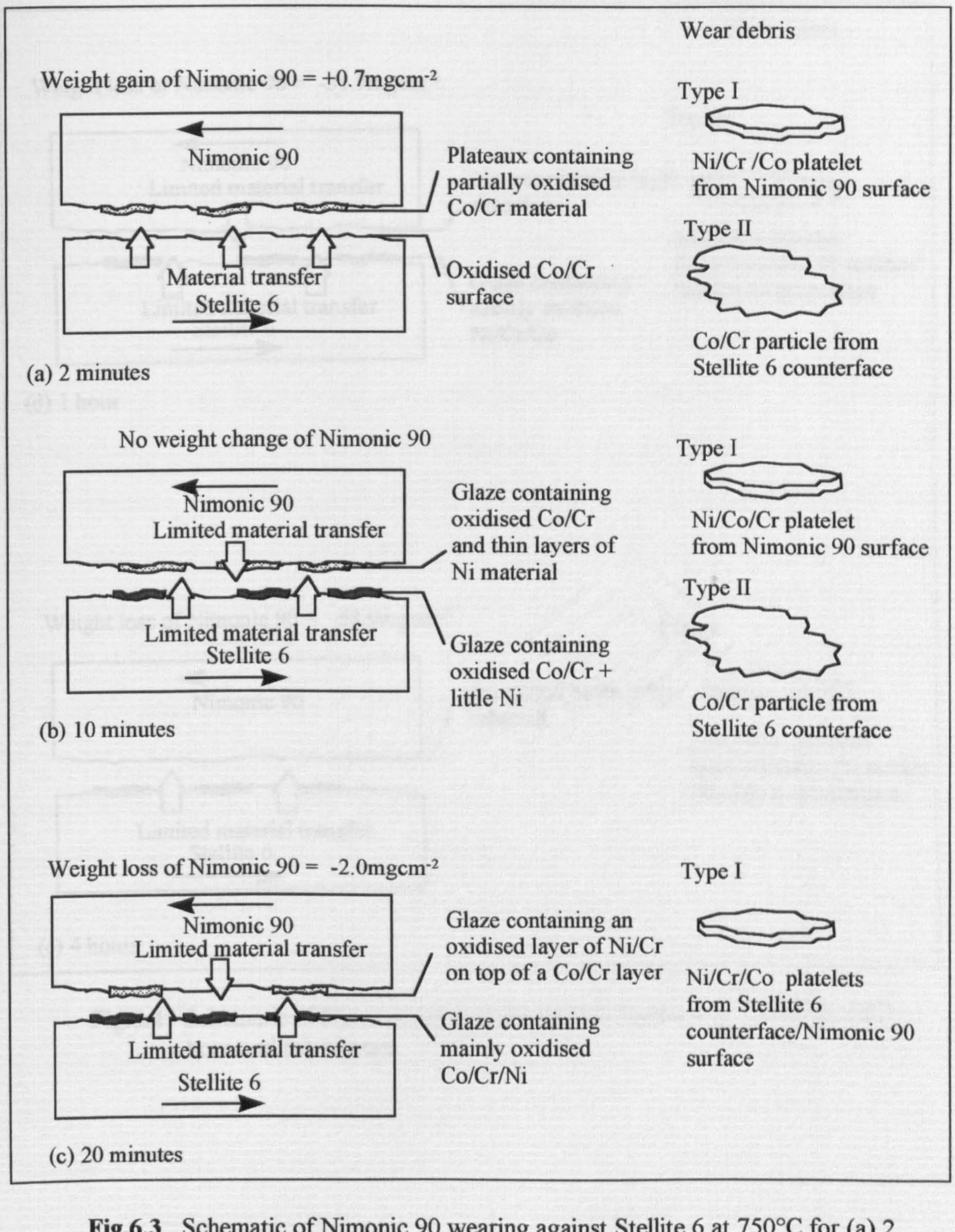

Fig.6.3 Schematic of Nimonic 90 wearing against Stellite 6 at 750°C for (a) 2 minutes, (b) 10 minutes and (c) 20 minutes

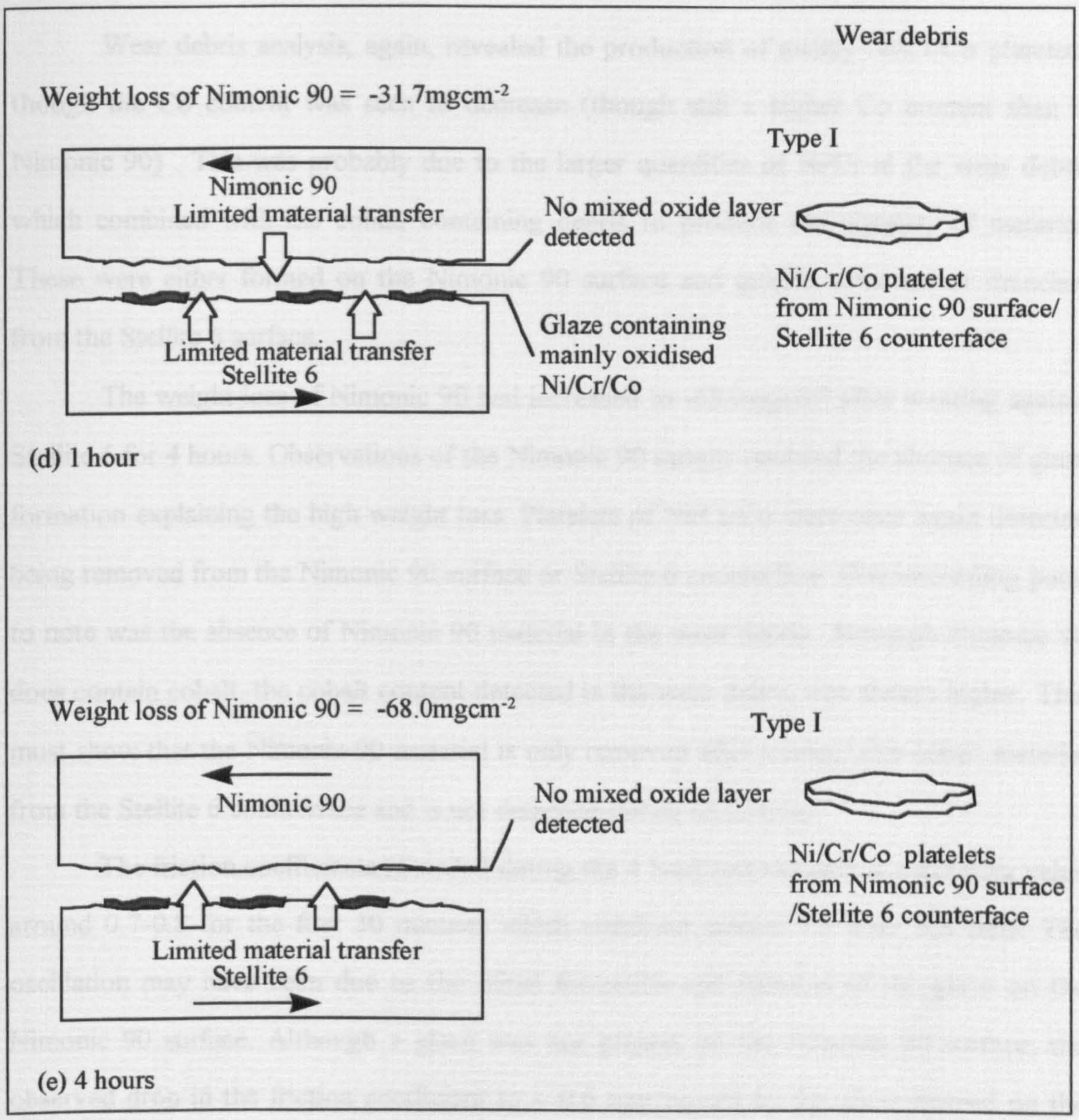

Fig.6.4 Schematic of Nimonic 90 wearing against Stellite 6 at 750°C for (d) 1 hour and (e) 4 hours

Wear debris analysis, again, revealed the production of mainly Ni/Cr/Co platelets, though the Co content was seen to decrease (though still a higher Co content than in Nimonic 90) . This was probably due to the larger quantities of Ni/Cr in the wear debris which combined with the cobalt containing debris to produce the platelets of material. These were either formed on the Nimonic 90 surface and quickly removed or detached from the Stellite 6 surface.

The weight loss of Nimonic 90 had increased to -68.0mgcm^{-2} after wearing against Stellite 6 for 4 hours. Observations of the Nimonic 90 sample revealed the absence of glaze formation explaining the high weight loss. Platelets of Ni/Cr/Co were once again detected being removed from the Nimonic 90 surface or Stellite 6 counterface. One interesting point to note was the absence of Nimonic 90 material in the wear debris. Although Nimonic 90 does contain cobalt, the cobalt content detected in the wear debris was always higher. This must show that the Nimonic 90 material is only removed after mixing with cobalt material from the Stellite 6 counterface and is not detached purely on its own.

The friction coefficients recorded during the 4 hour test showed an oscillating value around 0.7-0.8 for the first 30 minutes which stabilised around 0.6 after this time. The oscillation may have been due to the initial formation and removal of the glaze on the Nimonic 90 surface. Although a glaze was not present on the Nimonic 90 surface, the observed drop in the friction coefficient to ~ 0.6 was caused by the glaze formed on the Stellite 6 surface which was seen to develop after 10 minutes of wearing and remained present throughout the test. Continued fragmentation and compaction of the particles in this glaze probably led to a stronger glaze formed with a lower adherence force to the Nimonic 90 surface. This resulted in a reduction in the friction coefficient.

It is important to note that the glaze formed on the Ma956 wearing against Stellite 6 remained adherent and did not get detached. This contrasts to the behaviour of the glaze formed on Nimonic 90 which was removed.

6.2.3 Ma956 vs Incoloy 800 at 750°C

A schematic diagram of the wearing of Ma956 against Incoloy 800 at 750°C is shown in **Figs.6.5-6.6,** from 2 minutes to 4 hours.

Initially, the Ma956 sample showed a small weight increase of 3.2 $mgcm^{-2}$ after wearing for 2 minutes. The Ma956 surface was smeared with Incoloy 800, confirmed by the presence of Ni-containing material in **Fig.5.32a**, and was observed to suffer a degree of deformation and partial oxidation. The smearing of the Incoloy 800 material occurred because of the alloys low hardness of Hv183. Glazes were not observed on the surface of the Incoloy 800 counterface and the surface composition remained identical to that of the as-received Incoloy 800 indicating little, or no material transfer from the Ma956. Wear debris collected was mostly comprised of platelets with the same composition as Incoloy 800 indicating that they originated from the counterface.

After 10 minutes, the transfer of large mounds of Incoloy 800 material occurred onto the Ma956 surface. This was detected by XRD analysis indicating the presence of new Fe_2O_3 maghemite/$NiCr_2O_4$ phases on Ma956. The observed small weight increase of $+1.2mgcm^{-2}$ for the Ma956 sample indicated some loss of Ma956 material. However as only Ni/Cr/Fe containing debris was being detected, the Ma956 material must have been removed in combination with Incoloy 800 material. Glaze formation and material transfer were not detected on the Incoloy 800 counterface.

Glaze formation was however observed on the Incoloy 800 counterface after wearing against Ma956 for 20 minutes. The glazes were comprised of mainly Fe and Cr oxides having been either transferred from the Ma956 sample or originated entirely from the Incoloy 800 material. This would indicate a similar oxidation-scrape-reoxidation mechanism to that observed during the wearing of Nimonic 90 against Incoloy 800 at 750°C.

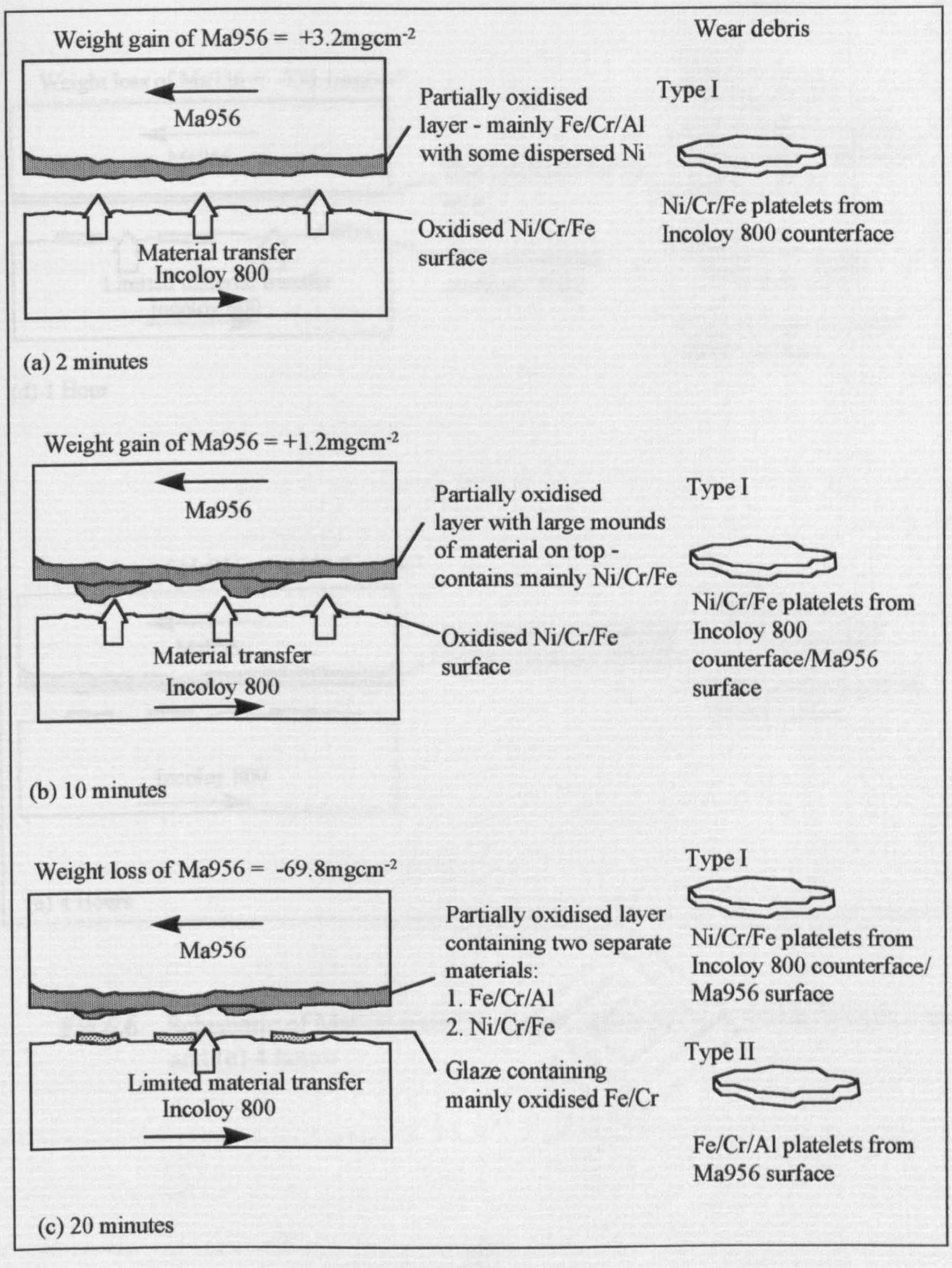

Fig.6.5 Schematic of Ma956 wearing against Incoloy 800 at 750°C for (a) 2 minutes, (b) 10 minutes and (c) 20 minutes

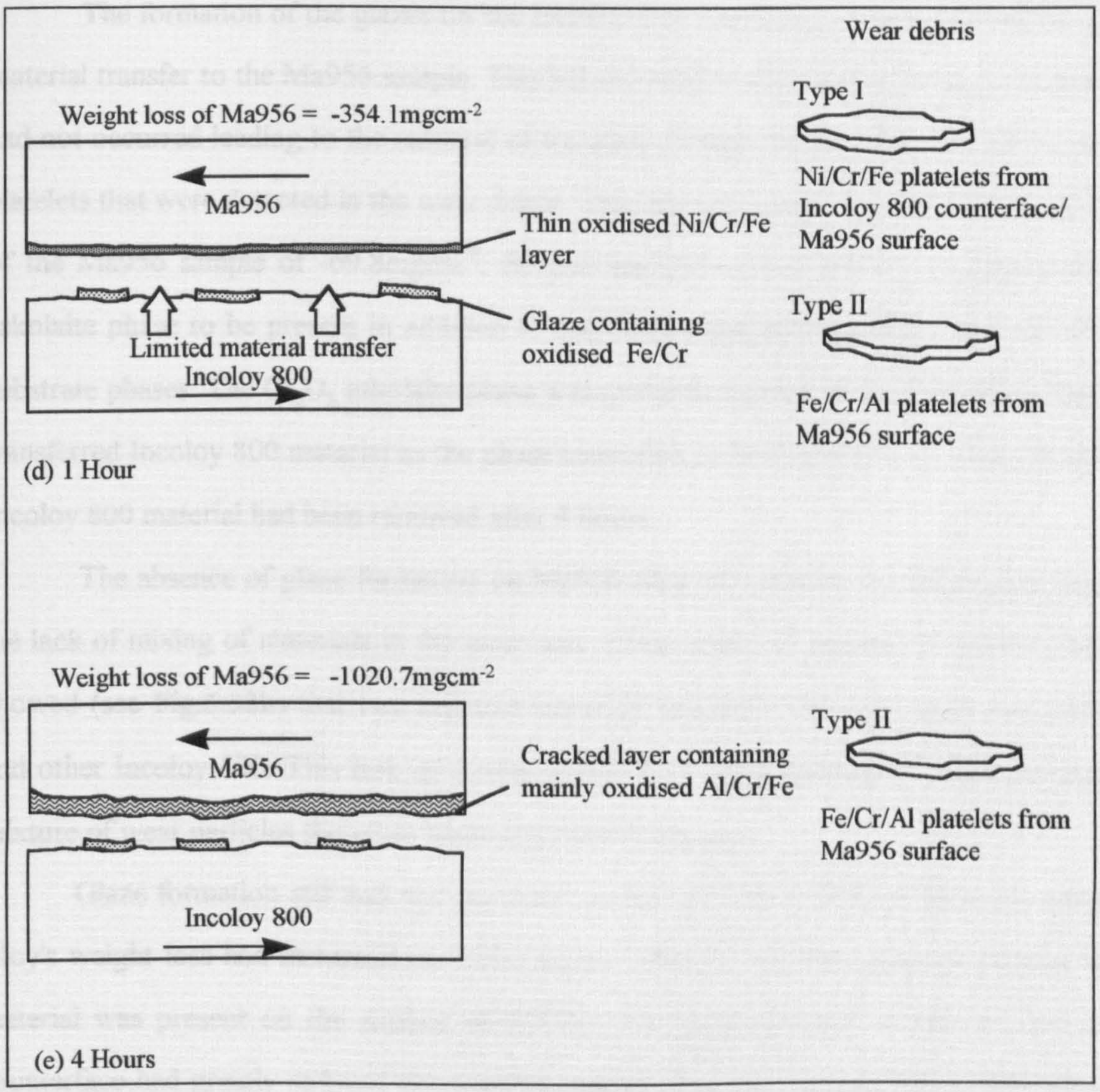

Fig.6.6 Schematic of Ma956 wearing against Incoloy 800 at 750°C for (d) 1 hour and (e) 4 hours

The formation of the glazes on the Incoloy 800 counterface prevented considerable material transfer to the Ma956 sample. This left the Ma956 unprotected as glaze formation had not occurred leading to the removal of the alloy through the formation of Fe, Cr & Al platelets that were detected in the wear debris. This also accounted for the high weight loss of the Ma956 sample of -69.8mgcm^{-2}. Surface analysis of the Ma956 revealed a Cr_2O_3 eskolaite phase to be present in addition to the Fe_2O_3 maghemite/$NiCr_2O_4$ and the Fe-Cr substrate phases. The Cr_2O_3 eskolaite phase was probably formed on Ma956 rather than on transferred Incoloy 800 material as the phase continued to be detected even when all of the Incoloy 800 material had been removed after 4 hours.

The absence of glaze formation on Ma956 after 20 minutes may have been due to the lack of mixing of materials in the wear scar. Cross-sectional analysis of Ma956 clearly showed (see **Fig.5.32b)** that two separate materials existed in the wear scar, one Ma956 and other Incoloy 800. This lack of mixing would deter the formation of a homogeneous mixture of wear particles therefore hindering glaze formation.

Glaze formation still had not occurred on Ma956 after 1 hour of wearing and the alloy's weight loss had increased to -354.1mgcm^{-2}. Only a very thin layer of Incoloy 800 material was present on the surface of Ma956. The glazes formed on the Incoloy 800 counterface had greatly reduced the material transfer from the Incoloy 800 which left the Ma956 even more exposed to damage.

The weight loss of the Ma956 sample was as high as -1020.7mgcm^{-2} after wearing for 4 hours. The glazes on the Incoloy 800 counterface had reduced material transfer to such an extent that only very small particles of Ni material could be observed on the surface of Ma956. The surface of the Ma956 was composed of a mixed oxide layer of Al, Cr and Fe. The oxide was very brittle and micrographs, as shown in **Fig.5.11b**, showed the layer to be cracked in a number of places leading to spallation. Wear debris produced was mainly Fe/Cr/Al platelets from the Ma956 surface.

The friction coefficient during the test, as shown in **Fig.5.4**, showed a steady fall from around 1 to a value around 0.4-0.5 after 90 minutes. The high values, initially recorded, occurred when adhesion was high during the transfer of Incoloy 800 to the Ma956 sample. However, as the wear time increased, glaze formation occurred on the Incoloy 800 counterface thereby reducing material transfer. At some point after 1 hour nearly all of the Incoloy 800 material initially transferred was removed from the surface of the Ma956 and this probably coincided with the stabilisation of the friction coefficient between 0.4-0.5 after 90 minutes.

The main difference between the wearing of Ma956 and Nimonic 90 against Incoloy 800 was that the surface of Ma956 underwent deformation, the Nimonic 90 surface remained undeformed. This is suprising as the hardness of Nimonic 90 (Hv242) is less than the hardness of Ma956 (Hv303). However, when other material properties are investigated, such as tensile strength and yield strength at 750°C (see **Fig.6.7**), one can see Nimonic 90 has greater strength properties than Ma956 at 750°C.

6.2.4 Ma956 vs Stellite 6 Counterface at 750°C

Ma956 showed much lower weight losses after wearing against Stellite 6 than compared to Incoloy 800 at 750°C. A schematic of the wearing process up to 4 hours is shown in **Figs.6.8-6.9**.

The Ma956 sample showed a weight gain of $+0.7 mgcm^{-2}$ after wearing against Stellite 6 for 2 minutes caused by oxidised Stellite 6 material transfer onto the surface of the Ma956. The Stellite 6 material collected on the surface of the Ma956 and developed as small wear resistant plateaux which provided wear protection for the rest of the Ma956 surface. The high hardness (Hv464) of the Stellite 6 prevented the smearing of the Ma956 surface with the Stellite 6 material.

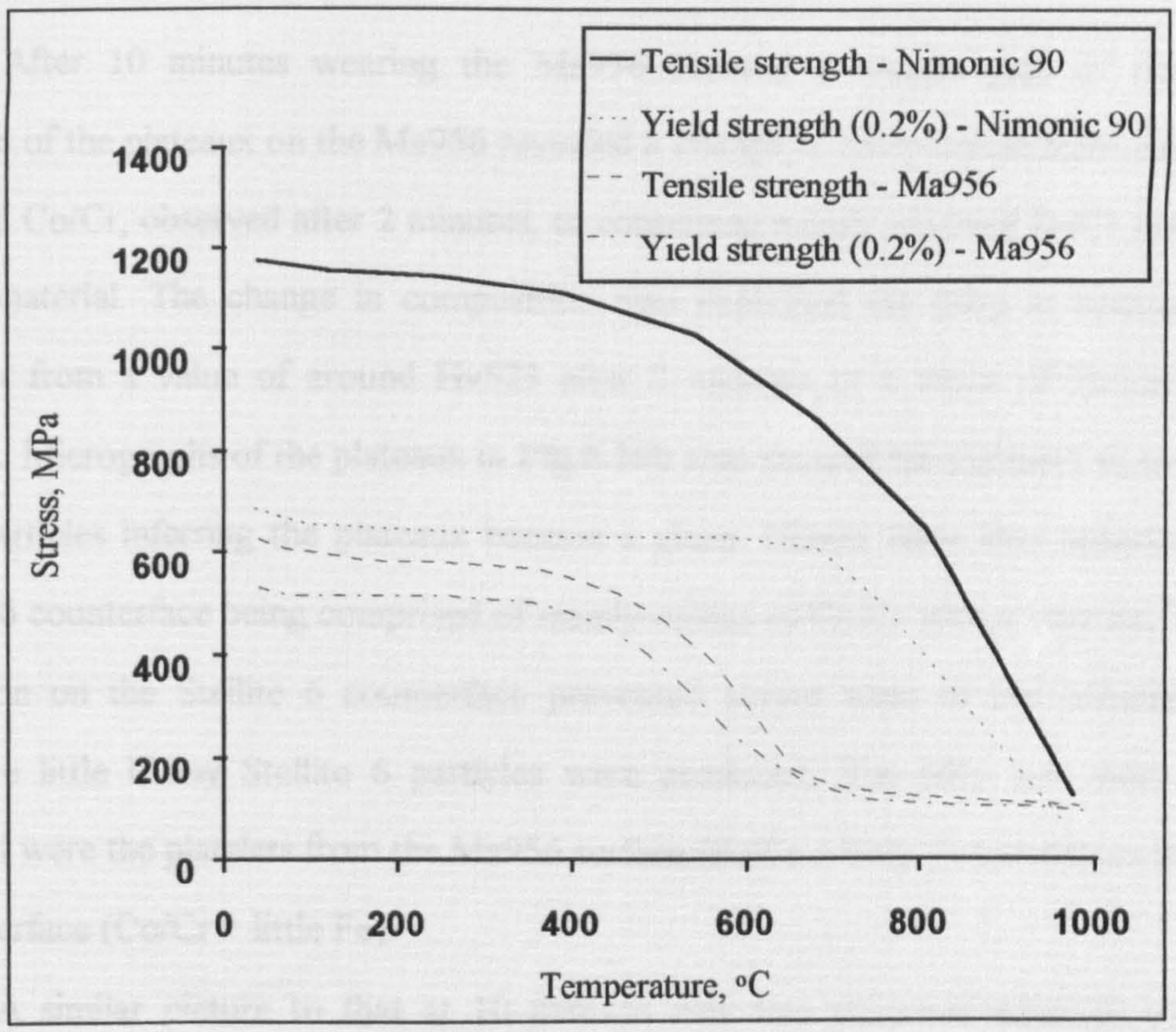

Fig.6.7 Variation of the tensile strength and yield strength with temperature for Nimonic 90 and Ma956 [107]

The micrographs, as shown in **Fig.5.26a**., reveals the Stellite 6 plateaux to be made up of layered material. The hardness of the Stellite 6 plateaux was Hv523, an increase of Hv59 compared to the as-received Stellite 6. The increase was probably due to work hardening of the Stellite 6 rather than glaze formation.

The higher amount of Fe detected on the Stellite 6 counterface after 2 minutes of wearing indicated material transfer from Ma956. Wear debris collected revealed three main types of particles. Two of the types were platelets, one containing mainly Fe/Cr with a little Co from the Ma956 surface and the other consisted of Co/Cr with a little Fe from the Stellite 6 counterface. The third type detected had a powder-like appearance and contained Co/Cr, originating from the Stellite 6 counterface. These were formed from Stellite 6 wear debris particles that had agglomerated together during the wear process but had not been flattened between the two wearing surface.

After 10 minutes wearing the Ma956 showed a weight gain of $+0.8mgcm^{-2}$. Analysis of the plateaux on the Ma956 revealed a change in composition from consisting of oxidised Co/Cr, observed after 2 minutes, to containing mainly oxidised Fe/Cr material and cobalt material. The change in composition also explained the drop in hardness of the plateaux from a value of around Hv523 after 2 minutes to a value of Hv368 after 10 minutes. Micrographs of the plateaux in **Fig.5.26b** also showed the plateaux to comprise of small particles inferring the plateaux became a glaze. Glazes were also observed on the Stellite 6 counterface being comprised of mainly oxides of Co/Cr with a little Fe. The glaze formation on the Stellite 6 counterface prevented severe wear of the counterface and therefore little if any Stellite 6 particles were produced. The only new wear particles detected were the platelets from the Ma956 surface (Fe/Cr + little Co) and from the Stellite 6 counterface (Co/Cr + little Fe).

A similar picture to that at 10 minutes was also observed after 20 minutes of wearing. Glazes were present on both the Stellite 6 counterface and the Ma956 sample. The glazes on the Ma956 were comprised of mainly oxides of Fe/Cr with a little cobalt seemingly well dispersed in the matrix. The cobalt on the Ma956 was probably present as the phase $CoCr_2O_4$ which was detected by XRD from 10 minutes to 4 hours. Micrographs of the glazes on Ma956, shown in **Fig.5.26c**., revealed that they were comprised of finer wear debris than those observed after 10 minutes of wear. The finer particles and the more even distribution of cobalt indicated that the glazes must have been constantly forming and being removed allowing the movement of particles and the breakdown of coarse wear debris into finer wear debris. The finer particles also allowed a more compact glaze to develop and this was shown in a higher hardness of the glaze of Hv502 compared to Hv368 after 10 minutes.

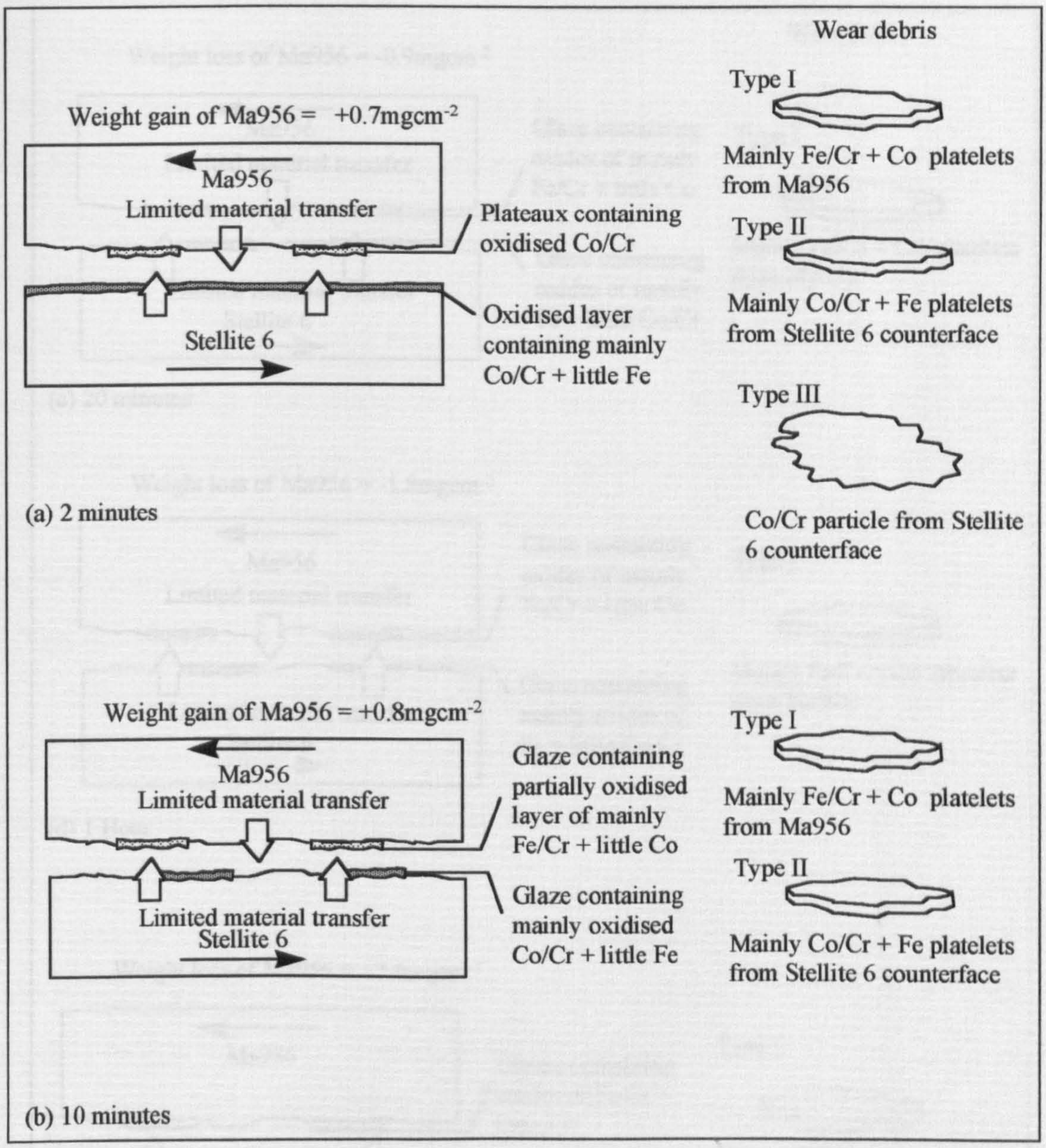

Fig.6.8 Schematic of Ma956 wearing against Stellite 6 at 750°C for (a) 2 minutes, and (b) 10 minutes

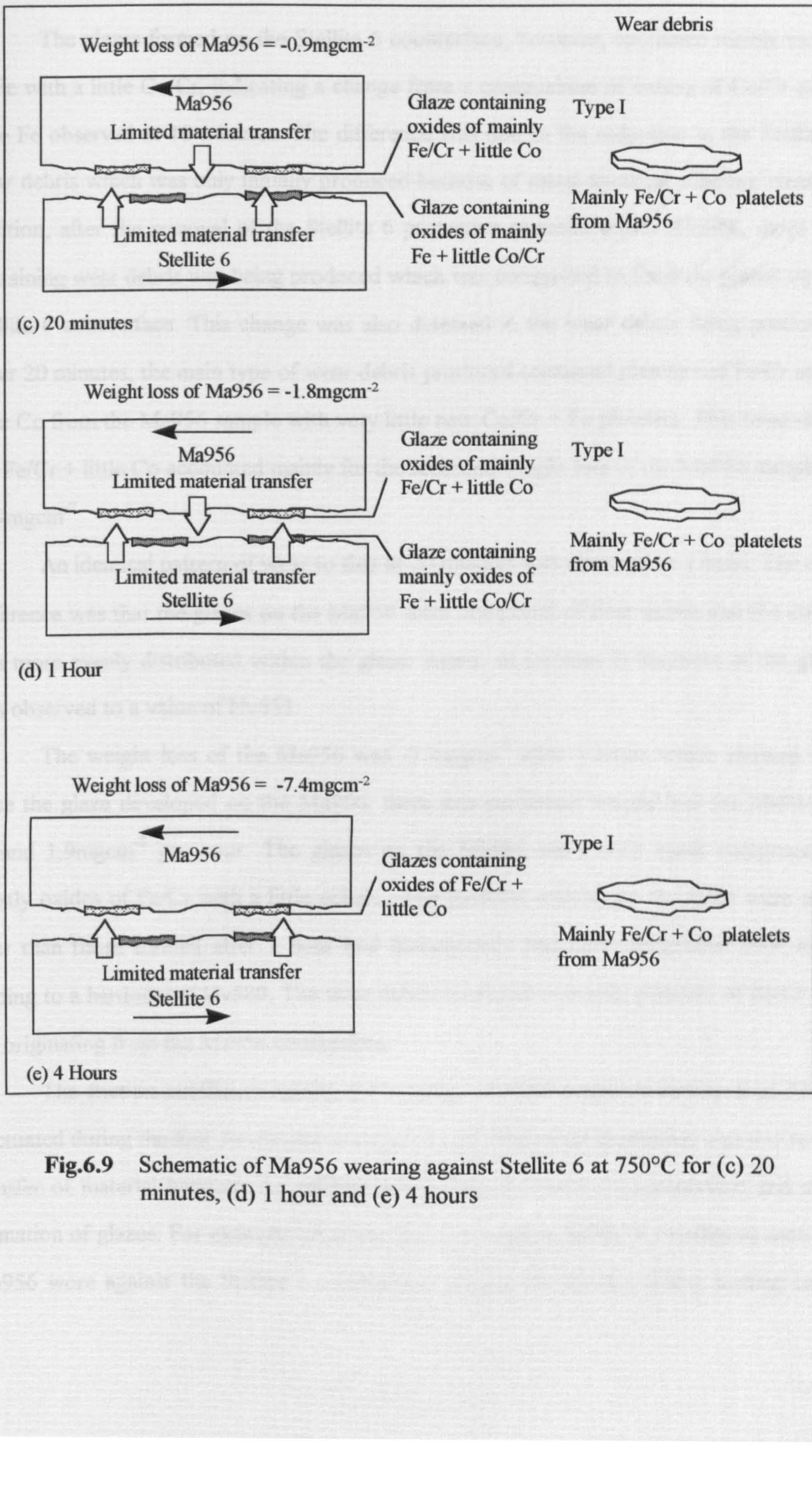

Fig.6.9 Schematic of Ma956 wearing against Stellite 6 at 750°C for (c) 20 minutes, (d) 1 hour and (e) 4 hours

The glazes formed on the Stellite 6 counterface, however, contained mainly oxides of Fe with a little Co/Cr, indicating a change from a composition of oxides of Co/Cr and a little Fe observed at 10 minutes. The difference was due to the reduction in the Stellite 6 wear debris which was only initially produced because of metal-to-metal adhesive wear. In addition, after the removal of the Stellite 6 protective plateaux on the Ma956, more Fe-containing wear debris was being produced which was compacted to form the glazes on the Stellite 6 counterface. This change was also detected in the wear debris being produced. After 20 minutes, the main type of wear debris produced contained platelets of Fe/Cr and a little Co from the Ma956 sample with very little new Co/Cr + Fe platelets. This removal of the Fe/Cr + little Co accounted mainly for the recorded weight loss of the Ma956 sample of $-0.9 mgcm^{-2}$

An identical pattern of wear to that at 20 minutes was observed at 1 hour. The only difference was that the glazes on the Ma956 were composed of finer debris and the cobalt was more evenly distributed within the glaze. Again, an increase in hardness of the glaze was observed to a value of Hv533.

The weight loss of the Ma956 was $-7.4 mgcm^{-2}$ after 4 hours which showed that once the glaze developed on the Ma956, there was consistent weight loss for Ma956 of around $1.9 mgcm^{-2}$ per hour. The glazes on the Ma956 were once again composed of mostly oxides of Fe/Cr with a little cobalt . The particles making up the glaze were even finer than those formed after 1 hour and consequently had been compacted even more leading to a hardness of Hv580. The wear debris consisted of mainly platelets of Fe/Cr and Co originating from the Ma956 counterface.

The friction coefficient during the wearing of Ma956 against Stellite 6 at $750^{o}C$ fluctuated during the first 30 minutes around 0.7 -0.8. The initial fluctuation was due to the transfer of material between the Ma956 sample and the Stellite 6 counterface and slow formation of glazes. For example, after the first two minutes Stellite 6 transferred onto the Ma956 wore against the Stellite 6 counterface causing like-on-like sliding leading to an

increase in the friction coefficient from to 0.7 to 0.8. However, once the wear debris was fine enough to form a well compacted glaze, the friction coefficient stabilised at a value around 0.6.

The main difference between Ma956 and Nimonic 90 during the wear against Stellite 6 seemed to be the mixing of the materials in the wear scar. During the wear of Ma956 against Stellite 6 the material seem to mixing well as shown in **Figs.5.33b-5.33c** by the distribution of cobalt material in the glaze on Nimonic 90. However, cross-sectional analysis of Nimonic 90 after wearing against Stellite 6 for the same length of time, revealed the two materials to be completely separate. This would have hindered the production of mixed wear particles thereby impeding glaze formation.

A complete description of the mechanism (s) responsible for the formation of glazes during high temperature wear is still not available. However, a tentative picture has emerged. Glaze formation during wear between two surfaces requires:

(i) the generation of wear debris - oxidised or non-oxidised which is subsequently oxidised

(ii) retention and mixing of the particles or with transferred material

(iii) the repeated deformation, fracture and oxidation producing increasingly finer particles encouraging further mixing

(iv) the presence of a strong surface or a layer to support the glaze

(v) sufficient glaze/substrate adhesion to prevent detachment of the glaze

(vi) sufficient cohesive strength of the glaze to prevent glaze breakdown

The effect of temperature is to influence the oxidation process, the deformation characteristics of the debris and the strength of the substrate layer beneath the glaze to support its formation. With these points in mind it is now possible to present a coherent summary explaining some of the observations discussed previously.

For Nimonic 90/Incoloy 800 counterface, the critical time for both systems to develop glazes was 20 minutes. The particles in the glaze on Nimonic 90, consisting of a layer of oxide of Fe on top of an oxidised Fe/Cr/Ni layer, became increasingly finer with increasing sliding time. The glaze on Incoloy 800 consisted of oxidised Fe/Cr particles. On Nimonic 90, glazes with high cohesive and adhesive strength developed following the classical pattern involving: transfer of Incoloy 800 , deformation, fragmentation and compaction of wear debris.

After 10 minutes, glaze formation occurred on both surfaces of the Nimonic 90/Stellite 6 counterface system. However, the strong glaze (Hv753) developed on Nimonic 90 lacked sufficient cohesion due to the lack of mixing as shown by the presence of two separate layers. This caused poor glaze/substrate adhesion leading to the detachment of the glaze.

The absence of glaze formation on Ma956 worn against Incoloy 800 at 750°C even after 4 hours can be ascribed to the observed lack of mixing (**Fig.5.28b**) on the surface between particles of Ma956 and the transferred Incoloy 800 material. Another contributing factor was the deterioration of the mechanical properties of Ma956 with temperature as indicated by its deformation. A critical time of 20 minutes was required for a Fe/Cr glaze to develop on the Incoloy 800

In the Ma956/Stellite 6 system where both surfaces developed glazes, the glaze formation again followed a classical pattern. The glaze on Ma956 consisted of oxidised Fe/Cr with Co and on Incoloy 800 it was composed of oxidised Fe and Co/Cr. The progressive wearing was accompanied by continued fragmentation and compaction of the particles in the glazes. Finally, strong glazes with very good cohesive strength and glaze/substrate adhesion emerged.

6.3 Effect of Temperature on the Wear Resistance of Ma956 Wearing Against Stellite 6

The temperature, as shown in **Fig.5.37**, did not have a major influence on the weight loss of Ma956 when worn against Stellite 6 between room temperature and 750°C. The weight loss of Ma956 generally decreased from room temperature to 750°C with only the result at 550°C not following this trend. Previous investigators [47] observed that increasing the temperature reduced the weight loss of the sample due to the formation a more wear-resistant glaze at the higher temperature. These tests were always conducted with like-on-like wearing with the resulting surface layer or glaze containing a similar chemical composition throughout the range of temperatures. However, in this investigation a change in the surface layer composition of Ma956 was observed. At room temperature and 350°C the surface film/plateaux contained mainly cobalt and chromium, transferred from the Stellite 6 counterface. This occurred because the temperature was not sufficient for glaze formation to occur on the Stellite 6 counterface to prevent considerable material transfer onto the Ma956. Glaze formation had also not occurred on the surface of Ma956 as indicated by the absence of a shiny surface and friction coefficient results which did not show a drop. The weight loss of Ma956 was still low, however, because the temperature was not sufficiently high to have a major detrimental effect on the strength properties of Ma956.

At 550°C and 750°C, the surface plateaux on the Ma956 was comprised of mostly Fe/Cr/Al oxides from the Ma956 but some material from the Stellite 6 counterface. The change in the composition was due to glaze formation on the Stellite 6 which limited Stellite 6 transfer to the surface. This decreased the amount of cobalt-containing wear debris available for plateaux formation. At both 550°C and 750°C , the surface of the plateaux was shiny and a friction coefficient drop was observed indicating the presence of a glaze. The glaze on Ma956 after wearing at 550°C was cracked in places and spallation of this glaze accounted for the higher weight loss recorded compared to other temperatures.

In addition, hardness values of the glazes revealed a higher hardness of Hv580 at 750°C compared to Hv486 at 550°C indicating greater compaction of the oxide debris particles. At 550°C, the temperature was obviously having a detrimental effect on the material properties of Ma956 but was too low for a very adherent and high strength glaze to be formed.

6.4 Effect of Preoxidation on the Wear Resistance of the ODS Alloys Against Incoloy 800 at 750°C

Preoxidation, overall, improved the wear resistance of the ODS alloys as shown by the weight losses in **Fig.5.40**. All of the preoxidised samples showed similar wear characteristics to those of the unoxidised samples - similar friction coefficient drops decreasing from 1.1-1.0 to 0.4-0.55, alloy surfaces covered in cracked smooth layers composed of mixed oxides of Fe,Cr and Al, and generation of wear debris consisting of two types of particles: one containing Fe/Cr/Ni and the other containing Fe/Cr/Al.

The improvement in the weight losses of preoxidised ODS samples is suggested to have stemmed from the preoxidised film, found to be Al_2O_3, which initially protected the Ma956 or slowed down the wear process. After the film was removed a similar wear mechanism to the unoxidised ODS alloys must have ensued as indicated by the similar microscopical and friction coefficient characteristics.

The thickness of this film was particularly relevant to the wear resistance, the thicker the film the greater the improvement in the wear resistance. For example, after 1 hour preoxidation of Ma956 the thickness of the alumina film was 0.5μm and the sample showed a weight loss of -788.1mgcm^{-2}. A large drop in the weight loss of Ma956 to -475.3mgcm^{-2} was recorded when the thickness of the film had increased to 1μm after 10 hours preoxidation. However, no increase in the oxide film thickness on Ma956 could be detected after 100 hours preoxidation and the weight loss had only slightly decreased to

-440.5mgcm^{-2}. The improvement in the wear resistance through preoxidation confirms other investigators [13-14] results about the benefits of preoxidation. However, in those studies the preoxidised film was seen to provide oxide debris for glaze formation. In this particular experiment, the preoxidised film was thin (0.5-1μm thick) and adherent to the substrate but did not lead to glaze formation. The improved wear resistance therefore stemmed not from production of oxidised wear debris but from providing a wear-protective film for the Ma956.

CHAPTER 7

CONCLUSIONS AND SUGGESTIONS FOR FUTURE WORK

7. CONCLUSIONS AND SUGGESTIONS FOR FUTURE WORK

This Chapter is divided into five main sections. The first Section comprises the conclusions from the wear studies conducted on alloys wearing against different counterfaces for 4 hours and Section 2 contains conclusions from wear tests using Ma956 and Nimonic 90 for 2 minutes to 4 hours. Section 3 and Section 4 report conclusions on the effect of temperature on wear resistance and the influence of preoxidation on wear resistance, respectively. Finally, suggestions for future work are considered in Section 5.

7.1 Wear Studies Using Different Counterfaces at Room Temperature and 750°C for 4 Hours

7.1.1 Ma956, PM2000 and PM2000SD

1. The ODS alloys all showed a similar pattern of wearing when worn against different counterfaces at different temperatures.
2. Lower weight losses were generally observed when the ODS alloys were worn at room temperature even though glaze formation was not observed.
3. The mechanism of room temperature wear seemed to be greatly affected by the hardness of the counterface.
4. Large amounts of the Incoloy 800 counterface (Hv183) was transferred during the wear with the ODS alloy. The material formed plateaux which work-hardened into wear-resistant surfaces on the ODS alloys.
5. Only limited material transfer was observed with the much harder Stellite 6 (Hv464) and Si_3N_4 (Hv1301) counterfaces at room temperature. A thin mixed oxide layer formed on the surface of the ODS alloys containing material from both wearing surfaces.
6. A range of different weight losses were recorded when the ODS alloys were worn against the counterfaces at 750°C.

7. Low weight losses and glaze formation were observed on the ODS alloys after wearing against the Stellite 6 counterface. The glaze was composed of mainly oxidised ODS material and a little oxidised Stellite 6 material.

8. A low weight loss and friction coefficient was observed when Ma956 was worn against Si_3N_4 at 750°C. A very thin layer containing mixed oxides from both wearing surfaces was observed on the Ma956. A glaze had formed at the very surface of this film.

9. Very high weight losses were observed when the ODS alloys were worn against Incoloy 800 at 750°C. Glaze formation was not observed on the ODS alloys.

10. Generally, the wear resistance of the alloys decreased with a decrease in hardness, i.e. wear resistance: PM2000SD (Hv363) > PM2000 (Hv311) > MA956 (Hv303).

7.1.2 Nimonic 80A (cast + HIPped) and Nimonic 90

11. Overall the Nimonic alloys showed a similar correlation to one another when tested against different counterfaces at different temperatures.

12. Room temperature testing again seemed to be greatly influenced by the degree of material transfer to the Nimonic surface. The degree of material transfer was itself influenced by the hardness of the counterface, the softer the counterface the higher the amount of transfer.

13. The material from the soft Incoloy 800 counterface was transferred at room temperature onto the surface of the Nimonics. The material formed wear resistant plateaux which protected the surface of the Nimonics leading to very small weight changes.

14. Only limited material transfer was observed with the hard Stellite 6 and Si_3N_4 counterfaces to the Nimonic surface. Thin mixed oxide layers were formed on the Nimonic, containing material from both wearing surfaces which provided only limited protection.

15. The Nimonic alloys showed a large range of weight losses when tested against the different counterfaces at 750°C.

16. Very low weight changes and glaze formation were observed when the Nimonic alloys were worn against Incoloy 800 at 750°C. The glaze formed was composed of material mostly from the Incoloy 800 counterface.

17. High wear rates were observed when the Nimonic alloys were worn against Stellite 6 at 750°C. Glaze formation occurred but the glazes were weak with poor adherence to the substrate leading to their continuous removal.

18. A very different wear resistance was seen when Nimonic 80A (cast) and Nimonic 90 were worn against Si_3N_4 at 750°C.

19. Nimonic 80A (cast) showed very poor wear resistance with glazes not being formed while glaze formation occurred on the Nimonic 90 sample leading to a very low weight loss. The difference stemmed from cobalt in the Nimonic 90 which through a mechanism as yet unclear, improved the adhesion and/or strength of the glaze on the Nimonic 90.

20. Nimonic 80A (cast) and Nimonic 80A (HIPped) showed similar wear properties and it was not possible to conclude that the processing route had an effect on the wear resistance.

7.1.3 TiAl

21. TiAl showed very good wear resistance against nearly all of the counterfaces at room temperature and 750°C.

22. The TiAl ordered structure provided a deformation and wear-resistant substrate for the formation of glazes/mixed oxides from the counterface material.

23. Very little if any of the TiAl material was detected in the surface film/glaze on the TiAl especially at 750°C.

24. Very high weight losses were observed when TiAl was worn against Si_3N_4 at room temperature.

25. This may have been due to the small covalent radii of Si and N which allowed them to enter the TiAl ordered lattice and disrupt the structure.

26. This made the TiAl structure susceptible to deformation and wear leading to high weight losses.

7.1.4 Comparisons

The counterface was seen to have a major effect on the wear resistance of all of the alloys especially at 750°C as shown in ***Table 7.1***. The effect was different depending upon the type of alloy. Alloys within their own group i.e. Nimonics or ODS alloys generally showed similar wear patterns. A relationship between hardness and wear resistance between the different groups was not found. The difference in wear resistance was thought to be due to the high temperature strength properties of the alloy and the strengthening mechanisms present. The chemical composition of the wear debris may also have had an effect with elements such as cobalt encouraging glaze formation in some cases.

In relation to the alloys use as valve and seat insert materials, the following combinations look the most promising:

TiAl (valve) vs Stellite 6 (seat insert)

Ma956 (valve) vs Stellite 6 (seat insert)

PM2000 (valve) vs Stellite 6 (seat insert)

PM2000SD (valve) vs Stellite 6 (seat insert)

It should be noted that combinations using the Incoloy 800 and Si_3N_4 counterfaces are not included. This is because either the wear rate was too high (Incoloy 800) or the fracture toughness of the counterface was too low (Si_3N_4).

7.2 Wear Studies on Nimonic 90 and Ma956 Worn Against Incoloy 800 and Stellite 6 at 750°C for 2 minutes-4 hours

7.2.1 Nimonic 90 vs Incoloy 800

27. Nimonic 90 showed a small weight increase and the surface was covered with glazes after wearing against Incoloy 800 at 750°C.

28. Material from the relatively soft Incoloy 800 counterface was transferred onto the Nimonic 90 surface but did not deform or wear the Nimonic 90 surface to any great extent.

29. A glaze was formed on the Nimonic 90 after 20 minutes from the transferred Incoloy 800 material. The Nimonic 90 provided a wear resistant surface for glaze formation to occur.

30. Glaze formation also occurred on the Incoloy 800 counterface after 20 minutes from mostly Incoloy 800 material.

7.2.2 Nimonic 90 vs Stellite 6

31. High wear losses were observed when Nimonic 90 was worn against Stellite 6 at 750°C.

32. Initially a small weight increase of the Nimonic 90 was recorded due to Stellite 6 transferred onto the surface of Nimonic 90 as small wear resistant plateaux.

33. Glaze formation on Nimonic 90 was observed after 10 minutes with the glazes being comprised of mainly Nimonic 90 material.

34. This change was associated with glaze formation on the Stellite 6 counterface which greatly reduced material transfer to the Nimonic 90 sample.

35. The glaze formed on the Nimonic 90 sample was not very adherent and a continuous removal and formation process was occurring. The destruction of the glaze happened at an increased rate due to the sample geometry which discouraged wear debris retention.

7.2.3 Ma956 vs Incoloy 800

36. Large weight losses of the Ma956 were observed due to the absence of glaze formation.

37. Incoloy 800 was initially transferred to the surface of MA956 deforming the Ma956 in the process.

38. Glaze formation occurred on the Incoloy 800 after 20 minutes thereby preventing further considerable material transfer to the surface of the Ma956. This led to the Ma956 being left unprotected leading to high wear rates.

39. Ma956 material was initially removed in combination with the Incoloy 800 material and latter without the counterface material.

7.2.4 Ma956 vs Stellite 6

40. Glaze formation on the Ma956 occurred leading to very small weight losses of the Ma956.

41. Initially only small amounts of Stellite 6 were transferred onto the Ma956 as wear-resistant plateaux due to the counterfaces high hardness (Hv464).

42. After 10 minutes the Stellite 6 plateaux on the Ma956 had been removed and a glaze had formed from this material and Ma956 material.

43. Glaze formation was observed on the Stellite 6 counterface after 10 minutes. The glazes were comprised of mainly Stellite 6 material but some material transferred from Ma956.

44. The glazes on the Ma956 and Stellite 6 continued to be present throughout the test with only their composition slightly changing.

45. The distribution and size of oxide particles in the glaze became more uniform and smaller with time indicating a continuous formation and removal process of the glazes.

7.2.5 Comparisons

The surface of Ma956 was seen to deform when worn against Incoloy 800 at 750°C but not the Nimonic 90 investigated under the same conditions. This was be due to the Nimonics high strength and creep resistance at 750°C compared to Ma956 as shown in **Fig.6.7**. In addition, glaze formation was observed on Nimonic 90 but was not detected on Ma956 after wearing against Incoloy 800 at 750°C. Glazes were not formed on Ma956 due to the lack of mixing between the transferred Incoloy 800 particles and the Ma956 wear debris. This hindered the production of homogeneous wear debris needed for glaze formation.

Nimonic 90 and Ma956 both deformed when worn against Stellite 6 because of the higher hardness and more abrasive nature of the counterface. An adherent glaze formed on the Ma956 but a weak glaze which spalled was observed on the Nimonic 90 alloy. This was because the Nimonic 90 and Stellite 6 were not mechanically mixing on the Nimonic 90 surface. As before, a non-homogenous mixture of wear debris particles was formed which hindered and weakened glaze formation on the Nimonic 90 alloy.

7.3 Effect of Temperature on the Wear Resistance of Ma956

46. The temperature did not have a major effect on the wear resistance of Ma956 when worn against Stellite 6, although glaze formation was only observed at 550°C and 750°C.

47. Generally, a small decrease in the weight loss was observed as temperature increased apart from the result at 550°C.

48. At room temperature and 350°C the surface layer of the Ma956 was composed of mainly Stellite 6 material.

49. At 550°C and 750°C glaze formation on the Stellite 6 counterface occurred preventing considerable Stellite 6 material transfer to the surface of the Ma956 sample. The glazes therefore formed on the Ma956 sample were composed of mainly oxidised Ma956 material with a small amount of oxidised Stellite 6 material.

50. The weight loss was highest at 550°C for two reasons: (a) the temperature was insufficient to form a large quantity of small oxide needed for glaze formation and (b) the temperature was high enough to have a major detrimental effect on the mechanical properties of the Ma956.

7.4 Effect of Preoxidation on the Wear Resistance of the ODS Alloys

51. Preoxidation was seen to improve the wear resistance of the ODS alloys when tested against Incoloy 800 at 750°C.

52. An increase in the preoxidation time of Ma956 improved the wear resistance. This was linked to the increased thickness of the oxide film formed on the Ma956 sample.

53. The improvement in wear resistance was due to the wear protective properties of the film and not the production of oxidised wear debris. The preoxidised film hindered the wear of the Ma956 until the film was completely removed and then the Ma956 followed a similar wear mechanism to the unoxidised sample.

Table 7.1 Comparison of wear performances of the alloys against the different counterfaces

Alloy	Temperature	Counterface		
		Incoloy 800	Stellite 6	Si_3N_4
Ma956	RT	good	fair	poor
	750°C	very poor	good	very good
PM2000	RT	good	poor	good
	750°C	very poor	very good	-
PM2000SD	RT	very good	poor	good
	750°C	very poor	very good	-
Nimonic 80A (cast)	RT	very good	fair	poor
	750°C	very good	very poor	very poor
Nimonic 80A (HIPped)	RT	good	poor	-
	750°C	very good	very poor	-
Nimonic 90	RT	very good	fair	very poor
	750°C	very good	very poor	very good
TiAl	RT	very good	very good	very poor
	750°C	very good	very good	very good

7.5 Future Work

Wear resistance of an alloy, especially high temperature wear resistance is becoming a more valuable property as demands for wear-resistant materials which can withstand harsher environments are increasing. Yet, still there is very little understanding of the mechanisms of wear. From this work is can be seen that the effect of the counterface on the wear resistance of an alloy may have been underestimated particularly at high temperature. A few suggestions are listed below with a view to extending this research and understanding some of the mechanisms in more detail:

(i) Confirm whether there is still formation or absence of glazes at a range of loads (7-30N) when testing at 750°C.

(ii) Investigate if one particular metal is causing or discouraging glaze formation on the alloys by using single metal counterfaces at 750°C i.e. Ma956 vs cobalt, Nimonic 90 vs cobalt etc.

(iii) Use TEM to examine the worn alloys for diffusion of counterface material with a view to investigating their effect on the structure of the alloy, i.e. TiAl vs Si_3N_4 at room temperature.

(iv) Study the factors controlling adherence of the glaze to the substrate through cross-sectional nanoindentation and XPS.

(v) Ascertain the role of preoxidised films on providing protective oxide films during the initial stages of wear of the ODS alloys.

(vi) Investigate the effect of the processing route on the wear resistance by testing Nimonic 80A (cast + HIPped) for longer periods at higher loads.

(vii) Use other alloys within a certain group i.e. other titanium aluminides to confirm if trends in the wear resistance can be related to the material group.

(viii) Reverse the sample geometry i.e. use Nimonic 90/Ma956 wheels and Incoloy 800/Stellite 6 block alloys to investigate the effect of changes in wear debris retention on glaze formation.

(ix) In addition to this fundamental research, valve and seat inserts can be manufactured and tested in the new engine built at British Gas, Loughborough. The material pairs are as follows:

TiAl (valve) vs Stellite 6 (seat insert)

Ma956 (valve) vs Stellite 6 (seat insert)

PM2000 (valve) vs Stellite 6 (seat insert)

PM2000SD (valve) vs Stellite 6 (seat insert)

REFERENCES

REFERENCES

[1] Giles W.S.

SAE Trans., 1967, Pub. No. 660471, p36.

[2] Kingston-Jones M.G., Thomas J.R. and Radcliff A.S

Diesel Engine Combustion Chamber Materials for Heavy Fuel Operation

Pub. by DTI, 1990.

[3] Naraismhan S.L., Larson J.M. and Whelan E.P.

Wear Characterisation of New Nickel Base Alloys for Internal Combustion Engine Valve Seat Applications

Pub. by Eaton Corporation, Michigan, 1980.

[4] Dowling W.E., Allison J.E., Swank L.R. and Sherman A.M.

SAE Special Publications: New Engine Design and Engine Component Technology, 1993, 972, p31.

[5] Kocis J.F.and Matlock W.M.

Met. Prog., 1975, 3, p58.

[6] Hannan E.S.

New Valve Materials for Diesel Engines

Int. conf., High Temp. Materials for Power Eng., Liege, Belgium, 24-27 Sept. 1990.

[7] Jones D.R.

SAE, 1980, 88 (7), p48.

[8] TRW Handbook, 1st Edition, 1993.

[9] Antony K.C.

J. of Metals, Feb 1983, p52.

[10] Cherrie J.M. and Vitcha E.T.

Met. Prog., Sept. 1971, p54.

[11] Nehrenberg A.E., Vitcha E.T. and Matlock W.M

Met. Prog., 1974, 106 (6), p67.

[12] Stott F.H, Lin D.S. and Wood G.C.

Corrosion Science, 1973, 133, p449.

[13] Stott F.H. and Mitchell D.R.G.

Surface Engineering, Volume I : Fundamentals of Coatings

Ed. P.K.Datta and J.S.Gray, 1993.

[14] Iwabuchi A., Hori K. and Kudo H.

The Effect of Temperature, Preoxidation and Presliding on the Transition from Severe Wear to Mild Wear for S45C Carbon Steel and SUS 304 Stainless Steel

Int. conf., Wear of Materials, New York, 1987.

[15] Sullivan J.L. and Granville N.W.

Trib. Int., April 1984, 17 (2), p63.

[16] Jiang J., Stott F.H., and Stack M.M.

Wear, 1995, 181, p20.

[17] Zum Gahr K.H.

Wear, 1988, 124, p87.

[18] Quinn T.F.J

Wear, 1992, 153, p179.

[19] Quinn T.F.J

Wear, 1994, 175, p199.

[20] Sullivan J.L. and Athwal S.S.

Trib. Int., June 1983, 16 (3), p123.

[21] Rigney D.A and Hirth J.P

Wear, 1979, 53, p345.

[22] Suh N.P.

Wear, 1973, 25, p111.

[23] Libsch T.A., Becker P.C. and Rhee S.K.

Wear, 1986, 110, p263.

[24] Archard J.F.

J. of Applied Physics, Aug. 1953, p.981.

[25] Hickl A.J.

Nickel-Base Alloys as Alternatives to Cobalt-BaseAlloys for P/M Wear and Environmental Resistant Components

Publ. by Cabot Corporation, Indiana, USA, 1981.

[26] Archard J.F. and Hirst W

Proc. R. Soc. London, Ser. A, 1959, 236, p397.

[27] Burwell J.T. and Strang C.D.

Proc.R. Soc. London, 1952, 212, p470.

[28] Department of Trade and Industry

Wear Resistant Surfaces in Engineering - a Guide to their Production, Properties and Selection, 1989

[29t] Hutchings

Tribology

Pub. by Arnold, London, 1992.

[30] Hailing J.

Introduction to Tribology

Pub. by Wykeham Publications, London, 1976.

[31] Rigney D.A.and Glaeser W.A.

Wear, 1978, 46, p241.

[32] Bhansali K.J.

Wear, 1980, 160, p95.

[33] Razavizadeh K. and Eyre T.S.

Wear, 1982, 79, p325.

[34] Childs T.H.C.

Trib.Int., December 1980, p.285.

[35] Quinn T.F.J.

ASLE Trans, 1978, 21, p778.

[36] Quinn T.F.J

Wear, 1971, 18, p413.

[37] Bowden F.B. and Tabour D.

The Friction and Lubrication of Solids: Pts 1 & II

Publ. by Oxford University Press, 1954 and 1964.

[38] Kubaschewski O. and Hopkins B.E.

Oxidation of Metals and Alloys

Pub. by Butterworths, London, 1962.

[39] Furey M.J.

ASLE Trans, 1964, 10, p.133

[40] Quinn T.F.J.

An Experimental Study of the Thermal Aspects of Sliding Contacts and their Relation to the Unlubricated Sliding of Steel

Int. conf., Tribology Convention, Gothenburg, Sweden, May 1969.

[41] Lin D.S., Stott F.H. and Wood G.C.

ASLE 73LC-1B-3, 1973, p.1.

[42] Stott F.H., Glascott J. and Wood G.C.

Wear, 1984, 97, p93.

[43] Barnes D.J., Wilson J.E., Stott F.H. and Wood G.C.

Wear, 1977, 45, p161.

[44] Stott F.H., Lin D.S., Wood G.C. and Stevenson C.W.

Wear, 1976, 36, p147.

[45] Stott F.H, Glascott J. and Wood G.C.

Proc. R. Soc., 1985, 402, p167.

[46] Stott F.H. and Glascott J.

Wear, 1987, 101, p78.

[47] Silence W.L.

ASME Trans., July 1978, 100, p.428.

[48] Bian S., Maj S. and Borland D.W.

Wear, 1993, 166, p1.

[49] Fischer A.

Wear, 1992, 152, p151.

[50] Rigney D.A.

Wear, 1994, 175, p63.

[51] Subramanian C.

Scripta Metallurgica et Materialia, 1991, 25, p1369.

[52] Subramanian C.

Wear, 1991, 151, p97.

[53] Subramanian C.

Wear, 1993, 161, p53.

[54] Clemow A.J.T. and Daniell B.L.

Wear, 1980, 61, p219.

[55] Wang Y. and Lei T.

Wear, 1996, 194, p44.

[56] Frenk A. and Kurz W.

Wear, 1994, 174, p81.

[57] Dao-Yuan W., De-Lin S. and Xin-Cheng G.

Wear, 1987, 119, p101.

[58] Yang. G.H. and Garrison W.M.

Wear, 1989, 129, p93.

[59] Ping L., Bahadur S. and Verhoeven J.D.

Wear, 1990, 138, p269.

[60] Agarwal S. and Ocken H.

Wear, 1990, 140, p223.

[61] Scholl M., Devanathan R. and Clayton P.

Wear , 1990, 135, p355.

[62] Todsen U.

Application and Optimisation of Materials in the Valve Train

Int. conf., Performance of High Temperature Materials in Heavy Duty

Reciprocating Engines, Cranfield, UK, 22nd March 1994.

[63] Stott F.H. and Wood G.C.

Trib. Int., August 1978, p211.

[64] Jiang J., Stott F.H. and Stack M.M.

Wear, 1994, 176, p185.

[65] Earles S.W.E. and Tenwick N.

Wear, 1972, 19, p287.

[66] Lanacster J.K.

Proc. Royal Soc., 1962, A273, p466.

[67] Takadoum J. and Roques-Carmes C.

Surface Coatings Technology, 1992, 52, p153.

[68] Hiratsuka K., Enomoto A. and Sasada T.

Wear, 1992, 153, p361.

[69] Takadoum J.

Wear, 1993, 170, p285.

[70] Buckley D.H. and Miyoshi K.

Wear, 1984, 100, p333.

[71] Zhou L., Fang L., Wang N.X. and Zhou J.E.

Trib. Int., 1994, 27 (5), p349.

[72] Miyoshi K.

Wear, 1990, 141, p35.

[73] Ravikiram A. amd Pramila Bai B.N.

J. Am. Ceram. Soc., 1995, 78 (11), p3025.

[74] Childs T.H.C and Mimaroglu A.

Wear, 1993, 162, p890.

[75] Buckley D.H.

Surface Effects in Adhesion, Friction, Wear and Lubrication

Publ. by Elsevier, Amsterdam, 1981.

[76] Goto H. and Buckley D.H.

Int. Conf., 5th Eurotrib , Helsinki, June 1989.

[77] Stachowiak G.W. and Stachowiak G.B.

Wear, 1989, 132, p151.

[78] Murray S.F. and Calabrese R.

Wear, 1994, 144, p277.

[79] Mokhtar M.O., Zaki M. and Shawki G.S.

Wear, 1980, 65, p.29.

[80] Budinski K.G.

Wear, 1991, 151, p203.

[81] Akagaki T. and Rigney D.A.

Wear, 1991, 149, p353.

[82] Zoroulis Z.A.

Wear, 1984, 96, p203.

[83] Miyoshi K. and Buckley D.H.

Wear, 1982, 77, p252.

[84] Zum Gahr K.H.

Wear, 1989, 133, p1.

[85] Iwabuchi A., Kubosawa H. and Hori K.

Wear, 1990, 139, p319.

[86] Waterhouse R.B. and Iwabuchi A..

Wear, 1985, 106, p303.

[87] Lee R.Y. and Eliezer Z.

Wear, 1984, 95, p165.

[88] Overs M.P., Harris S.J. and Waterhouse R.B.

Wear, 1982, 74, p315.

[89] Hamdy M.M. and Waterhouse R.B.

Wear, 1981, 71, p237.

[90] Schunke J.N., Sudarshan T.S. and Srivatsan T.S.

Wear, 1988, 125, p.211.

[91] Kazimierzak B., Prignon J.M. and Fromont R.I.

Materials and Design, April 1992, 13 (2), p67.

[92] Kazimierzak B., Prignon M., Lecomte-Mertens C., Coutsouradis D.

Fe Base ODS Alloys with Improved Mechanical Strength.

Int. conf., High Temperature Materials for Power Engineering, Liege, Belgium, 24-27 Sept 1990.

[93] Haghi M. and Anand L.

Met. Trans. A, Feb.1990, 21A, p353.

[94] Ruhle M. and Korb. G.

Novel ODS Super Alloys Mamufacture and Properties

Int. conf., Heat-Resistant Materials, Fontana, USA, Sept 1991.

[95] Hack G.A.J. and Fronsko A.L.

Oxide Dispersion Strengthened Superalloys for High Temperatures

Int. conf., Australasian Conference on Materials for Industrial Development, Christchurch, New Zealand, 24-26th August 1987.

[96] Quadakkers W.J., Elschner A., Holzbrecher H. and Schmidt K.

Mikrochim. Acta, 1992, 107, p197.

[97] Hedrich H.D.

Properties and Applications of Iron-Base ODS Alloys

Int. conf., New Materials by Mechanical Alloying Techniques, FRG, 1989.

[98] Smith G.D., Barbadillo J.J. and Fischer J.J

Exploring the Temperature and Environmental Limits for MA ODS Alloys based on High Temperature Corrosion Performance

Int. conf., PM Aerospace Materials, Lausanne, Switerland, 4-6th Nov. 1991.

[99] Kazimierzak B., Prignon M. and Coutsouradis D.

Metal Powder Report, Oct. 1990, 45 (10), p699.

[100] Quaddakkers W.J.

Werkstoffe und Korrosion, 1990, 41, p659.

[101] Bennett M.J. and Houlton M.R.

Comparison between the Oxidation Behaviour of FeCrAlloy Stainless Steel and the Ma956 Oxide Dispersion Strengthened Alloy

Int. conf., High Temp. Materials for Power Eng., Liege, Belgium, 24-27 Sept. 1990.

[102] Sporer D. and Korb G.

PM2000 - An Iron Base ODS Sheet Alloy for Advanced Combustion Systems and the other High Temperature Applications in Corrosive Environments

Int. conf., PM Aerospace Materials, Lausanne, Switzerland, 4-6th Nov. 1991.

[103] Allison J.E., Sherman A.M. and Bapna M.R.

J. of Metals, March 1987, p15.

[104] Blenkinsop P.A.

Titanium Science and Technology

Pub. by Oberursel, Germany, 1985.

[105] Eylon D., Fujishiro S, Postans P.J. and Froes F.H.

J. of Metals, 1984, 36 (11), p55.

[106] Jette P. and Sommer A.

Titanium for Energy and Industrial Applications

Publ. by Warrendale, USA, 1981.

[107] Inco Alloy Product Handbook

Pub. No.IAI-38, 1988.

[108] Woods M.E. and McNulty W.D.

SAE Paper 910951, 1991.

[109] Schreiner M., Kamo R., Walson R. and Liang W.

SAE Paper 870418, 1987.

[110] Johnson M.P., Moorhouse P. and Nicholls J.R.

Diesel Engine Combustion Chamber Materials for Heavy Fuel Operation,

Publ. by DTI, 1990.

[111] Kocis J.F.and Matlock W.M.

Met. Prog., 1975, 3, p58.

[112] Blau P.J.

Wear, 1981, 72, p.55.

[113] Razavizadeh K.and Eyre T.S.

Wear, 1983, 87, p261.